Zebrafish disease modelling identifies a link between type I interferon signalling and cholesterol dysregulation in Aicardi-Goutières syndrome and brain endothelial cells

A thesis submitted to the University of Manchester for the degree of Doctor of Philosophy in the Faculty of Biology, Medicine and Health

2022

Sarah E. Withers

School of Biological Sciences, Division of Neuroscience and Experimental Psychology

Table of Contents

Word count: 46239

List of Figures

List of Tables

List of Abbreviations

25HC	25-hydroxycholesterol
ABCG1	ATP binding cassette subfamily G member 1
ACAT	Acyl-coenzyme A cholesterol acyltransferase
ADAR1	Adenosine deaminase acting on RNA
AGS	Aicardi-Goutières syndrome
AIM2	Absent in melanoma 2
ATF3	Activating transcription factor 3
ATV	Atorvastatin
BBB	Blood brain barrier
BCA	Bicinchoninic acid
BMDM	Bone marrow derived macrophages
bp	base pair
BSA	Bovine serum albumin
CANDLE	Chronic atypical neutrophilic dermatosis with lipodystrophy and elevated temperatures
Cas9	CRISPR associated protein 9
CDC	Cholesterol-dependent cytolysin
cGAS	Cyclic GMP-AMP synthase
CH25H	Cholesterol 25-hydroxylase
CMV	Cytomegalovirus
CNS	Central nervous system
CRFB	Cytokine receptor family B
CRISPR	Clustered regularly interspaced palindromic repeats
CSF	Cerebrospinal fluid
Ctrl	Control
CTTF	Corrected total fail fluorescence
cyp51a1/CYP5A1	Cytochrome P450 family 51 subfamily A member 1
dhcr24/DHCR24	24-Dehydrocholesterol reductase
DHCR7	7-dehydrocholesterol reductase
DLV	Dorsal longitudinal vein
DMSO	Dimethyl sulfoxide
DNA	Deoxyribonucleic acid
dNTP	Deoxynucleoside triphosphate
dpf	Days post fertilisation
dsDNA	Double stranded DNA
dsRNA	Double stranded RNA
ebp/EBP	3 beta-hydroxysteroid-delta 8, delta 7-isomerase
ER	Endoplasmic reticulum

F	Forward primer
FDFT1	Farnesyl-diphosphate farnesyltransferase 1
FDPS	Farnesyl diphosphate synthase
GCS	Glasgow coma score
GGPP	Geranylgeranyl pyrophosphate
gRNA	Guide RNA
h	hours
hCMEC/D3	Human brain microvascular endothelial cells
HIV	Human immunodeficiency virus
hmgcr/HMGCR	3-hydroxy-3-methylglutaryl-coA reductase
HMGCS1	3-hydroxy-3-methylglutaryl-coA synthase 1
hpf	Hours post fertilisation
HSD17B7	Hydroxysteroid 17-β dehydrogenase
HSV	Herpes simplex virus
HUVEC	Human umbilical vein endothelial cells
ICH	Intracerebral haemorrhage
IFIH1	IFN-induced helicase C domain-containing protein 1
IFITM3	Interferon induced transmembrane protein 3
IFN	interferon
IFNAR	Interferon α/β receptor
IFNα	Interferon alpha
IFNβ	Interferon beta
IL-17	Interleukin 17
IL-1β	Interleukin 1β
IL-8	Interleukin 8
INSIG	Insulin-induced gene 2
IQR	Interquartile range
IRF3/9	Interferon regulatory factor 3/9
isg12/ISG12	interferon stimulated gene 12
isg15/ISG15	interferon stimulated gene 15
ISRE	IFN-stimulated response elements
JAK	Janus Kinase
LDL	Low density lipoproteins
LDLR	Low density lipoprotein receptors
LINE-1	Long interspersed element 1
LSM11	LSM11, U7 small nuclear RNA associated
LSS	Lanosterol synthase
LXR	Liver X Receptor
MAVS	Mitochondrial anti-viral signalling protein
MDA	Melanoma differentiation associated protein 5

Min	minute
mi-RNA	Micro-RNA
MO	Morpholino
mRNA	Messenger RNA
MS	Multiple sclerosis
MS222	Tricaine methansulfonate
msmo1/MSMO1	Methylsterol monooxygenase 1
MsV	Mesencephalic vein
MtA	Metencephalic atery
MVD	Mevalonate diphosphate decarboxylase
MVK	Mevalonate kinase
NF-κβ	Nuclear factor kappa-beta
NLRP3	NOD-, LRR- and pyrin domain-containing protein 3
NSDHL	NAD(P) dependent steroid dehydrogenase-like
OSBP	Oxysterol binding protein
PAM	Protospacer-adjacent motif
PAMP	Pathogen associated molecular pattern
PBMC	Peripheral blood mononuclear cell
PBS	Phosphate buffered saline
PCR	Polymerase chain reaction
PCSK9	Proprotein convertase subtilisin/kenin type 9
PFA	Paraformaldehyde
PMVK	Phosphomevalonate kinase
PrA	Prosencephalic artery
PRR	Pattern recognition receptors
PTU	Phenylthiourea
qPCR	Quantitative PCR
R	Reverse primer
RGC	Radial glial cells
RNA	Ribonucleic acid
RNASEH2 (A,B,C)	Ribonuclease H2
RNA-seq	RNA-sequencing
RNU7-1	RNA, U7 small nuclear 1
rpm	revolutions per minute
RQ	Relative quantification
rsad2/RSAD2	Radical S-adenosyl methionine domain containing 2
RSEM	RNA-seq by expectation maximisation
RT	Room temperature
RTI	Reverse transcriptase inhibitor
RWD	Relative wound density

s	seconds
samhd1	SAM domain and HD domain-containing protein 1
SAVI	STING-associated vasculopathy with onset in infancy
SC5D	Stearoyl-CoA desaturase
SCAP	SREBP cleavage activator protein
SEM	Standard error of the mean
SLE	Systemic lupus erythematosus
SLO	Streptolysin O
SOCS	Suppressor of cytokine genes
sqle/SQLE	Squalene epoxidase
srebf1	sterol regulatory element binding transcription factor 1
SREBP	Sterol regulatory element binding protein
ssDNA	Single stranded DNA
STAT1/2	Signal transducer and activator of transcription
STING	Stimulator of interferon genes
SZ 58-035	Sandoz
TAE	Tris-acetate-EDTA
TBK	TANK binding kinase
TdT	Terminal deoxynucleotidyl transferase
TM7SF2	Delta- 14-sterol reductase
TNFα	Tumour necrosis factor alpha
TOAST	Trial of ORG in 10172 in acute stroke treatment
TPM	Transcript per million
TREX1	Three primer repair exonuclease
TUNEL	Terminal deoxynucleotidyl transferase dUTP nick end labelling
TYK2	Tyrosine kinase 2
USP18	Ubiquitin carbxy-terminal hydrolase 18
VAMP	Vesicle-associated membrane protein
VAPA	VAMP-associated protein A
VZV	Varicella zoster virus
WT	Wild type

Abstract

Aicardi Goutières Syndrome (AGS1-9) is a rare inflammatory mediated encephalopathy which occurs due to mutations in genes involved in the sensing, regulation and metabolism of self-nucleic acid species. Proteins implicated in AGS play an essential role in self-non-self-discrimination, which helps explain the excessive type I interferon (IFN) production and large upregulation of interferon stimulated genes (ISGs) that occurs in AGS patients. This strong antiviral response is thought to largely contribute to the devastating nature of the condition, which results in significant physical and neurological disability. AGS patients can also suffer from sub-type specific symptoms, such as cerebrovascular disease which only manifests in patients with mutations in *SAMHD1* (AGS5). Indeed, AGS5 represents a monogenic form of inflammatory based stroke, and can be utilised to provide unique insight into the mechanisms and causes behind more common forms of stroke, such as viral infections as a risk factor, whereby excessive type I IFN signalling as an antiviral mechanism may be related to the onset of stroke. Moreover, antiviral signalling has also been attributed to cholesterol dysregulation, an additional clinical risk factor for both ischaemic and haemorrhagic stroke.

To date, few mouse models successfully replicate the vast clinical phenotypes observed in AGS patients, with none phenocopying the neurological manifestations which are one of the hallmarks of the condition. Contrastingly, transient knockdown of the *samhd1* gene in a zebrafish larval model appeared to recapitulate a number of clinically relevant phenotypes, including neurological aspects of the disease, as observed by the presence of intracerebral haemorrhage (ICH) in the larvae. Therefore, zebrafish may offer specific advantages over mice when modelling AGS pre-clinically. As such, the central aim of this PhD was to characterise a novel stable mutant zebrafish model of AGS5 to increase understanding of SAMHD1-induced AGS, and the associated cerebrovascular disease.

Zebrafish disease modelling of AGS5 revealed the presence of a number of neurological phenotypes, not previously identified in the existing pre-clinical models, reinforcing the usefulness of zebrafish as a model organism to study AGS. Furthermore, the zebrafish exhibited cerebrovascular deficits and dysregulation of the cholesterol biosynthesis pathway, which was also observed in an AGS patient RNAseq dataset. Further investigation of the type I IFN signalling relationship with cholesterol in human brain endothelial cells, identified cholesterol dysregulation following treatment of the oxysterol 25 hydroxycholesterol (25HC), produced downstream of type I IFN. A reduction in cholesterol from the plasma membrane acted to alter the normal functioning properties of the brain endothelial cells. Taken together, we propose that these data in zebrafish and human cells provide new mechanistic insight into how cholesterol dysregulation, as a result of antiviral signalling, may lead to the generation of cerebrovascular deficits and stroke.

Declaration

I declare that no portion of the work referred to in the thesis has been submitted in support of an application for another degree or qualification of this or any other university or other institute of learning

Copyright statement

Experimental Contributions

Chapter 3- All experiments were designed, performed and analysed by myself, with the exception of the generation of the *samhd1*$^{\Delta 23/\Delta 23}$ model, which was generated by Dr. Paul Kasher, prior to the start of this PhD project.

Chapter 4- All experiments were designed, performed and analysed by myself, with the exception of the AGS patient RNA sequencing data. Whereby RNA was extracted from AGS patient whole blood by Dr Gillian Rice, RNA sequencing was performed by the Manchester Genomic Technologies facility and the subsequent analysis was performed by Dr. Charles Rowlands, under the supervision of Dr. Tracy Briggs.

Chapter 5- All experiments were designed, performed and analysed by myself and Dr. Victor Tapia Olivares. We both performed replicates for each of the *in vitro* experiments described within the chapter.

Acknowledgements

Completing a PhD is such a mammoth task, and one which is impossible to complete alone. I feel extremely grateful for all of the support I have received, and there are so many people who have helped me get to the finishing line of this PhD.

Firstly, my supervisors, Paul, Stuart and Tracy. Thank you so much for your supervision and guidance over the course of the PhD, you have all provided me with invaluable knowledge and I feel extremely lucky to have had you all as part of my supervisory team. A special thank you to Paul, who truly went above and beyond as a supervisor, and was always there to help and sympathise with all of the many, many zebrafish related issues.

A massive thank you to the Kasher lab and the Brain Inflame Group, old and new. It has been an absolute pleasure to work in a lab group with so many lovely, helpful individuals and thank you all for the laughs, the drinks, the retreats, the parties, and the general silliness. I feel very privileged to have worked with so many fantastic people. A big thank you to Siobhan for being there from the start and being my lab big sister, teaching me the ways of the fish, and then becoming my go-to gig pal! Thank you to Victor, who taught me everything I know about *in vitro* work, and who always answered my 100s of questions, no matter how trivial they were.

Thank you to the MRC for funding my PhD work, and also the EWS educational trust who awarded me with an exceptional contribution grant throughout the duration of my PhD. Additionally, I would like to thank all of those who helped me from the University of Manchester by providing training and resources: all of the staff at the Biological Services Unit who cared for all of the fish and the Bioimaging core facility and genomic technologies core facility.

My life in Manchester has been made that much brighter thanks to my amazing and wonderful friends: Lucy and Molly thank you for your infectious optimism and positivity. My Pencarrow Girls: Lina, Amy and Jade. We really went through it all from 3 years in our lovely house. Celebrating the highs, and getting through the lowest of the lows (curtesy of the global pandemic) together. You are all amazing and I thank you so much for your friendship, love and support which came in the form of club nights in the kitchen, outdoor movie nights, BBQs and so much more. Lina, you also deserve a medal for living with me during my last few months of the PhD, thank you for keeping me sane and laughing, being my unofficial therapist, and just generally being the Lorelai to my Lorelai (because no-one wants to be Rory).

A massive thank you to my family: mum, dad and Luke. Your unwavering support and guidance throughout this journey is so appreciated. You have been my personal cheerleaders, always knowing what to say to keep my spirits up and you have always believed in me and my abilities. This thesis is dedicated to you. Finally, thank you to Jack who has been there every step of the way. You are rock, my support system all the way from the other side of the country. I cannot wait to finally start this new chapter together.

Chapter 1: Introduction

1.1 Aicardi-Goutières syndrome and the type I interferonopathies

1.1.1 Aicardi-Goutières syndrome

Aicardi-Goutières syndrome (AGS) is a rare monogenic disease, which comprises part of the larger disease class known as the type I interferonopathies. Since the 1980s, inappropriate exposure to type I interferon (IFN) has been shown to be detrimental in developing mammals, resulting in growth arrest, delay in organ maturation, and death (Gresser et al., 1980). Following this pre-clinical observation, two paediatric neurologists: Jean Aicardi and Françoise Goutières described comparable results in a group of young infants. These patients presented with mainly neurological symptoms, manifesting as intracranial calcifications, brain atrophy and microcephaly, coupled with a large increase in intrathecal IFN-α production and lymphocytosis, despite no indication of a viral infection (Aicardi and Goutieres, 1984; Lebon et al., 1988). The lack of identifiable infection was intriguing, as the clinical phenotypes observed had significant overlap with the sequelae of *in utero* congenital viral infection (Crow and Livingston, 2008). Instead, this alluded to a genetic basis of this disease, and since the original identification of these symptoms, pathogenic variants in nine different genes have been revealed, with their corresponding genetic loci termed AGS1-9. There are thought to be approximately 500 families affected by AGS worldwide, making it the most common type I interferonopathy, and also the most well studied. (Crowl et al., 2017).

1.1.2 Additional type I interferonopathies

Type I interferonopathies are a relatively new disease class, first described in the medical lexicon in 2011 to group together three distinct Mendelian syndromes all characterised by excessive type I IFN release (AGS, spondyloenchondrodysplasia, and monogenic forms of systemic lupus erythematosus (SLE)) (Crow, 2011). Fuelled by enhanced clinical knowledge and understanding, screening assays, and next-generation sequencing, there are now 38 discrete genotypes, responsible for 13 syndromes which are all considered type I interferonopathies (Crow and Stetson, 2021). Alongside the three originally described syndromes, current literature includes syndromes such as proteasome-associated autoinflammatory syndromes, ISG15 and USP18 deficiency, Singleton-Merten syndrome and STING-associated vasculopathy with onset in infancy (SAVI) (d'Angelo et al., 2021).

Notably, there is a distinct overlap of clinical features found across the type I interferonopathies, particularly with regards to the central nervous system (CNS) and the skin, which suggests that type I IFN is directly a large contributor to the pathology. However, this has yet to be ascertained, and may yet just represent an association with the disease rather than a causal relationship (Rodero and Crow, 2016). Arguments for type I IFN being a disease biomarker rather than a pathological factor stem from the largely heterogeneous clinical presentation of each syndrome, despite the evident phenotypic overlap. For example, SAVI patients present with profound pulmonary disease, a symptom not identified in other type I interferonopathies (Crow and Manel, 2015). However, Rodero and Crow argue that the differences could instead be attributed to multiple biological consequences

of protein dysfunction, coupled with distinct expression patterns of affected genes, causing phenotypes in specific locations (Rodero and Crow, 2016).

The genes implemented in causing dysregulated type I IFN production can be grouped based on the function of the gene products, with the majority acting directly on nucleic acid substrates, involved in the metabolism, regulation or sensing of deoxyribonucleic acid (DNA) or ribonucleic acid (RNA). Other groups of genes are involved in type I IFN receptor signalling, the maintenance of mitochondrial integrity and proteasomal functioning, whilst a small number of genes have an as yet undefined role relating to type I IFN (Crow and Stetson, 2021). Ultimately, upon mutation, these genes represent a failure of self versus non-self discrimination and the highly distinctive roles and intracellular location of each gene acts to increase our understanding of innate immunity, in particular the role of the type I IFN pathway, in both health and disease.

1.2 Genetic mechanisms of AGS

Currently, nine sub-types of AGS have been identified. These involve mutations in *TREX1*; the three nonallelic components of the *RNASEH2* complex *(RNASEH2A, B, C*); *SAMHD1; ADAR1; IFIH1; LMS11* and *RNU7-1* (Crow et al., 2006a; Crow et al., 2006b; Rice et al., 2009; Rice et al., 2014; Rice et al., 2012; Uggenti et al., 2020). Each gene encodes a protein with an integral role in intracellular nucleic acid sensing, processing or metabolism (Table 1.1). Upon mutation, there is disruption to the nucleic acid homeostasis within the cell, recognised by intracellular DNA and RNA sensors, which activate the cyclic GMP-AMP synthase (cGAS), Stimulator of interferon genes (STING) (cGAS-STING) pathway, or the Mitochondrial antiviral-signalling protein (MAVS pathway) respectively, causing type I IFN induction (Fig 1.1).

Table 1.1- Molecular function of AGS-related proteins, and the mechanism behind innate immune signalling pathways following mutation

Abbreviations: ssDNA: single stranded DNA; dsDNA: double standed DNA; dsRNA: Double stranded RNA; cGAS: cyclic GMP-AMP synthase; STING: Stimulator of interferon genes; dNTP: deoxynucleotide triphosphate; MDA5: Melanoma differentiation associated protein 5; MAVS: Mitochondrial antiviral-signalling protein.

Gene	Protein Function	Proposed mechanism of IFN activation
Three prime repair exonuclease (***TREX1***)	DNA exonuclease targeting products of reverse transcriptase activity (ssDNA and dsDNA) (Mazur and Perrino, 1999)	Following loss of function, DNA species accumulate and are detected by the cGAS-STING pathway (Gao et al., 2015)
Ribonuclease H2 (***RNASEH2B, 2C, 2A***)	Endonuclease complex that degrades RNA in RNA-DNA heteroduplexes. These are products of RNA transcription and reverse transcription (Cerritelli and Crouch, 2009)	Following loss of function, there is suggested to be an increase in cytosolic RNA-DNA hybrids leading to an increase in DNA damage, thought to activate the cGAS-STING pathway (Mackenzie et al., 2016).
SAM and HD Domain containing deoxynucleoside triphosphate triphosphohydrolase (***SAMHD1***)	dNTPase which regulates the intracellular dNTP pool (Goldstone et al., 2011)	Following loss of function, endogenous dNTPs accumulate, leading to loss of genome integrity and activation of the cGAS- STING pathway (Kretschmer et al., 2015)
Adenosine Deaminase acting on RNA (***ADAR1***)	dsRNA-editing enzyme, deaminates adenosine to inosine (Hogg et al., 2011)	Loss of function leads to generation of abnormally immunogenic dsRNA species, recognised by the RNA-sensing pathway involving MAVS (Rice et al., 2012)
IFN-induced helicase C domain-containing protein 1 (***IFIH1***)	Encodes MDA5, a dsRNA sensor (Kato et al., 2006)	Gain of function mutation results in a lower activation threshold to enable sensing of endogenous dsRNA, and the MAVS pathway is activated (Rice et al., 2014)
LSM11, U7 small nuclear RNA associated (***LSM11***) RNA, U7 Small nuclear 1 (***RNU7-1***)	Both proteins form components of the replication-dependent histone pre-mRNA processing complex (Mowry and Steitz, 1987; Pillai et al., 2003)	Upon loss of function mutation, there is a disturbance of histone protein composition, leading to the sensing of nuclear DNA through cGAS-STING (Uggenti et al., 2020)

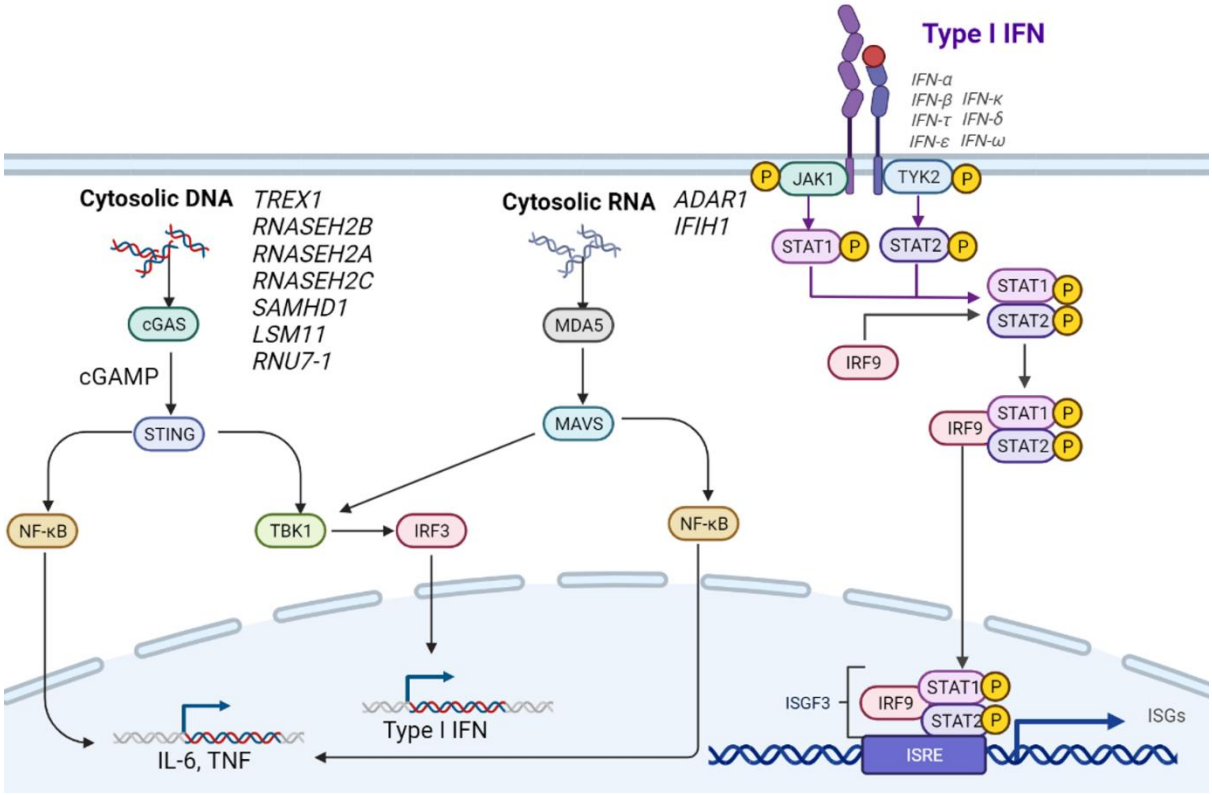

Figure 1.1- Activation of the antiviral signalling pathway following AGS mutations

Cytosolic DNA and RNA are recognised by cytosolic sensors. Mutations in *TREX1, RNASEH2B, 2A, 2C, SAMHD1, LMS11* and *RNU7-1* cause either the build-up of cytosolic DNA, or result in abnormal sensing of DNA. The DNA binds to cGAS and catalyses the synthesis of cGAMP. cGAMP binds to and activates STING, leading to activation of two distinct pathways. The NF-κB pathway leads to the expression of pro-inflammatory genes, whilst TBK-1 and IRF3 result in type I IFN expression. The cytosolic RNA pathway is initiated by mutations in *ADAR1* and *IFIH1*. MDA5 recognises long double stranded RNA, resulting in downstream activation of the adaptor protein MAVS. Subsequently, the TBK-1 and NF-κB pathways are activated, akin to the DNA sensing pathway. The type I IFN produced from the IRF3 transcription factor can act in an autocrine and paracrine fashion, through binding to the IFNAR receptors. This initiates the activation of the JAK/STAT signalling cascade. JAK1 and TYK2 phosphorylate each other's tyrosine residues and the intracellular tail of the receptor, establishing a docking site for STAT1 and STAT2 to bind. Phosphorylation of STAT1 and STAT2 recruits the transcription factor IRF9, together forming the ISGF3 complex which translocates into the nucleus to bind to ISRE and initiate the induction of ISGs. Abbreviations: cGAS: cyclic GMP-AMP (cGAMP) synthase; STING: Stimulator of interferon genes; TBK: serine/threonine protein kinase; IRF3/9: interferon regulatory factor 3/9; NF-κB: nuclear factor kappa beta. MDA5: melanoma differentiation-associated protein 5; MAVS: mitochondrial antiviral-signalling protein; JAK: janus kinase 1; TYK2: tyrosine kinase 2; STAT1/2: signal transducer and activator of transcription; ISRE: IFN-stimulated response elements.

1.3 Type I IFN

Type I IFN forms one of the three distinct IFN families, along with type II IFN (IFNγ) and type III IFN (IFNλ1, IFNλ2, IFNλ3). Type I IFN is made up of 13 partially homologous IFNα subtypes, one IFNβ and also a number of poorly defined subtypes: IFNε, IFNτ, IFNκ, IFNω, IFNδ and IFNζ (Pestka et al., 2004). As a result, the discussions around type I IFN are focussed on the most well characterised subtypes: IFNα and IFNβ.

Type I IFNs are key components of the innate immune response, and are known as antiviral cytokines. The antiviral properties of type I FN have been recognised *in vivo* as early as the 1960's, when IFN was shown to be rapidly upregulated following viral infection of mice, long before the production of antibodies against the viral insult (Isaacs and Hitchcock, 1960). This can now be attributed to the different arms of the immune system, with IFN belonging to the innate immune system to produce a rapid response to infection, leaving the adaptive immune system to produce pathogen specific antibodies at a later time point. The importance of IFN in an antiviral context was then confirmed using IgG antibodies against IFN, which made resistant mice susceptible to the viral infections hepatitis and influenza (Haller et al., 1979; Virelizier and Gresser, 1978).

All nucleated cells can produce type I IFN, following the activation of pattern recognition receptors (PRRs) that recognise microbial products and other pathogen-associated molecular patterns (PAMPs). These can be found in the cytosol, as highlighted in Fig 1.1 with cGAS and MDA5, which identify nucleic acid species. Additionally, PRRs are also present on the cell surface and endosomal compartments where similar signalling mechanisms are utilised to produce type I IFN from other pathogen associated molecular patterns (McNab et al., 2015).

Following the production of type I IFN, the response is three-fold. Firstly, type I IFN binds to the heterodimeric transmembrane receptor Interferon α/β receptor (IFNAR), formed of IFNAR1 and IFNAR2 subunits, initiating the canonical type I IFN signalling pathway (Fig 1.1). This cumulates in the transcription of a number of ISGs, which largely facilitate an antiviral state through inhibition of viral entry, transcription and replication (Crosse et al., 2018). Most cells are capable of responding directly to IFN, in order to induce ISG expression. Notably, both type I IFN and ISGs can act in an autocrine and paracrine fashion, to augment a response throughout neighbouring cells, in order to limit the spread of infection (Ivashkiv and Donlin, 2014). Further discussions on specific ISGs can be found in section 1.10.2.

Secondly, type I IFNs regulate other components of the innate immune system to establish a balance between promoting antigen presentation and natural killer cell expansion, whilst also limiting damaging immune responses, which may arise from other immune cells, such as neutrophils, monocytes and innate lymphoid cells (Lee and Ashkar, 2018). Lastly, type I IFNs interact with the adaptive immune system by promoting the development of high-affinity antigen-specific T and B cell responses which facilitate immunological memory (Ivashkiv and Donlin, 2014; McNab et al., 2015). It should be noted that this type I IFN response is attributed to acute viral infections.

The importance of the antiviral type I IFN response has been well established following the discovery of inborn errors of immunity in humans. These are a collection of mutations that compromise the expression/ function of components of the IFN signalling pathway. Loss of IFNAR1, IFNAR2, signal transducer and activator of transcription 1/2 (STAT/2), (interferon regulatory factor 9) IRF9, janus kinase 1 (JAK1) and tyrosine kinase 2 (TYK2) proteins have all been associated with an increased susceptibility to severe/recurrent viral infections, and can even cause reactions to live-attenuated viral vaccines (Duncan et al., 2021).

Despite the vital role type I IFN plays in innate immunity, it is of equal importance to be able to suppress IFN signalling when the viral threat has been removed. Mechanisms have evolved, through the actions of pro-inflammatory cytokines such as interleukin (IL)-1, to downregulate cell surface IFNAR expression through internalisation of the receptor, which acts to limit IFN binding (Ivashkiv and Donlin, 2014). Type I IFNs are also capable of inducing the expression of suppressor of cytokine genes (SOCS) and ubiquitin carbxy-terminal hydrolase 18 (USP18) which form a negative feedback loop to limit the IFN response. These proteins compete with STAT to bind to the IFNAR receptors, and suppress JAK activity, or displace JAK from binding to IFNAR (Sarasin-Filipowicz et al., 2009; Yoshimura et al., 2007). However, these feedback mechanisms can become ineffective following chronic type I IFN production, and in some instances, mutations in components of the regulatory machinery: USP18 and ISG15 (a modulator of USP18) are known type I interferonopathy causative genes, with the mutations leading to excessive type I IFN production (Meuwissen et al., 2016; Zhang et al., 2015).

Interestingly, chronic viral infections can also be worsened by a persistent type I IFN response, through a number of immunosuppressive effects induced by the cytokine which act to impede viral control. This may be observed in Human Immunodeficiency Virus (HIV) infection, whereby IFN acts to reduce T cell clonal expansion, to restrict infection of $CD4^+$ T cells (McNab et al., 2015).

Conversely, type I IFN can also trigger inflammation and tissue damage following chronic viral infection (Davidson et al., 2014). These detrimental effects of type I IFN have been widely described within the CNS, where astrocytes and microglia have been shown to be the primary producers of the cytokines, essential for when pathogens may breach the blood brain barrier (BBB) (Akiyama et al., 1994; Lieberman et al., 1989). Transgenic mice producing excessive amounts of IFNα from astrocytes developed encephalopathy, intracranial calcifications and neurodegeneration, with disturbed synaptic plasticity, similar to the phenotypes observed in AGS and other type I interferonopathy patients (Akwa et al., 1998; Campbell et al., 1999). Despite the manifestation of the neurological phenotypes, these mice were also protected against lymphocytic choriomeningitis virus infection, highlighting the need for type I IFN production within the CNS, although there appears to be a delicate balance between the beneficial antiviral properties and neurotoxicity (Akwa et al., 1998).

1.4 Symptoms of AGS

The heterogeneity of type I interferonopathies has already been alluded to, and this phenotypic variation is also apparent within sub-types of the same condition, such as AGS. Whilst complete understanding of the direct cause of the symptoms is not fully elucidated, the toxic nature of type I IFN is well established to be involved, and most likely the causative agent behind a number of symptoms, as discussed in section 1.1.2 (Rodero and Crow, 2016).

Following the identification of a number of genes implicated in AGS, a partial genotype-phenotype correlation was observed, allowing further characterisation of the disease into five distinct syndromic

groups. Given the very recent discovery of AGS8-9 (Uggenti et al., 2020), there is insufficient patient phenotypic detail to include here, thus descriptions below are only provided for AGS1-7 patients.

'Classical' AGS symptoms are observed across all sub-types, where the patients present with the typical hallmarks of the condition, first identified by Jean Aicardi and Françoise Goutières. This manifests as a prenatal or infantile onset, reminiscent of a congenital viral infection, causing microcephaly, motor dysfunction, epileptic seizures, white matter disease and intracranial calcifications (Aicardi and Goutieres, 1984; Crow and Livingston, 2008). Moreover, the identification of elevated IFNα in both the periphery and the cerebrospinal fluid (CSF), coupled with lymphocytosis within the CSF are also key indicators of AGS, found across all sub-types (Aicardi and Goutieres, 1984; Crow et al., 2015)

There is also a later onset form, manifesting after the first year of life, with a range of 1.00-17.68 years (Piccoli et al., 2021). This form frequently causes neurological regression, following an initial period of normal development. The symptoms are similar to those found in classical AGS, although there is some variation within the severity of neurological symptoms, as a proportion of patients have no abnormalities identified through imaging (D'Arrigo et al., 2008; Piccoli et al., 2021).

Whilst these two distinct manifestations of the disease can occur across all sub-types, there are also sub-type specific phenotypes. Mutations in *ADAR1, IFIH1* and *RNASEH2B* can cause non-syndromic spastic paraparesis confined to the lower limbs (Crow et al., 2014). *ADAR1* patients can also present with bilateral striatal necrosis (La Piana et al., 2014; Livingston et al., 2014a). Lastly, *SAMHD1* patients can develop cerebrovascular disease, which can manifest in a number of ways, including stenosis, moyamoya, aneurysms, intracerebral haemorrhage (ICH) and ischaemic stroke (Ramesh et al., 2010; Thiele et al., 2010). A full list of the symptoms associated with each subtype can be found in table 1.2.

Interestingly, to add further complexity to the condition, intra-familial variability is also apparent, whereby siblings harbouring the same mutation may present in vastly different ways. One may exhibit severe neurological impairment, and the other with only mild symptoms, and normal intellect (Livingston and Crow, 2016; Vogt et al., 2013). These discrepancies within the clinical penetrance can only be explained by further genetic or environmental factors. The leading hypothesis for intra-sibling variation is infection, whereby the induction of an innate immune response could increase the expression of key sensors above the critical threshold, resulting in aberrant detection of self nucleic acids, and the progression to symptomatic disease (Crow and Stetson, 2021). This mechanism has already been identified as a potential trigger for disease in *ADAR-1* related bilateral striatal necrosis (Livingston et al., 2014a).

Table 1.2- Known symptoms associated with mutations in AGS1-7 genes

† two *TREX1* patients have suffered from a cerebrovascular event, †† One *SAMHD1* patient, also with a heterozygous lesion in *ADAR1.* Table adapted from (Livingston and Crow, 2016)

Symptom	*TREX1*	*RNASEH 2B*	*RNASEH 2C*	*RNASEH 2A*	*SAMHD1*	*ADAR1*	*IFIH1*
Motor dysfunction (dystonia/spasticity)	✓	✓	✓	✓	✓	✓	✓
Non syndromic Spastic paraparesis		✓				✓	✓
Microcephaly	✓	✓	✓	✓	✓	✓	✓
Intracranial calcifications	✓	✓	✓	✓	✓	✓	✓
White matter abnormalities	✓	✓	✓	✓	✓	✓	✓
Cerebral atrophy	✓	✓	✓	✓	✓	✓	✓
Seizures	✓	✓	✓	✓	✓	✓	✓
Cerebrovascular disease	✓†				✓		
Bilateral striatal necrosis						✓	
Demyelinating peripheral neuropathy	✓	✓	✓	✓	✓	✓	
Glaucoma	✓	✓	✓	✓	✓		✓
Chilblains	✓	✓	✓	✓	✓	✓	✓
Liver abnormalities	✓	✓	✓	✓	✓	✓	✓
Neonatal Thrombocytopenia/ pancytopenia	✓	✓	✓	✓	✓	✓	✓
Cardiomegaly	✓		✓	✓			✓
Cardiomyopathy	✓		✓				✓
Aortic calcification							✓
CSF lymphocytosis	✓	✓	✓	✓	✓	✓	✓
Elevated type I IFN in blood/CSF and ISG	✓	✓	✓	✓	✓	✓	✓
Hormonal dysfunction	✓	✓		✓	✓	✓	✓
Chronic lymphocytic leukaemia					✓††		
Autoimmune features	✓	✓	✓	✓	✓	✓	✓
Joint contractures	✓				✓		✓
Scoliosis		✓					

1.5 Treatments for AGS and the type I interferonopathies

The treatment strategies for type I interferonopathies are limited, however, two small clinical trials and a number of individual case studies have focussed on the therapeutic potential of JAK inhibitors (Gomez-Arias et al., 2021; Sanchez et al., 2018; Vanderver et al., 2020). Figure 1.1 highlights the

position of JAK within the type I IFN signalling pathway. Following engagement of the IFNAR receptor by type I IFN, phosphorylation of JAK1, TYK2 and the intracellular tail of the IFNAR receptor creates a docking site for STAT1 and STAT2. Phosphorylated STAT1 interacts with phosphorylated STAT2 and IRE9, becoming the interferon-stimulated gene factor 3 (ISGF3) complex, which translocates to the nucleus to initiate transcription of ISGs (Hadjadj et al., 2021). Therefore by targeting JAK, the type I IFN signalling pathway is largely inhibited.

JAK inhibitors are an existing drug class, currently approved for the treatment of rheumatoid arthritis (Genovese et al., 2016). The clinical trials generated a number of positive outcomes following treatment with the JAK inhibitor baracitinib. In chronic atypical neutrophilic dermatosis with lipodystrophy and elevated temperatures (CANDLE) patients, baracitinib normalised inflammatory markers, such as the ISG signature, and also aspects of metabolic disease, including improved body mass index values, compared to pre-treatment (Sanchez et al., 2018). In the same study, baracitinib treatment for SAVI patients improved cutaneous inflammation and halted the development of gangrene. Furthermore, SAVI patients exhibited a decrease in lung inflammation and stabilisation of lung fibrosis. Despite these improvements, there was no normalisation of inflammatory markers, which was observed in the CANDLE patients (Sanchez et al., 2018). In AGS patients, baracitinib treatment also improved cutaneous inflammation and reduced the ISG score. Neurological improvement was also described, with an increase in patients reaching new milestones and acquiring new skills (Vanderver et al., 2020). However, changes in neurological phenotypes are difficult to assess due to the complex nature of the condition, which presents with differential onset and disease progression (Hadjadj et al., 2021). Moreover, there is the additional challenge of CNS penetration of the drug, whereby only 10% of a different JAK inhibitor: ruxolitinib has been measured in the CSF compared to the blood in AGS patients (Neven et al., 2020).

There are a number of side-effects which may occur following JAK inhibitor treatment, including anaemia and leukopenia, cardiovascular disease, cancer and proneness to infection (Hadjadj et al., 2021). Infection is the most commonly described side-effect, as the treatment dampens the immune response, causing a low level of immunosuppression. Fortunately, due to the multitude of signalling pathways involved within the immune system, JAK pathways are not always implemented following infection. This is the case for activating cytokines such as IL-1, IL-8, IL-17 and tumour necrosis factor alpha (TNFα), and may account for the lower levels of serious infection identified in JAK inhibitor treated patients than expected (Hadjadj et al., 2021).

Alongside JAK inhibitors, reverse transcriptase inhibitors (RTIs) have been trialled as a treatment option in AGS. Endogenous retroelements are mobile genetic elements, formed from the integration of retroviruses into the human genome throughout evolution, where they make up ~50% of the genome (Mu et al., 2016). Within the cell, retroelements can be transcribed to RNA and DNA through reverse transcription mechanisms, whereby they represent a potential source of immunostimulatory nucleic acids (Rice et al., 2018). The actions of TREX1, RNASEH2A, B, C and SAMHD1 have been implicated in controlling the levels of retroelements to ensure they do not rise above the immunostimulatory threshold, and this function is perturbed following mutation (see section 1.6 for

additional SAMHD1 functions). Following treatment with HIV-1 reverse transcriptase therapy, AGS patients exhibited a reduction in type I IFN signalling, resulting in a lower ISG signature. Interestingly, patients also presented with increased cerebral blood flow, alluding to an effect on cerebral status which highlights the ability of RTIs to target the CNS (Crow et al., 2020; Rice et al., 2018). A follow-up study is planned to investigate the mechanisms by which RTIs limit IFN signalling and may challenge neuroinflammation (Crow et al., 2020).

1.6 SAMHD1

SAMHD1 was first shown to be associated with AGS in 2009, when it was introduced as a protein with unknown functions. Mutations in *SAMHD1* are thought to be responsible for 13% of all known AGS cases (Crow et al., 2015; Rice et al., 2009). In the subsequent years following identification as an AGS causing gene, there has been a plethora of literature describing multiple functions of the protein (fig 1.2).

The most well characterised role of SAMHD1 is that of a deoxynucleoside triphosphohydrolase (dNTPase), which is the function thought to be altered in AGS5. All mutations in AGS5 patients present with defects in SAMHD1's enzymatic ability, reducing the essential oligomerisation required for dNTPase activity (Coggins et al., 2020; Goldstone et al., 2011) (see table 1.1). The dNTPase function has also identified SAMHD1 as a viral restriction factor, most notable for HIV-1, with the restriction properties most likely occurring due to depletion of the intracellular dNTP pool, which acts to restrict the virus's reverse transcription step, preventing replication of the viral genome within the cell (Goldstone et al., 2011). This viral restriction factor property has also classified *SAMHD1* as a non-classical ISG, whereby *SAMHD1* expression is upregulated through induction of IRF3 following PRR activation, and levels are regulated via micro-RNA expression (miR-181a and miR-155) in monocytes in response to type I IFN (Riess et al., 2017; Yang et al., 2016).

SAMHD1 also plays important roles within cell cycle progression, cell division and DNA damage repair (Coggins et al., 2020). Cell cycle progression and cell division require the dNTPase function of SAMHD1, and upon mutation, the imbalanced pool of dNTPs can become a source of DNA replication stress, which halts replication fork progression during cell division and increases mutagenesis. Moreover, genomic instability can also be attributed to dysregulated dNTPs, which induce a type I IFN response from the DNA damage, sensed by intracellular DNA sensing pathways, such as cGAS-STING, (Kretschmer et al., 2015). With regards to DNA repair, SAMHD1 has been shown to facilitate homologous recombination of double strand breaks before cytosolic ssDNA can be recognised and trigger a type I IFN response, a function also impaired following *SAMHD1* mutation (Coquel et al., 2018). These functions of SAMHD1 also offer an explanation as to why somatic mutations in the gene have been implicated in a number of different cancers, and it is suggested that AGS5 patients are also at a higher risk of developing cancer, despite only one case currently identified in patients (Clifford et al., 2014; Coquel et al., 2019).

Lastly, SAMHD1 has been recognised as an inhibitor of long interspersed element 1 (LINE-1): an endogenous retroelement (Zhao et al., 2013). Following mutation in *SAMHD1*, an upregulation in

LINE-1 nucleic acid species have been identified, and it is hypothesised that an increase in LINE-1 by-products and intermediates can trigger a cGAS-STING upregulation of type I IFN, further contributing to the AGS pathophysiology (Coggins et al., 2020).

As previously highlighted, cerebrovascular disease frequently manifests in AGS5 patients, but this particular phenotype is unique to *SAMHD1* mutations (apart from two exceptional cases in *TREX1* patients) (Ramesh et al., 2010; Thiele et al., 2010). None of the known functions help to explain why these phenotypes could arise due to mutations in *SAMHD1*, alluding to a potentially as yet undescribed function of SAMHD1 related to neurovascular integrity (Ramesh et al., 2010). Interestingly, AGS5 is not the only type I interferonopathy which can cause cerebrovascular disease. A recent gain of function mutation in the *STAT2* gene (involved in the type I IFN signalling cascade) resulted in ICH, in both identified patients (Duncan et al., 2019). This suggests there may be a small defined number of proteins involved in the innate immune response and type I IFN signalling which may have downstream actions on the cerebrovasculature.

Moreover, whilst only SAMHD1 and STAT2 variants have been shown to cause cerebrovascular disease, chilblains and cutaneous vasculopathy are frequently observed symptoms within the type I interferonopathies. These observations may therefore suggest that type I IFN is capable of causing inflammation of the peripheral vasculature, but only able to extend into the cerebral vessels following mutation of SAMDH1 and STAT2 (Volpi et al., 2016). One hypothesis could be related to the distinct expression patterns of these proteins. For example, whole tissue microarray from human donors identified constitutive expression of SAMHD1 protein in the vascular endothelium, including the CNS. This could be related to the viral restriction properties of the enzyme, in particular with herpes simplex virus, whereby the virus can readily invade the endothelium (Schmidt et al., 2015). However, until full expression profiles have also been established from the other AGS causative genes, we are unable to determine whether differential expression plays a role in the cerebrovascular phenotypes.

Like all AGS subtypes, astrocytes have been suggested to be the primary source of increased type I IFN within the CNS (Cuadrado et al., 2013). Given the anti-angiogenic properties of type I IFN, if excessive levels are identified in the developing brain, it could lead to abnormal vessel formation and thus be associated with the cerebrovascular abnormalities associated with AGS5. However, type I IFN within the CNS, does not provide an explanation as to why none of the other sub-types develop these phenotypes. Regardless, AGS5 is fascinating as a rare monogenic form of cerebrovascular disease, and though increased understanding of how the specific cerebrovascular manifestations arise following mutations in SAMHD1, we may be able to apply these findings to more common forms of cerebrovascular disease.

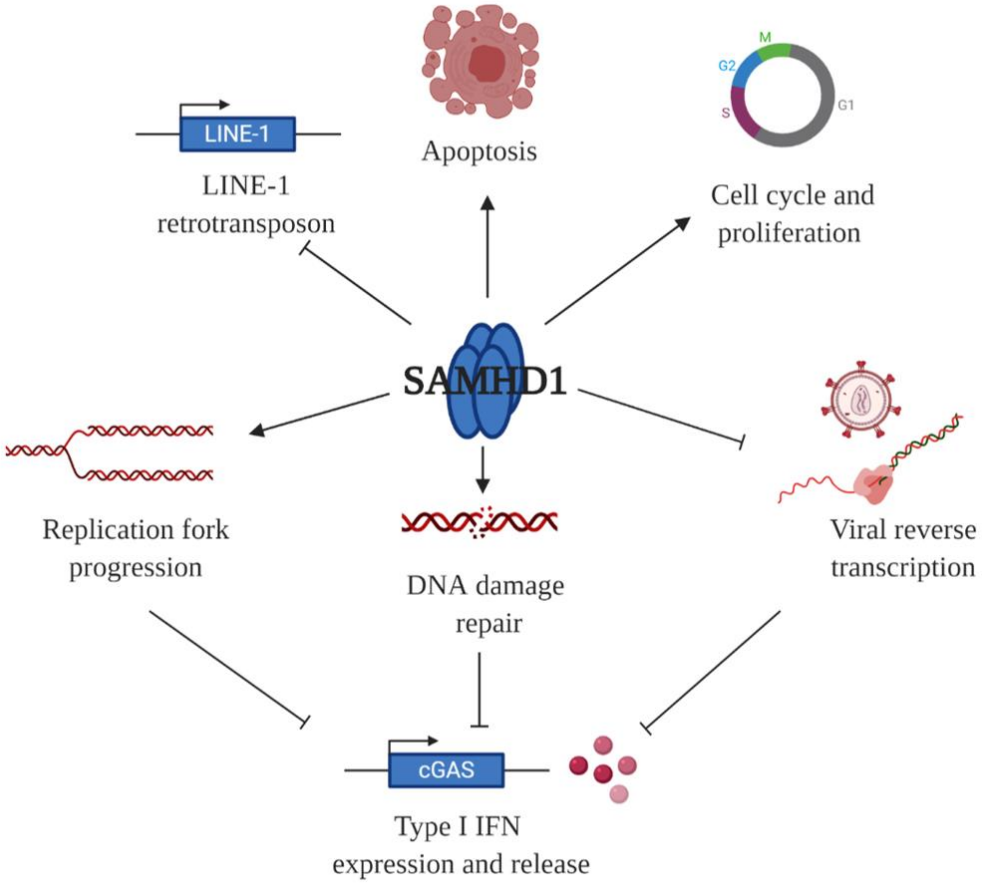

Figure 1.2- Known functions of SAMHD1

SAMHD1 has a plethora of distinct biological roles but is best recognised as a viral restriction factor, via dNTPase activity. The enzyme can also facilitate reparation of DNA damage, replication fork progression and inhibit the LINE-1 retrotransposon. If unregulated these mechanisms can lead to the induction of a type I IFN response, thus SAMHD1 is also a negative regulator of type I IFN. SAMHD1 is also implicated in more general biological mechanisms, such as cell proliferation and apoptosis. Figure adapted from (Coggins et al., 2020)

1.7 Existing pre-clinical rodent models of AGS

The number of small case studies and larger multi-centre studies involving AGS patients have been invaluable at increasing our understanding of the disease, and ultimately have been responsible for identifying the causative genes leading to aberrant type I IFN signalling. Patient material, such as post-mortem tissue and immortalised cell lines have also been utilised to examine the effects of loss/gain of function in certain tissues/ cell types. However, global defects across the whole body cannot be established using post mortem or *in vitro* material alone, and the lack of available patient derived resources presents an additional problem, due to the rare nature of the disease. Thus there has been a need to develop effective pre-clinical models of AGS. Numerous pre-clinical AGS models have now been generated for each genetic subtype of AGS (excluding AGS8-9 due to the recent discovery). The majority have been modelled in mice, and are associated with largely variable phenotypes with regards to fully recapitulating the human condition.

1.7.1 Trex1

The primary phenotype developed in *Trex1*$^{-/-}$ mice was inflammatory pericarditis, and inflammation was also identified in other organs, excluding the brain (Gall et al., 2012; Morita et al., 2004; Stetson et al., 2008). Interestingly, there are a proportion of AGS1 patients who present with heart disease, which this model may be mimicking, however there was a complete lack of neurological phenotype observed in these animals (Crow et al., 2015). Despite this, the *Trex1*$^{-/-}$ mouse has been useful at elucidating the exonuclease properties of Trex1, which were largely reduced upon gene loss. Furthermore, crossing the *Trex1*$^{-/-}$ mice with *Tmem173*$^{-/-}$ (STING deficient mice) rescued the multi-organ inflammation found in the model, which revealed the link between Trex1 loss of function and the cGAS-STING pathway (Gall et al., 2012).

1.7.2 Rnaseh2

Loss of function in any subunit from the *Rnaseh2* complex in mice results in embryonic or perinatal lethality, elucidating the essential role *Rnaseh2* plays in genomic stability (Hiller et al., 2012; Pokatayev et al., 2016; Reijns et al., 2012). Moreover, mouse embryos with a point mutation in *Rnaseh2a* displayed increased expression of ISGs, and mouse embryonic fibroblasts from these mutants demonstrated a link between this ISG activation and the cGAS-STING pathway, in a similar manner to the *Trex1*$^{-/-}$ mice (Pokatayev et al., 2016). Interestingly, no neuroinflammatory phenotype was observed, although this could be attributed to the early age of death associated with these models. As a result, conditional knockouts of *Rnaseh2* have been generated in brain specific cell types to determine the presence of neurological disease and neuroinflammation. Deletion of the whole *Rnaseh2* complex in both astrocytes and neurons produced a lack of disease signs in the animals, although once astrocytes had been isolated from the mice and studied *in vitro*, signs of increased DNA damage and ISG expression were observed (Bartsch et al., 2018). More recently, a second conditional model targeting *Nestin* positive cells (neuroprogenitor cells) in mice did successfully recapitulate a number of the neurological phenotypes, including cerebellar atrophy, white matter defects and neuroinflammation. Interestingly, these findings were proposed to be a result of DNA damage within the brain, as opposed to the direct effect of type I IFN, which had previously been suggested (Lavin and Yeo, 2021).

1.7.3 Adar1

In a similar manner to the *Rnaseh2*$^{-/-}$ mice, loss of *Adar1* is also embryonically lethal in mice, as established through models generated prior to the discovery of the gene's involvement in AGS (Hartner et al., 2004; Hartner et al., 2009; Wang et al., 2004). These studies were the first to identify a link between *Adar1* and regulation of type I IFN, alongside the essential function of Adar1 in the maintenance of haematopoiesis in the foetal liver. However, no neurological phenotype was identified, which may be attributed to the embryonic lethality, as described in the *Rnaseh2* models. Knocking out the Ifnar receptor only partially rescued the embryonic lethality phenotype, indicating

that excessive type I IFN responses are not the primary reason for the fatality associated with the model (Mannion et al., 2014). Conversely, crossing *Adar1*$^{-/-}$ mice with *Mda5*$^{-/-}$ *or Mavs*$^{-/-}$ mice (components of the intracellular RNA sensing pathway) rescued the phenotype to produce live births, confirming the role of *Adar1* in preventing the sensing of endogenous dsRNA as non-self by *Mda5* (Liddicoat et al., 2015; Mannion et al., 2014).

1.7.4 Ifih1

Only one mouse model encompassing the *Ifih1* mutation has been generated which relates to AGS7. The resulting model, obtained through mutagenesis screening, identified a gain of function missense mutation, and was found to be embryonically viable (Funabiki et al., 2014). The main characteristics observed in this model included excessive type I IFN production, and multi-organ inflammation, similar to what was observed in *Trex1*$^{-/-}$ mice, although the primary organ affected was the kidneys, with a distinct lack of inflammation within the brain (Funabiki et al., 2014). This model was originally utilised as a model of SLE, prior to the identification of *IFIH1* as a causative gene in AGS.

1.7.5 Samhd1

Lastly, *samhd1*$^{-/-}$ mice appear to produce the mildest phenotypes of all the rodent pre-clinical models. The mice are viable and appear healthy, with only a slight ISG phenotype in the spleen (Behrendt et al., 2013; Rehwinkel et al., 2013). These models were useful, however, in helping to elucidate the normal functioning of the Samhd1 protein, linking gene loss to an accumulation of dNTPs, and a reduction in viral restriction capabilities.

Each of the rodent pre-clinical models for AGS1-7 have been useful at increasing understanding of the functioning of the genes affected, where a link between type I IFN and gene mutation has been consistently established. However, the lack of neurological phenotypes questions the effectiveness of the models, and the species they were created in. Aside from rodent models of AGS, mutations in *adar1*, *ifih1* and *samhd1* have been modelled in embryonic zebrafish (*Danio rerio*), and will be discussed in the following zebrafish disease modelling section (section 1.8).

1.8 Zebrafish disease modelling

1.8.1 Zebrafish as a model organism

Zebrafish possess many benefits as an *in vivo* model, and we have previously suggested that some of the limitations associated with rodent pre-clinical models of disease may be compensated for by zebrafish models, which can be thought of as an intermediate between *in vitro* and higher order *in vivo* systems (Withers et al., 2020). Firstly, the high fecundity of adult breeding pairs results in hundreds of genetically similar offspring following each breeding session, generating large sample sizes for experimentation. The zebrafish offspring are produced through *ex-vivo* fertilisation, which, coupled with rapid development, and transparency of the embryonic and larval stages, allows for

non-invasive *in vivo* imaging, making them an attractive organism to study vertebrate developmental biology. (Eisen, 1996; Kimmel et al., 1995).

In recent years, the zebrafish has become more than the prototypical developmental biology model, with greater potential being recognised. The ease of genetic manipulation introduced the concept of zebrafish as a model of human disease, facilitated by the identification of the zebrafish genome sharing ~70 % homology with humans, and 82% of disease causing human proteins also possessing a zebrafish orthologue (Howe et al., 2013; Lieschke and Currie, 2007). Following this, the generation of tissue specific transgenic reporter animals have been widely utilised which allow for live-imaging of cells and tracking of intracellular processes to study molecular mechanisms (Choe et al., 2021) Moreover, the small size and relative abundance of larvae makes them an ideal target for high-throughput drug-screening, whereby compounds can be absorbed by the animal following addition to larval water, and any subsequent phenotypic changes can be assessed within the larvae to determine drug effectiveness (MacRae and Peterson, 2015).

1.8.2 Generating zebrafish models of disease

Genetic modification within the zebrafish genome can be transient or permanent. Transient techniques include morpholinos (MOs), which are oligonucleotides that can be injected into a fertilised zygote at the one cell stage. MOs bind to messenger RNA (mRNA) at the transcription start site (ATG), preventing ribosome assembly and inhibiting translation of mRNA into a polypeptide. Additionally, some MOs can bind to pre-mRNA at splice sites, to modify splicing, causing intron inclusions, or exon excisions, which will affect the resulting polypeptide, if formed at all (Moulton, 2017). MOs are a quick and easy way to examine the effect of a gene knock-down, but their transient nature arises from the inability to permanently integrate into the genome, thus the effects can only be studied during the first few days following injection before the MO is diluted out. Moreover, MOs are being utilised less, due to the identification of off-target effects associated with MO injections (Bedell et al., 2011). This questions the validity of MO models, although guidelines have been published with the gold standard being to phenocopy a MO model with a stable permanent mutant zebrafish model, which aims to identify true effects directly attributed to the gene of interest (Eisen and Smith, 2008; Stainier et al., 2017). As an alternative, clustered regularly interspaced repeat (CRISPR) interference (CRISPRi) has been utilised to reversibly silence gene expression at a transcriptional level (Rossi et al., 2015).

Stable zebrafish disease models can be generated through random mutagenesis using chemical mutagens such as N-ethyl-N-nitrosourea, to create huge libraries of stable mutants. However this method is limited by the unlikely chance of modelling specific disease-associated mutations (Kettleborough et al., 2013). Targeted gene-editing is a more common approach for disease modelling, which is performed using the technology behind engineered nucleases, such as zinc finger nucleases, transcription activation-like effector nucleases, and the most commonly implemented method: CRISPR - CRISPR-associated protein 9 (Cas9) (Doyon et al., 2008; Hwang et al., 2013; Sander et al., 2011). With CRISPR-Cas9 technology, a specific targeted guide RNA

(gRNA) directs the Cas9 endonuclease to the desired target site, which is upstream of a protospacer-adjacent motif (PAM). Cas9 cleaves the DNA to form a double strand break, and the subsequent DNA repair mechanisms cause the desired mutations. Non-homologous end joining creates knockout alleles to enable loss of function investigation, whilst homology-directed repair creates a knock-in allele (Adamson et al., 2018).

All of these methods have been widely implemented to generate zebrafish models of human disease. This is also facilitated by zebrafish forming the major organs by 24 hours post fertilisation (hpf), which allows diseases affecting specific organs to be modelled from an early time point (Santoriello and Zon, 2012). As a result, zebrafish have been used to successfully model haematopoietic disorders, cancer, cardiovascular disease, muscle disorders, kidney disease, CNS disorders and inflammation, whereby genetic or chemical inducers of a disease phenotype can be identified and studied to improve understanding of disease mechanisms (Santoriello and Zon, 2012).

1.8.3 The zebrafish Immune System

The functionality of the zebrafish immune system is well conserved to human, which reinforces their usefulness at modelling different aspects of inflammation (Xie et al., 2020). The innate arm of the immune system develops first, with macrophages identified from 15 hours post fertilisation (hpf) and neutrophils from 18 hpf (Bennett et al., 2001; Herbomel et al., 1999). Both cell types resemble their human counterparts, with neutrophils possessing segmented nuclei, granules and the expression of myeloperoxidase (Lieschke et al., 2001). Moreover, developing zebrafish also possess specific glial cells, which help contribute to the innate immune response within the CNS. After the first macrophages have migrated into the CNS, the cells begin to differentiate into microglia, from ~ 60 hpf, distinguishable from macrophages by the expression of distinct genes such as *p2y12*, and an altered morphology, characterised by highly active processes (Herbomel et al., 2001; Sieger et al., 2012). Radial glial cells (RGCs) are precursors to astrocytes, and until recently, were proposed to act as a functional substitute for astrocytes in zebrafish. However, a recent study identified the transformation of RGCs into astrocyte-like cells at 48 hpf (Chen et al., 2020). These cells were revealed to possess additional similarities to mammalian astrocytes, such as close association with synapses, expression of glutamine synthetase and astrocyte tiling behaviour (Chen et al., 2020). The presence of these innate immune cells facilitates the study of the inflammatory response in developing zebrafish larvae, and has been utilised in different models, such as tail wounding-induced inflammation, chemical-induced inflammation and mutation-induced inflammation (Xie et al., 2020)

Another aspect of the innate immune response that is functionally conserved, is the antiviral response, initiated by IFN. In zebrafish, four type I IFN genes have been characterised: *ifnphi1-4*, although only *ifnphi1* and *ifnphi3* are active during larval stages, with *ifnphi2* only expressed in adults, and *ifnphi4* possessing little activity (Aggad et al., 2009). *Ifnphi1* and *ifnphi4* are classified as group I IFN, and *ifnphi2* and *ifnphi3* known as group II IFNs. Group I IFNs bind to the cytokine receptor family B (CRFB) 1 and CRFB5 complex, whilst group II IFNs bind to a CRFB2 and CRFB5 complex (Aggad et al., 2009; Levraud et al., 2007). The classification of fish IFN genes relative to mammalian

IFNs has been relatively controversial (Langevin et al., 2013). Originally, it was proposed that due to zebrafish IFN genes consisting of five exons and four introns, there was greater overlap with human type III IFN, which also possess the same number of exons and introns. However, following the identification of the crystal structures of zebrafish IFNs, there was found to be a characteristic type I IFN architecture, leading to these cytokines being described in a similar manner to mammalian type I IFNs (Hamming et al., 2011; Langevin et al., 2013). As a result, zebrafish larvae respond to a number of viral insults by inducing a significant group I IFN (*ifnphi1* and *ifnphi3*) response, from as early as 24 hpf, leading to the upregulation of a number of ISGs, and other anti-viral genes, such as PRRs, and other pro-inflammatory cytokines (Levraud et al., 2007; Levraud et al., 2019; Palha et al., 2013; Widziolek et al., 2021). A number of the ISGs generated following viral infection possess orthologues in humans, highlighting a core ancestral ISG repertoire, whilst others were found to be fish specific (Briolat et al., 2014; Levraud et al., 2019). Thus, the aspects of the antiviral response which are conserved reinforce the usefulness of zebrafish as a model to study type I IFN signalling and innate immunity.

The cell types involved in expressing *ifnphi1* in zebrafish larvae have been identified as predominantly hepatocytes and neutrophils following infection with chikungunya virus, as observed in a Tg*(ifnphi1:*mCherry) reporter line (Palha et al., 2013). Interestingly, the relationship between the antiviral response and the adaptive immune system cannot be determined in zebrafish larvae, due to the lack of a mature adaptive immune system until 4-6 weeks post fertilisation (Lam et al., 2004). This allows for examination of the innate immune system in isolation from the adaptive immune system.

1.8.4 Zebrafish models of type I interferonopathies

Modelling certain diseases in zebrafish can also be beneficial when other species are not the most effective at recapitulating the human pathology, such as the mouse models of AGS.

The most well characterised zebrafish model of AGS has been the transient *samhd1* MO model. The *samhd1* morphant possessed a significant ISG response, coupled with increased global *ifnphi1* expression. The morphants also presented with spontaneous ICH, thus recapitulating an aspect of the cerebrovascular disease commonly identified in AGS5 patients (Kasher et al., 2015). The ICH phenotype was the first neurological phenotype seen across any of the pre-clinical models of AGS, suggesting zebrafish may be an appropriate species to perform AGS disease modelling. However, as discussed, transient knock-downs using MO's may present with off-target effects, and so a permanent stable mutant line was required to fully model AGS5, which was a primary aim of this project. The *samhd1* MO study also produced an *adar1* MO, although it was less thoroughly characterised than the *samhd1* morphants (Kasher et al., 2015). The resulting *adar1* morphants exhibited a large upregulation of ISGs, alongside severe developmental deficiencies, akin to what was observed in the mice models.

In addition, a stable zebrafish *ifih1* mutant has been generated. However, this model harboured a loss of function mutation, as opposed to a gain of function mutation which is found in AGS patients.

As such, this model was not produced to model AGS7 and the aberrant activation of the intracellular RNA sensing pathway, rather, the model was utilised to rescue the overexpression of immune-regulated genes in a mutant line with an upregulated IFN response (Rajshekar et al., 2018).

AGS is not the only type I interferonopathy where zebrafish models appear to more accurately recapitulate the human condition than rodent models. Mutations in *RNASET2* cause RnaseT2-deficit leukodystrophy. Interestingly, *RNaseT2*$^{-/-}$ rats do possess a neuroinflammatory phenotype, but lack any white matter abnormalities, which is a key hallmark of the condition. Moreover, the model fails to exhibit any signs of systemic inflammation (Sinkevicius et al., 2018). Conversely, an *rnaset2* mutant zebrafish model successfully identified white matter abnormalities in adults, thought to be attributed to microglial dysfunction which is apparent from embryonic development. (Hamilton et al., 2020; Haud et al., 2011). The mutants also presented with consistent locomotion deficits throughout life, and an increase in ISG expression.

Rutherford and colleagues made a number of compelling arguments for the use of zebrafish models versus rodent models of type I interferonopathies which may help to explain the increased success associated with zebrafish models. Crucially, type I interferonopathies often develop *in utero*, with a large number of patients present with symptoms during the first year of life. This early disease progression can easily be modelled in the zebrafish during the embryonic and larval stages. Conversely, rodent models are characterised postnatally, usually at early adulthood, allowing the possibility that some phenotypes may be missed at these later time points (Rutherford et al., 2020).

Additionally, the environment in which zebrafish and rodents reside is vastly different. Rodents live in a relatively sterile environment compared to zebrafish and are exposed to less pathogens which may potentially modify a phenotype as pathogen exposure through infection has been proposed to be key in dictating disease severity in AGS and may account for phenotypic variation between patients and occasionally siblings (Crow and Stetson, 2021; Livingston et al., 2014a). In particular, a picornavirus has been recently identified in a number of research zebrafish aquaria (Balla et al., 2020).The larvae investigated throughout the study exhibited no overt phenotype, instead an ISG specific reporter line Tg(*isg15*:GFP) was utilised to demonstrate the activation of the innate immune system. This, understandably, may act as a confounding factor when directly examining the type I IFN response in a zebrafish model of a type I interferonopathy, and more importantly, may generate pseudo-phenotypes in WT fish which are responding to the viral infection, leading to difficulties assessing inflammatory phenotypes in mutant fish lines (Rutherford et al., 2020). However, although potentially increasing the complexities of phenotyping, the presence of pathogens in the environment can also be a benefit in the context of disease modelling, as it more accurately mimics the pathogen rich environment that humans are continually exposed to throughout life (Rutherford et al., 2020).

Lastly, a more general observation on zebrafish as a model organism is that zebrafish are relatively outbred, compared to laboratory rodents (Rutherford et al., 2020). This results in the accumulation of polymorphisms that vary between animals of the same genetic background, which can be suggested to more closely mimic the heterogeneity of the human population, especially with regards

to AGS and other type I interferonopathies, where different disease manifestations can occur following the same gene mutation (Crow et al., 2015).

1.9 Cerebrovascular disease

1.9.1 Overview

Cerebrovascular disease is a general term used to describe any condition which disrupts cerebral blood flow through the vasculature. The brain only makes up 2% of total body mass, but is the most energy-intensive organ, utilising ~50% of total glucose within the human body (Chandra et al., 2017a). As such, any perturbations in the transport of glucose and other essential nutrients and oxygen via the blood will have detrimental effects on the brain tissue. This can result in the most common form of cerebrovascular disease: stroke, which manifests as either ischaemic (occlusion of blood vessels) or haemorrhagic (blood vessel rupture).

Alterations to the cerebrovasculature can be intrinsic and attributed directly to alterations within the blood vessels. Examples include stenosis, which cause narrowing of the vessels, and a reduction in blood flow. Alternatively, inflammation of the vasculature can act to damage the arterial wall, disrupting blood flow, or creating arterial tears. Extrinsic factors leading to stroke include the presence of cerebral venous thrombosis and cerebral emboli, which cause blockages within the vasculature (Chandra et al., 2017b).

Stroke is the second highest cause of death worldwide, eclipsed only by ischaemic heart disease (Collaborators, 2019). Moreover, high morbidity observed in stroke survivors is attributed to 50% chronic disability associated with patients. Ischaemic stroke is the most common form of stroke, accounting for 80% of total stroke, with haemorrhagic stroke making up the remaining 20% (Donkor, 2018). Despite the lower prevalence of haemorrhagic stroke, it is the most severe form of the disease, resulting in 40% mortality rate at one-month post-ictus (An et al., 2017).

Both sub-types of stroke can be further divided depending on the mechanism by which the stroke occurs, and the location. The Trial of Org 10172 in Acute Stroke Treatment (TOAST) classification, characterised ischaemic stroke into five sub-types: large artery thrombotic strokes, attributed to atherosclerotic plaques; lacunar strokes caused by small penetrating artery thrombosis; cardiogenic embolic strokes; cryptogenic strokes; and other causes, such as substance abuse (Adams et al., 1993). Contrastingly, haemorrhagic stroke is generally characterised based on the location of the vessel rupture and bleed: resulting in either ICH or subarachnoid haemorrhage (SAH).

The pathogenesis of stroke will not be discussed here, however a more detailed review on the pathogenesis process and the need for a translational pipeline of pre-clinical ICH research can be found in Appendix 1 (Withers et al., 2020).

1.9.2 Risk factors for stroke

Despite the distinct aetiologies attributed to ischaemic and haemorrhagic stroke, risk factors for both stroke types exhibit large levels of clinical overlap, resulting in inconsistent knowledge regarding the relative role of specific ischaemic and haemorrhagic risk factors (Andersen et al., 2009). Non-modifiable risk factors for both stroke types include age, sex, race/ethnicity and genetic factors (Boehme et al., 2017). We have already introduced genetics as a risk factor for cerebrovascular disease with AGS5, whereby a monogenic mutation in *SAMDH1* can lead to both ischaemic and haemorrhagic stroke. These are attributed to cerebral large artery disease, manifesting as stenosis, moyamoya (stenosis with compensation in the form of collateral circulation, where smaller existing vessels begin to enlarge), and aneurysms (du Moulin et al., 2011; Ramesh et al., 2010; Thiele et al., 2010). However, the aetiology behind the cerebrovascular manifestations in AGS5 patients is still poorly understood. Conversely, other, more common genetic diseases have been attributed to ischaemic and haemorrhagic stroke, such as familial amyloid angiopathy, and inherited forms of small vessel disease (Boehme et al., 2017).

Genetic risk factors can be characterised as non-modifiable and modifiable, due to the interaction between genes and the environment. Additional modifiable risk factors that are predominantly identified in ischaemic stroke patients include diabetes, atrial fibrillation and other cardiac causes, such as previous myocardial infarction (Andersen et al., 2009). Conversely, smoking and high alcohol intake have been found to correlate more closely to haemorrhagic stroke in one study, whilst other studies have shown no clear relationship with only haemorrhagic stroke, instead identifying ischaemic stroke to also be affected by these factors (Andersen et al., 2009). However, hypertension is one modifiable risk factor which widely accepted for both stroke types (O'Donnell et al., 2010).

Two additional modifiable risk factors for both ischaemic and haemorrhagic stroke are dylipidaemia and infection, which will be discussed in greater detail in sections 1.9.3 and 1.9.4.

1.9.3 Cholesterol dysregulation in ICH

Cholesterol dysregulation has been an established risk factor for ischaemic stroke for many years, with hypercholesterolaemia facilitating the development of atherosclerotic plaques, which then act to occlude the cerebrovasculature (Hackam and Hegele, 2019; Prospective Studies et al., 2007; Tirschwell et al., 2004; Wouters et al., 2005). Contrastingly, the inverse association has been identified in ICH, whereby low cholesterol appears to be a risk factor. The most powerful example of this was from a retrospective case-control study, which identified a significant decline in total cholesterol and low-density lipoproteins (LDL) in the six months prior to the generation of an ICH, when compared to non-cerebrovascular disease controls (Phuah et al., 2016). This reduction in circulating cholesterol, lipoproteins and triglycerides has been highlighted in a number of different studies (Chen et al., 2017; Sun et al., 2019; Valappil et al., 2012; Wang et al., 2013). To complement these findings, reduced lipid levels have been shown to worsen stroke outcomes. The Taiwanese stroke registry study concluded that cholesterol levels below 160 mg/dL significantly increased the

severity of the stroke, according to both the Glasgow Coma Score (GCS) and the National Institute of Health Stroke Scale, followed by an increased 3- month mortality (Chen et al., 2017). This was also observed in a Helsinki ICH study, where lowered lipid levels worsened the GCS (Mustanoja et al., 2013). Alternatively, higher levels of LDLs have been indicative of smaller haematoma volumes and lower mortality rates (Chang et al., 2018).

One hypothesis for hypocholesterolaemia as a risk factor for ICH relates to the integral roles cholesterol plays within the cerebrovasculature. A reduction in circulating cholesterol could equate to less cholesterol within the plasma membranes of the endothelium, weakening the vessel and increasing susceptibility to rupturing (Valappil et al., 2012). Additionally, it has been proposed that low cholesterol may play a role in promoting arterial smooth muscle necrosis, which also acts to impair the integrity of the endothelium (Wang et al., 2013). However, it is unlikely that low cholesterol as a sole factor causes spontaneous rupture of the vessels, suggesting an additional risk factor is present. Hypertension has been identified in >80% of patients with reduced cholesterol who went on to develop an ICH (Chen et al., 2017; Phuah et al., 2016). Hypertension coupled with increased vascular fragility due to reduced cholesterol, could provide a potential mechanism, as the vasculature is not equipped to handle the increased blood pressure, resulting in damage and rupture.

The underlying cause of hypocholesterolaemia in ICH patients is unclear, but may include malnutrition, anaemia and hyperthyroidism (Duntas and Brenta, 2018; Shalev et al., 2007; Wang et al., 2013). Another possible cause for hypocholesterolaemia is a systemic inflammatory response, prior to the haemorrhage, such as an infection (Filippas-Ntekouan et al., 2017; Phuah et al., 2016), which will be discussed in more detail below.

1.9.4 Cerebrovascular disease and viral infection

Viral infections constitute another risk factor for cerebrovascular disease, attributed to increased prevalence of both ischaemic and haemorrhagic stroke. It is of note that viruses are not the only organism implicated in stroke: a number of bacterial, parasitic and fungal infections have also been associated with stroke onset (Miller and Elkind, 2016). Identifying mechanisms responsible for causing stroke after viral infections is challenging, however the proposed mechanisms include infection-related platelet activation and aggregation, inflammation-induced thrombosis, impaired endothelial function and damage, infection-provoked cardiac arrhythmias and dehydration-induced thrombosis (Elkind et al., 2020). Discussed below are several viruses known to be associated with both ischaemic and haemorrhagic stroke. However, the distinct mechanisms causing either ischaemic or haemorrhagic stroke are not clearly defined, which further highlights the need for future experimentation on viral infection, or the antiviral response in order to elucidate the specific effects on the cerebrovasculature.

Herpesviruses are one family largely associated with cerebrovascular disease, with different mechanisms proposed for each virus described. Following a systematic review and meta-analysis on Cytomegalovirus (CMV) and atherogenesis, a strong correlation was noted (Ji et al., 2012). Further experimentation of *in vivo* models of CMV, suggested that CMV can directly activate a sub-

set of platelets which exacerbates the formation of platelet-leukocyte aggregates, alongside promoting neutrophil extravasation and accelerating atherosclerosis (Assinger et al., 2014).

Contrastingly, varicella zoster virus (VZV) has been shown to directly infect the cerebral vasculature. After infection with VZV, which primarily causes chickenpox, the virus remains latent in the neuronal ganglia. Upon reactivation, the virus can travel transaxonally to cerebral arteries, causing an active infection, and leading to pathological vascular remodelling (Nagel and Gilden, 2014). The remodelling causes the development of a thickened tunica intima thought to contribute to vascular occlusion and ischaemia. Conversely, a disruption of the tunica media has been hypothesised to contribute to aneurysm formation and haemorrhage via a reduction in medial smooth muscle cells, leading to loss of vascular integrity (Nagel and Bubak, 2018; Nagel and Gilden, 2015). Whilst less studied, Herpes Simplex Virus (HSV)-2 is proposed to cause vasculopathy and stroke through a similar mechanism to VZV. Moreover, HSV-1 can cause vasculopathy with encephalitis, and ischaemic and haemorrhage stroke following infection are suggested to occur following perivascular inflammation, necrosis and capillary and small vessel congestion (Fan et al., 2020).

Interestingly, all herpesviruses discussed can act as opportunistic infections in immunocompromised individuals, which may account for the increase in cerebrovascular disease found in these populations. One such population, are HIV patients. HIV has a complex relationship with stroke, as infection with the virus increases the likelihood of developing many traditional risk factors for stroke, such as hypertension, dyslipidemia and diabetes. Moreover, the advent of anti-retroviral treatment has been found to increase the incidence of stroke in HIV positive individuals partially attributed to the increase in life expectancy from the treatment (Ismael et al., 2020; Singer et al., 2013).

Despite this, there is also evidence to suggest that the virus directly associates with cerebrovascular disease, independent of con-current infection and traditional risk factors (Behrouz et al., 2016; D'Ascenzo et al., 2015). Whilst incompletely understood, HIV-1 may directly invade the cerebral arteries, akin to VZV to cause vasculopathy. Post-mortem human brain samples from HIV patients highlighted increased arterial inflammation within the adventitial intima (Gutierrez et al., 2016; Nagel et al., 2010). Severe vascular re-modelling has been identified in HIV infected individuals, and can manifest via two extremes: The first being the generation of atherosclerotic arteries, causing thickening of the arterial walls and resulting in stenosis. This process is likely through the actions of HIV activating immune cells and endothelial cells, along with modifying lipid levels. Secondly, extreme thinning of the media and elongation of the artery (dolichoesasia) have been found in post-mortem patients (Gutierrez et al., 2015). Moreover, aneurysm formation has also been identified in patients (Kossorotoff et al., 2006).

Lastly, hepatitis C virus (HCV) is also associated with cerebrovascular disease (Adinolfi et al., 2013; Tseng et al., 2015). In a similar mechanism to HIV infection, inflammation induced atherosclerosis is hypothesised to be a contributing factor for the generation of ischaemic stroke. Moreover, HCV can replicate within endothelial cells and the atherosclerotic plaque, which may result in the destabilisation of the plaque, causing occlusive or embolic stenoses (Adinolfi et al., 2013).

Contrastingly, a separate hypothesis for ICH has been proposed following HCV infection. This is based on the actions of HCV on the liver, whereby the resulting liver disease may impair coagulation functions, increasing the risk of ICH (Tseng et al., 2015).

Overall, these examples highlight a clear association between viral infections directly damaging the cerebrovascular unit, which is exacerbated by the immune response, in an attempt to limit the viral spread, and this relationship may lead to the development of stroke.

1.10 Viral infection and cholesterol dysregulation

1.10.1 Viruses altering intracellular lipid homeostasis

As discussed in section 1.3, type I IFN is one of the key contributors to an effective antiviral response. The activation of the IFN pathway leads to the expression of ISGs which have evolved to target the pathways required by viruses to successfully infect and replicate within the body. Viruses are metabolically inert, and as such, they rely on the host cell to generate the components required for replication (Sumbria et al., 2020). This is achieved through manipulation of the cellular metabolism in order to produce a bioenergetically favourable environment to replicate. This can be via inducing a high glucose metabolism, and also changing the nature of lipid metabolism (Sumbria et al., 2020).

Before viruses can act to alter intracellular metabolism, they first have to invade the host cell, which generally occurs via two distinct mechanisms: direct fusion with the plasma membrane, or through receptor mediated endocytosis. These processes require specific compositions of the plasma membrane. For example, enveloped viruses, such as HIV, directly fuse with the membrane at the boundary of cholesterol rich domains, in an area with tension between ordered and disordered surfaces (Yang et al., 2015). Other enveloped viruses engage lipid-binding proteins, such as phosphatidylserine, which is bound by phagocytic cell receptors (TIM and TAM) to enable endocytosis (Ketter and Randall, 2019). Alternatively, non-enveloped viruses' target receptors localised to cholesterol/ sphingomyelin-enriched microdomains, as has been observed in rubella virus (Otsuki et al., 2018).

Together, this highlights the importance of lipid membrane composition in viral entry. As a result, a key aspect of the type I IFN response is to generate ISGs which target viral entry. This is achieved by interfering with lipids within the plasma membrane, and altering cholesterol homeostasis within endosomes to prevent viral release into the cytosol (Majdoul and Compton, 2021).

1.10.2 Type I IFN and cholesterol dysregulation

The most well established link between type I IFN and cholesterol dysregulation as an antiviral response comes from the ISG cholesterol 25-hydroxylase (CH25H). This is an endoplasmic reticulum (ER) bound enzyme that catalyses the oxidation of cholesterol to the oxysterol 25-hydroxycholesterol (25HC).

25HC acts to inhibit viral entry and replication (Fig 1.3). Firstly, viral entry is targeted through the actions of acyl-coA cholesterol acyltransferase (ACAT). ACAT is an ER-localised enzyme, activated by 25HC that converts free accessible cholesterol in the ER membrane to cholesterol esters which are stored as lipid droplets within the cytosol (Abrams et al., 2020). This reduction in free cholesterol is thought to trigger rapid cholesterol remodelling on the plasma membrane and is utilised to restrict viral fusion. This mechanism has been implicated *in vitro* to reduce entry of the virus SARS-CoV-2, and bacterial pathogens, including *L.monocytogenes* and *S.flexneri (*Abrams et al., 2020; S. Wang et al., 2020). Moreover, 25HC directly interacts with the plasma membrane, independent from actions with ACAT. The oxysterol can change lipid head group spacing, alongside altering the position, orientation and accessibility of cholesterol, all of which act to modulate the fluidity of the membrane, to evade viral entry (Gale et al., 2009; Olsen et al., 2011).

If viruses are able to evade the initial membrane defences initiated by 25HC and enter the cell, 25HC can also exert its effects on more general lipid metabolism. This is established through actions on the two cholesterol homeostasis pathways, modulated by the transcriptional regulators sterol regulator-binding protein (SREBP) and Liver X Receptor (LXR). When cholesterol and 25HC levels are low, SREBP binds to the SREBP cleavage activator protein (SCAP), forming a SREBP-SCAP complex on the ER. SCAP contains a sterol sensing domain, and when ER cholesterol levels are depleted, it chaperones SREBP to the golgi apparatus, whereby SREBP is cleaved by site 1 and site 2 proteases (S1/2P) to become a mature transcription factor. (Cyster et al., 2014).

Conversely, in the presence of 25HC, the oxysterol binds to the membrane-spanning ER protein: insulin-induced gene 2 (INSIG2), which form SREBP/INSIG/SCAP complexes that are retained in the ER, unable to be processed by the Golgi, thus halting cholesterol biosynthesis. High cholesterol has a similar effect to 25HC binding to INSIG, whereby cholesterol binds to SCAP, and forms the same SREBP/INSIG/SCAP complex (Cyster et al., 2014). Moreover, 25HC has been shown to directly induce proteasomal degradation of HMGCR in macrophages, to further limit cholesterol biosynthesis and cholesterol availability to viruses and other pathogens (Lu et al., 2015).

The relationship between the transcriptional regulator LXR and 25HC is the inverse of that described for SREBP, as the LXR pathway is involved in the absorption, degradation, transportation and excretion of cholesterol, and so is largely upregulated following 25HC generation. A number of genes are expressed following LXR activation, including *CH25H*, which demonstrates a positive feedback loop, to ensure sufficient quantities of 25HC are produced. *(*Liu et al., 2018a*).* Moreover, 25HC causes the upregulation of cholesterol efflux transporters, such as ATP-binding cassette transporter A1 and G1 (ABCA1/G1) (Zhao et al., 2020).

CH25H is not the only ISG which manipulates lipids to prevent viral entry. The interferon-induced transmembrane proteins (IFITM) family, consists of five members, with the most well characterised in the context of viral restriction, being IFITM3 (Majdoul and Compton, 2021). IFITMs have been shown to increase plasma membrane rigidity, helping to prevent pore formation, which would allow viral entry. This mechanism is thought to be similar to the effects 25HC displays within the plasma

membrane (K. Li et al., 2013). Moreover, IFITM3 alters cholesterol distribution via another distinct mechanism. Vesicle-associated membrane protein (VAMP)-associated protein A (VAPA) interacts with oxysterol-binding protein (OSBP) to transfer cholesterol from the ER to other organelles. IFITM3 also interact with VAPA, antagonising the VAPA-OSBP function, and preventing the trafficking of cholesterol to various intracellular compartments. Instead, there is a build-up of cholesterol in late endosomal compartments/ multivesicular body. As a number of viruses enter cells via endocytosis, the accumulation of cholesterol within the endosome through the actions of IFITM acts to block viral release into the cytosol (Amini-Bavil-Olyaee et al., 2013). Thus highlighting another antiviral mechanism involving intracellular cholesterol redistribution.

Type I IFN can also cause the upregulation of micro-RNAs (mi-RNAs). One particular miRNA (miR-342-5p) was shown to be upregulated in *Ch25h*$^{-/-}$ mice and exerted similar effects to 25HC, including inhibition of sterol biosynthesis via transcriptional regulation of SREBP. In murine bone marrow derived macrophages (BMDMs) this also reduced total cholesterol levels (Robertson et al., 2016). The group hypothesised that within cells, CH25H and 25HC are responsible for a rapid reduction in cholesterol synthesis, prior to degradation by activating transcription factor 3 (ATF3), which acts as a negative regulator of type I IFN responses. Subsequently, miR-342-5p is induced to promote a more sustained fine-tuning of sterol metabolism (Robertson and Ghazal, 2016).

Interestingly, this type I IFN and cholesterol relationship has been shown to be bidirectional, whereby a reduction in the mevalonate pathway, induced by silencing *HMGCR* in macrophages, has resulted in an increase in *IFNB1* and ISG expression. Moreover, replenishing *SREBP2*$^{-/-}$ cells with cholesterol acted to attenuate the type I IFN response (York et al., 2015).

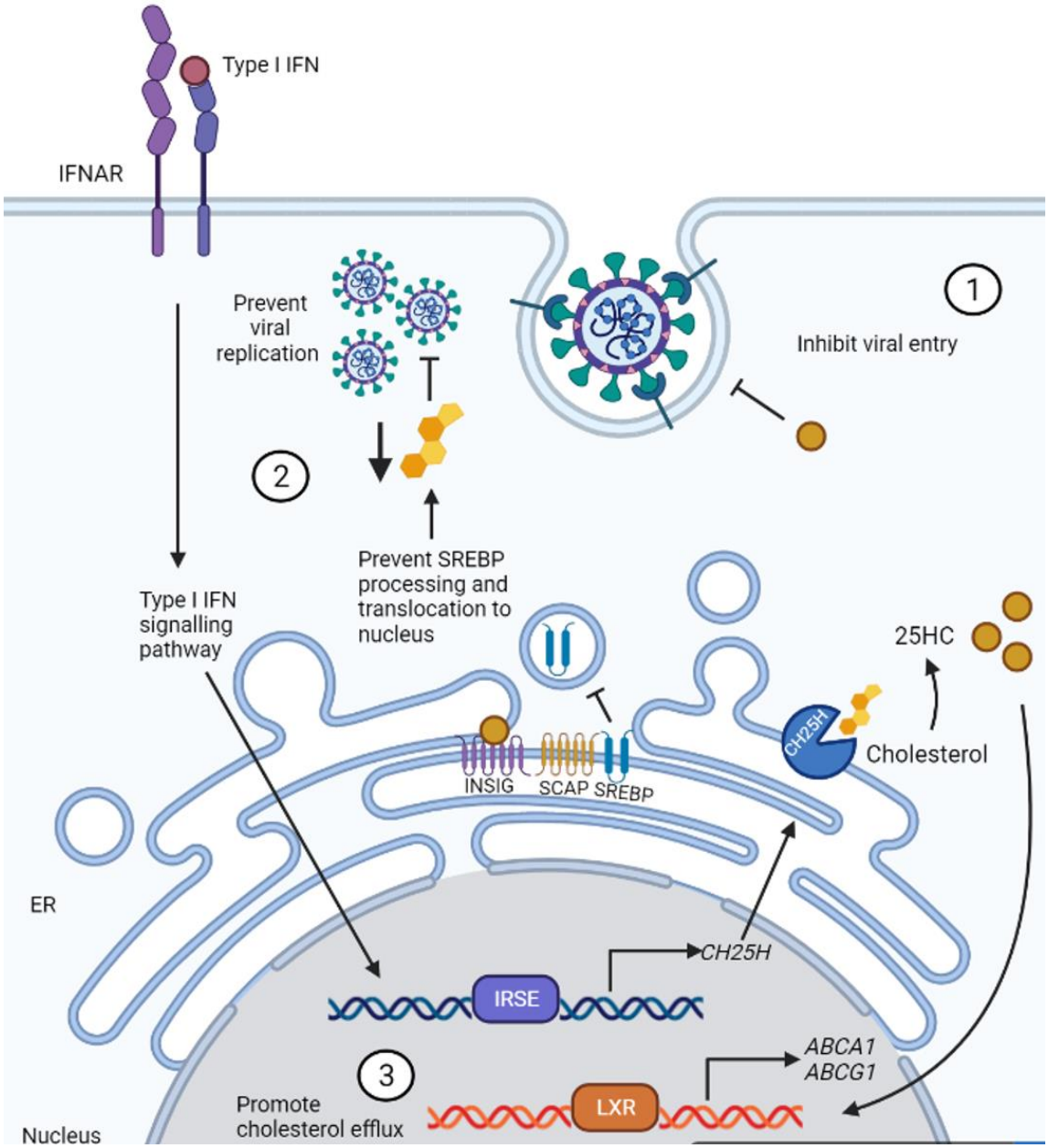

Figure 1.3- Antiviral mechanisms of CH25H/25HC

Following binding of type I IFN to IFNAR the canonical type I IFN signalling pathway ensues, leading to the expression of *CH25H*. CH25H is an ER bound enzyme that converts cholesterol into 25HC, which exerts anti-viral effects via 3 primary mechanisms. 1) 25HC alters plasma membrane cholesterol distribution via the actions of ACAT, preventing viral entry. 2) 25HC binds to INSIG, which forms an INSIG/SCAP/SREBP complex in the ER, whereby SREBP is retained, unable to undergo processing in the golgi and be translocated to the nucleus. SREBP is the master sterol transcription factor, and so this reduces *de novo* cholesterol levels, required by viruses for replication. 3) 25HC activates the LXR transcription receptor family, promoting the expression of cholesterol efflux transporters, as an additional mechanism to reduce available cholesterol in the cell for viral replication. Abbreviations: IFNAR, interferon α/β receptor; ER, endoplasmic reticulum; IRSE, interferon-stimulated response elements; LXR, liver X receptor; CH25H, cholesterol 25 hydroxylase; ABCA1/G1, ATP binding cassette subfamily A member 1/ G1; 25HC, 25- hydroxycholesterol.

1.10.3 CH25H/25HC in inflammation

Aside from these well characterised effects of CH25H and 25HC in facilitating an anti-viral response, the oxysterol also possesses distinct pro- and anti-inflammatory responses. 25HC is capable of inducing the production of pro-inflammatory cytokines such as IL-1β, IL-6, IL-8 and macrophage colony-stimulating factor, as observed in monocytes/macrophages within atherosclerotic plaques (Liu et al., 1997; Zhao et al., 2020). Moreover, 25HC is proposed to play a role in the generation of foam cells within the atherosclerotic process, which may be due to the effects on cholesterol esterification and the formation of lipid droplets (Gold et al., 2012). Furthermore, IL-1β release has been proposed to occur following the assembly of the NOD-like receptor protein 3 (NLRP3) inflammasome, initiated by 25HC (Jang et al., 2016). Contrastingly, other studies have described more anti-inflammatory functions of 25HC. By suppressing SREBP activity, 25HC has been shown to inhibit both NLRP3 and absent in melanoma 2 (AIM2) inflammasome activation, and the subsequent production of IL-1β and other pro-inflammatory cytokines (Dang et al., 2017; Reboldi et al., 2014).

Whilst there are no definite answers regarding the conflicting reports on the pro- and anti-inflammatory effects of 25HC, it has been suggested that different concentrations may elicit different responses. With nanomolar concentrations exerting protective anti-inflammatory effects and micromolar concentrations producing the more detrimental pro-inflammatory phenotypes observed (Zhao et al., 2020). Moreover, different treatment times could also be attributed to these discrepancies, and this may be observed in acute versus chronic viral infections, although further experimentation is required to confirm this.

1.11 Summary and aims

AGS is a devastating rare genetic auto-inflammatory disease characterised by aberrant type I IFN signalling. Over the past 40 years, the advancement in genomic technologies has enabled the identity of nine causative genes to be established. The existing pre-clinical rodent models of AGS are lacking in their ability to fully recapitulate the human condition. However, zebrafish have recently emerged as an effective organism to study a vast number of diseases, and a transient knockdown of the *samhd1* gene in a zebrafish larval model did manage to more accurately mimic AGS, suggesting that zebrafish may represent a useful organism to model the disease.

Aim 1: To validate and further demonstrate that zebrafish represent an effective pre-clinical model organism for AGS research, by characterising a stable mutant *samd1* zebrafish model.

AGS5, caused by mutations in the *SAMHD1* gene, is of particular interest, because it is a unique sub-type of AGS whereby patients frequently exhibit cerebrovascular disease, representing a monogenic form of inflammatory based stroke. Rare monogenic diseases can provide unique insight into the mechanisms that underpin more common forms of related diseases. The mechanisms behind cerebrovascular disease are complex, with many factors working synergistically to result in ischaemic and haemorrhagic strokes. As such, as well as improving our understanding of disease mechanisms in SAMHD1-related AGS, studying this rare condition may also provide unique insight

into the influence of excessive type I IFN on the development of cerebrovascular disease, in general, particularly in the context of viral infection and stroke risk.

Aim 2: To utilise the *samhd1* zebrafish model to further study the generation of cerebrovascular complications that arise in AGS5

From aim 2, we identified an apparent relationship between mutations in *samhd1* and cholesterol biosynthesis within the zebrafish model. Mutations in the AGS causative genes are linked to antiviral signalling, and alterations to intracellular cholesterol are commonly implemented as an antiviral mechanism to prevent viral entry and replication. We are interested in this relationship between antiviral signalling and cholesterol dysregulation in the context of cerebrovascular disease, as viral infection and low and high cholesterol levels have been attributed as risk factors for both ischaemic and haemorrhagic stroke. Therefore, we hypothesise that excessive type I IFN signalling can lead to cerebrovascular deficits and stroke via modulation of cholesterol synthesis and metabolism. This led us to examining this relationship in an *in vitro* human brain endothelial cell line to observe the effects with the cerebrovasculature

Aim 3: To study the role of the type I IFN signalling and cholesterol relationship in human brain endothelial cells

Chapter 2: Materials and Methods

2.1 List of reagents

Table 2.1- Laboratory reagents

Name	Protocol	Recipe
E3 Embryo Media	Zebrafish husbandry and embryo collection	4% Instant Ocean, 500 µl methylene blue in 1 L dH_2O
4% MS222	Larvae termination	2 g Tricaine, 10.5 ml Tris (pH 8.0) in 500 ml dH_2O
4% Paraformaldehyde (PFA)	Fixing embryonic tissue	10 ml 16% PFA (Alfa Aesar) in 30 ml Phosphate-buffered saline (PBS)
50X TAE buffer	Gel electrophoresis	121 g Tris base, 50 ml 0.5 M EDTA (pH 8.0), 28.5 ml acetic acid in 500 ml dH_2O
0.003% Phenylthiourea (PTU)	Whole mount immunofluorescence and staining protocols	30 mg of PTU in 1 L of methylene blue- free E3 media
O-Dianisidine stain	Haemoglobin stain	6 mg o-dianisidine (Sigma), 4 ml of 100% ethanol, 100 µl 1M sodium acetate (pH 4.5), 210 µl 30% H_2O_2 into 5.69 ml dH_2O
1% PBSTx	Whole mount immunofluorescence and staining protocols	200 ml PBS and 2 ml Triton X-100
Blocking Buffer	Whole mount immunofluorescence	10% normal goat serum, 1% Bovine serum albumin (BSA), 1% Dimethyl sulfoxide (DMSO) in PBSTx
Terminal deoxynucleotidyl transferase (TdT) mixture	Terminal deoxynucleotidyl transferase dUTP nick end labelling (TUNEL) staining	TdT reaction buffer (94 µl), TdT (enzyme) (4 µl), EdUTP nucleotide mixture (2 µl) per tube.
TUNEL Supermix	TUNEL staining	2630 µl 1X Click-iT Plus TUNEL reaction buffer, 67 µl copper protectant, 3.7 µl Alexa Fluor picolyl azide

0.2% Calcein solution	Calcein staining	2 g of calcein powder in 1 L of ddh_2O. pH with NaOH to pH7.
Total cholesterol reaction mix	Cholesterol assay	22 µL cholesterol assay buffer, 1 µL cholesterol probe, 1 µL enzyme mix, 1 µL cholesterol esterase per sample
Free cholesterol reaction mix	Cholesterol assay	23 µL cholesterol assay buffer, 1 µL cholesterol probe, 1 µL enzyme mix per sample.

2.2 Zebrafish

2.2.1 Zebrafish Husbandry

Adult zebrafish husbandry was approved by The University of Manchester Animal Welfare and Ethical Review Board, and all experiments were performed in accordance with U.K Home Office regulations (PPL: P132EB6D7). The zebrafish in this study were raised and maintained at The University of Manchester Biological Services Unit, under standard conditions, with adults housed in mixed sex tanks with a recirculating water supply at 28 °C under a 14/10 hour light/dark cycle, as previously described (Westerfield, 2000).

2.2.2 Generation of *samhd1*$^{\Delta 23/\Delta 23}$ mutant line

The line was generated using CRISPR Cas-9 technology prior to the start of this PhD project. gRNA was designed by inputting the *samhd1* exon 4 sequence into CHOPCHOP (Montague et al., 2014) to produce a list of appropriate sequences, and to provide information of any off-target sequences- none of which were identified. Synthesis of the gRNA and cas9 RNA have been described previously (Badrock et al., 2020). The resulting RNAs were mixed with 0.05% phenol red, 120 mM KCl and 20 mM HEPES, ph7.0, and ~1 nl of the mix was injected into the yolk of wild type (WT) AB fertilised eggs at the one cell stage to produce F0 crispants. These were assessed for indels using Hyp188I restriction analysis and raised to adulthood before outcrossing onto a WT background (F1). Following this, Sanger sequencing was performed on PCR amplicons to check for the presence of the mutation in the F1 generation, using primers that flanked the guide RNA binding site (forward primer 5'-GTGTTTAATGACCCCATCCA-3'; reverse primer: 5'-CCTATGGAGTGCTCAAATCG-3') and through the use of the University of Manchester Genomic Technologies Core Facility.

To generate the amino acid sequence, the zebrafish WT *samhd1* transcript was obtained from Ensembl (Cunningham et al., 2022) and inputted into ExPASy for translation (Gasteiger et al., 2003). For the *samhd1*$^{\Delta 23/\Delta 23}$ sequence, the 23 bp deletion determined by sanger sequencing was removed from the WT transcript, before also being translated.

The *samhd1*$^{\Delta 23/\Delta 23}$ line was crossed onto the endothelial cell specific transgenic line: Tg(*fli1*:EGFP) generated previously (Lawson and Weinstein, 2002) for analysis of the gross cerebrovasculature.

2.2.3 Embryo collection

Adult breeding pairs were set up for each experiment, with *samhd1*$^{\Delta 23/\Delta 23}$ adult females crossed with *samhd1*$^{\Delta 23/\Delta 23}$ adult males to produce all homozygous mutant offspring. Additionally, *samhd1*^{WT} adult females were crossed with *samhd1*^{WT} males to produce all WT offspring. Following breeding complications with the *samhd1*^{WT} adult fish, which abruptly ceased to produce fertilised eggs, the *samhd1*^{WT} fish were replaced with WT AB fish, to produce the WT offspring. Fertilised eggs were collected following natural spawning of the adult pairs, and were incubated at 28 °C in fresh E3 medium. The embryos were staged according to standard guidelines (Kimmel et al., 1995). The fish are classified as embryos until 4 days post fertilisation (dpf) and larvae from thereafter (4-5 dpf). As such, this terminology will be used throughout, depending on the age of the fish. After termination of the experiment, all embryos/larvae were killed prior to protected status (5 dpf) using a lethal dose of MS222 anaesthesia, and freezing.

2.2.4 PTU treatment

A number of imaging experiments required an increase in the optical transparency of the embryos. To facilitate this, embryos were bathed in 0.003% PTU (table 2.1) ~32 hpf to inhibit pigmentation, thus reducing the requirement for bleaching steps when performing these protocols. The embryos were maintained in the PTU E3 media, which was refreshed every 24 h, until the embryos were taken for harvesting.

2.2.5 Embryo dechorionating

From 1 dpf, embryos were manually dechorionated prior to fixing in PFA for imaging protocols, or for drug treatments. Using two pairs of jewelers forceps (Merck, F6521), the chorion was cut open, releasing the embryo into the petri dish, whist the chorion was removed.

2.2.6 Locomotion assay

Swimming was measured from 3 – 5 dpf in WT and *samhd1*$^{\Delta 23/\Delta 23}$ larvae. Firstly, prior to selection for the assay, all larvae were briefly anaesthetised using 0.02% MS222 in E3 medium to remove any locomotor function bias. For the assay, 24 larvae were randomly selected from each group, and upon recovery from anaesthesia, were individually placed into a 24 well plate (1 larvae per well), containing 1 ml of fresh methylene-blue-free E3 medium. The DanioVision camera chamber and ethovision XT software (Noldus, version 11) was used to determine the cumulative time spent mobile by the larvae. Swimming movement of each larvae was tracked in the X and Y plane for 10 minutes (min), using a

white light stimulus to initiate a startle response every 60 seconds (s). Locomotion was measured in 3 independent replicates, with n=22-24 larvae per replicate.

2.2.7 Atorvastatin treatment

Pharmacological inhibition of the enzyme *hmgcr* using statins is a known brain haemorrhage inducer in zebrafish embryos due to proposed effects of the enzyme in stabilising cranial vessels (Crilly et al., 2018; Eisa-Beygi et al., 2013). Atorvastatin (ATV; Merck) was used for this purpose, and was solubilised in distilled water to a stock concentration of 0.5 mM. At ~32 hpf groups of n=20 WT or *samhd1*$^{\Delta 23/\ \Delta 23}$ embryos were added to 1 well of a 6 well plate containing increasing ATV concentrations diluted in PTU E3 media: untreated; 0.25 µM, 0.5 µM, 1 µM and 1.5 µM. The embryos were incubated overnight, and at ~54 hpf imaged for the presence of haemorrhages in the head, using a Leica M205 FA Stereo fluorescence microscope with a 5x/0.50 PlanAPO LWD objective, captured using a DFC 425 camera (Lecia) and processed using LAS AF v3.1.0.8587 software (Leica). The percentage of embryos with haemorrhages within each treatment/genotype group was determined from 3 independent replicates.

2.2.8 Ruxolitinib treatment

The JAK inhibitor ruxolitinib (Selleckchem) was used for rescue experiments. A stock solution of 10 mM was generated by dissolving into DMSO. Following WT and *samhd1*$^{\Delta 23/\Delta 23}$ adult fish breeding, 20 fertilised eggs at the gastrula stage (6 hpf) were added to 1 well of a 6 well plate containing 2 µM ruxolitinib in E3 media. The water was changed 1 day later to PTU E3 media, with fresh addition of the drug. At 48 hpf, the embryos were harvested for the individual rescue outcomes: microcephaly and TUNEL staining.

2.3 Whole-mount stains

2.3.1 Fixing embryos

WT and *samhd1*$^{\Delta 23/\Delta 23}$ embryos were killed using an overdose of MS222 at 2 dpf, and fixed in 4% PFA (Table 2.1) overnight at 4 °C. The PFA was removed and samples washed in 0.4-1% PBSTx (stain dependent) before being dehydrated into increasing concentrations of methanol, until 100% methanol where the embryos were stored at -20 °C until use.

2.3.2 TUNEL staining

At 2 dpf, WT and *samhd1*$^{\Delta 23/\Delta 23}$ embryos were stained following an adapted protocol from the manufacturer of Click- iT Plus TUNEL assay kit (Invitrogen). Methanol dehydrated embryos were rehydrated into 0.4% PBSTx following washes with a series of decreasing methanol solutions.

Samples were then treated with 1X proteinase K, diluted 1:25 in PBS from a 25X stock solution (from Invitrogen assay kit), for 40 min. Following proteinase K removal, the samples were washed in 0.4% PBSTx prior to a 10 min incubation in ice cold acetone. A short (20 min) re-fixing of samples in 4% PFA at room temperature (RT) was followed by 3 washes in 0.4% PBSTx. Afterwards, the samples were left for 10 min to equilibrate in the TdT buffer. When the buffer was removed, 100 µl of TdT reaction mixture (table 2.1) was added, and the samples incubated at 37 °C for 2 hours (h). Samples were then washed twice in a 3% BSA solution in 0.25% PBSTx. Following this, the TUNEL supermix (Table 2.1) was combined with 10X TUNEL reaction buffer additive, and 100 µl of the solution was added to the samples, before a 30 min incubation period at 37 °C in the dark. The samples were washed twice in 3% BSA in 0.25% PBSTx, before they were placed in PBS, in preparation for imaging. For imaging, samples were mounted in a lateral position in 80% glycerol on a nunc glass base dish 12 mm (Thermo Fisher) and imaged on a Leica M205 FA Stereo fluorescence microscope using a 5x/0.50 PlanAPO LWD objective, captured using a DFC 365FX camera and processed using LAS AF v3.1.0.8587 software (Leica). Images were analysed using the manual cell counting software on Image J (version 1.52a). n= 6-8 embryos, per each biological replicate, repeated 7 independent times (3 for initial cell death analysis, and 4 for ruxolitinib rescue).

2.3.3 Measuring Microcephaly

Fixed WT and *samhd1*$^{\Delta 23/\Delta 23}$ embryos at 2 dpf were transferred into 1% PBSTx, and did not undergo methanol dehydration. To image the samples, 80 % glycerol was added to the embryos which were placed into a nunc glass base dish 12 mm. The samples were individually imaged in a ventral orientation using a Leica M165FC light stereo microscope with DFC7000T camera, and processed using LAS-X v3.3.3.16958 software (Leica). To assess for microcephaly, the distance between the eyes was measured alongside full length of the embryo (µm). The head/ body ratio was determined from these 2 values, and normalised to the average WT head/body ratio, to produce a microcephaly index (ratio). Measurements were obtained using Image J (version 1.52a). n=8 embryos per group, for each biological replicate, repeated 6 independent times (3 for initial microcephaly measurements, and 3 for ruxolitinib rescue).

2.3.4 Calcein Staining in live larvae

Protocol adapted from (Du et al., 2001). Live WT and *samhd1*$^{\Delta 23/\Delta 23}$ larvae at 5 dpf were immersed in a petri dish of 0.2% calcein solution (table 2.1) for 5 min. Upon completion, the larvae were washed 3X in methylene blue-free E3 medium, each wash lasting 10 min, to allow unbound calcein to diffuse out of tissues. The larvae were then anaesthetised using 0.02% M2SSS, and individually mounted in a dorsal orientation using 1.5% low melt agarose (Promega), maintained at RT, prior to imaging on a Leica M205 FA Stereo fluorescence microscope with a 5x/0.50 PlanAPO LWD objective, captured using a DFC 365FX camera and processed using LAS AF v3.1.0.8587 software (Leica). The calcein stain was used to identify any intracranial calcifications- independent of the normal

staining pattern calcein produces. Small fluorescent specks on the dorsal portion of the brain were classed as calcifications, and larvae were scored based on the presence or absence of these specks. n=6-8 larvae per group, repeated 3 independent times.

2.3.5 Gross cerebrovasculature imaging of Tg(*fli1:*EGFP) line

WT and *samhd1*$^{\Delta 23/\Delta 23}$;Tg(*fli1*:EGFP) embryos were imaged at 3 dpf using light sheet microscopy to analyse the gross cerebrovasculature. Randomly selected larvae were anaesthetised using 0.02% MS222 and mounted in 1.5% low-melt agarose, maintained at RT. Images were acquired using a W plan-Apochromat 20X/1.0 UV-VIS objective for light-sheet microscope (Carl Zeiss Lightsheet Z.1) and processed with ZEN imaging software (version 2.3). Embryos were imaged dorsally and Maximum intensity projection composites were generated from z-stack images. n=8 embryos per genotype, from one independent replicate.

2.3.6 ZNP-1 staining

Protocol adapted from (Lin et al., 2021). Fixed and dehydrated WT and *samhd1*$^{\Delta 23/\Delta 23}$ embryos at 2 dpf were rehydrated from 100% methanol to 1% PBSTx. The samples were treated with a 10 µg/ml proteinase K solution for 40 min at RT, before 3X washes in 1% PBSTx. The samples were placed into ice-cold acetone for a 10 min incubation, before being washed in 1% PBSTx. Following this, the samples were re-fixed in 4% PFA for 20 min at RT and after PFA removal, samples were washed 3X in 1% PBSTx. A blocking solution (Table 2.1) was added to the samples for 4 h with gentle rocking on a gyro-rocker (Stuart). After blocking, samples were incubated with a mouse anti-zebrafish znp-1 antibody (1:500, Developmental Studies Hybridoma Bank) in blocking solution overnight at 4 °C with gentle rocking. Samples were washed with 1% PBSTx and incubated overnight with goat anti-mouse Alexa 488 antibodies (1:500, Invitrogen) without light at 4 °C, with gentle rocking. Upon removal of the secondary antibody the samples were washed 3X in 1% PBSTx, before being placed in a nunc glass base dish 12 mm and mounted laterally in 80% glycerol. Samples were imaged on a Leica M205 FA Stereo fluorescence microscope with a 5x/0.50 PlanAPO LWD objective, captured using a DFC 365FX (Leica) camera and processed using LAS AF v3.1.0.8587 software (Leica). n=7-8 embryos per group, repeated 5 independent times. Images were analysed on Image J (version 1.52a) where the number of motor nerve terminals was manually counted from the cloaca to the end of the tail. In addition, corrected total tail fluorescence (CTTF) was obtained using the following equation:

$$CTTF = Integrated\ density - (area\ of\ tail\ region * mean\ fluorescence\ of\ background\ readings)$$

2.3.7 Haemoglobin stain

Live WT and *samhd1*$^{\Delta 23/\ \Delta 23}$ embryos at 3 dpf were anaesthetised using MS222 and transferred into glass bijoux's. E3 media was removed, and replaced with 1 ml of the haemoglobin stain (table 2.1). Embryos were incubated in the dark for 30 min at RT. Following stain completion, the embryos were washed 3X in dH_2O and fixed in 4 % PFA overnight at 4 °C. For imaging, embryos were mounted in 80% glycerol and imaged on a Leica M205 FA Stereo fluorescence microscope with a 5x/0.50 PlanAPO LWD objective, captured using a DFC 365FX (Leica) camera and processed using LAS AF v3.1.0.8587 software (Leica). n=100 embryos per group from one independent replicate.

2.3.8 Recording blood flow

WT and *samhd1*$^{\Delta 23/\Delta 23}$ embryonic cerebral blood flow was measured on the light sheet microscope. This was performed at 3 dpf where randomly selected embryos were anaesthetised using 0.02% MS222 and mounted in 1.5% low-melt agarose, maintained at RT. The brightfield setting was used to focus on the blood flow in the head, and a 30 s recording was made using Open Broadcaster Software (OBS) studio screen capture software (version 23.0.2). For analysis, the regions of interest was selected using the DanioScope (Noldus version 1.1) software over the dorsal longitudinal vein (DLV) and the heart, allowing the flow percentage and heart rate to be established. n=5 embryos per groups, from 3 independent replicates.

2.4 Genotyping

2.4.1 Primers for genotyping and SYBR green qPCR

Table 2.2- List of primer sequences used in zebrafish for genotyping and SYBR GREEN qPCR

Forward (F) and reverse (R) primers for each gene target. Primers were synthesised by Eurofin Genomics.

Gene	Sequence (5'-3')
hprt1	F: GGACTTCATCCTCAAGAG R: GTTCTAGCAGCGTCTTCATCG
samhd1	F: AGAACATCATCTGCCGCCGG R: CCAGTTCCTTCGCCCAGTCC

2.4.2 Fin Clipping

Adult fish were briefly anaesthetised using 0.02% MS222, and the tip of the caudal fin was removed using a scalpel. The fish were then recovered in fresh system water and monitored for recovery

signs. Until completion of the genotyping, (approx. 3-5 days), the fish were singly housed in genotyping drawers, before being re-grouped with adults of the same genotype.

2.4.3 DNA extraction

To extract DNA, 100 µl of 50 mM NaOH was added to the dissected caudal fin. Following this, the samples were heated for 20 min at 95 °C, before being cooled on ice for 2 min, with the addition of 10 µl TRIS-HCL (pH 8.0). Lastly the samples were vortexed and centrifuged at max speed (14,800 revolutions per minute (rpm)) for 1 min, before using the supernatant in the polymerase chain reaction (PCR).

2.4.4 PCR

PCR amplification was performed using a PCR master mix (Thermo Scientific) containing the *Taq* DNA polymerase, dNTPs and reaction buffer with 4 mM $MgCl_2$. This was mixed with the zebrafish *samhd1* exon 4 primers (Table 2.2) at a concentration of 10 µg/ml, and the extracted DNA from the fin clips. A touch down (65-55 °C) protocol was used (Table 2.3) on a thermocycler (Genepro).

Table 2.3- PCR programme required for *samhd1*$^{\Delta 23/\Delta 23}$ genotyping

Required temperature and time cycles for the touchdown (65-55) protocol

Step	Temperature (°C)	Time (s)
Denature	95	240
Touchdown anneal	65-55	180
Repeat 10 cycles		
Denature	95	30
Anneal	60	30
Elongate	72	30
Repeat 35 cycles		
Elongate	72	600
Hold	4	Indefinitely

2.4.5 Gel electrophoresis

PCR amplicons were assessed using agarose gel electrophoresis to determine the different genotypes. For the gel, 2.5% agarose (bioline) was added to 150 ml of 1X TAE buffer and 15 µl SafeView dye (NBS Biologicals Ltd) to visualise the DNA. The gel moulds were set and samples loaded into wells using 5X loading dye (New England BioLabs) alongside a 25 bp (base pair) DNA

ladder (Bioline). Samples were separated for ~45 min at 120 V and imaged under a UV transilluminator (Syngene). Example genotyping gel shown below.

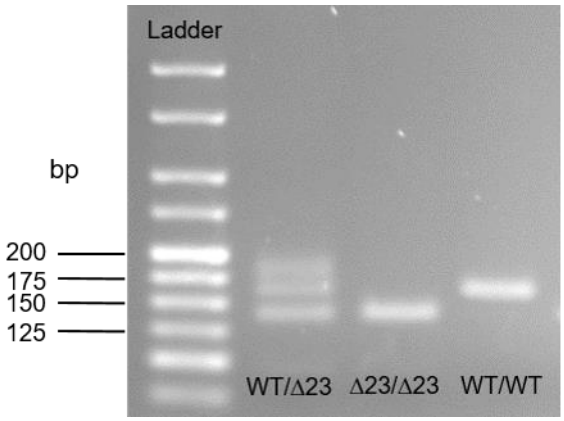

Figure 2.1- Representative PCR gel obtained from genotyped *samhd1* heterozygous incross fish

WT/Δ23, Δ23/Δ23 and WT/WT bands are indicated on the gel. Exon 4 of the *samhd1* gene is 161 bp, whilst the 23 bp deletion produces a band size of 138 bp.

2.5 Zebrafish Gene Expression Analysis

2.5.1 RNA Extraction

Total RNA was collected from whole embryos at 2 and 5 dpf, and larval heads at 5 dpf. For whole body extraction groups of 20 embryos/ larvae per replicate were given an overdose of MS222 before being collected into a 1.5 ml Eppendorf. For larval heads, 30 larvae were required to generate enough RNA for one independent replicate. Following an overdose of MS222, a needle and a pair of forceps were used to decapitate the larvae, and the head was collected into a 1.5 ml Eppendorf.

All samples were washed in PBS prior to the addition of 250 µl TRIzol (Invitrogen). Each tube was then manually homogensised using a microfuge tube pestle (Astral Scientific). Next, 75 µl of chloroform was added to each tube and agitated vigorously before centrifugation at 10,000 rpm for 15 min at 4 °C. Following centrifugation, the homogenate formed three distinct layers: a clear aqueous layer containing the RNA, a debris containing interphase, and a lower organic phase containing DNA and proteins. The aqueous upper phase layer was transferred to new tubes, and the RNA precipitated using 0.8 volumes of isopropanol incubated at -20 °C for 30 min. Precipitate was pelleted following centrifugation at 10,000 rpm for 15 min at 4 °C, and was subsequently washed in 250 µl of 75% RNase-free filter sterilised ethanol, and centrifuged for a further 10 min at 8000 rpm at 4 °C. The remaining ethanol was air dried from the pellet, and the pellet resuspended in 20 µl RNase-free H_2O (Invitrogen). RNA was purified with a DNase I treatment (Applied Biosystems) prior to quantification on a spectrophotometer (Nanodrop 1000, Thermo Fisher)

2.5.2 cDNA synthesis

To generate complementary DNA (cDNA) sequences from the RNA, 800 ng of RNA was incubated with 1 µl of reverse transcriptase and 10 µl buffer mix (including dNTPs) from the High-Capacity RNA-to-cDNA kit (Applied Biosystems). The samples were made up to 20 µl with RNase-free H_2O and heated to 37 °C for 1 h, followed by termination of the reaction at 95 °C for 5 min.

2.5.3 Quantitative PCR (Taqman)

For gene expression analysis of quantitative PCR (qPCR) using Taqman reagents, the Taqman Universal PCR Master Mix (Applied Biosystems) was used. The probes and references can be found in Table 2.4. The relative abundance of each target transcript was normalised to the expression level of *hprt1,* with the WT samples acting as the calibrators. The StepOnePlus real time PCR machine (Thermo Fisher) was used for the experiments with the Applied Biosystems StepOne Software (version 2.1) to acquire the data using the Comparative C_T ($\Delta\Delta C_T$) programme. Relative gene expression quantification values (RQ) were obtained following an adapted protocol previously described (Vandesompele et al., 2002). Data were obtained from 5 independent replicates.

2.5.4 Quantitative PCR (SYBR green)

SYBR green qPCR was used to measure *samhd1* expression in 5 dpf larvae. Synthesised cDNA was added to the *samhd1* and *hprt1* primers, (Table 2.2) and power SYBR Green master mix (Applied Biosystems). The same StepOne machine and software were used to obtain RQ values (2.5.3). Data from 4 independent replicates.

Table 2.4- Zebrafish Taqman probes

All genes used for qPCR, including the probe reference

* Custom Probe sequence can be found in supplementary Figure 1 of (Kasher et al., 2015)

Gene	Taqman Probe reference
isg12	Dr03140917_g1
isg15	Custom made probe, using the Custom Taqman Assay Design Tool (Life Technologies)*
rsad2	Dr03896954_m1
stat1b	Dr03151121_m1
cyp51	Dr0314750_m1
dhcr24	Dr03423142_m1
ebp	Dr03076172_m1
msmo1	Dr03133463_m1
sqlea	Dr03131215_g1
hmgcrb	Dr03128326_m1
srebf1	Dr03093012_m1
hprt1	Dr03095135_m1
gfap	Dr03079978_m1
nptx2a	Dr03118566_m1
pcna	Dr03093294_m1
cldn5b	Dr03096124_s1
elav13	Dr03131531_m1

2.6 AGS patient samples

All AGS patient data was obtained by researchers at the Manchester Centre for Genomic Medicine, including Dr. Tracy Briggs, Dr. Gillian Rice and Dr. Charles Rowlands, who acquired the patient material, performed RNA sequencing and the gene expression analysis.

2.6.1 Acquisition of patient material

Whole blood from AGS patients with confirmed mutations in *TREX1, RNASEH2A, 2B, 2C, SAMDH1, ADAR1* and *IFIH1* was taken to allow for whole genome RNA sequencing, and has been described previously (Rice et al., 2013). In addition, non-AGS patient age-matched controls were obtained. Briefly, AGS patients were identified through either direct clinical contact with the appropriate physicians, or through a referral process. The use of patient materials has been approved from the

Leeds (East) research ethics committee (reference number: 10/H1307/132), whilst consent was also obtained from parents of the affected patients.

2.6.2 RNA extraction and short-read sequencing

The RNA extraction method for RNA sequencing has been described previously (Rice et al., 2013; Rice et al., 2018). Briefly, blood was collected into PAXgene tubes (PreAnalytix) and kept at RT between 2-72 h before being frozen at -20 °C until RNA extraction. Total RNA was extracted from whole blood with a PAXgene RNA isolation kit (PreAnalytix). RNA concentration was assessed with a spectrophotometer (FLUOstar Omega, Labtech), and 1 µg of mRNA from each sample was diluted into 20 µl nuclease-free water. Subsequently, the quality and integrity of the RNA samples were assessed using a 2200 TapeStation (Agilent Technologies). A poly-A enrichment library was then generated using the TruSeq® Stranded mRNA assay (Illumina), according to the manufacturer's protocol, and 76 bp (+ indices) paired-end sequencing carried out on an Illumina HiSeq 4000.

2.6.3 RNA sequencing alignment and gene expression analysis

Raw sequencing output was demultiplexed (allowing one mismatch) and the Binary Base Call (BCL) sequence file format, was converted to the text-based sequencing data file format (FASTQ) using Illumina's bcl2fastq software, version 2.17.1.14. Low quality bases and adaptor sequences were trimmed using Trimmomatic, and reads aligned to the Genome Reference Consortium Human Build 37 (GRCh37) genome using the two-pass mode of the Spliced Transcripts Alignment to a Reference (STAR) aligner (v2.5.3a) , as well as to the transcriptome according to the GENCODE v19 human gene annotation (downloaded from https://www.gencodegenes.org/human/release_19.html). For each patient sample, the RNA-Seq by Expectation Maximization (RSEM) software package (v1.3.0) was used to calculate gene expression values, in transcripts per million (TPM), for all genes described in Chapter 4. Subsequently, fold change was determined from TPM values, by dividing the individual values for each gene by the average control value. Lastly, the fold change values were then Log transformed (Log2).

2.7 Cell culture

2.7.1 hCMEC/D3 cell culture

The immortalised human cerebral microvascular endothelial cell line (hCMEC/D3) was purchased from Merck (UK). hCMEC/D3 cells were maintained in either T25 or T75 cm^2 flasks pre-coated with rat tail collagen type I (Enzo life sciences) diluted in PBS 1:100 and incubated at 37 °C for at least 30 min. The cells were grown in EndoGRO-MV Complete Culture Media (Millipore) with the following supplements: 5% Fetal Bovine Serum (FBS), L-glutamine (10 mM), EndoGRO-LS supplement (0.2

%), heparin sulphate (0.75 U/ ml), ascorbic acid (50 µg/ml), hydrocortisone hemisuccinate (1 µg/ml), recombinant human epidermal growth factor (rh EGF) (5 ng/ml), penicillin 1 U/ml and streptomycin 0.1 mg/ml. Cells were maintained at 37 °C in a humidified atmosphere with 5 % CO_2. hCMEC/D3s were passaged at 80-90 % confluency using 1X trypsin-EDTA (Sigma) to detach from the flask.

2.7.2 Human MDM culture

Methods for obtaining human monocyte derived macrophages (MDMs) have been described previously (Gritsenko et al., 2020). Leucocyte cones from healthy donors were obtained from the national blood transfusion service (Manchester, UK) with full ethical approval from the Research Governance, Ethics, and Integrity Committee at the University of Manchester (ref. 2018-2696-5711). Human peripheral blood mononuclear cells (PBMCs) were isolated from the cones by density centrifugation using a 30% Ficoll® gradient. The PBMC layer was separated and washed with MACS buffer (PBS, 0.5% BSA, 2mM EDTA) to ensure platelet removal. Monocytes were positively selected from PBMCs by magnetic $CD14^+$ MicroBeads (Miltenyi) for 15 min at 4 °C before being eluted using a LS column (Miltenyi). For monocyte differentiation into macrophages, the monocytes were plated for 7 days at 750,000 cells/well in 12 well plates, in RPMI-1640 medium, supplemented with 2 mM L-glutamine, 10% FBS, penicillin 1 U/ml, streptomycin 0.1 mg/ml and 0.5 ng/ml M-CSF (Peprotech). On day 3, half of the media was removed and replaced with fresh media.

2.8 *In vitro* treatments

2.8.1 IFNβ treatment

IFNβ (TONBO Biosciences) was solubilised in a 0.1% BSA in PBS solution, to a stock concentration of 10 µg/ml, and was added to the wells at a final concentration of 20 ng/ml. 0.1% BSA in PBS was used as the vehicle control (Ctrl) for IFNβ treatment.

2.8.2 25HC treatment

25HC (Sigma) was solubilised in ethanol to a stock concentration of 10 mM, and was added to the wells at a final concentration of 5 µM. Moreover, a 25HC dose response was also used as a treatment with the following final concentrations: 0.2; 1; 5; 25 µM. Ethanol was used as the vehicle Ctrl for 25HC treatment.

2.8.3 Co-treatments

Cholesterol (Sigma) was solubilised in ethanol to a stock concentration of 10 mM, and was added to the wells at a final concentration of 10 µM for SLO assay and 50 µM for scratch assay. Ethanol was used as the vehicle Ctrl.

Desmosterol (Avanti) was solubilised in Dimethylformamide (DMF) to a stock concentration of 50 mM, and was added to the wells at a final concentration of 10 µM. DMF was used as the vehicle Ctrl.

The ACAT inhibitor, Sandoz 58-035 (SZ 58-035) was solubilised in DMSO to a stock solution of 80 mM, and added to wells at a final concentration of 10 µM. DMSO was used as the vehicle Ctrl.

2.9 *In vitro* gene expression analysis

2.9.1 hCMEC/D3 cells

A 4 h and 24 h stimulation was applied for IFNβ and 25HC treatment of hCMEC/D3 cells. Cells were seeded overnight at a density of 350,000 cells/ml for 4 h treatment, and 300,000 cells/ml for 24 h treatment in a 24 well plate (Corning), prior to the addition of IFNβ and 25HC (see section 2.8). The treatments were incubated in the wells for the designated time, and cell lysates were collected.

2.9.2 Human MDMs

A 24 h stimulation was applied for IFNβ and 25HC treatment of human MDMs. Following monocyte differentiation (2.8.2), cells were treated with IFNβ and 25HC (see section 2.8). After treatment, cells lysates were collected.

2.9.3 RNA extraction and cDNA synthesis

Following the 4 h or 24 h treatment of hCMEC/D3 and MDMs, the media was removed from each well, followed by the addition of 300 µl of TRIzol reagent (Invitrogen). Scraping the cells with a 1000 µl pipette tip was used to ensure full detachment of cells. The subsequent RNA extraction protocol and cDNA synthesis has already been described with zebrafish larvae (see sections 2.5.1 and 2.5.2). The only difference being 65 µl of chloroform added to each sample rather than 75 µl.

2.9.4 SYBR green qPCR from hCMEC/D3 cells and MDMs

SYBR green qPCR was used to measure ISGs and sterol genes in the samples, and followed a similar protocol as already described (see section 2.5.4). Synthesised cDNA was added to the primers (Table 2.5), and the power SYBR Green master mix (Applied Biosystems). The StepOnePlus real time PCR machine (Thermo Fisher) was used for the experiments with the Applied Biosystems StepOne Software (version 2.1) to acquire the data using the Comparative C_T ($\Delta\Delta C_T$) programme. Data was normalised to the expression of two housekeeping genes: *HPRT1* and *18S* and RQ values were obtained following the method described previously, and used for zebrafish gene expression data (Vandesompele et al., 2002). The RQ values were then Log transformed (Log2). Each

condition/time point was repeated on 4-5 different passages for hCMEC/D3 cells and from 4 individual blood donors in human MDMs.

Table 2.5- List of primer sequences for SYBR Green qPCR

F and R primers for each gene target

Gene	Sequence (5'-3')
HPRT1	F: CAGGCGAACCTCTCGGCTTT R: GGGTCGCCATAACGGAGCC
18S	F: GTAACCCGTTGAACCCCATT R: CCATCCAATCGGTAGTAGCG
CH25H	F: AACGTCACACTGCTCGGGTG R: GTGGTCCTCCACGGAAAGCC
ISG15	F:CAGCACCTACGAGGTACGGC R: TTCCCCTCGAAGGTCAGCCA
RSAD2	F: AGGGCAACCTTCTGGCTGCTA R: TTGCACTGGCGAGTGAAGTGAT
IFITM3	F: CATCCCAGTAACCCGACCGC R: GCTGGCCACTGTTGACAGGA
DHCR24	F: CCACATGCTTAAAGAACCACGGC R: CAGGAGAACCACTTCGTGGAAG
ABCG1	F: GAGGGATTTGGGTCTGAACTGC R: TCTCACCAGCCGACTGTTCTGA
HMCGR	F: GACGTGAACCTATGCTGGTCAG R: GGTATCTGTTTCAGCCACTAAGG
SQLE	F: CTCCAAGTTCAGGAAAAGCCTGG R: GAGAACTGGACTCGGGTTAGCT

2.10 Cholesterol lipid measurements in hCMEC/D3 cells

2.10.1 Cholesterol ester assay

hCMEC/D3 cells were seeded overnight at a density of 200,000 cells/ml in a 6 well plate and left overnight. 25HC and vehicle Ctrl was added to the wells for a 48 h incubation (see section 2.8.2). Afterwards, cell lysates were collected. Following this, the cells were trypsinised, spun down and resuspended in 1 ml PBS. Next, 100 µl of each sample was taken for the BCA assay to measure protein concentration (see section 2.10.2), whilst the remaining 900 µl was re-spun and the resulting cell pellet used for the cholesterol assay.

The samples were taken for total and free cholesterol measurements, performed according to manufacturer's protocol for the Cholesterol/Cholesterol Ester Assay Kit (Abcam). Briefly, cell pellets were resuspended with 200 µl extraction buffer (Table 2.1) and sonicated in an Ultrasonic cleaning bath (VWR, Avantor) for 15-30 min. The cells were then centrifuged for 10 min at 11,000 rpm at 4°C. The organic phase was transferred to a new Eppendorf and air-dried at 50 °C until full chloroform evaporation. The samples were then vacuumed for 3 h on the Genevac™ miVac (SP scientific) to remove all remaining solvents, leaving a lipid droplet.

The droplet was dissolved in 200 µl of the cholesterol assay buffer and 25 µl of this solution was mixed 1:1 with one of two assay reaction mixes, depending on total or free cholesterol measurement (Table 2.1). Samples were plated alongside a set of known cholesterol standards (0-5 µg) in a clear bottom 96 well plate and incubated for 1 h at 37 °C in the dark. The absorbance was read at 570 nm on a FLUORstar Omega plate reader (BMG labtech) and total and free cholesterol concentrations were established based on a standard curve from the cholesterol standards. Cholesterol was expressed as µg/µl. From these values, cholesterol ester concentrations could be established by removing the free cholesterol concentration from the total cholesterol concentration.

To determine the cholesterol concentrations of each sample relative to the protein concentration, cholesterol was converted to µg/ml, and divided by protein concentration to produce cholesterol/protein (µg), used to compare between different samples. Experiments were performed as 4 replicates of different passages of hCMEC/D3 cells.

2.10.2 Analysis of cell number by total protein assay (bicinchoninic acid assay)

Total protein in the cell lysate of treated hCMEC/D3 cells was assessed as an indirect measure of cell number. Protein concentration was determined prior to the cholesterol assay, to establish cholesterol concentrations relative to the protein content. A Pierce™ bicinchoninic acid assay (BCA) Protein Assay Kit (Thermo Scientific) was performed following manufacturer's instructions. Absorbance was read at 570 nm on a FLUORstar Omega plate reader (BMG labtech), and protein concentration was calculated from the standard curve. Total protein was expressed as µl/ml.

2.11 SLO assay

A 4 h and 24 h stimulation was applied for 25HC treatment for the SLO assay. Cells were seeded overnight at a density of 300,000 cells/ml for 4 h treatment, and 250,000 cells /ml for 24 h treatment, in a black clear-bottom 96 well plate (CELLSTAR). Initially, cells were treated with 25HC or vehicle Ctrl (see section 2.8.2). Subsequent 24 h experiments included co-treatment of 25HC with cholesterol, desmosterol or SZ 58-035 (see section 2.8.3).

Following completion of treatment, the EndoGro (Merck) media was removed, and replaced with 40 µl Opti-MEM (Gibco) with 0.5 µM TO-PRO-3 (ThermoFisher). The bacterial toxin Streptolysin O

(SLO) (Sigma) was activated at 100 U/µl with 20 mM dithiothreitol (DTT) (Merck), 30 min prior to imaging, at 37 °C.

An initial baseline image was acquired on the IncuCyte Zoom Live Cell Analysis system using a 10x/1.22 Plan Fluor OFN25 objective for the phase contrast and red filter. Following the baseline image, SLO was added to each well at a final concentration of 2 U/ µl, and an image was obtained 1 h later. Following the 1 h image, 2.5 µl of 0.05% triton was added to each well to cause 100% cell death, and allow the percentage of cell death to be identified from the assay.

The number of dead cells was determined through the basic analyser software (Essen BioScience), used for the quantification of fluorescent objects and based on a number of defined characteristics, such as area, eccentricity and fluorescent intensity. The percentage of cell death was established by dividing the number of dead cells at the 0 h and 1 h time point, with the number of dead cells in the 0.05% Triton time point for each well. Each condition/ time point was repeated on 2-6 different passages of hCMEC/D3 cells

2.12 Scratch assay

A 3 h and 24 h pre-treatment stimulation was applied for 25HC treatment for the scratch assay. For the 3 h incubation, cells were seeded at a density of 400,000 cells/ml in a 96-well ImageLock plate (Essen BioScience) not collagen coated and left for 1 h. Then the cells were treated with 25HC and vehicle Ctrl (see section 2.8.2) for 3 h prior to generation of the scratch.

Conversely, for the 24 h treatment, cells were seeded at a density of 250,000 cells/ml in a 24 well plate and left overnight. The cells were then treated with 25HC or vehicle Ctrl for 20 h. Subsequently, the cells were re-suspended and re-seeded to a density of 400,000 cell/ml in a 96-well ImageLock plate, where the protocol then followed the 3 h treatment. The 24 h treatment also encompassed the co-treatment of the cells, as previously described in the SLO assay (2.11) whereby the 25HC treated wells were co-treated with cholesterol, desmosterol (10 µM) or SZ-58-035 for the 24 h period.

After the 4 h following seeding, EndoGro media with treatments was temporarily removed and replaced with PBS. Wells were then scratched using a 96-pin IncuCyte WoundMaker Tool (Essen BioScience) and washed two times with PBS, and replaced with the original EndoGro and treatment media. Phase contrast images were acquired at 2 h intervals for a period of 24 h on an IncuCyte Zoom Live Cell Analysis system using a 10x/1.22 Plan Fluor OFN25 objective. The IncuCyte Scratch Wound Analysis Software Module (Essen BioScience) was used to quantify relative wound density. Relative wound density (RWD) is a measure (%) of the density of the wound region relative to the density of the cell region:

$$\%RWD(t) = \frac{w(t) - w(0)}{c(t) - w(0)} x100$$

Where w(t)=Density of wound region at time, (t) and c(t)=Density of cell region at time, (t).

Each condition/time point was repeated on 2-6 different passages of hCMEC/D3 cells.

2.13 Statistical analysis

All data were analysed with GraphPad Prism 8.1.2 (GraphPad Software Inc) using the appropriate tests (further details stated in the figure legends throughout the results chapters). Data were tested for normality using the D-Agostino-Pearson test. This test uses skewness and kurtosis to quantify how far away the distribution is from Gaussian, relating to asymmetry and shape, moreover, how far these values differ from the expected value with a Gaussian distribution is computed. The resulting parametric data are presented as mean ± standard error of the mean (SEM). Non-parametric data are presented as median ± interquartile range (IQR). Details of replicates are recorded in the figure legend. Statistical significance was accepted at *P<0.05, **P<0.01, ***P<0.001 and ****P<0.0001.

Chapter 3: Characterising the use of a stable mutant zebrafish model to recapitulate the classical symptoms of Aicardi-Goutières syndrome

3.1 Introduction

AGS is a rare type I interferonopathy with nine identified genetic subtypes (AGS1-9), involving mutations in *TREX1*, the three non-allelic components of *RNASEH2 (RNASEH2A-C), SAMHD1, ADAR1, IFIH1, LSM11* or *RNU7-1* (Crow et al., 2006a; Crow et al., 2006b; Rice et al., 2009; Rice et al., 2014; Rice et al., 2012; Uggenti et al., 2020). Each protein is involved in intracellular nucleic acid sensing, processing or metabolism, and upon mutation, the genes cause an increase in, or abnormal processing or sensing of endogenous nucleic acid species at levels above the immunostimulatory threshold (Crowl et al., 2017). This is recognised by intracellular DNA and RNA sensors, leading to chronic activation of the type I FN pathway (Crow and Stetson, 2021).

One of the main diagnostic criteria across all AGS subtypes is elevated type I IFN levels and an IFN signature, which is classified as increased expression of a panel of ISGs (Rice et al., 2013). Other clinical manifestations, ubiquitous across all genetic sub-types, are called 'classical' AGS symptoms, and include white matter abnormalities, intracranial calcifications, microcephaly and motor defects, thus categorising this disease as an encephalopathy due to the large number of neurological features (Crow et al., 2015; Livingston and Crow, 2016).

Whilst many patients across AGS1-9 do share a number of these classical symptoms, it is of note that AGS as a whole is an extremely heterogeneous disease, with large differences in symptom severity observed in patients within and between genetic sub-types (Adang et al., 2020; Crow et al., 2015). Furthermore, there are sub-type specific symptoms, including *ADAR1* related bilateral striatal necrosis and *SAMHD1*-related cerebrovasculopathy (Crow et al., 2015).

As AGS is a rare disease, with around 500 families affected worldwide, it is important to develop pre-clinical models to study the condition, due to limited availability of patient derived material, such as primary cells (Crowl et al., 2017). Although immortalised cell lines from patients have provided significant insight into the loss of gene function, global defects across the whole-body system are not possible to assess *in vitro*, leading to the development of a number of *in vivo* AGS models, the majority of which have been generated in mice. Unfortunately, none of these AGS models have been able to fully recapitulate the human condition. Some models develop varying degrees of IFN related inflammation, but there is a consistent lack of a neurological phenotype in rodents. Conversely, other AGS mouse models are not embryonically viable (Rutherford et al., 2020).

Non-mammalian *in vivo* models of AGS have been generated in zebrafish, producing loss of function models in *ifih1*, *adar1* and *samhd1. ifih1* presents in AGS patients as a gain of function mutation, thus this model was used to rescue overexpression of immune-regulated genes in a mutant line with an upregulated IFN response, rather than as a direct model of AGS7 (Rajshekar et al., 2018; Rutherford et al., 2020). A transient model of AGS5 (*samhd1* MO) has been described that is the first to show a neurological phenotype in the form of ICH, along with a robust global type I IFN and ISG response (Kasher et al., 2015). *SAMHD1*-related AGS is of particular interest due to patients frequently developing cerebrovascular disease. Indeed, as AGS5 represents a monogenic form of

cerebrovascular disease, understanding this condition may provide useful insights into the more common, non-inheritable forms of the disease, such as stroke.

Zebrafish models of disease are becoming increasingly popular tools for pre-clinical disease modelling, for a plethora of reasons (see introduction 1.8). Arguably the most important is the relative ease of genetic manipulation in zebrafish, with the ability to generate transient and stable mutants quickly and efficiently. This, coupled with high fecundity and optical transparency, makes them an ideal species for disease modelling, as an alternative or in parallel with rodent models (Eisen, 1996).

MO models are a valuable starting point for disease modelling, but like all models there are caveats associated with them, such as off-target effects, which may interfere with the phenotypes observed (Eisen and Smith, 2008). Thus it is important to model the disease in a stable mutant line. Herein, we describe the generation of a novel CRISPR-cas9 stable mutant *samhd1* zebrafish model, and the subsequent characterisation of the classical AGS symptoms in order to validate the zebrafish as a useful pre-clinical model of AGS.

3.2 Results

3.2.1 Generation of a 23 bp deletion in the *samhd1* gene using CRISPR-Cas9 technology

Following on from the *samhd1* morphant model, which successfully recapitulated aspects of the AGS5 phenotype, a stable mutant zebrafish line was subsequently generated to facilitate long term disease characterisation (Kasher et al., 2015). To generate a stable *samhd1* loss of function model, a gRNA was designed using the CHOPCHOP software, targeting exon 4 of the *samhd1* gene (Fig. 3.1a). The gRNA and Cas9 were co-injected into WT fertilised eggs at the one-cell stage producing F0 crispants, which were assessed for indels using restriction diagnostics, and raised to adulthood prior to outcrossing onto a WT background to create an F1 generation. Sanger sequencing (Fig. 3.1b) of the F1 generation revealed a 23 bp deletion in exon 4 of the mutants, thus the line was designated the name *samhd1*$^{\Delta 23}$. To determine whether this mutation resulted in a loss of transcript, RNA was harvested from WT and *samhd1*$^{\Delta 23/\Delta 23}$ larvae at 5 dpf, allowing qPCR analysis of the *samhd1* gene, where the mutants elicited almost a complete loss in *samhd1* expression compared to WT larvae ($P<0.05$) (Fig. 3.1c). We also wanted to corroborate the mutation at the protein level using western blotting, as gene expression levels do not necessarily equate to protein levels. However, due to the absence of a reliable antibody, we were not able to measure samhd1 at the protein level. As an alternative, we compared the amino acid sequence from the WT zebrafish samhd1 protein to the homozygous mutant protein (Fig. 3.1d). Following the 23 bp deletion in exon 4 of the *samhd1* gene, there is a premature stop codon, producing a truncated amino acid sequence. The stop codon is before the predicted HD domain, which is thought to be responsible for the enzymatic activity of samhd1, thus suggesting that the resulting protein, if any, is largely truncated and will be non-functional (Beloglazova et al., 2013).

Together, these data confirm that CRISPR-Cas9 successfully generated a 23 bp deletion in exon 4 of the *samhd1* gene in zebrafish, resulting in a significant reduction in *samhd1* gene expression, and a truncated amino acid sequence of the samhd1 protein.

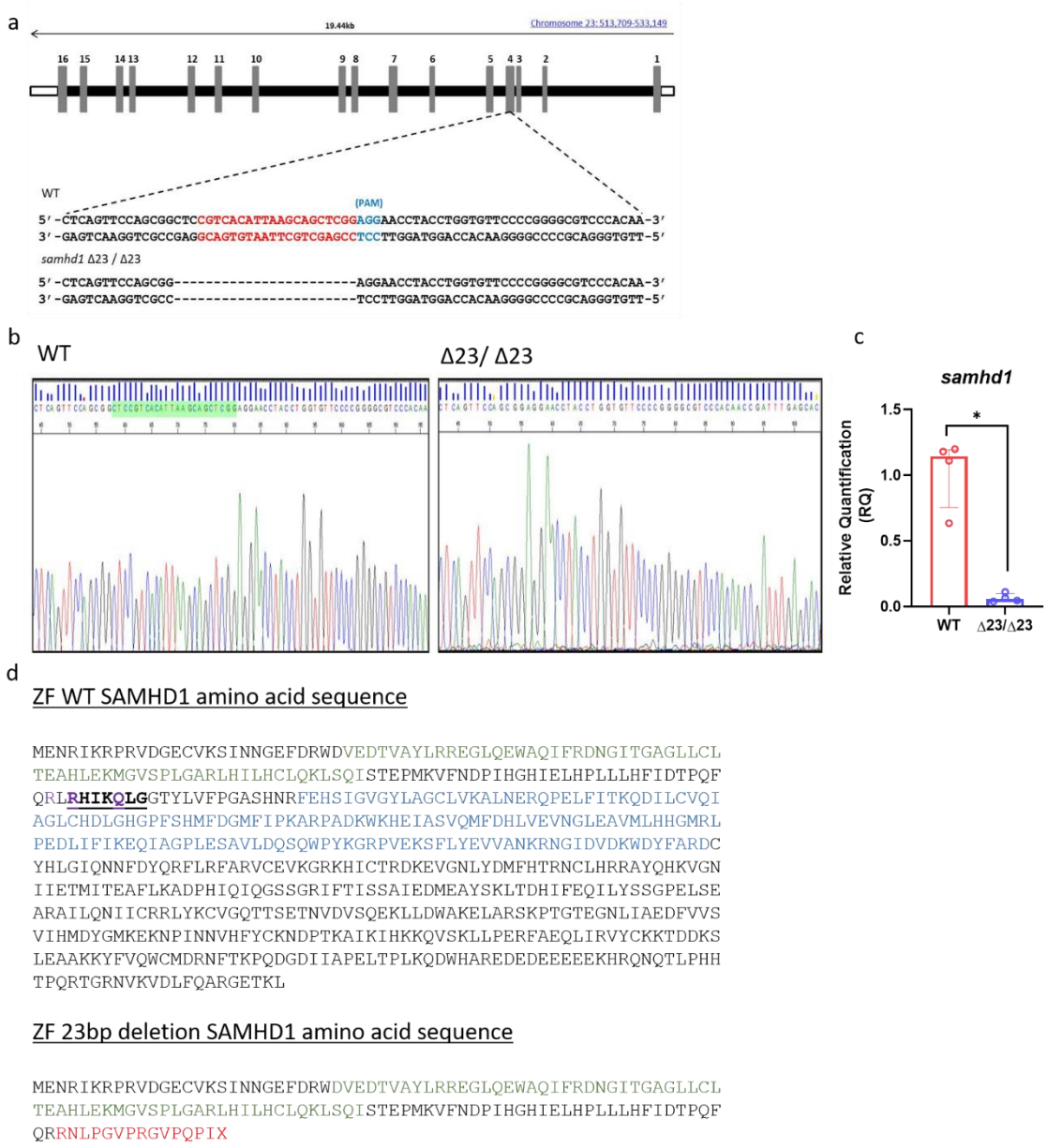

Figure 3.1- CRISPR-Cas9 induced 23 bp deletion in exon 4 of the zebrafish samhd1 gene

a) gRNA sequence (red) designed to target a site within exon 4 to initiate a 23 bp deletion in the injected embryos. b) Sanger sequencing of WT and *samhd1*$^{\Delta 23/\Delta 23}$ mutants from fish derived from an F1 generation incross. Green highlighted area on WT sequencing is the site of the 23 bp deletion, resulting in a frameshift on the mutant sequencing c) qPCR analysis of *samhd1* gene expression in 5 dpf WT and *samhd1*$^{\Delta 23/\Delta 23}$ larvae. Data analysed using Mann Whitney U test and presented as median ± IQR (* P=0.0286). n=20 larvae per group, per biological replicate, repeated 4 times. d) Amino acid sequence for WT samhd1 protein and mutant samhd1 protein. Green denotes predicted SAM domain, whilst blue denotes predicted HD domain, absent in mutant protein. Black underlined and bolded amino acids represent the CRISPR targeted sequence in the WT protein, and purple amino acids represent the location of pathogen mutations in AGS5 patients. Red sequence denotes the change in amino acids following mutation, cumulating in a premature stop codon.

3.2.2 Loss of *samhd1* is associated with a variable increase in ISG expression in *samhd1*$^{\Delta 23/\Delta 23}$ larval heads

One of the primary hallmarks across all AGS subtypes is the excessive upregulation of type I IFN, and the subsequent ISG signature, which is often used as a clinical diagnostic tool (Crow et al., 2015; Garau et al., 2019; Rice et al., 2013). The upregulation of type I IFN and ISG expression has also been observed in a number of pre-clinical models of AGS, including the *samhd1* MO model (Kasher et al., 2015). Therefore a similar result was also expected in the *samhd1*$^{\Delta 23/\Delta 23}$ larvae.

Pilot experiments using RNA from whole larvae, similar to the method performed in the *samhd1* MO model, did not exhibit any effect on ISG expression (data not shown). We hypothesised this may be the result of the MO being a more severe model than the stable mutant. Therefore, a different method was utilised to try and observe the presence of an ISG response.

The primary site of IFNα production in AGS patients is in the CSF, thus suggesting the CNS elicits a greater type I IFN response and subsequent ISG signature, than the periphery. This finding may begin to account for the severe neurological phenotypes observed in AGS (Lodi et al., 2021). In an attempt to phenocopy this observation in the *samhd1*$^{\Delta 23/\Delta 23}$ model, we chose to subsequently measure ISG expression in larval heads, allowing us to determine an ISG signature from a clinically relevant location, and potentially removing out any 'diluted effect' from the previous RNA extraction method utilising whole larvae.

RNA was extracted from larval heads, at 5 dpf, when the larvae are optimal size for head/brain removal. The expression of the ISGs *isg15*, *rsad2* and *stat1b* were previously shown to be upregulated in either the MO model, AGS patients, or both. (Kasher et al., 2015; Rice et al., 2013). *isg15* is another ISG which followed a similar pattern to the other three, thus the rationale for looking at the expression patterns of only these four ISGs is because they provided the most reliable and comparable results compared to the other ISGs identified in the MO and patients.

Although not statistically significant, due to high levels of variation, a pattern was evident (Fig 3.2). It appeared that a number of replicates within the *samhd1*$^{\Delta 23/\Delta 23}$ group exhibited large upregulations in ISG expression, resulting in excess of 200 fold increases for *isg12* and *stat1b*. However, these same genes also possessed replicates with no difference in expression when compared to the WT group. Therefore, these data highlights the heterogeneity observed within the zebrafish model, which appears to mimic the human condition, where variations in symptoms and ISG signatures are readily observed (Rodero and Crow, 2016).

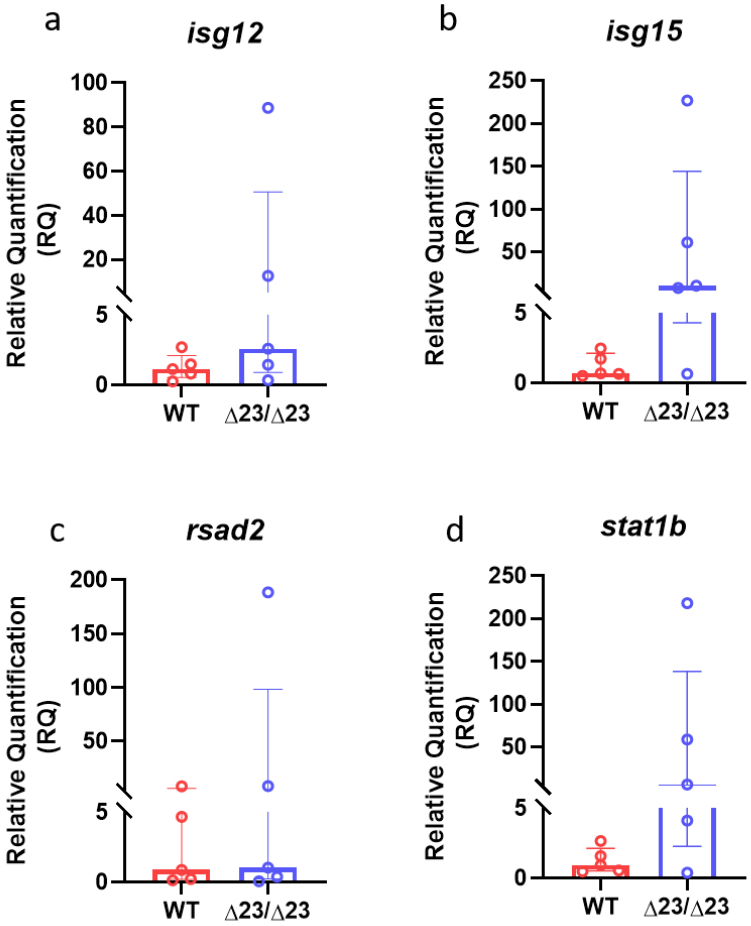

Figure 3.2- ISG expression in isolated *samhd1*$^{\Delta 23/\ \Delta 23}$ larval heads indicates a variable ISG phenotype.

a-d) RNA was extracted from WT and *samhd1*$^{\Delta 23/\ \Delta 23}$ larval heads at 5 dpf, requiring 30 heads per biological replicate, repeated 5 times. A panel of ISG Taqman probes: *isg12, isg15, rsad2* and *stat1b* were used and normalised to the housekeeper gene *hprt1*. Data analysed by a Mann-Whitney U test between WT and *samhd1*$^{\Delta 23/\ \Delta 23}$ groups for each gene, and was presented as median ± IQR.

3.2.3 *samhd1*$^{\Delta 23/\Delta 23}$ embryos exhibit a number of clinically relevant neurological phenotypes

3.2.3.1 Loss of samhd1 expression causes microcephaly in samhd1$^{\Delta 23/\Delta 23}$ *embryos*

Aside from the substantial type I IFN response observed in AGS patients, severe neurological manifestations are another important aspect of the disease. Patients can present with a range of symptoms all affecting the CNS, which further play a vital role in the debilitating nature of the condition (Crow et al., 2015; Livingston and Crow, 2016). To characterise neurological phenotypes in the zebrafish model, we looked firstly at head size, as microcephaly is a common clinical manifestation of AGS (Aicardi and Goutieres, 1984; Lanzi et al., 2002; Orcesi et al., 2009). Microcephaly has been well characterised in a number of zebrafish models of disease using different measurement protocols (Faundes et al., 2021; Jobst-Schwan et al., 2018; Stankiewicz et al., 2017). The method used in this study was to measure the distance between the eyes after ventral imaging of fixed embryos at 2 dpf, as indicated by the blue arrow in Fig 3.3a-b. Full body length was also measured to determine a head to body length ratio, also referred to as a microcephaly index, which was normalised to the mean of the WT group (Fig. 3.3e). This value was necessary to prove that the mutants developed small heads, in the absence of shortened body length, thus ruling out 'short stature' which is not characteristic of AGS. This microcephaly index was found to be significantly reduced by 15% in the mutants ($P<0.0001$), indicating that loss of *samhd1* causes smaller head sizes in zebrafish.

3.2.3.2 samhd1$^{\Delta 23/\Delta 23}$ *embryos present with enhanced cell death in the head*

Previous studies have suggested that microcephaly can be attributed to an increase in neuronal cell death (Stankiewicz et al., 2017). In order to determine the cellular basis of the microcephaly, TUNEL staining was used to identify dead cells in the head region. Manual counting of dead cells in the indicated region from the representative images revealed a significant increase in cell death in the *samhd1*$^{\Delta 23/\Delta 23}$ embryos, ~3X higher than what was observed in the WT embryos ($P<0.001$) (Fig.3.4). This provided the first evidence that loss of the *samhd1* gene in zebrafish increases cell death in the head and could potentially explain the microcephaly. Moreover, the cell death could act as a measure of cerebral atrophy, which also occurs in AGS patients, likely a result of neuronal loss.

3.2.3.3 samhd1$^{\Delta 23/\Delta 23}$ *embryos do not exhibit any alterations to the expression of brain specific markers*

After identifying the significant increase in cell death in the embryonic head, we next measured expression levels of different brain cell markers, including for general cell proliferation (*pcna*), BBB formation (*clnd5*) neurones (*elavl3, nptx2a*), and astrocytes (*gfap*). We found no difference between the expression levels of the WT and *samhd1*$^{\Delta 23/\Delta 23}$ embryos at 2 dpf for any of the genes measured (Fig. 3.5).

3.2.3.4 Calcein staining of larval heads did not identify the presence of intracranial calcifications in samhd1$^{\Delta 23/\Delta 23}$ larvae

The final brain specific phenotype we looked to characterise in the *samhd1*$^{\Delta 23/\Delta 23}$ model was intracranial calcifications, which are often associated with type I interferonopathies, including all subtypes of AGS (Livingston et al., 2014b; Uggetti et al., 2009). Calcein is a fluorescent chromophore that specifically binds to calcium, and has been used in zebrafish research to study bone growth and development (Hosen et al., 2013). A previous study observed ectopic calcification in the cranium using calcein staining, indicating this dye may be useful to study brain calcifications in the context of AGS research (Apschner et al., 2014). The larvae were anaesthetised with MS222 and live stained with calcein at 5 hpf. Calcein only effectively stains from approximately 5 dpf, therefore we were unable to stain the larvae at the same time point used for assessing the other neurological phenotypes (2 dpf). In both the WT and *samhd1*$^{\Delta 23/\Delta 23}$ larvae there were no ectopic calcifications found within the brain region (Fig.6), suggesting either intracranial calcifications are not observed in this model, or the calcein was ineffective.

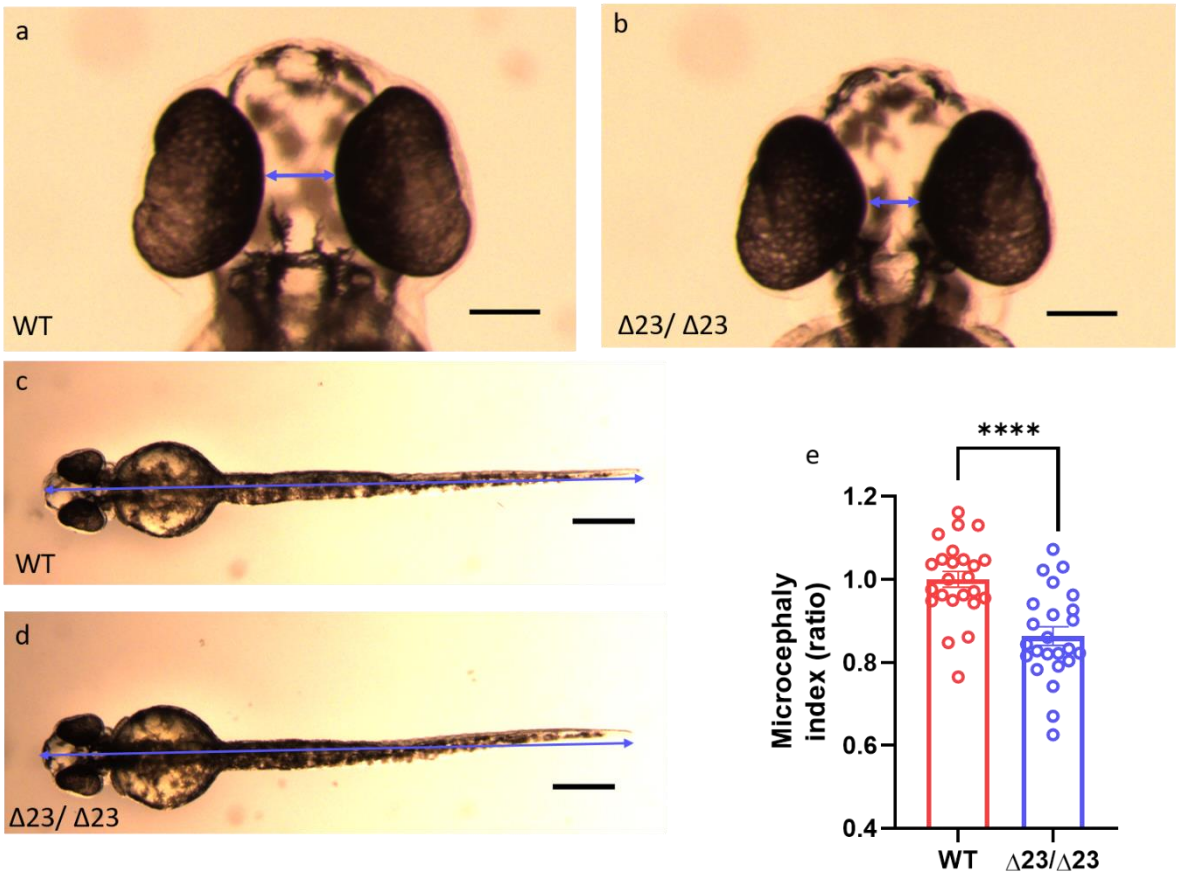

Figure 3.3- *samhd1*$^{\Delta 23/\ \Delta 23}$ embryos exhibit a microcephaly phenotype

a-d) Representative images of fixed WT and *samhd1*$^{\Delta 23/\ \Delta 23}$embryos at 2 dpf, imaged ventrally. Images were taken on a Leica M165FC light stereo microscope. All images processed on image J. Blue arrows indicate the distance between the eyes measured (a-b) and total body length measurements (c-d) .n=8 larvae per group, for 3 biological replicates. Scale bar = 100 µm for heads, and 250 µm for full length e) Microcephaly index (ratio) determined by distance between eyes and body length. Data analysed using unpaired t test (****P<0.0001) and presented as mean ± SEM.

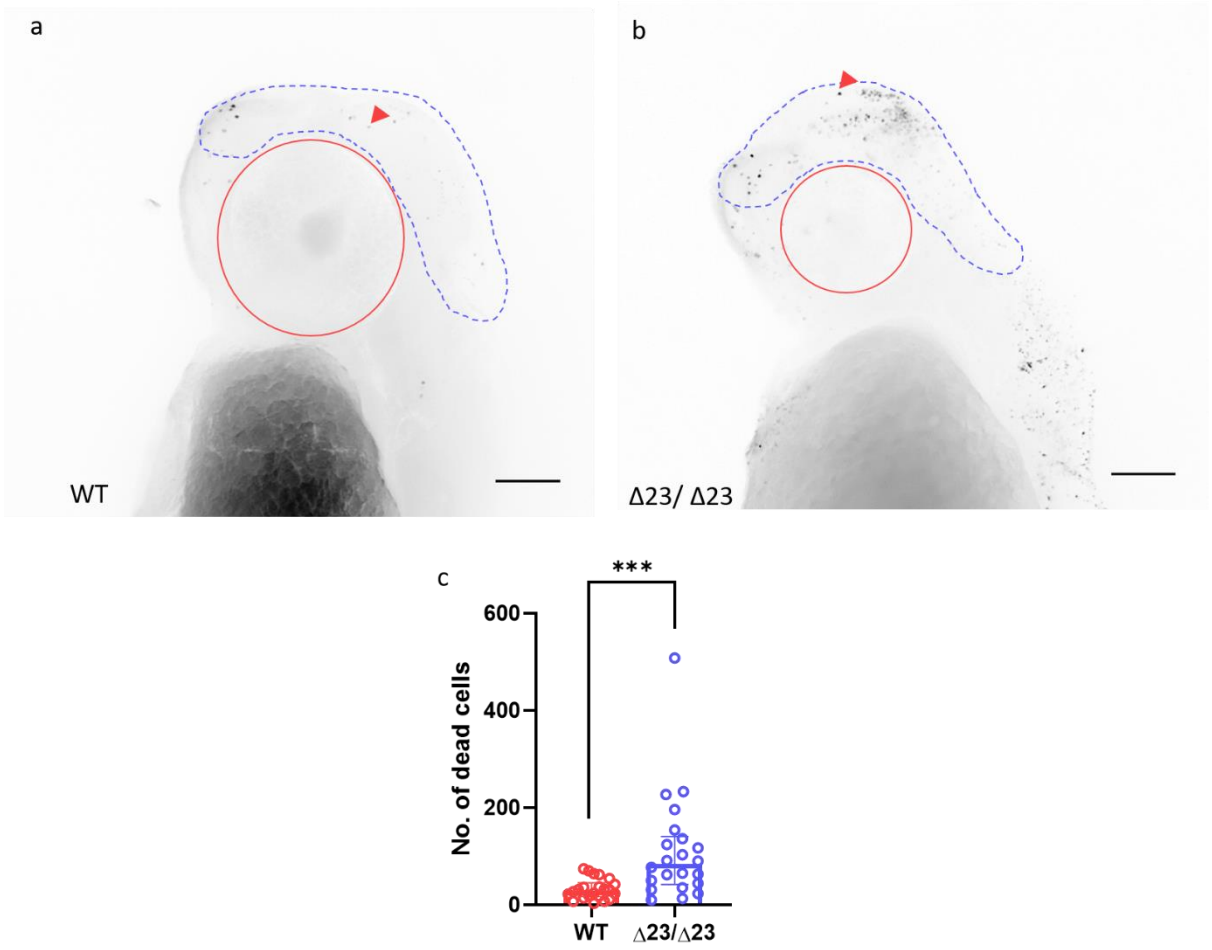

Figure 3.4- *samhd1* $^{\Delta 23/\ \Delta 23}$ embryos present with enhanced head cell death

a+b) representative images from WT and *samhd1*$^{\Delta 23/\ \Delta 23}$ TUNEL stained embryos at 2 dpf, imaged laterally on a Leica M205 FA upright stereomicroscope. . Blue dotted line indicates the area of interest for cell counting: the forebrain to hindbrain region, excluding the eyes, mouth and ears. The dead cells counted for analysis are represented by the red triangle. n= 6-8 larvae per group, with 3 biological replicates. Images processed and inverted on ImageJ. Scale bar = 100 µm. c) Quantification of the number of dead cells in the head of WT and samhd1$^{\Delta 23/\ \Delta 23}$ embryos. Data analysed using Mann Whitney test (***P<0.001) and presented as median ± IQR.

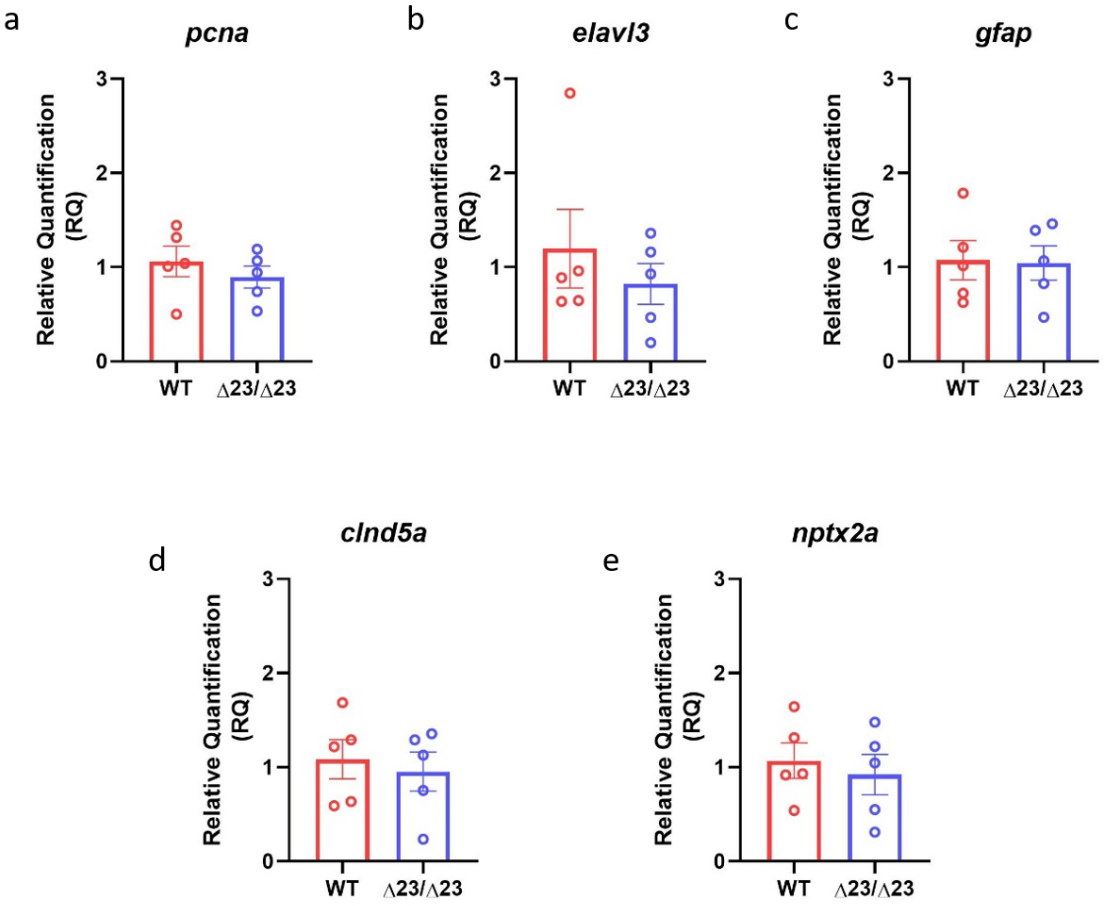

Figure 3.5- samhd1$^{\Delta 23/\Delta 23}$ embryos do not have altered expressions of brain cell markers

RNA was extracted from whole body WT and samhd1$^{\Delta 23/\ \Delta 23}$ embryos at 2 dpf, n= 20 embryos per sample, per biological replicate, repeated 5 times. A panel of brain cell marker Taqman probes: *pcna, elavl3, gfap, clnd5a, nptx2a* were used to identify any alterations in expression levels between WT and *samhd1*$^{\Delta 23/\ \Delta 23}$embryos, normalised to the housekeeper gene *hprt1*. Data analysed using an unpaired t test between WT and samhd1$^{\Delta 23/\ \Delta 23}$ for each gene and presented as mean ± SEM

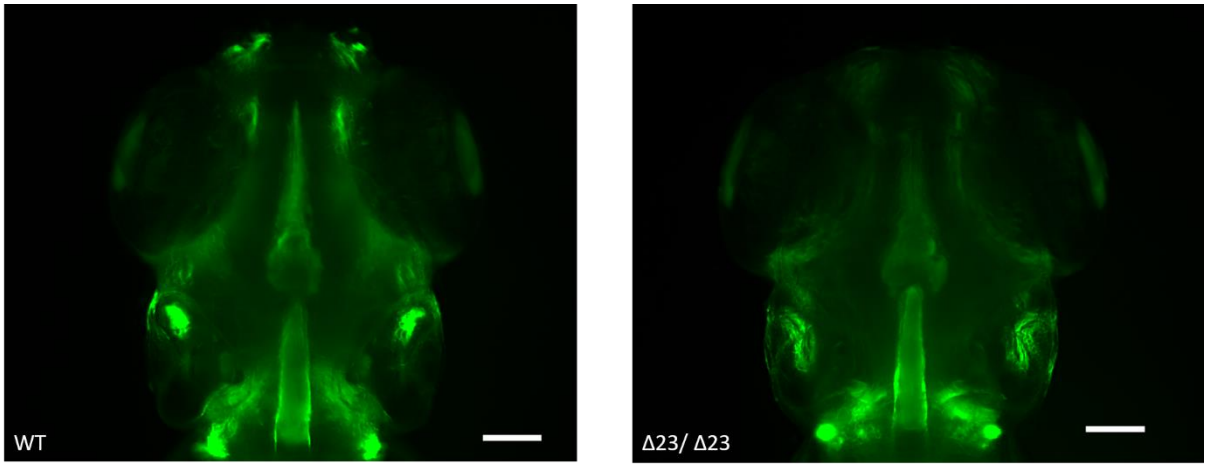

Figure 3.6- Absence of intracranial calcifications in samhd1$^{\Delta 23/\Delta 23}$ larvae

Representative images from calcein staining of WT and samhd1$^{\Delta 23/\Delta 23}$ larvae at 5 dpf. Larvae were anaesthetised in MS222 and stained with calcein before being imaged dorsally on a Leica M205 FA upright stereomicroscope. n=6-8 larvae per group, with 3 biological replicates. Scale bar= 100 µm

3.2.4 *samhd1*$^{\Delta 23/\Delta 23}$ larvae exhibit a locomotor deficit

3.2.4.1 samhd1$^{\Delta 23/\Delta 23}$ *larvae present with a reduction in swimming time at 4 dpf*

We next wanted to identify whether the microcephaly and increased cell death in the *samhd1*$^{\Delta 23/\Delta 23}$ model led to functional defects. From a clinical perspective, a wide range of motor defects are observed across all AGS subtypes (Crow et al., 2015). Swimming behaviour can be readily assessed in zebrafish larvae as a readout for motor dysfunction, as observed in other zebrafish models of disease (Crilly et al., 2018). We tracked swimming behaviour in the larvae between 3-5 dpf using DanioVision software. Interestingly, the time course identified no difference in movement at 3 dpf and 5 dpf between the genotypes. However, there was ~50% reduction in the swimming time at 4 dpf in the *samhd1*$^{\Delta 23/\Delta 23}$ larvae ($P<0.01$), indicating that loss of *samhd1* expression leads to a loss of motor function (Fig. 3.7).

3.2.4.2 A subtle reduction in znp-1 staining could contribute to the swimming deficits in samhd1$^{\Delta 23/\Delta 23}$ *larvae*

znp-1 is used as a marker of differentiating spinal motor neurons, and has been used previously in zebrafish models of hereditary spastic paraplegias, whereby impairment of neuronal outgrowth was identified (Butler et al., 2010). To examine the cellular contribution associated with the swimming deficit, whole mount staining using an anti-znp-1 antibody was performed to characterise the spinal motor nerves. Whilst there didn't appear to be any impairment in the growth and development of the motor axons between genotypes, the staining highlighted reduced fluorescence in the trunk region, potentially indicating a small reduction in the number of primary motor nerves in the mutants

compared to the WT group, but too subtle to observe structural impairments. As such, this difference was not statistically significant (Fig 3.8). The number of motor nerve segments stained per embryo, was also counted, to account for any neurodevelopmental delay. These counts showed a small variation in segment numbers across both groups. However, a larger proportion of the *samdh1*$^{\Delta 23/\Delta 23}$ embryos were found to possess smaller numbers of segments in their trunk region than the WTs, alluding to a slight neurodevelopmental delay in the mutants, akin to what is observed in AGS patients. These data suggest that the motor deficits observed in the *samdh1*$^{\Delta 23/\Delta 23}$ larvae may in part be attributed to subtle differences within the spinal motor neurons.

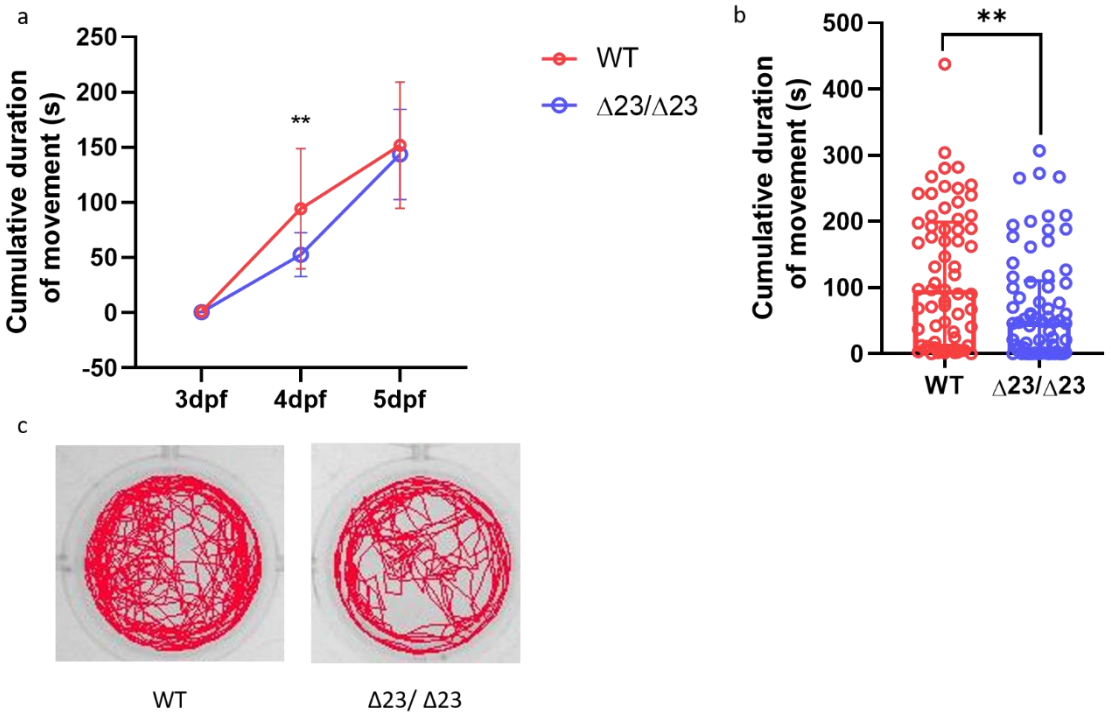

Figure 3.7- samhd1$^{\Delta 23/\Delta 23}$ larvae exhibit a locomotor deficit

a+b) *samhd1* $^{\Delta 23/\Delta 23}$ larvae exhibited a significant decrease in cumulative duration of movement at 4 dpf, which was improved by 5 dpf. n=22-24 larvae per group, with 3 biological replicates. Data analysed using a Mann Whitney U test between each time point (**P<0.001). 4 dpf movement presented as median ± IQR c) Representative examples of the swimming tracks obtained at 4 dpf on the DanioVision software between WT and *samhd1*$^{\Delta 23/\Delta 23}$ larvae.

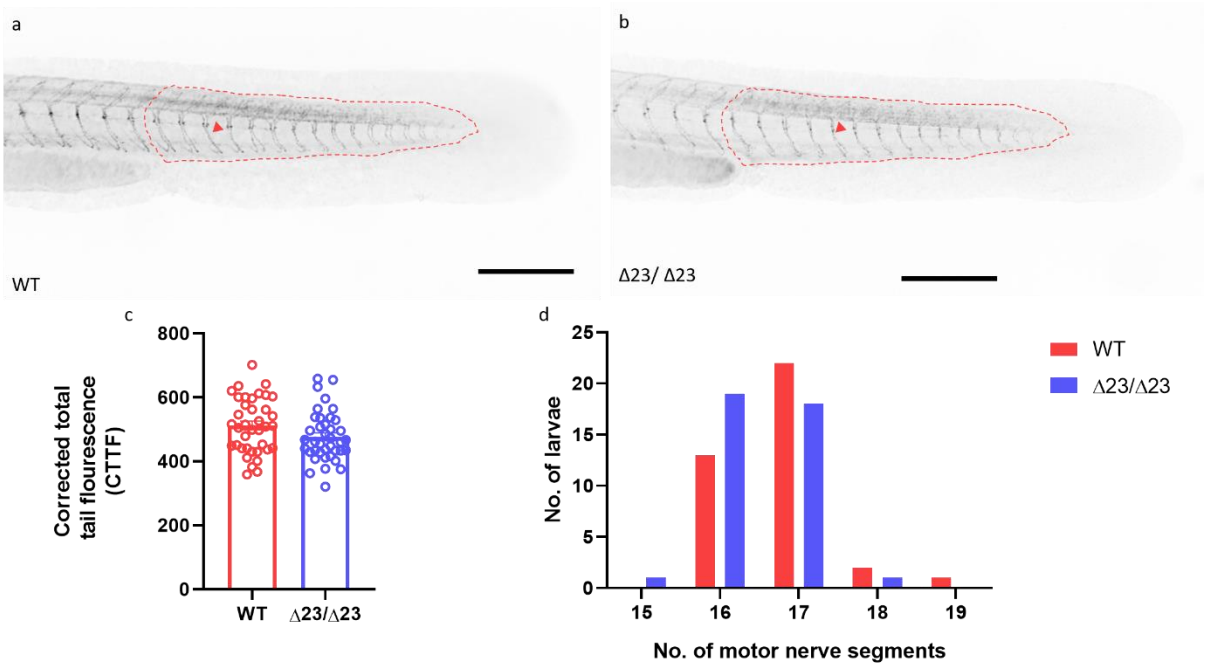

Figure 3.8- A subtle reduction in znp-1 staining could contribute to the swimming deficits seen in *samhd1*$^{\Delta 23/\Delta 23}$ larvae

a+b) Representative images from the trunk region of WT and *samhd1*$^{\Delta 23/\Delta 23}$ embryos at 2 dpf, stained with a znp-1 antibody and imaged laterally on a Leica M205 FA upright stereomicroscope. Red dotted line marks the area where fluorescence was measured, and also where the number of motor nerve segments were counted. Red triangle indicates a motor nerve segment. n= 7-8 larvae per group, with 5 biological replicates. Scale bar= 250 µm. Images processed and inverted on Image J, after the fluorescence was measured c) The CTTF was measured in WT *samhd1*$^{\Delta 23/\Delta 23}$ embryos. Data analysed by an unpaired t test, and presented as mean ± SEM. d) Number of motor nerve segments within marked area for WT and *samhd1*$^{\Delta 23/\Delta 23}$ embryos.

3.2.5 The Janus Kinase inhibitor ruxolitinib does not rescue microcephaly or brain cell death phenotypes in *samhd1*$^{\Delta 23/\Delta 23}$ embryos

The JAK pathway is activated following type I IFN binding to IFNAR receptors, and results in the transcription of ISGs (see introduction Fig.1.1 for schematic of pathway). As a result, it is an ideal pathway to target in AGS and other type I interferonopathies to block the signal transduction following IFN binding to the receptor. This is the mechanism of action by which JAK inhibitors exert their effects, and as such, JAK inhibitors have been identified as a potential treatment for a number of type I interferonopathies, including AGS (Vanderver et al., 2020). Therefore, we assessed whether the JAK inhibitor, ruxolitinib, was capable of rescuing the microcephaly and brain cell death phenotypes observed in the *samdh1*$^{\Delta 23/\Delta 23}$ embryos. Embryos were treated with 2 µM of ruxolitinib via water bath incubation from 6-48 hpf. Embryos were subsequently fixed for either microcephaly measurements or TUNEL staining. Ruxolitinib treatment did not affect either phenotype (Fig 3.9). However, given that ruxolitinib treated WT embryos did not develop a significant increase in cell death or microcephaly, it suggests that the drug was safely tolerated in the zebrafish embryos, but did not exert any beneficial effects.

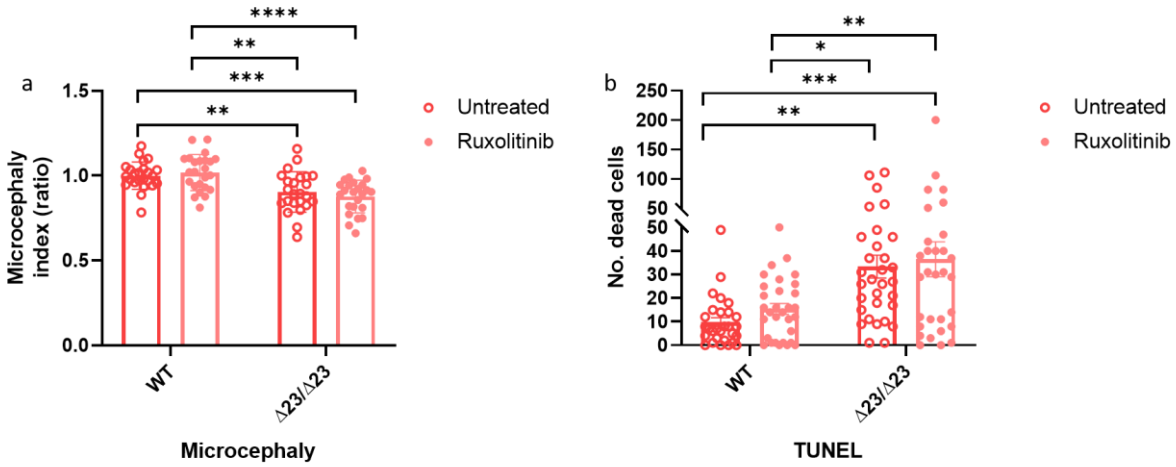

Figure 3.9- The JAK inhibitor ruxolitinib does not rescue the cell death or microcephaly phenotypes observed in *samhd1* $^{\Delta 23/\Delta 23}$ larvae

Ruxolitinib was added to E3 media from 6- 48 hpf. Afterwards embryos were fixed for microcephaly measurements or TUNEL staining a) The microcephaly index was calculated based on distance between eyes and full body length in 48 hpf fixed embryos. Data was analysed with a two- way ANOVA with tukey post hoc analysis (**P=<0.01, ***P=<0.001, ****P=<0.0001) Data presented as mean ± SEM b) Number of dead cells determined by TUNEL staining of 48 hpf fixed embryos. Data also analysed with a two way ANOVA with tukey post hoc analysis (*P<0.05, **P<0.01, ***P<0.001). Data presented as mean ± SEM.

3.3 Discussion

The primary aim of this study was to generate and characterise a stable mutant zebrafish model of AGS5 as a continuation of the work performed previously in the lab with the transient *samhd1* morphant model. The morphant exhibited both classical AGS symptoms, with the increase in ISG expression and type I IFN producing cells, whilst also producing a cerebrovascular phenotype frequently observed in AGS5 patients (Kasher et al., 2015). (N.B: Identification and characterisation of the sub-type specific phenotypes in *samhd1*$^{\Delta 23/\Delta 23}$ is the subject of chapter 4.)

Prior to publication of the *samhd1* morphant, AGS modelling had been performed solely in mice, resulting in a range of phenotypes across all sub-types. *Samhd1*$^{-/-}$ mice appeared healthy, with only a mild ISG phenotype in the spleen (Behrendt et al., 2013; Rehwinkel et al., 2013). Similarly *Trex1*$^{-/-}$ mice and *Ifih1*^{gof} mice did not present with any neurological symptoms. They did, however, have severe multi-organ inflammation, particularly myocarditis and nephritis respectively (Funabiki et al., 2014; Gall et al., 2012; Morita et al., 2004; Stetson et al., 2008). On the opposite end of the severity spectrum, *Rnaseh2*$^{-/-}$ and *Adar1*$^{-/-}$ models were not embryonically viable. (Hartner et al., 2004; Mannion et al., 2014; Pokatayev et al., 2016; Reijns et al., 2012; Wang et al., 2004).

As can be ascertained from these murine models, there is not one which manages to phenocopy multiple aspects of the disease, thus making it difficult to utilise these models for translational AGS research. Most importantly, the lack of neurological phenotypes observed questions their effectiveness as true AGS models.

Whilst the aforementioned *samhd1* morphant model was novel in displaying neurological phenotypes, there are many reasons why MOs are not used in the long term study of disease. Their effects are transient as MOs cannot permanently integrate into the genome, thus can only be studied during the first few days following injection. Furthermore, off-target effects are not uncommon, which makes it difficult to state that phenotypes identified are directly correlated to the effect of one targeted gene (Bedell et al., 2011). To increase the validity of these MO models, guidelines have been published with the gold standard being to phenocopy a MO model with a stable mutant line (Eisen and Smith, 2008; Stainier et al., 2017). This is the route we took to validate the model and to further demonstrate that zebrafish represent the most useful model organism for pre-clinical AGS research.

The *samhd1* line was generated using CRISPR-Cas9, where exon 4 was targeted. This exon is in the same location of the splice site MO to maintain consistency. Several human mutations have also been identified in exon 4 of the *SAMHD1* gene, thus also providing clinical relevance (Rice et al., 2009). The 23 bp deletion was successful in significantly reducing the expression levels of *samhd1* in the homozygous mutant zebrafish larvae. Unfortunately, this loss in gene function was not able to be confirmed in protein level, due to issues with the samhd1 antibody, which had worked previously for the *samhd1* morphant paper (Kasher et al., 2015). This loss of effectiveness may be due to inter-batch variation, and, as a result, we were unable to successfully measure samhd1 levels in the zebrafish larvae. Therefore we had to make the assumption that the significant reduction in transcript

would also equate to loss in protein levels. Based on the amino acid sequence of the mutant samhd1 protein, a premature stop codon after the 23 bp deletion in exon 4 of the *samhd1* gene generated a truncated amino acid sequence, further suggesting a loss in samhd1 protein. Moreover, the mutated amino acid sequence does not contain the predicted HD domain, which is responsible for the enzymatic properties of samhd1 (Beloglazova et al., 2013). Taken together this implies that if any truncated forms of the protein are produced, they would be non-functional. It would have been useful to confirm this by measuring the dNTPase activity in the *samhd1*$^{\Delta 23/\Delta 23}$ model.

Overall, the resulting mutant zebrafish were viable and healthy on appearance, with no breeding issues observed in homozygotes.

The first phenotype characterised in the mutant was the type I IFN response, which is one of the most important hallmarks of AGS, and was successfully phenocopied in the *samhd1* morphants. As aforementioned, we used a different method of sample preparation in this study compared to the *samd1* MO paper. This being the use of RNA extracted from larval heads instead of whole larvae, thus we are unable to make direct comparisons between the models, due to the difficulties associated with identifying an ISG response from whole larval RNA in the *samhd1*$^{\Delta 23/\Delta 23}$ model. Therefore, we chose to isolate larval heads for the ISG measurements, which also established additional clinical relevance, as evidence suggests higher levels of type I IFN are present in the CSF of AGS patients, when compared to the periphery (Lodi et al., 2021).

Our data exhibited large variation across multiple replicates, and as such we were unable to confirm a consistent and statistically significant ISG phenotype. However, it is obvious that a portion of the larvae do express large quantities of a number of ISGs, when compared to the WT larvae. In the future to look more closely at the expression patterns of individual larvae, we could perform in-situ hybridisation of different ISGs, which would provide a more accurate picture of the intra-larval variation.

The environment may contribute to the variation observed. A novel picornavirus has recently been identified in multiple research aquaria around the world, including the Manchester Biological Services Unit (Balla et al., 2020). The presence of a virus would undoubtedly affect any investigation into antiviral immune signalling, as any infected fish would begin to mount an antiviral type I IFN response (*ifnphi* in zebrafish). Thus this would act as a confounding factor for researching the *samhd1*$^{\Delta 23/\Delta 23}$ model. It has not yet been ascertained whether any of the WT or *samhd1*$^{\Delta 23/\Delta 23}$ fish are infected, and as such, further investigation is required.

Aside from environmental factors, one potential reason for the discrepancy observed between ISG expression in the mutant and morphant could be that the MO did induce a large ISG response as an off-target effect. This is due to a large transcriptomic study researching the common genetic signatures of MO injected zebrafish, which highlighted increased expression of several ISGs (Lai et al., 2019). However, the only ISG in that study which was also measured in the *samhd1* MO was *isg15*, and so does not account for the increase in other genes.

Another possibility could be the result of a phenomenon known as genetic compensation. This biological process accounts for the differences in severity of phenotypes between MO and mutant models, with the MO generally producing a more severe response. It is hypothesised that this occurs due to the presence of maternally provided wild-type mRNAs within the yolk sac, which may be able to compensate for the loss of gene function. By contrast, the translation of these mRNAs can be blocked by MOs, hence the more severe phenotypes, and could potentially explain why the samhd1 MO model exhibited a large ISG response in whole larvae, compared to *samhd1*$^{\Delta 23/\Delta 23}$ larvae (Stainier et al., 2017).

Alternatively, the loss of gene function evoked by germline mutation can, with time, cause direct upregulation of other genes to compensate for the loss (Rossi et al., 2015). This may be what we are experiencing with the *samhd1*$^{\Delta 23/\Delta 23}$ model and rather than excessive uncontrolled ISG responses, a negative regulator of type I IFN and ISGs is upregulated to control the levels. To further investigate genetic compensation, there are several experiments which could be performed, including RNA sequencing, to compare gene expression levels between the mutant and morphant. In particular, the expression of SOCS genes could be examined. Alternatively, western blotting could be performed to determine the presence of phosphorylated stat2 protein, which could also act as a negative regulator of the type I IFN signalling pathway. However, finding a stat2 antibody which works in zebrafish may be problematic.

Another difficulty associated with characterising the type I IFN phenotype was the inability to use the Tg(*ifnphi1*:mCherry) transgenic line (Kasher et al., 2015; Palha et al., 2013). This is due to the large variation found in the number of *ifnphi1* positive cells in WT untreated larvae, whereby within the same clutch a single larvae could present with > 200 positive cells, and another larvae with <10, thus questioning the reliability of the line. However, this may also be related to potential picornavirus infection, where further investigation is required.

Zebrafish possess four IFN genes equivalent to mammalian type I IFN: *ifnphi1-4*, whereby *ifnphi1* and *ifnphi3* are the only two expressed in zebrafish at the larval stages (Langevin et al., 2013). This reporter line enables all *ifnphi1* expressing cells to be identified through fluorescence as a result of mCherry expression, thus generating a dynamic model, whereby the location and identity of the cells can be established through live-imaging and FACS-sorting (Kasher et al., 2015; Palha et al., 2013). This is an experiment which should be re-visited in the future on the *samhd1*$^{\Delta 23/\Delta 23}$ mutant line.

Two neurological symptoms were successfully phenocopied from AGS patients to the *samhd1*$^{\Delta 23/\Delta 23}$ model: microcephaly and enhanced brain cell death. Microcephaly is not unique to AGS, but is commonly attributed to range of neurodevelopmental disorders, and can be measured in zebrafish embryos (Faundes et al., 2021). The increase in brain cell death observed in *samhd1*$^{\Delta 23/\Delta 23}$ embryos could be indicative of cerebral atrophy, or a more general readout for brain damage.

A link between microcephaly and brain cell death in zebrafish models of disease has been suggested previously. It was hypothesised that observing both microcephaly and brain cell death is the result of secondary microcephaly, whereby postnatal reduction of dendritic processes, myelination and

synaptic connections cause microcephaly (Stankiewicz et al., 2017). This aligns with the phenotypes found in the *samhd1*$^{\Delta 23/\Delta 23}$ model, and also AGS patients who develop progressive microcephaly after birth, rather than in utero (Crow et al., 2015) . This also fits with a cerebral atrophy phenotype, despite not observing a reduction in the expression of a number of brain markers, especially *elavl3* and *nptx2a* which are neuronal markers. It was hypothesised that a reduction in neurons, due to excessive cell death, would reduce neuronal marker expression, alongside *pcna* expression, which is a cell proliferation marker. Additional co-stains should be performed in the future with the TUNEL stain to elucidate the cell type/s undergoing increased cell death within the brain.

One common way in which neurological disability can manifest is though motor skill deficits. In AGS these can range from spastic paraparesis, to global developmental delay (Adang et al., 2020). To assess motor function in the zebrafish, larval swimming was tracked over a 10 minute period using the DanioVision software. A three day time course was initiated from 3- 5 dpf to determine whether any effect on swimming was observed consistently. At 3 dpf there was no difference between either group, likely a result of the lack of movement from both WT and *samhd1*$^{\Delta 23/\Delta 23}$ larvae. At 4 dpf a significant reduction in swimming was observed, suggestive of a motor deficit. Interestingly, this deficit did not persist beyond this time point, suggesting motor dysfunction is transient and can resolve quickly. One potential explanation could be a result of the regenerative capabilities of zebrafish larvae, and whilst the larvae are continuing to develop, neurological disabilities may be ameliorated. This would also provide rationale for why *samhd1*$^{\Delta 23/\Delta 23}$ zebrafish grow into healthy, viable breeding adults. In the future, the TUNEL stain and microcephaly should also be measured at later time points, such as 5 dpf, to determine whether other associated phenotypes resolve as the larvae develop, which would indicate a very small window of pathology within this model.

Whilst the brain cell death and microcephaly may account for the motor deficits, we hypothesised that spinal motor neurons may also be playing a role in the reduction of movement. The znp-1 antibody was applied to stain motor neurons along the spinal cord, and to also assess branching of the caudal primary motor neurons, where several segments could be viewed from the areas analysed. Whilst not significant, a trend towards a decrease in the fluorescence intensity in the mutants was observed compared to the WTs, coupled with a higher number of mutants exhibiting less motor neuron segments from the cloaca to the tip of the tail. However, this is not enough evidence to suggest these subtle phenotypes are a cause for the locomotion deficits found at 4 dpf. In the future, it would be useful to co-stain with TUNEL to see whether increased cell death was found amongst the neuronal tracts of the mutants. Moreover, znp-1 staining was performed on 2 dpf embryos, to corroborate with the other neurological phenotypes, therefore, staining at 4 dpf would be useful to make direct comparisons between the significant reduction in movement and motor nerve staining.

AGS has been referred to as the most common leukodystrophy which presents with intracranial calcifications, thus representing another important diagnostic factor (Tonduti et al., 2018). However, intracranial calcifications were not identified in the *samhd1*$^{\Delta 23/\Delta 23}$ larvae. This could be due to some issues with study design, which could be improved upon in the future. Firstly, calcification is not

widespread in zebrafish until after 5 dpf, suggesting that the staining was not successful because the levels of calcium in the cranium, if any, were too low to be detected. This could have been confirmed further by performing other known calcium and mineralisation stains such as alizarin red and van kossa to increase the chances of observing any form of ectopic calcifications at that early time point (Apschner et al., 2014). Furthermore, calcein staining in larvae older than 5 dpf would be useful to determine the presence of calcifications as the calcium levels in the fish increase. However, we ultimately believe it is important to identify calcifications whilst the zebrafish are still in the larval/juvenile stages, as clinically, intracranial calcifications are found in early childhood (Tonduti et al., 2018).

Since the early 2000's, zebrafish have been utilised as a pre-clinical model for drug screening, due to the ease of drug administration and high reproductive capabilities (Parng et al., 2002). As a result, there have been a number of compounds identified from zebrafish screens which are in/about to enter clinical trials (Cully, 2019). In this study, there was no immediate requirement for a multi-compound screen as JAK inhibitors are already approved clinically for the treatment of AGS and other type I interferonopathies. This is, however, not to suggest that in the future broader drug screens will not be utilised in the *samhd1*$^{\Delta 23/\Delta 23}$ model.

The JAK inhibitors have generally been shown to possess beneficial effects in relieving multiple symptoms in AGS- in particular the skin inflammation and ISG scores (Vanderver et al., 2020). Neurological improvement is mixed, and likely a result of the heterogeneity of the condition which can lead to differential disease progression (Hadjadj et al., 2021). Given this initial success of JAK inhibitors in treating AGS patients, we sought to treat the *samhd1*$^{\Delta 23/\Delta 23}$ embryos with JAK inhibitors.

Due to the *samhd1*$^{\Delta 23/\Delta 23}$ model not possessing any skin lesions, or a consistent, robust ISG phenotype, it was the neurological phenotypes that the rescue experiments aimed to target, with the knowledge that JAK inhibitor effectiveness was already varied with these phenotypes clinically. Ruxolitinib was the JAK inhibitor used in this study, due to previous effective use in zebrafish (although not for treatment of a type I interferonopathy) (Lim et al., 2016). The drug was not successful in reducing head cell death or rescuing the microcephaly phenotype, however ruxolitinib also did not exacerbate these effects, indicating that the drug is safely tolerated in zebrafish. However, there are several limitations to this experiment. Firstly, there is no confirmation that the drug was taken up successfully by the fish. Ideally, ISG expression between untreated and treated embryos would have been measured as a control, however this wasn't feasible due to the large variation between ISG expressions observed in *samhd1*$^{\Delta 23/\Delta 23}$ larvae. Alternatively, we could have measured the levels of different components downstream of JAK, such as the transcription factor IRF9, and the ISGF3 complex, via western blotting.

Secondly, DNA damage rather than IFN signalling has recently been hypothesised to be the cause of neural dysfunction in a neuro-progenitor conditional *Rnaseh2b*$^{-/-}$ mouse model (Aditi et al., 2021; Lavin and Yeo, 2021). RNASEH2B and SAMHD1 proteins work via different mechanisms, with mutations resulting in an increase in cytosolic DNA-RNA hybrids, and an accumulation in dNTPs

respectively. Despite these differences, (Aditi et al., 2021) provides the first evidence that the neurological phenotypes identified may not be a direct result of excessive type I IFN release, perhaps explaining why the neurological phenotypes may be so difficult to improve in AGS patients with JAK inhibitor treatment.

To conclude, this study continued the work initiated by the *samhd1* MO model, which enabled us to generate a stable mutant pre-clinical model of AGS. This model also exhibited several clinically relevant phenotypes, with the most interesting being the identification of neurological differences, not previously found in either the *samhd1* morphant, or pre-clinical rodent models, thus validating *samhd1*$^{\Delta 23/\Delta 23}$ zebrafish as a useful and effective pre-clinical model. Whilst ruxolitinib was unable to rescue cell death and microcephaly, we believe this model has the potential to be utilised for other treatment strategies, and for further characterisation of AGS, looking more specifically at the role which *samhd1* plays in the disease progression, and the development of cerebrovascular disease, unique to AGS5 patients.

Chapter 4: Investigating the presence of cerebrovascular disease in the *samhd1*$^{\Delta 23/\Delta 23}$ model

4.1 Introduction

It is currently unknown why AGS patients can develop sub-type specific symptoms. All nine genes possess specific intracellular roles, but, upon mutation, a similar antiviral response is initiated, cumulating in excessive type I IFN production and downstream ISG expression, which is thought to account for the symptoms observed in the disease (Rodero and Crow, 2016). Despite this, key differences have resulted in the further categorisation of AGS1-7 subtypes into five phenotypic groups, reinforcing the heterogeneity of the condition (N:B AGS8-9 are not included in this characterisation due to the recent discovery of *LSM11* and *RNU7*-1 as AGS causing genes). The groups are: 'classical' AGS, found across all sub-types (characterised in the *samhd1*$^{\Delta 23/\Delta 23}$ model in chapter 3); spastic-dystonic syndrome, presenting after 1 year of life, causing neurological regression, or a slower progressive disease development, also found across all sub-types; *ADAR1*-related bilateral striatal necrosis; non-syndromic spastic paraparesis found in *RNASEH2B, ADAR1* and *IFIH1* patients; and *SAMHD1* related cerebrovasculopathy (Crow et al., 2020).

SAMHD1 related cerebrovasculopathy affects a significant proportion of AGS5 patients, and can manifest in a multitude of ways, including ischaemic and haemorrhagic stroke, aneurysms, stenosis and moyamoya, all of which present in childhood (du Moulin et al., 2011; Ramesh et al., 2010; Thiele et al., 2010; Xin et al., 2011). The known function of SAMHD1 as a dNTPase helps to explain the viral restriction factor and ISG capabilities of the protein, whereby the intracellular dNTP pool is depleted upon viral entry as to not be utilised for viral replication. This function is also essential in cellular homeostasis, necessary for cell cycle progression and cell division (Coggins et al., 2020; Goldstone et al., 2011). However, these roles of SAMHD1 do not easily explain the early on-set cerebrovascular disease identified in AGS5 patients. This alludes to a previously undefined cerebrovascular function for SAMHD1 and a distinct genetic cause of childhood-onset stroke that is not influenced by the common co-morbidities associated with non-syndromic stroke in the general population. As such, studying the role of SAMHD1 within the cerebrovasculature may not only help to elucidate AGS5 pathophysiology, but may provide new insight into genetic risk factors and mechanisms associated with cerebrovascular disease in general.

Whilst a potential explanation for cerebrovascular disease in AGS5 patients could link the detrimental effects of type I IFN and the ISGs to defects within the cerebral vessels, this does not easily explain why these phenotypes are not observed in other AGS subtypes. Interestingly, cerebrovasculopathy has been identified in other rare type I interferonopathies, such as the recently discovered *STAT2* gain of function mutation, whereby haemorrhagic stroke was observed in both patients in the study (Duncan et al., 2019).

Potentially also linked to type I IFN and activation of the innate immune system, a number of viral infections have also been implicated as a risk factor for cerebrovascular disease. This includes CMV, VZV, HSV, HIV and HCV (Adinolfi et al., 2013; Behrouz et al., 2016; D'Ascenzo et al., 2015; Fan et al., 2020; Ji et al., 2012; Nagel and Gilden, 2014; Tseng et al., 2015). The mechanism behind cerebrovascular disease following infection is poorly understood, but has been proposed to involve

endothelial dysfunction, due to damage, inflammation and the activation of immune cells, although further experimentation would help decipher a specific role of type I IFN and the downstream antiviral signalling, which may be contributing to the development of cerebrovascular disease (Elkind et al., 2020). This may also align with AGS5, if a similar mechanism of action is established.

The *Samhd1*$^{-/-}$ mouse models did not display any form of cerebrovascular disease, whilst a significant proportion of *samhd1* morphant zebrafish exhibited spontaneous ICH (Behrendt et al., 2013; Kasher et al., 2015; Rehwinkel et al., 2013). The mechanism behind ICH in the *samhd1* morphant was not elucidated. However, additional zebrafish models of ICH exist, where the mechanisms have been established, such as in *notch3* and *arhgef7b* (encodes βpix) mutants. Mutations in these genes affects the BBB function and vascular stability respectively, cumulating in ICH (Liu et al., 2007; Wang et al., 2014). In addition, a known chemical inducer of ICH in zebrafish larvae is atorvastatin (ATV). ATV reduces *de novo* cholesterol biosynthesis by inhibiting the rate limiting enzyme HMGCR. A reduction in cholesterol and other essential lipids such as geranylgeranyl pyrophosphate (GGPP) reduces the activation of Rho GTPases, which are important regulators of vascular permeability and tight junction formation. Thus, implying that low cholesterol acts to alter the cerebrovascular integrity in the zebrafish model, generating an ICH phenotype (Eisa-Beygi et al., 2013).

Indeed, low cholesterol has been identified as a clinical risk factor for the development of ICH (Chen et al., 2017; Phuah et al., 2016; Sun et al., 2019; Valappil et al., 2012; Wang et al., 2013). This is the inverse of ischaemic stroke, whereby high cholesterol has long been established as a risk factor, as cholesterol acts to facilitate the development of atherosclerotic plaques, resulting in occlusions and blockages within the cerebrovasculature (Boehme et al., 2017).

The underlying mechanisms behind low cholesterol and ICH are unknown, but are proposed to be related to the important structural roles that cholesterol plays within the cell membrane, as a vital component of the phospholipid bilayer, maintaining the integrity and fluidity of the membrane (Grouleff et al., 2015; Simons and Ikonen, 2000). *In vitro* studies have shown cholesterol to play a role in the generation and stabilisation of adheren junctions, which act to regulate the permeability of the endothelial layers, and thus the vasculature (Corvera et al., 2000). Therefore, a reduction in cholesterol could lead to vessel weakness and an increased susceptibility to rupturing (Valappil et al., 2012). Moreover, low cholesterol may promote arterial smooth muscle necrosis, further acting to impair the integrity of the endothelium (Wang et al., 2013)

However, low cholesterol alone is unlikely to be the sole factor that results in ICH, more probable is the presence of additional risk factors, such as hypertension. High blood pressure coupled with weakened endothelium could provide a mechanism for how these patients develop ICH. This is corroborated by >80% of ICH patients with hypocholesterolaemia also presenting with hypertension (Chen et al., 2017; Phuah et al., 2016).

It has been proposed that a systemic inflammatory response prior to the stroke, such as an infection, may contribute to cholesterol dysregulation (Phuah et al., 2016). The antiviral response initiated by type I IFN can act to alter intracellular cholesterol as viruses alter cellular lipid metabolism to facilitate

their replication within cells to meet the anabolic requirements of the viral lifecycle, and to evade host defences (York et al., 2015). If the host can endogenously inhibit the pathway, it can protect the cell and environment by preventing viral entry and replication (Cyster et al., 2014). This is suggested to happen due to the actions of type I IFNs inducing specific ISGs that alter intracellular cholesterol production, including inhibition of the major sterol transcription factor: SREBP to reduce *de novo* cholesterol biosynthesis.

There appears to be a complex relationship between specific risk factors for cerebrovascular disease, which include viral infection/antiviral signalling and cholesterol dysregulation. These factors seemingly can work independently, or synergistically, to result in a stroke phenotype. By utilising the monogenic form of cerebrovascular disease, as observed in AGS5 patients, we may begin to elucidate these underlying mechanisms and start to understand how the more general cerebrovascular risk factors of viral infection and hypocholesterolaemia, can manifest.

In this chapter, we aimed to firstly assess the presence of any cerebrovascular disease manifestations in the *samhd1*$^{\Delta 23/\Delta 23}$ model, and subsequently, to determine a potential mechanism behind the development of cerebrovascular disease. This lead to the identification of a cholesterol dysregulation in the *samhd1*$^{\Delta 23/\Delta 23}$ fish.

Lastly, to establish whether cholesterol dysregulation was a samhd1 specific relationship, which could begin to provide a potential explanation for AGS5 specific cerebrovascular disease in the patients, we next examined cholesterol biosynthesis gene expression across all AGS sub-types with the aim to further understanding of the relationship between antiviral signalling and cholesterol.

4.2 Results

4.2.1 *samhd1*$^{\Delta 23/\Delta 23}$ embryos do not exhibit gross cerebrovascular abnormalities

Following the characterisation of classical AGS symptoms (chapter 3), we next sought to investigate the presence of AGS5 specific cerebrovascular phenotypes in the *samhd1*$^{\Delta 23/\Delta 23}$ model. To begin to establish the presence of these disease phenotypes in the mutant embryos, we first examined the gross cerebrovasculature.

The *samhd1*$^{\Delta 23/\Delta 23}$ mutation was crossed onto the endothelial cell specific transgenic reporter line: Tg(*fli1:*EGFP) to produce *samhd1*$^{\Delta 23/\Delta 23}$; Tg(*fli1:*EGFP) (Lawson and Weinstein, 2002). At 3 dpf, the head regions of Tg(*fli1:*EGFP) (WT) and *samhd1*$^{\Delta 23/\Delta 23}$; Tg(*fli1:*EGFP) positive embryos were imaged dorsally using light sheet microscopy to identify the presence of any gross structural vascular abnormalities (Fig 4.1). This analysis revealed considerable intra-larval variation in cerebrovascular development across both Tg(*fli1:*EGFP) and *samhd1*$^{\Delta 23/\Delta 23}$; Tg(*fli1:*EGFP) groups, making subsequent comparative observations between genotypes difficult.

Interestingly, it appeared that the *samhd1*$^{\Delta 23/\Delta 23}$; Tg(*fli1:*EGFP) embryos possessed a higher density of cranial vessels, when compared to Tg(*fli1:*EGFP) embryos. However, this difference may be attributed to subtle differences in developmental stages, whereby the Tg(*fli1:*EGFP) embryos appeared slightly delayed in comparison to the mutants. However, importantly, key cranial vessels including the prosencephalic artery (PrA), the mesencephalic vein (MsV), and the metencephalic artery (MtA) were observable and no clear differences were identified between genotypes. These vessels were chosen as they are amongst the first to be developed and can be identified from 1.2 dpf (Isogai et al., 2001). As such, from these images alone, we conclude that no detectable gross differences in cerebrovascular architecture exist between Tg(*fli1:*EGFP) and *samhd1*$^{\Delta 23/\Delta 23}$; Tg(*fli1:*EGFP) groups at 3 dpf.

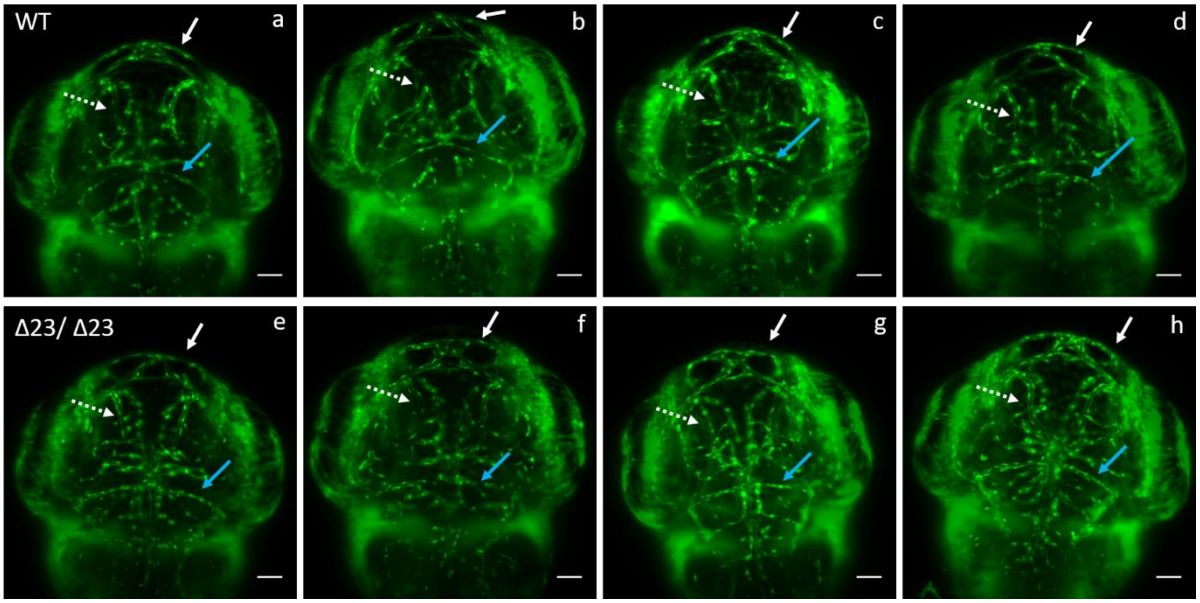

Figure 4.1- No observable cerebrovascular abnormalities are present in *samhd1* $^{\Delta 23/\Delta 23}$; Tg(*fli1*:EGFP) embryos

Tg(*fli1*:EGFP) and *samhd1*$^{\Delta 23/\Delta 23}$; Tg(*fli1*:EGFP) embryos were imaged dorsally at 3 dpf using light sheet microscopy to observe gross cerebrovascular structures, a-d are representative WT embryo images, and e-h *samhd1*$^{\Delta 23/\Delta 23}$ embryo images. n=8 embryos imaged per genotype. Scale bar is 100 µm. The arrows denote a subset of vessels: white solid= prosencephalic artery (PrA), white dashed = mesencephalic vein (MsV), Blue= metencephalic artery (MtA).

4.2.2 *samhd1*$^{\Delta 23/\Delta 23}$ embryos do not have altered cerebral blood flow

Alongside morphological changes to the vasculature being a key indicator of cerebrovascular disease, abnormal patterns of blood flow have also been implicated. It has been hypothesised that high blood flow may be protective against the formation of vascular abnormalities, whilst low blood flow can induce detrimental effects (Rodel et al., 2019). Furthermore, low blood flow can be indicative of blockages within the blood vessels, representative of ischaemic stroke. The optical transparency of zebrafish embryos facilitated cerebral blood flow measurements to be taken from live, anaesthetised animals to investigate blood flow discrepancies at 3 dpf. The DanioScope (Noldus version 1.1.) software was used to determine % flow activity from the DLV and heart rate over a 30 second period (Fig.4.2). We found no difference in blood flow rates across the two genotypes, which was reinforced by the similar heart rates, acting as a global blood flow control. This indicates that the mutant embryos do not exhibit an alteration to cerebral blood flow as a result of *samhd1* mutation. DLV was chosen as the MsV identified in Fig 4.1 drains into the DLV, therefore it acted to further corroborate the lack of cerebrovascular abnormalities described above.

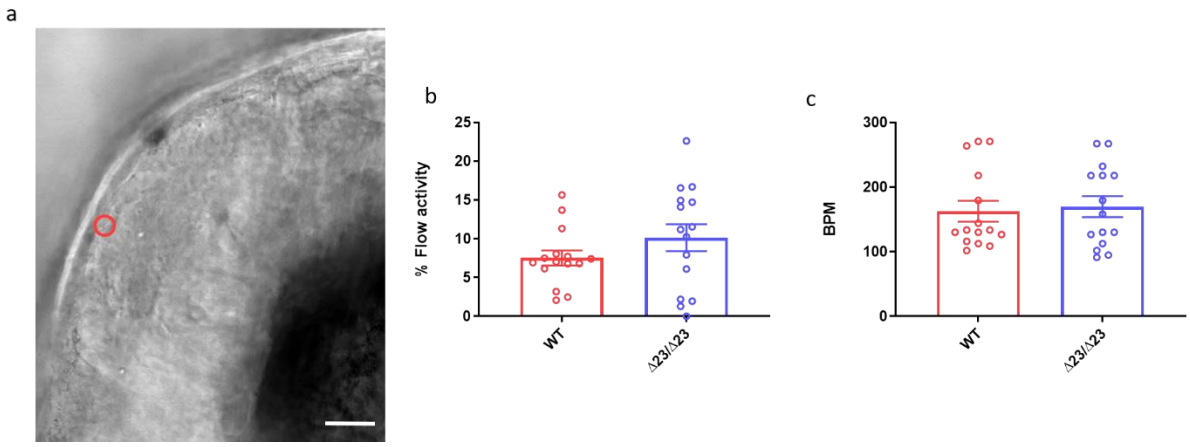

Figure 4.2- *samhd1*$^{\Delta 23/\Delta 23}$ embryos do not have altered cerebral blood flow

Cerebral blood flow was measured in *samhd1*$^{\Delta 23/\Delta 23}$ and WT embryos at 3 dpf. Embryos were briefly anaesthetised with MS222, and light sheet microscopy was used to record blood flow from the DLV for 30 seconds. a) Brightfield screenshot from light sheet microscope video recording, taken with OBS studio. Embryos were recorded in lateral orientation. Red circle marks the recorded region within the DLV. b) Videos from blood flow were analysed using the DanioScope software, where % flow activity was calculated to correspond to cerebral blood flow. n=5 per group, with 3 biological replicates. Scale bar is 100 µm. Data analysed using an unpaired t test, and presented as mean ± SEM. c) Heart rate was obtained as a control for global blood flow. n=5 per group, with 3 biological replicates. Data analysed using an unpaired t test, and presented as mean ± SEM.

4.2.3 A small sub-set of *samhd1*$^{\Delta 23/\Delta 23}$ embryos developed micro-thrombotic events in the brain

We next aimed to characterise the presence of any stroke phenotypes, as AGS5 patients can present with both ischaemic and haemorrhagic stroke (du Moulin et al., 2011; Ramesh et al., 2010; Thiele et al., 2010). Whilst no changes to cerebral blood flow were observed in the mutants (Fig 4.2), the measurements were taken solely from one representative vessel (DLV), therefore ischaemia in other brain regions could not be discounted. As such, to determine the presence of a wider ischaemic stroke phenotype, we chose to examine the whole larval brain. To identify the presence of cerebral thrombi, *samhd1*$^{\Delta 23/\Delta 23}$ and WT embryos were stained with the haemoglobin stain o-dianisidine at 3 dpf (Fig 4.3). Although not observed in any WT embryos, we observed apparent cerebrovascular blockages in 6% of *samhd1*$^{\Delta 23/\Delta 23}$ embryos. Blockages were determined when the staining was thicker than that of individual blood cells within the vessels, as observed in a previously characterised cerebral micro-thrombi zebrafish embryonic model (Zhu et al., 2020). Whilst only encompassing a small percentage of the total embryos imaged, this could suggest a slight pre-disposition of *samhd1*$^{\Delta 23/\Delta 23}$ embryos developing thrombotic events, compared to WT.

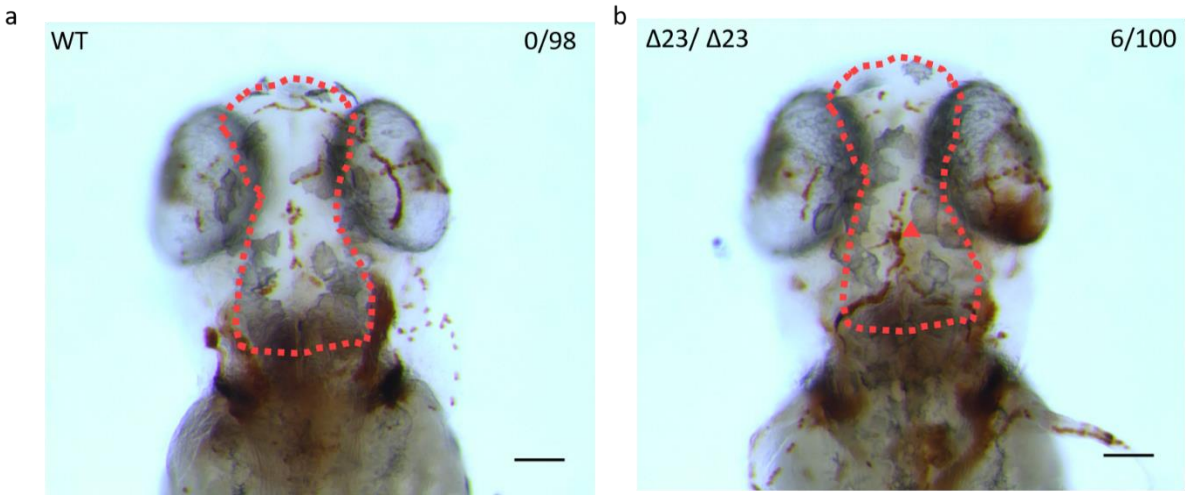

Figure 4.3- A small sub-set of *samhd1*$^{\Delta 23/\Delta 23}$ embryos appear to develop micro-thrombotic events

a+b) Live WT and *samhd1*$^{\Delta 23/\Delta 23}$ embryos were stained with the haemoglobin stain o-dianisidine at 3 dpf, and subsequently post-fixed in PFA prior to imaging on the Leica M205 FA upright stereomicroscope, Scale bar= 50 µm. Red dotted line represents the area of interest, whilst the red arrow denotes possible micro-thrombi in a *samhd1*$^{\Delta 23/\Delta 23}$ embryo. n=98/100 embryos, per group, from one independent experiment.

4.2.4 A small sub-set of *samhd1*$^{\Delta 23/\Delta 23}$ embryos develop spontaneous brain haemorrhages, and the embryos also have an increased susceptibility to haemorrhaging with low dose statin treatment

Next, we sought to investigate the presence of brain haemorrhages in the *samhd1*$^{\Delta 23/\Delta 23}$ model, as ICH is another prominent cerebrovascular manifestation in AGS5 patients (du Moulin et al., 2011; Ramesh et al., 2010; Thiele et al., 2010). Indeed, the *samhd1* MO model exhibited ICH (Kasher et al., 2015), and we too, observed a small proportion (~5%) of *samhd1*$^{\Delta 23/\Delta 23}$ embryos that developed brain haemorrhages under baseline conditions.

Pharmacological inhibition of the HMGCR pathway, using statins, has previously been shown to induce brain specific haemorrhages in zebrafish embryos (Crilly et al., 2018; Eisa-Beygi et al., 2013). The haemorrhages arise due to a reduction in *de novo* cholesterol biosynthesis, as described previously. As only a small percentage of the embryos spontaneously haemorrhaged in the *samhd1*$^{\Delta 23/\Delta 23}$ model at baseline, we next tested whether the *samhd1* mutants may be more susceptible to brain haemorrhage following exposure to a low concentration of ATV. Following water bath incubation at ~30 hpf, ATV induced haemorrhages were consistently identified from ~52 hpf. Overall, the incidence of haemorrhages increased in a dose-dependent manner for both groups, with the highest dose of 1.5 µM causing bleeds in 100 % of embryos in both WT and *samhd1*$^{\Delta 23/\Delta 23}$ groups. Interestingly, compared to WT, there was a significant increase in ICH rates in the *samhd1*$^{\Delta 23/\Delta 23}$ embryos at the lower doses of 0.25 µM ($P<0.05$) and 0.5 µM ($P<0.05$) ATV: 17% versus 38 %, and 63% versus 87% respectively. These data suggest that the *samhd1*$^{\Delta 23/\Delta 23}$ embryos possess an inherent weakness in cerebral blood vessels that is exacerbated following ATV treatment.

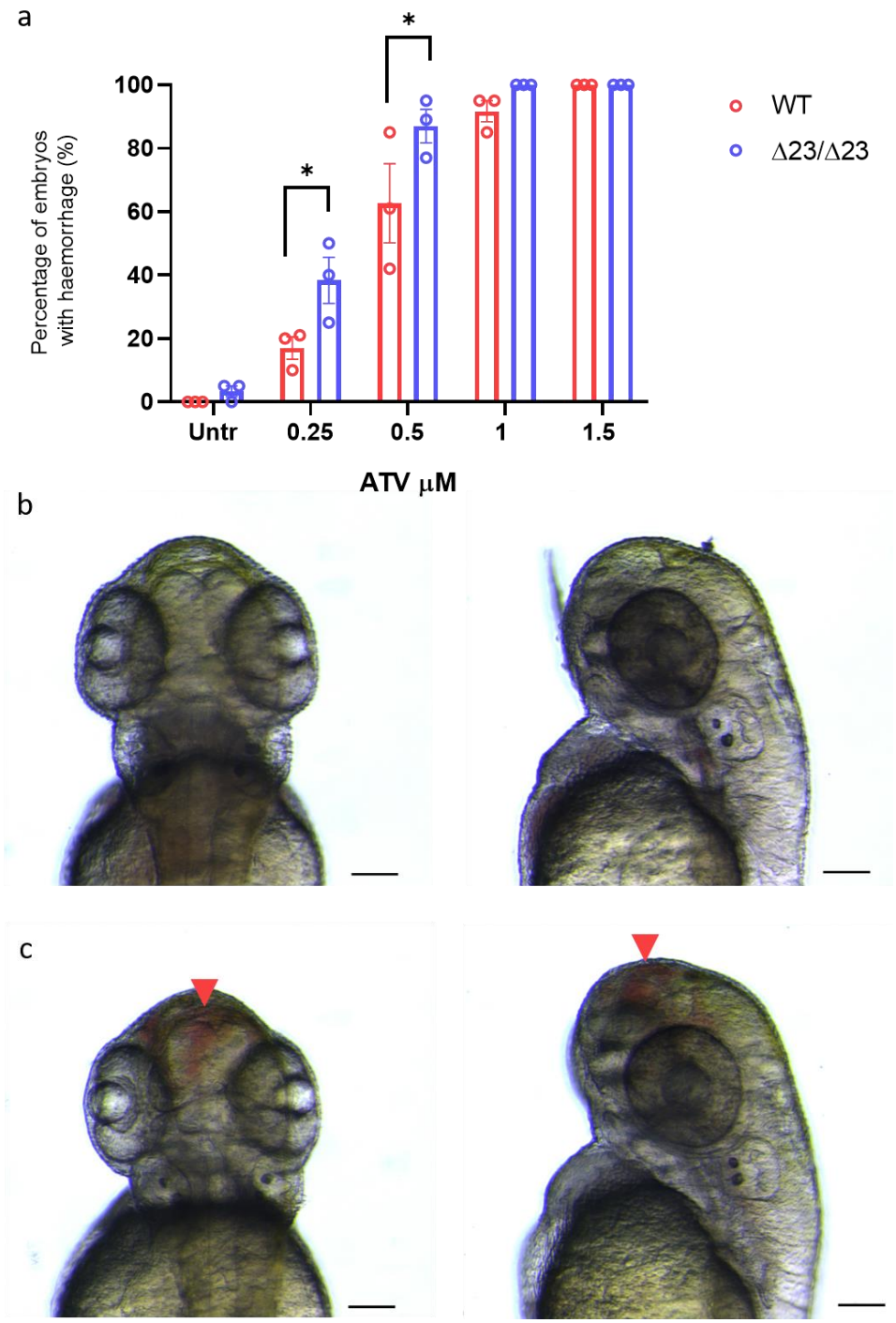

Figure 4.4- *samhd1*$^{\Delta 23/\Delta 23}$ embryos have increased susceptibility to ICH with low dose ATV treatment

a) WT and *samhd1*$^{\Delta 23/\Delta 23}$ embryos were treated with increasing concentrations (0.25-1.5 µM) of ATV added via water bath incubation, and scored based on the presence or absence of blood in the brain. n=20 embryos treated per group, with the percentage of animals per group which developed haemorrhages determined, repeated 3 times. Data analysed using a two-way ANOVA with sidak's multiple comparisons test (*P<0.05). b+c) Representative images taken on Leica M205 FA upright stereomicroscope of dorsal (left) and lateral (right) larval heads without brain haemorrhages (b) and with brain haemorrhages (c). Red arrow denotes haemorrhages. Scale bar is 50 µm.

4.2.5 A subtle cholesterol biosynthesis dysregulation is apparent in *samhd1*$^{\Delta 23/\Delta 23}$ larvae

We next sought to elucidate the potential mechanism responsible for causing increased susceptibility to brain haemorrhage in the *samhd1* mutant. Pharmacological inhibition of *hmgcr* using ATV alluded to a potential involvement of the cholesterol biosynthesis pathway (Eisa-Beygi et al., 2013). This is due to a significantly higher proportion of mutants developing ICH with lower, 'sub threshold' concentrations of ATV, indicating that the mutants may possess a baseline cholesterol deficiency. We postulated that this deficiency could exceed the threshold required for cerebrovascular stability when inhibited further following ATV treatment. We then suggested that samhd1 may possess a relationship with the cholesterol biosynthesis pathway, and upon absence/reduction of samhd1, as found in the *samhd1*$^{\Delta 23/\Delta 23}$ model, it could lead to cholesterol dysregulation, specifically within the cerebrovasculature. To test this hypothesis, we measured the expression levels of a number of cholesterol biosynthesis genes in *samhd1*$^{\Delta 23/\Delta 23}$ larval heads (in order to more closely align with specific cerebrovasculature expression). The cholesterol biosynthesis pathway is complex with multiple arms and a large number of enzymes involved to generate the end product of cholesterol. Therefore, we chose to examine the expression of a number of cholesterol-related enzyme genes from all areas of the pathway as illustrated in Fig 4.5.

The expression levels of the chosen cholesterol biosynthesis genes (*cyp51a1, dhcr24, ebp, hmgcr, msmo1, sqle, srebf1*) were measured using RNA extracted from larval heads (5 dpf). Whilst the expression levels varied between the different biosynthesis genes measured, *dhcr24* expression was significantly reduced in *samhd1*$^{\Delta 23/\Delta 23}$ larval heads by ~50% compared to WT larvae ($P<0.05$), with *hmgcr* and *sqlea* also reduced by a similar amount, although not reaching significance. This potentially reveals a subtle cholesterol biosynthesis dysregulation within the *samhd1*$^{\Delta 23/\Delta 23}$ larvae, although we cannot confirm whether this is a *samhd1* specific event.

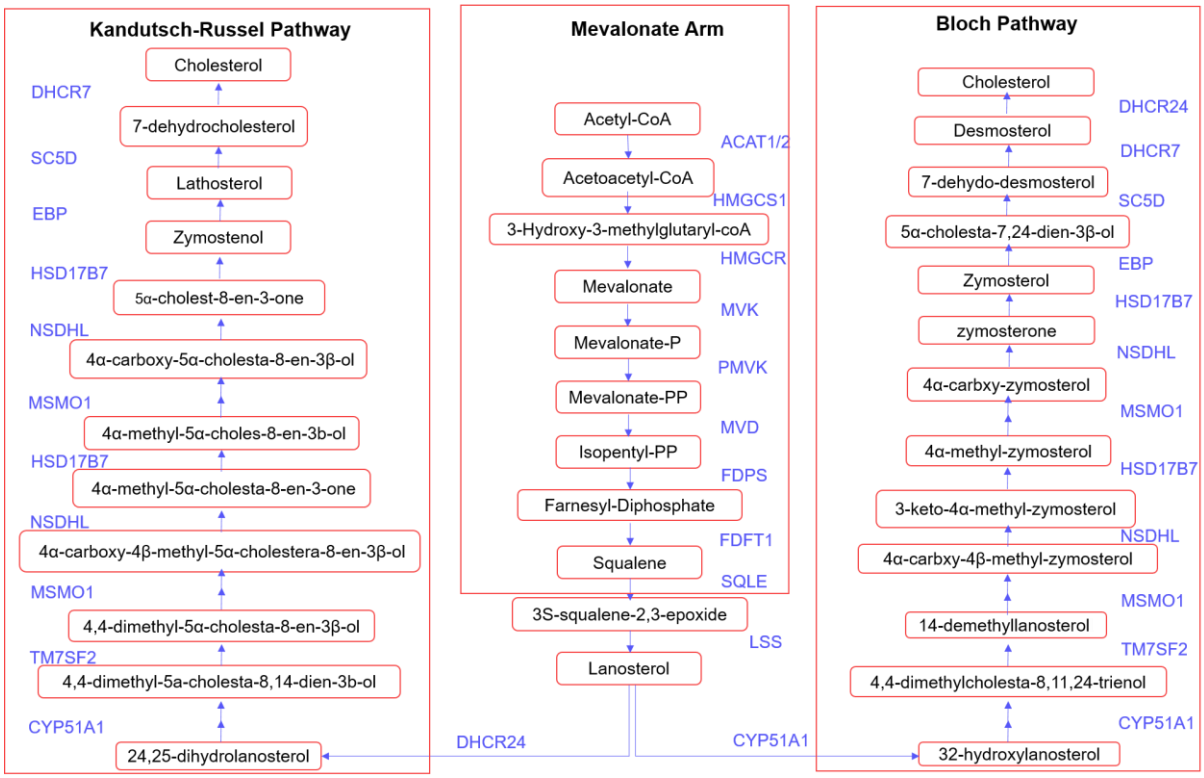

Figure 4.5- Schematic of the cholesterol biosynthesis pathway

The Mevalonate arm of the pathway is required to generate lanosterol, which then enters the Kandutsch-Russel pathway or the Bloch pathway. The enzymes for cholesterol biosynthesis are transcribed following activation of the master sterol transcription factor (SREBP1/2). Several cross-over sites occur along between the Bloch and Kandutsch-Russel pathway, whereby DHCR24 is utilised to enhance usage of the Kandutsch-Russel pathway (Mitsche et al., 2015). Figure adapted from (Robertson et al., 2016).

Abbreviations: ACAT1/2: acetyl-coenzyme A acetyltransferases; HMGCS1: 3-hydroxy-3-methylglutaryl-coA synthase 1; HMGCR: 3-hydroxy-3-methylglutaryl-coA reductase; MVK: Mevalonate kinase; PMVK: Phosphomevalonate kinase; MVD: Mevalonate diphosphate decarboxylase; FDPS: Farnesyl diphosphate synthase; FDFT1: Farnesyl-diphosphate farnesyltransferase 1; SQLE: Squalene epoxidase; Lanosterol synthase; DHCR7: 7-dehydrocholesterol reductase; SC5D: Stearoyl-CoA desaturase 5; EBP: 3beta-hydroxysteroid-delta 8, delta 7-isomerase; HSD17B7: Hydroxysteroid 17-beta dehydrogenase 7; NSDHL: NAD(P) dependent steroid dehydrogenase-like; MSMO1: Methylsterol monooxygenase; TM7SF2: delta 14-sterol reductase; CYP51A1: Cytochrome P450 family 51 subfamily A member 1.

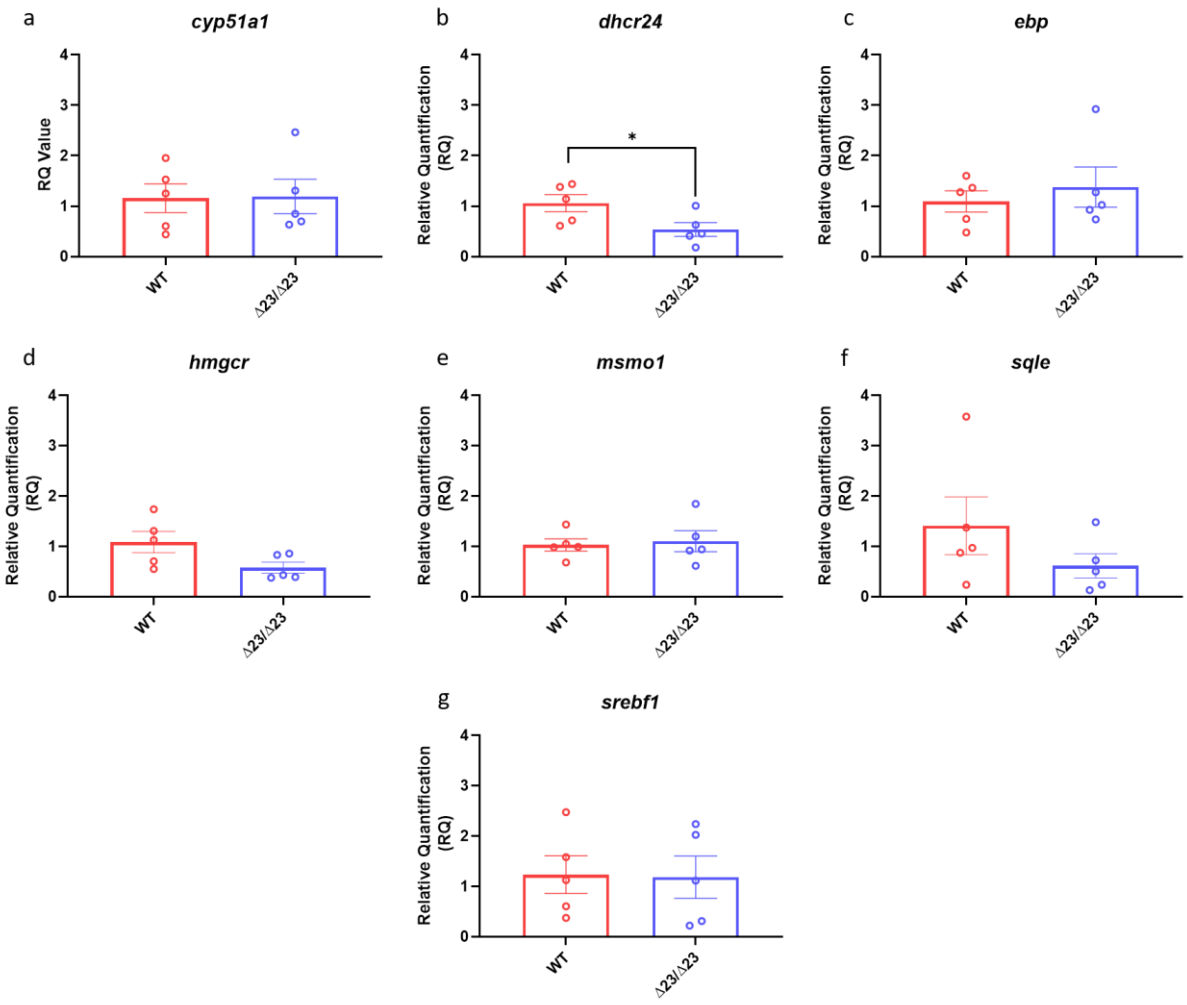

Figure 4.6- *samhd1*$^{\Delta 23/\Delta 23}$ larvae possess a subtle cholesterol biosynthesis dysregulation

a-g)- RNA was extracted from *samhd1*$^{\Delta 23/\Delta 23}$ and WT larval heads at 5 dpf, with n= 30 heads per group, per biological replicate, repeated 5 times. A panel of Taqman probes targeting a series of cholesterol biosynthesis genes were used: *cyp51a1, dhcr24, ebp, hmgcr, msmo1, sqlea, srebf1*. Expression was normalised to the housekeeper gene *hprt1*. Data analysed using an unpaired t test (*P<0.05) and presented as mean ± SEM.

4.2.6 RNA sequencing data reveals a cholesterol biosynthesis dysregulation in AGS patient whole blood

We had proposed that cholesterol dysregulation may provide a novel mechanism for the development of cerebrovascular disease in AGS5 patients, as observed in the *samhd1*$^{\Delta 23/\Delta 23}$ model. However, the relationship between type I IFN and cholesterol dysregulation has been well established in immune cells *in vitro* whereby IFN treatment reduces cholesterol biosynthesis as an antiviral mechanism to inhibit viral entry and replication (Blanc et al., 2011; York et al., 2015). Interestingly, this relationship has also been observed clinically, in patients undergoing IFN treatment for HCV, cancer and multiple sclerosis (MS) (Borden et al., 1990; Coppola et al., 2006; Shinohara et al., 1997). Thus suggesting that cholesterol dysregulation may be IFN specific, not SAMHD1 specific, and so could be identified across all AGS sub-types. This led us to investigate the relationship between type I IFN and cholesterol in AGS1-7 patients, who suffer from excessive type I IFN production and a subsequent ISG signature.

Following acquisition of AGS1-7 patient whole blood, RNA was extracted for RNA sequencing analysis. The RSEM software was used to compute TPM values for each cholesterol biosynthesis gene, across the AGS1-7 patients. All genes encode enzymes found across the entirety of the cholesterol biosynthesis pathway (see Fig 4.5): *ACAT2, CYP51A, DHCR7, DHCR24, EBP, HMGCR, HMGCS, HSD17B, LSS, MSMO1, MVD, NSDHL, SC5D* and *SQLE.* Of the 14 genes examined, *ACAT2, CYP51A, DHCR24, EBP, HSD17B, MSMO1, MVD, NSDHL* and *SC5D* were all found to be significantly upregulated in patients *with ADAR1, RNASEH2A,2B,2C* or *SAMHD1* mutations (Fig 4.7 and Fig 4.8). Overall, *SAMHD1* patients exhibited upregulation in eight genes, followed by *RNASEHB/C* patients with seven genes, *ADAR1* patients with six genes, and *RNASEH2*A with one gene. Whilst *IFIH1* patient data has been included in Fig 4.7 and 4.8, the small sample size (n=2), meant it was excluded from any statistical analysis. Given what has been alluded to within the literature, this upregulation of cholesterol biosynthesis gene expression is the inverse of what was hypothesised to occur following chronic type I IFN exposure.

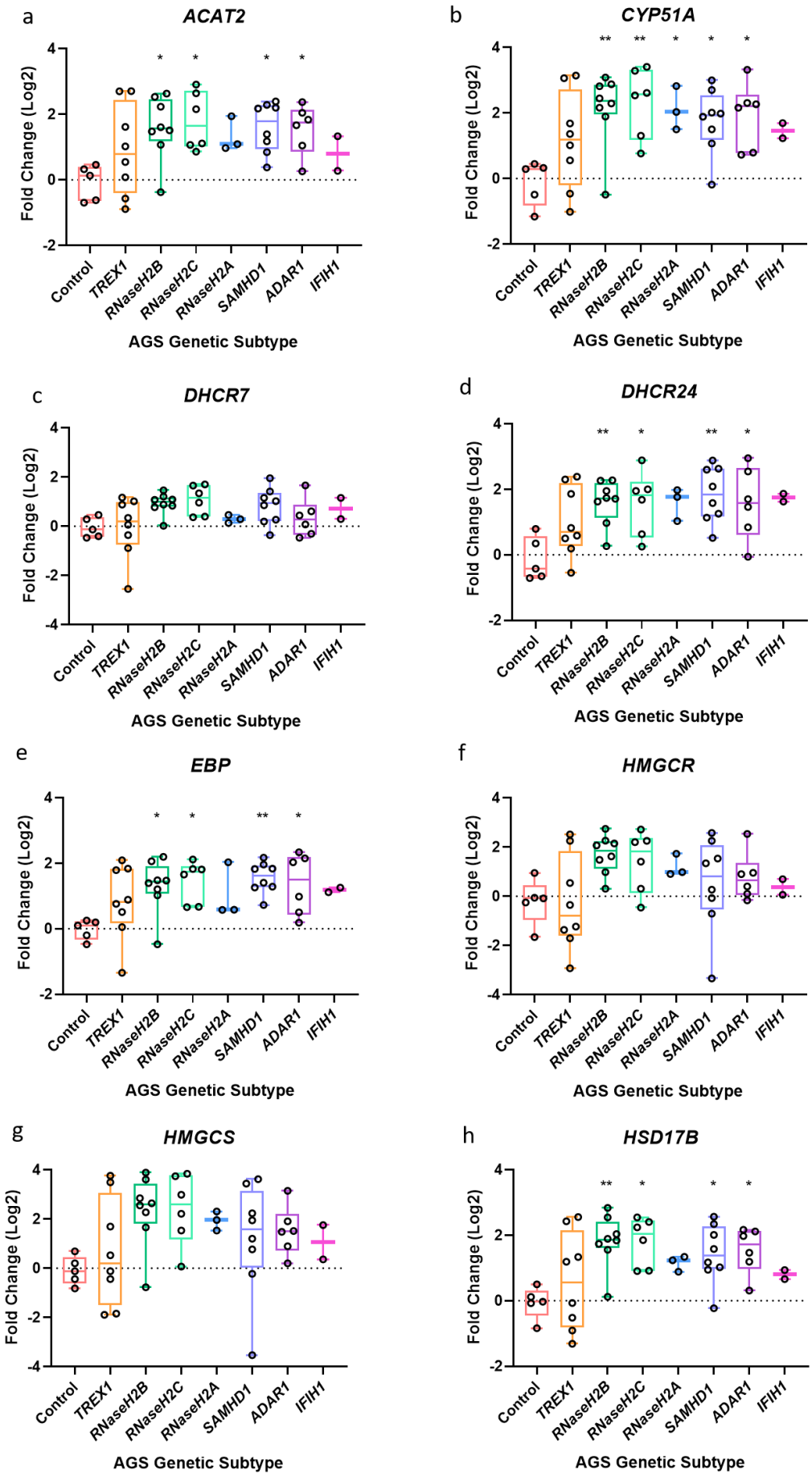
a
ACAT2
b
CYP51A
c
DHCR7
d
DHCR24
e
EBP
f
HMGCR
g
HMGCS
h
HSD17B
Fold Change (Log2)
Control
TREX1
RNaseH2B
RNaseH2C
RNaseH2A
SAMHD1
ADAR1
IFIH1
AGS Genetic Subtype

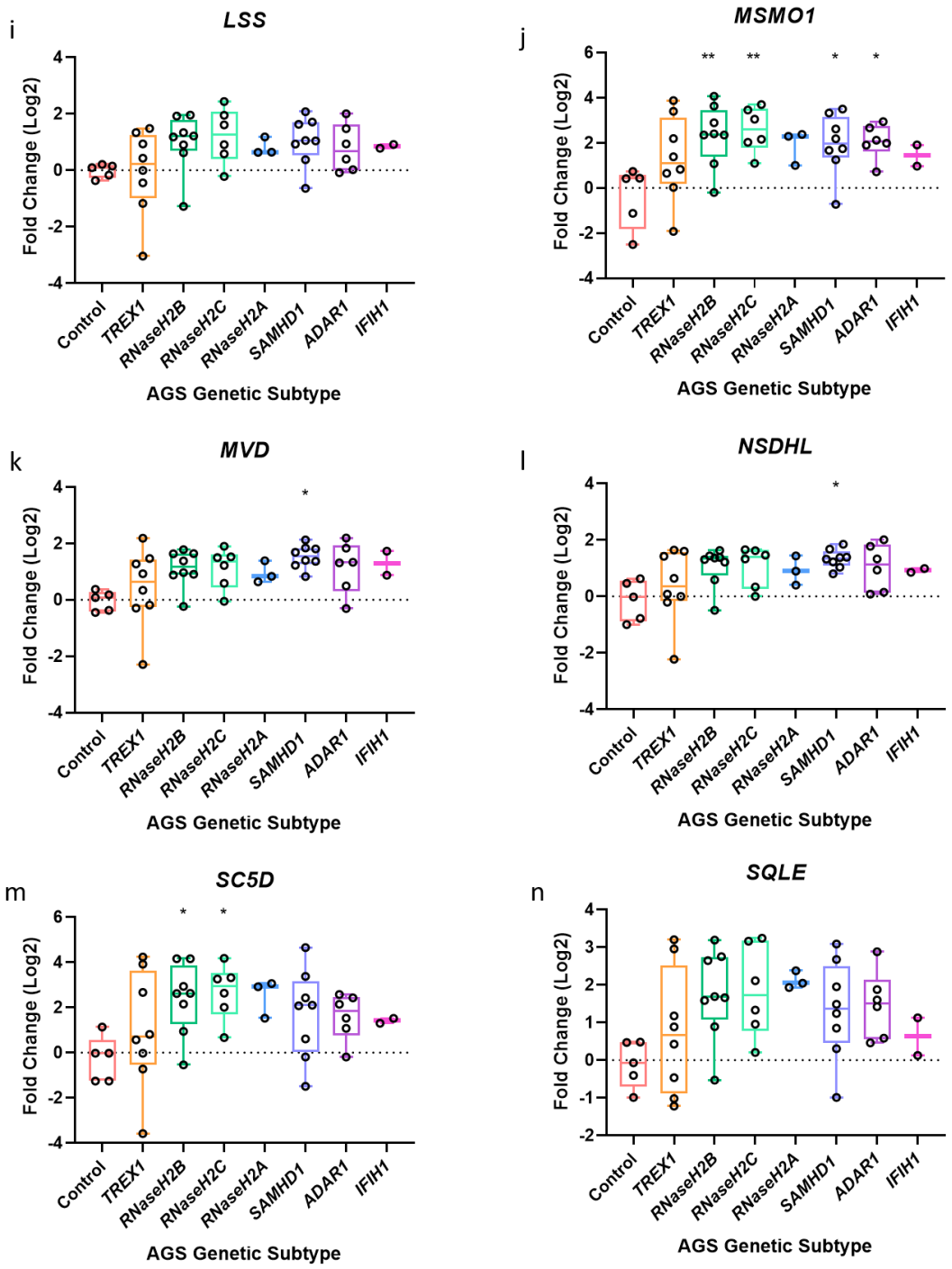

Figure 4.7- RNA sequencing data reveals an increase in cholesterol biosynthesis gene expression observed in AGS1-7 patients

RNA from AGS1-7 patient whole blood was analysed using the RSEM software to determine the TPM of each cholesterol biosynthesis gene, for the AGS patients. Data was then normalised to an age-matched control group, and transformed into log2 before plotting. a-n) box and whisker plots for the expression of *ACAT2, CYP51A, DHCR7, DHCR24, EBP, HMGCR, HMGCS, HSD17B, LSS, MSMO1, MVD, NSDHL, SC5D, SQLE* in AGS1-7 subtypes. Sample sizes for each AGS subtype, n=5 control, n=8 *TREX1*, n= 8 *RNaseH2B*, n=6 *RNaseH2C*, n=3 *RNaseH2A*, n=8 *SAMHD1*, n=6 *ADAR1*, n=2 *IFIH1*. Data analysed using a one way ANOVA, with Dunnetts multiple comparison test, only comparing each AGS gene with the control group. (*P <0.05, **P <0.01).

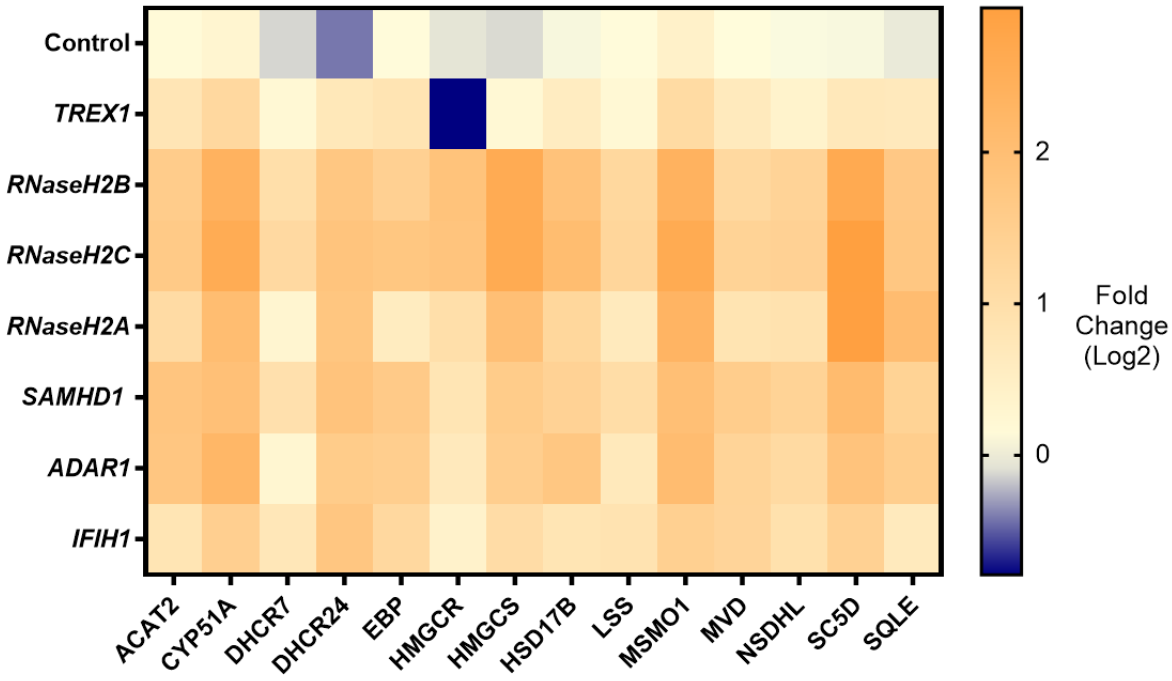

Figure 4.8- Heat map of cholesterol biosynthesis gene expression across AGS1-7 patients

RNA sequencing Fold Change (Log2) data from Fig 4.6 was applied to produce a heat map for visualisation of expression differences in each AGS subtype compared to age matched control group. The median Fold Change (Log2) value was used to plot the heat map points for each cholesterol biosynthesis gene from the AGS1-7 subtypes.

4.3 Discussion

Cerebrovascular disease is frequently observed in AGS5 patients (Crow et al., 2015; du Moulin et al., 2011; Ramesh et al., 2010; Thiele et al., 2010). As such, it has been hypothesised that this phenotype reveals an uncharacterised role of the SAMHD1 protein relating to vascular homeostasis (Kasher et al., 2015; Ramesh et al., 2010). The aim for this chapter was to assess whether cerebrovascular defects were detectable in the *samhd1*$^{\Delta 23/\Delta 23}$ zebrafish model, and if present, begin to elucidate the mechanisms behind cerebrovascular manifestations by utilising the *samhd1*$^{\Delta 23/\Delta 23}$ zebrafish model as a monogenic form of cerebrovascular disease.

Cerebrovascular abnormalities are identified clinically using angiograms, whereby stenosis, aneurysms and moyamoya have been readily observed in AGS5 patients (Ramesh et al., 2010; Thiele et al., 2010). To investigate whether these vasculature changes were also apparent in the zebrafish embryonic vessels, the *samhd1*$^{\Delta 23/\Delta 23}$; Tg(*fli1:*EGFP) transgenic line was employed and imaged using light sheet microscopy. *fli1* encodes for an endothelial cell marker expressed from early developmental stages in zebrafish (Lawson and Weinstein, 2002). The gross cerebrovasculature of the WT and *samhd1*$^{\Delta 23/\Delta 23}$ embryos was compared to that of the developing zebrafish neurovascular anatomy atlas coupled with a study into larval hindbrain development (Isogai et al., 2001; Ulrich et al., 2011).

Overall, we cannot provide firm conclusions based on the images obtained for two main reasons. Firstly, it was apparent that the WT and *samhd1*$^{\Delta 23/\Delta 23}$ embryos were at subtly different developmental stages at the point of imaging, with the mutants appearing more developmentally advanced than the WT embryos- likely attributed to slight differences in timing of egg fertilisation between the two strains. From the rapid development of the cerebrovasculature described in the literature, a 1-2 h delay between WT and *samhd1*$^{\Delta 23/\Delta 23}$ embryos can result in obvious alterations within the cerebrovasculature (Isogai et al., 2001; Ulrich et al., 2011).

Secondly, another experimental error involved the imaging. Rather than dorsally imaging the fish by creating stacks through the whole brain, it would have been preferable to generate two independent image stacks. This would have allowed for a separation between the dorsal and ventral vessels to make them more easily identifiable. As the approach taken was to image the whole brain, from a dorsal perspective, it resulted in the loss of a significant proportion of the ventral cerebrovasculature, thus hindering the ability to directly compare WT and *samhd1*$^{\Delta 23/\Delta 23}$ embryos. As such, future studies should focus on further optimisation of the imaging techniques.

Accordingly, we chose to focus solely on the dorsal vasculature, and identified the PrA, MsV and MtA in both WT and *samhd1*$^{\Delta 23/\Delta 23}$ mutant groups, and noted no obvious abnormalities surrounding these vessels. However, as discussed, more in-depth imaging, coupled with better aligned egg fertilisation should be implemented and this experiment revisited to provide a more definitive answer regarding cerebrovascular abnormalities in the samhd1$^{\Delta 23/\Delta 23}$ model.

Following future studies, if a lack of apparent cerebrovascular abnormalities is maintained, there may be a suitable explanation. An *in vitro* study determining the effect of AGS gene knock-down in brain endothelial cells observed no changes in angiogenesis (Cuadrado et al., 2015a). The group suggested that an intrinsic knockdown of *SAMHD1* and the other AGS genes, was not sufficient to affect the vasculature, instead the high levels of type I IFN within the environment is a more probable explanation for changes observed in endothelial cells, due to the anti-angiogenic properties of the cytokine (Cuadrado et al., 2015a). As discussed in chapter 3, we were unable to directly measure type I IFN levels in the *samhd1*$^{\Delta 23/\Delta 23}$ larvae, and whilst the larvae exhibited a variable, but apparent ISG response, ISGs can be expressed independently of type I IFN, so this indirect read-out may not correlate exactly with type I IFN levels. As a result, it would be useful to revisit type I IFN quantification, to ensure the mutants are producing type I IFN that can interact with the cerebrovasculature.

To assess cerebrovasculature function in the *samhd1*$^{\Delta 23/\Delta 23}$ model, cerebral blood flow was measured, using the DLV as a representative vessel. The MsV identified in the gross cerebrovasculature imaging drains into the DLV, thus we hypothesised that if any vascular abnormalities were missed in the MsV, we would be able to identify them by recording cerebral blood flow downstream of the vessel. Moreover, the DLV is a large, easily distinguishable vessel, and readily identifiable on each embryo to facilitate continuity.

The results highlighted no differences in cerebral blood flow within the DLV. This corresponds to the lack of cerebrovascular malformations observed. In a previous zebrafish model of cerebral cavernous malformations, the abnormalities found in the larvae resulted in a slowing of blood flow, indicating this method is a useful readout for cerebral malformations. (Rodel et al., 2019). However, a caveat with this method was only using one representative vessel to take measurements. A more thorough approach would have been to take multiple vessel measurements across the whole cerebrovasculature to generate a more accurate representation of cerebral blood flow.

Following the lack of cerebrovascular abnormalities found in the *samhd1*$^{\Delta 23/\Delta 23}$ embryos, we next aimed to test for a stroke phenotype. In an attempt to establish a full picture of any ischaemic events in the larvae, the haemoglobin stain o-dianisidine was performed to identify any large accumulations of blood within the vessels, which could be indicative of a micro-thrombi, as previously described in a ponatinib- induced zebrafish larval model of ischaemic stroke (Zhu et al., 2020). Interestingly, a small proportion of *samhd1*$^{\Delta 23/\Delta 23}$ embryos did appear to have a blockage within the vasculature. These blockages were characterised by consistent block staining of a section of a vessel, making it appear thicker or bulging. Due to the small sub-set of the population which did go on possess these thrombotic-like events, we cannot conclude that the *samhd1*$^{\Delta 23/\Delta 23}$ embryos possess an ischaemic stroke phenotype. However, this does suggest that what we observe in the zebrafish model is a large level of heterogeneity, mirroring what is observed in the AGS5 patients with regards to a cerebrovascular disease phenotype.

Haemorrhagic stroke was the last cerebrovascular phenotype characterised. From the *samhd1* MO model, it had been established that transient knock-down of the *samhd1* gene in zebrafish embryos did give rise to a spontaneous haemorrhaging phenotype (Kasher et al., 2015). Whilst a small proportion of *samhd1*$^{\Delta 23/\Delta 23}$ embryos did haemorrhage under baseline conditions, this was a highly reduced frequency than observed in the *samhd1* morphants. However, as discussed in chapter 3, it is not uncommon for MO models to produce more severe phenotypes in comparison to the stable mutant counter-parts (Place and Smith, 2017).

We hypothesised that the stable mutants may possess a more subtle defect within the cerebrovascular unit, which in isolation, is insufficient to cause spontaneous ICH, but may be attributed to an increased proneness to haemorrhage. Following low doses of ATV, we observed an increased susceptibility to developing ICH. ATV causes haemorrhages by inhibiting the rate limiting enzyme in cholesterol biosynthesis (HMGCR), which acts to lower cholesterol and other lipid synthesis within the nascent vessels as previously described, and the lipids have integral structural roles within the vasculature, such as the formation of tight junctions between endothelial cells (Eisa-Beygi et al., 2013). It would have been useful to confirm this mechanism of action in ATV treated embryos in this study, by measuring either cholesterol biosynthesis gene expression, or cholesterol at the lipid level.

As low dose ATV induced ICH occurred with increased frequency in the mutant embryos, it suggested they already possess a weakened cerebrovasculature, potentially due to alterations within the cholesterol biosynthesis pathway, which is exacerbated with the addition of low dose ATV. As a result, we chose to look at gene expression of a number of cholesterol biosynthesis genes. Across the panel of seven genes analysed, *dhcr24* was significantly downregulated compared to WT larvae, with *hmgcr* and *sqle* expression also reduced, although not reaching significance. *dhcr24* has a very important role in cholesterol biosynthesis, as it is the final enzyme that converts desmosterol to cholesterol in the Bloch pathway, and also enhances usage of the kandutsch-Russel pathway to generate cholesterol (Mitsche et al., 2015). Therefore, a significant reduction in this enzyme suggests that less cholesterol is being produced and fits with the hypothesis of lower cholesterol increasing the likelihood of vessel rupture and haemorrhaging in the *samhd1*$^{\Delta 23/\Delta 23}$ model. This should be confirmed by measuring cholesterol lipid levels within the larval heads.

The relationship between low cholesterol and ICH has been identified clinically, where a significant decrease in total cholesterol and LDLs have been measured in the serum of ICH patients (Phuah et al., 2016; Segal et al., 1999; Sun et al., 2019; Valappil et al., 2012; Wang et al., 2013). As a result, hypocholesterolaemia is now a readily accepted clinical risk factor for haemorrhagic stroke. The reason behind the reduction in cholesterol is still unknown, but the main theories suggest either a nutritional deficiency, or a systemic inflammatory response prior to the haemorrhagic event (Phuah et al., 2016; Wang et al., 2013). Such an inflammatory response may be attributed to infection, and interestingly, viral infections are an independent risk factor for ICH, whereby HIV, HCV, HSV and VZV all increase the risk of ICH (Behrouz et al., 2016; Hauer et al., 2019; Nagel and Gilden, 2015;

Nagel et al., 2010; Tseng et al., 2015). It is of note that other infectious agents can cause ICH, and also all the viral infections mentioned can lead to ischaemic stroke. Therefore, the mechanisms behind viral infection leading to stroke are still yet to be elucidated due to the multiple manifestations the same virus can produce.

Viral infections as a risk factor for stroke also align with AGS, whereby the body responds as though it is under constant viral attack- and in AGS5, this can result in both haemorrhagic and ischaemic strokes, which are often fatal. We suggested that SAMHD1 may possess an as yet undiscovered role relating to cholesterol biosynthesis to account for some of the cerebrovascular phenotypes, which are not identified in the other AGS subtypes. However, given the recent identification of a different type I interferonopathy causing ICH in patients (*STAT2* mutation), coupled with the evidence that the antiviral response initiated by type I IFN results in cholesterol dysregulation, it suggests that this mechanism is not SAMHD1 specific. Alternatively, cholesterol dysregulation could be a type I IFN specific event and so cerebrovascular disease in AGS5 patients may be attributed to a different role of the protein (Duncan et al., 2019; Robertson and Ghazal, 2016; Robertson et al., 2016; York et al., 2015; Zhou et al., 2020).

Conversely, cerebrovascular disease could arise due to the differential location of SAMHD1 within the body compared to other AGS genes, causing location specific phenotypes (Rodero and Crow, 2016). Whole tissue microarray from human donors identified SAMHD1 within the vascular endothelium in the CNS, which may provide an explanation for why mutations in SAMHD1 cause cerebrovascular events, due to specific inflammation within the cerebrovasculature (Schmidt et al., 2015). However, before this can be confirmed, the expression patterns of the other AGS genes should also be established. We attempted to identify the expression patterns of *samhd1* in both WT and *samhd1*$^{\Delta 23/\Delta 23}$ embryos using whole-mount in situ hybridisation, however the staining was not successful, and thus is an experiment that should be revisited in the future, to confirm whether samhd1 is found within the cerebrovasculature in the fish.

To confirm whether the cholesterol dysregulation was a SAMHD1-specific effect, or more widely related to IFN signalling, we investigated cholesterol biosynthesis gene expression in AGS1-7 patients. RNA sequencing data from whole blood of AGS patients revealed a significant upregulation in a number of cholesterol biosynthesis genes, this trend being consistently identified across all AGS sub-types, except from *TREX1* patients. Whilst this is an interesting observation, it is of note that the samples sizes used were extremely low. The highest number of patient samples received was eight from *RNASEH2B*, *SAMHD1* and *TREX1* patients, and the lowest was two from *IFIH1* patients (unable to form part of the analysis). Furthermore, only five age matched controls were obtained. The low number of available patients highlights a significant limitation with research on rare diseases, and reinforces the need to generate suitable *in vivo* models of AGS, which can help direct the research and increase disease understanding in a larger sample size than what is available clinically.

The upregulation in cholesterol biosynthesis gene expression in whole blood of AGS patients was the inverse of what was hypothesised to occur. The literature has shown that type I IFN responses

result in a downregulation of cholesterol biosynthesis as an antiviral defence mechanism *in vitro* (Cyster et al., 2014; York et al., 2015). Moreover, HCV patients treated with IFNα exhibited a reduction in serum cholesterol and associated lipoproteins. Interestingly, in this study, there was a significant acute decline in total serum cholesterol following 1-2 weeks of treatment, which then steadily increased back to baseline levels for the remainder of the treatment (Shinohara et al., 1997). This suggests that there may be a difference between acute and chronic time exposure to type I IFN, coupled with differences between exogenous administrations and endogenous production of the cytokine. Moreover, there may be differences between cholesterol biosynthesis gene expression and how well that translates to cholesterol lipid levels, which also should be considered.

We believe this is the first study to have researched the effect of cholesterol biosynthesis in a type I interferonopathy, and we hypothesise that the upregulation is most likely a result of a negative feedback mechanism to ensure cells maintain their structural integrity and are not damaged by chronically low levels of *de novo* cholesterol. This feedback process is well established and involves the cholesterol sensing machinery in the ER. SCAP contains a sterol sensing domain, and, upon depletion of ER cholesterol levels, it binds to the transcription factor SREBP and facilitates its transportation from the ER to the golgi apparatus so SREBP can be processed by S1/S2P. Following this, SREBP is activated and migrates to the nucleus to transcribe cholesterol biosynthesis genes (Cyster et al., 2014). This cholesterol biosynthesis process may be facilitated by the downregulation of specific ISGs, in particular *CH25H*, which is involved in reducing cholesterol biosynthesis as an antiviral mechanism.

The upregulation of cholesterol biosynthesis gene expression observed across all AGS subtypes (except *TREX1* patients) suggests that SAMHD1 does not possess a specific function associated with cholesterol biosynthesis, and thus we cannot conclude that this dysregulation results in AGS5 patients being more susceptible to cerebrovascular disease than other AGS subtypes. However, we speculate that this novel finding may explain the mechanism behind one of the classical AGS symptoms, observed in all subtypes: intracranial calcifications. It has been suggested that these calcifications can arise as a result of increased levels of small dense LDL cholesterol causing the hardening and calcification surrounding the intracranial vessels (Yao et al., 2020). However, this was measured in adults following ischaemic stroke, whereby atherosclerosis is a common risk factor, and calcification is readily associated with plaque formation (Boren et al., 2020). There is no literature to suggest the aetiology behind calcifications in AGS and other type I interferonopathies, and it is highly unlikely to be a result of the environmental influences which cause arterial calcification in atherosclerotic patients' e.g. high cholesterol diet. Therefore, it could suggest dysregulation in *de novo* cholesterol biosynthesis may manifest in the same way. To help establish this, cholesterol lipid levels could be measured in AGS patients to present a more accurate representation of how well biosynthesis gene expression translates to the lipid level.

In this chapter we aimed to investigate the presence of cerebrovascular disease in the *samhd1*$^{\Delta 23/\Delta 23}$ model. As with the classical symptoms, the embryos exhibited more subtle phenotypic changes, which highlighted a neurovascular weakness, leading to a proneness to haemorrhaging with low

dose ATV treatment. This observation enabled us to explore the possibility of a cholesterol dysregulation within the *samhd1*$^{\Delta 23/\Delta 23}$ larvae, which was present at the gene expression level. RNA sequencing data from AGS patients did not correlate with cholesterol dysregulation being a SAMHD1 specific event. It did, however, lead us to discover a novel observation regarding cholesterol biosynthesis dysregulation across multiple AGS sub-types, although the direction of the dysregulation was the opposite of what was found in the *samhd1*$^{\Delta 23/\Delta 23}$ model. Understandably, we are unable to make direct comparisons regarding the cholesterol dysregulation between the zebrafish and AGS patient data, as cholesterol biosynthesis gene expression was determined from different types of sample: zebrafish tissue, and patient whole blood. However, the *samhd1*$^{\Delta 23/\Delta 23}$ model did play a pivotal role in identifying a different direction of cholesterol dysregulation in AGS patients.

These findings will establish a new line of research to study the role of cholesterol in the type I interferonopathies, with more focus on patient data, and how this dysregulation may account for, or exacerbate, existing symptoms. Moreover, these findings propelled additional research on the complex relationship between type I IFN, cholesterol dysregulation and stroke, focusing specifically on brain endothelial cells (chapter 5).

Chapter 5: An investigation into the effect of innate immune mediators on the sterol metabolic network and functionality of human brain endothelial cells

5.1 Introduction

The risk factors associated with cerebrovascular disease are highly diverse, ranging from purely genetic causes, as observed in AGS5 patients (Chapter 4) to environmental challenges. ICH is the most severe form of cerebrovascular disease, resulting in 40% mortality rate at one month post ictus (An et al., 2017).

VZV, HSV, HCV and HIV infection have all been associated with both ICH and ischaemic stroke risk (Behrouz et al., 2016; Hauer et al., 2019; Nagel and Gilden, 2014; Nagel et al., 2010; Tseng et al., 2015). Focusing on ICH, the mechanism behind vessel rupture is not fully understood. However, each of these viruses can penetrate the BBB, and as such, one suggested mechanism of how infection leads to ICH focuses on direct damage caused by the virus within the cerebrovasculature, resulting in inflammation of the endothelium (vasculitis) and vasculopathy (Nagel et al., 2010). Vasculopathy manifests as weakening of the neurovascular unit, due to increased permeability from the collective actions of cytokines, chemokines and proteases released downstream of inflammation (Hauer et al., 2019). Additionally, HCV is thought to cause ICH via a different mechanism, involving the alteration of coagulation (Tseng et al., 2015).

Infection has also been proposed to contribute to hypocholesterolaemia (Filippas-Ntekouan et al., 2017), which is an additional risk factor for haemorrhagic stroke (Phuah et al., 2016; Valappil et al., 2012; Wang et al., 2013). Although the precise mechanisms underpinning hypocholesterolaemia as a risk factor are not currently well understood, it is thought to link to cerebrovascular stability, due to the vital role cholesterol plays within the plasma membrane in the endothelium (Valappil et al., 2012). We hypothesise this may manifest via a similar mechanism as the ATV model of ICH in zebrafish, as described in chapter 4 (Eisa-Beygi et al., 2013). Moreover, it has been proposed that low cholesterol may promote arterial smooth muscle necrosis, also acting to impair the integrity of the cerebrovasculature (Wang et al., 2013). There are multiple mechanisms by which hypocholesterolaemia can occur, including active inflammation, in particular, through the actions of IFNs. This is highlighted by the reduction in total serum cholesterol and various lipid fractions observed in cancer, HCV and MS patients treated with IFN as a therapeutic (Borden et al., 1990; Coppola et al., 2006; Shinohara et al., 1997).

Type I IFNs are produced following the detection of a virus by an intracellular PRR (see introduction 1.3), and can act in an autocrine, paracrine or systemic fashion to bind to IFNAR on the recipient cell, and initiate a signalling cascade cumulating in the transcription of a number of ISGs, which contribute to host defence, inflammation, signalling mechanisms, transcription and immunomodulation (Lee and Ashkar, 2018) . Excessive induction of type I IFN and ISGs due to mutations in a number of genes involved in nucleic acid metabolism, regulation or sensing can cause AGS and other type I interferonopathies, as discussed in previous chapters.

CH25H is an ISG which encodes an enzyme that catalyses oxidation of cholesterol to 25HC. 25HC belongs to a class of endogenous oxysterols, and exerts antiviral effects via actions on the

intracellular sterol pathway (Liu et al., 2013). This is an important target as cholesterol is widely utilised by viruses for entry into cells and for replication, thus, reducing the amount of cholesterol available to the pathogen has a protective role by attenuating the infection (York et al., 2015). The mechanisms by which 25HC manipulates sterol metabolism are through targeting the major sterol transcription factor SREBP and rate limiting enzyme in sterol biosynthesis HMGCR, thus reducing *de novo* biosynthesis. (Adams et al., 2004; Lu et al., 2015). Furthermore, 25HC redistributes existing intracellular cholesterol, achieved by removing free cholesterol from the membrane, which is often utilised by different infectious agents, such as viruses and bacteria, to enter the cells (Abrams et al., 2020; S. Wang et al., 2020; Zhou et al., 2020). Lastly, 25HC activates the LXR transcription factors, which are known to regulate the absorption, degradation, transport and excretion of cholesterol (Lehmann et al., 1997; Liu et al., 2018b; Zhao et al., 2020). It has been proposed that within the endothelium, cholesterol homeostasis is necessary for angiogenesis, barrier function and the shear stress response, thus, alterations to intracellular cholesterol can impair these normal functions (Tan et al., 2020; Yamamoto et al., 2020).

We hypothesise there is a complex relationship between viral infection leading to a type I IFN response that results in cholesterol dysregulation. If this dysregulation manifests within the cerebrovasculature, it may cause an endothelial weakness, increasing susceptibility to ICH. This could occur in individuals who suffer from additional ICH risk factors, such as hypertension, whereby the fragile cerebrovasculature is too weak to handle the increased blood pressure, resulting in damage and rupture. Hypertension has been identified in >80% of ICH patients who were also found to suffer from hypocholesterolaemia, providing rationale for this hypothesis (Chen et al., 2017; Phuah et al., 2016).

As such, this chapter aimed to focus on the role of the type I IFN response and intracellular cholesterol relationship within the cerebrovasculature. This has been poorly explored up to date, and so these studies may provide new evidence regarding the interactions between infection, hypocholesterolaemia and ICH.

This was achieved by firstly determining the response of human brain endothelial cells to type I interferon stimuli (IFNβ and 25HC), and whether subsequent alterations to intracellular cholesterol could be observed. Following this, we aimed to establish a link between alterations within intracellular cholesterol and the functional properties of brain endothelial cells, to observe any changes that may arise, thus reinforcing the importance of cholesterol within the cerebrovasculature.

5.2 Results

5.2.1 hCMEC/D3 cells respond to IFNβ treatment through ISG upregulation

The presence of IFNAR receptors on the surface of endothelial cells has already been established *in vitro* in a human umbilical vein endothelial cell line (HUVECs), thereby indicating that IFN can directly interact with the endothelium *in vitro*, causing down-stream signalling effects (Jia et al., 2018). However, as different vascular beds exhibit distinct gene expression and functionality, it was necessary to treat human brain microvascular endothelial cells (hCMEC/D3) with type I IFN in order to verify an antiviral response in a brain-specific endothelial cell type (Reynolds et al., 2014). This has only been shown once previously in hCMEC/D3 cells, whereby poly I:C was used to activate toll like receptor 3 on the cells, resulting in endogenous IFNβ production and downstream ISG expression (J. Li et al., 2013).

IFNβ treatment of hCMEC/D3 cells did produce an antiviral effect, classified as an increase in ISG expression. A concentration of 20 ng/ml was used, due to previous effective use whilst examining the relationship between interferon and intracellular cholesterol within BMDMs (Zhou et al., 2020).

The expression of *RSAD2, ISG15, CH25H* and *IFITM3* were measured, and IFNβ treatment was found to induce a significant upregulation in the expression of *RSAD2* ($P<0.0001$) and *ISG15* ($P<0.0001$), following a 4 h and 24 h treatment (Fig 5.1a-b), which equated to ~18 fold increase in *RSAD2* expression compared to Ctrl for both time points. *CH25H* ($P<0.05$) and *IFITM3* ($P<0.001$) expression was only significantly upregulated following 24 h treatment (Fig 5.1c-d), resulting in ~4 fold increase in gene expression compared to Ctrl. Together, these data indicates that brain endothelial cells can directly respond to type I IFN by initiating the downstream expression of ISGs.

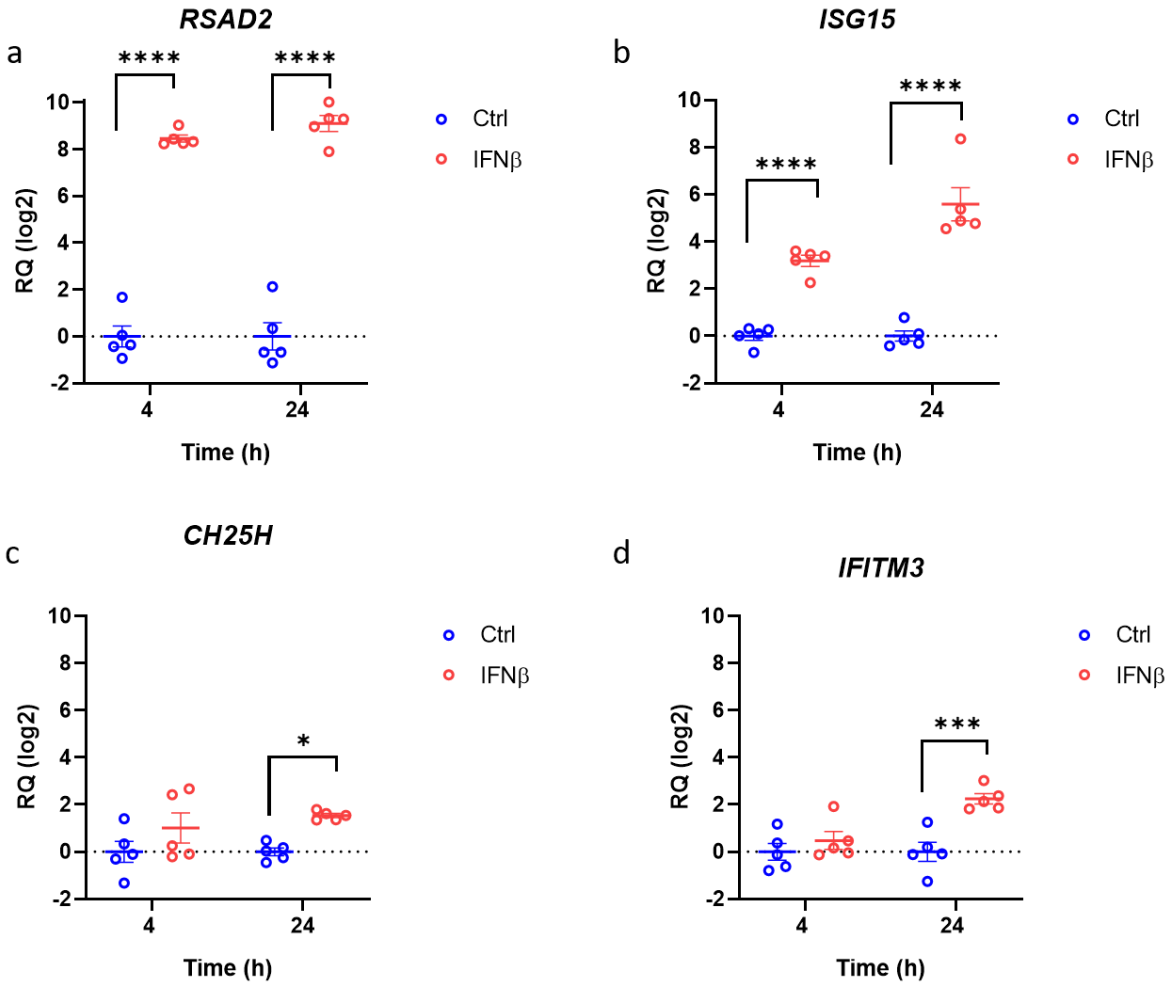

Figure 5.1- hCMEC/D3 cells respond to IFNβ treatment through ISG upregulation

a-d) hCMEC/D3 cells were seeded at a density of 92105 cells/cm^2 (4 h treatment) or 78947 cells/cm^2 (24 h treatment) in a 24 well plate and left overnight prior to treatment of IFNβ at a final concentration of 20 ng/ml, or 0.1% BSA in PBS as a Ctrl for either 4 h or 24 h. Cell lysates were collected and RNA extracted for qPCR analysis. The expression of *RSAD2, ISG15, CH25H* and *IFITM3* were determined, and normalised to the housekeeper genes *18S* and *HPRT1*. Data presented as mean ± SEM from 5 biological replicates, and analysed by a two-way ANOVA followed by sidak's post-hoc analysis. *P <0.05, ***P<0.001, ****P<0.0001

5.2.2 25HC, but not IFNβ, alters sterol gene expression in hCMEC/D3 cells

As previously described, CH25H produces the oxysterol 25HC, which acts to decrease sterol synthesis by inhibition of the master transcription factor SREBP. Due to the upregulation of CH25H in hCMEC/D3 cells following IFNβ treatment (Fig 5.1c), we hypothesised this would be coupled with a downregulation of sterol biosynthesis genes via actions on SREBP (see chapter 4, Fig 4.5 for cholesterol biosynthesis pathway). This was not observed, with *HMGCR, DHCR24* and *SQLE* all exhibiting no changes in expression (Fig 5.2a-c).

Additionally, 25HC activates the LXR transcription factors, which are known inducers of cholesterol efflux pathways (Liu et al., 2018a). Therefore we also measured the expression of one of the cholesterol efflux transporters: *ABCG1*, where no change in expression patterns were identified. Together, these results suggest that the upregulation of *CH25H* was not sufficient to generate adequate levels of 25HC, to alter the sterol pathway at the genetic level.

In other cell types treated with type I IFN, 25HC is produced and acts as a paracrine and autocrine factor, to elicit alterations to cholesterol on different cells (Blanc et al., 2013). Due to the lack of effect observed from IFNβ treatment on hCMEC/D3 cells, we next treated the cells directly with 25HC, to mimic a paracrine response. We surmised this could more accurately represent the environment *in vivo*, with 25HC being largely produced by immune cells responding to the actions of type I IFN, as opposed to endogenous production of 25HC in endothelial cells (Blanc et al., 2013; Diczfalusy et al., 2009). A concentration of 5 μM was used, a concentration within the upper levels of inhibition for a number of different viral and bacterial infections, such as SARS-CoV-2, HIV and *L.monocytogenes* indicating that this concentration of 25HC is highly effective for the antiviral and antibacterial properties of the oxysterol (Abrams et al., 2020; Liu et al., 2013; S. Wang et al., 2020)

25HC did not significantly affect expression of *RSAD2, ISG15, CH25H* or *IFITM3* (Fig 5.3). This is the opposite of what has been observed previously, whereby 25HC treatment in a human hepatoma cell line caused increased *CH25H* expression, via activation of the LXR pathway (Liu et al., 2018a). *RSAD2, ISG15* and *IFITM3* resulted in a varied expression across all replicates, however these followed a similar pattern as the Ctrl group, thus resulting in no difference.

Conversely, 25HC treatment significantly altered expression of all sterol related genes (Fig 5.4). This was identified by a ~2 fold reduction in *HMGCR* expression following 4 h treatment ($P<0.05$), which was further reduced to ~3 fold at 24 h ($P<0.0001$*). DHCR24* ($P<0.05$) and *SQLE* ($P<0.05$) were only significantly downregulated at 24 hr, also leading to a ~3-4 fold reduction in gene expression, potentially as a down-stream effect from the reduction in *HMGCR* expression at the 4 h time point. Moreover, there was a significant ~6 fold increase in *ABCG1* expression at 24 h ($P<0.01$). Together, gene expression changes suggest 25HC acts to decrease *de novo* cholesterol biosynthesis and increase cholesterol efflux in hCMEC/D3 cells, although the actual alterations to cholesterol efflux and overall cholesterol biosynthesis have not been fully elucidated.

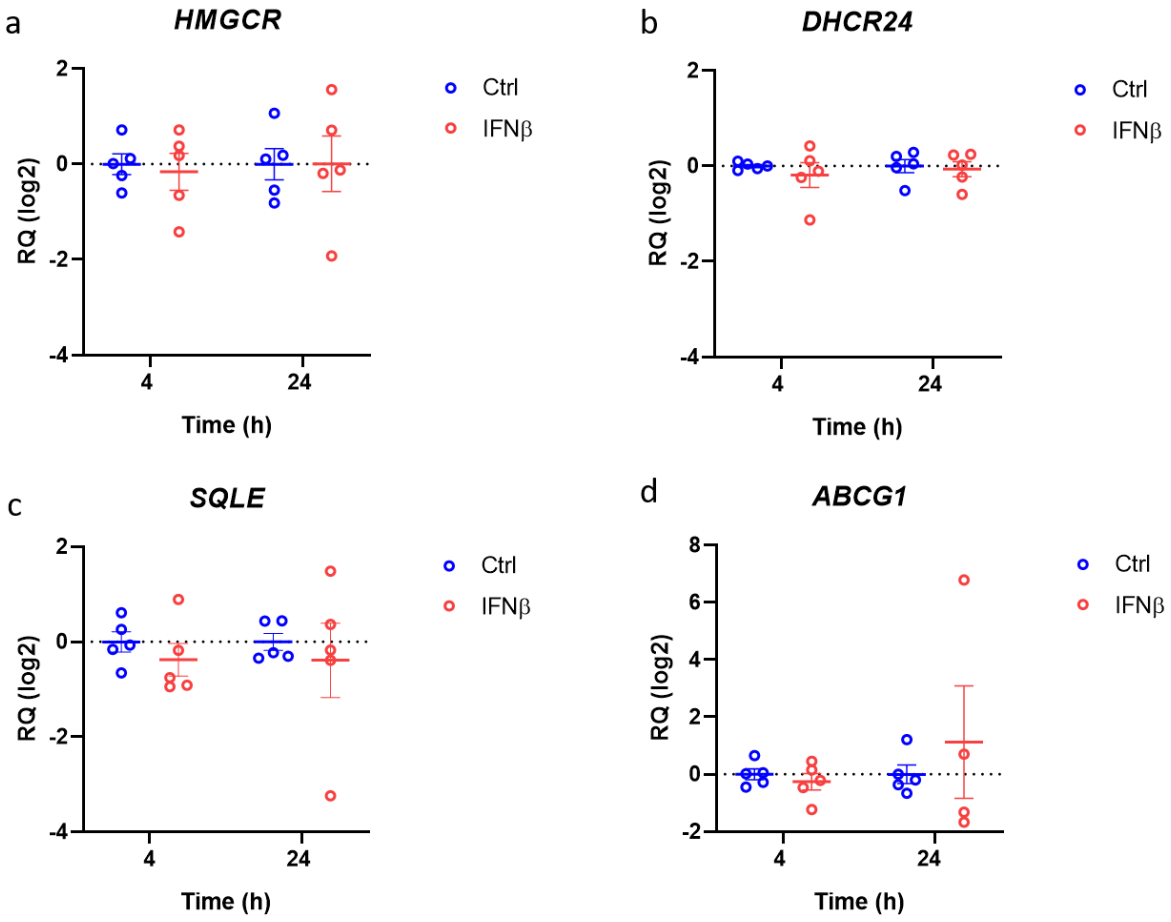

Figure 5.2– IFNβ treatment on hCMEC/D3 cells has no effect on sterol related gene expression

hCMEC/D3 cells were seeded at a density of 92105 cells/cm^2 (4 h treatment) or 78947 cells/cm^2 (24 h treatment) in a 24 well plate and left overnight prior to treatment of IFNβ at a final concentration of 20 ng/ml or 0.1% BSA in PBS as a Ctrl for either 4 h or 24 h. Cell lysates were collected and RNA extracted for qPCR analysis. The expression of *HMGCR, DHCR24, SQLE* and *ABCG1* were determined, and normalised to the housekeeper genes *18S* and *HPRT1*. Data presented as mean ± SEM from 5 biological replicates, and analysed by a two-way ANOVA followed by sidak's post-hoc analysis.

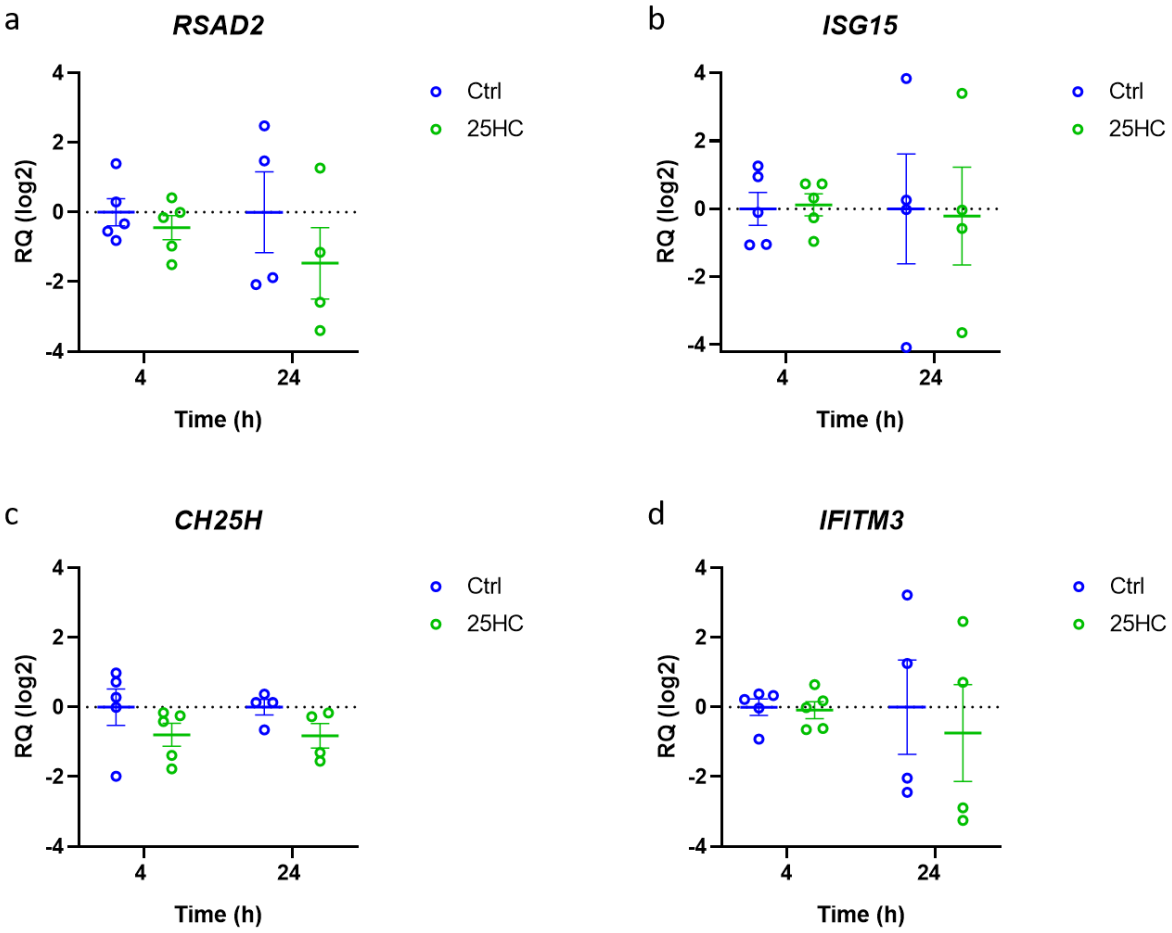

Figure 5.3- 25HC treatment has no effect on ISG expression in hCMEC/D3 cells

a-d) hCMEC/D3 cells were seeded at a density of 92105 cells/cm^2 (4 h treatment) or 78947 cells/cm^2 (24 h treatment) in a 24 well plate and left overnight prior to treatment of 25HC at a final concentration of 5 µM, or ethanol as a Ctrl for either 4 h or 24 h. Cell lysates were collected and RNA extracted for qPCR analysis. The expression *of RSAD2, ISG15, CH25H* and *IFITM3* were determined, and normalised to the housekeeper genes *18S* and *HPRT1*. Data presented as mean ± SEM from 5 biological replicates, and analysed by a two-way ANOVA followed by sidak's post-hoc analysis.

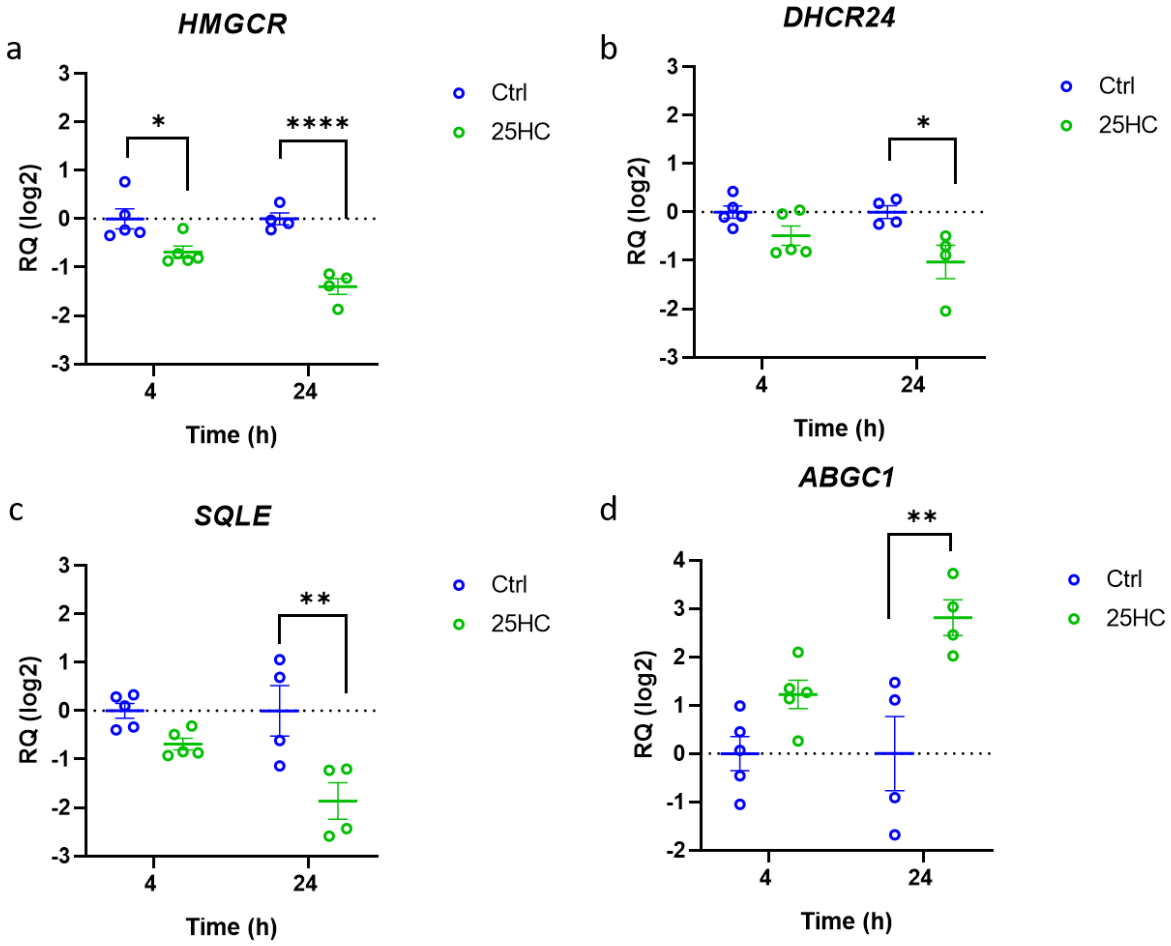

Figure 5.4- 25HC alters sterol related gene expression in hCMEC/D3 cells

a-d) hCMEC/D3 cells were seeded at a density of 92105 cells/cm^2 (4 h treatment) or 78947 cells/cm^2 (24 h treatment) in a 24 well plate and left overnight prior to treatment of 25HC at a final concentration of 5 µM, or ethanol as a Ctrl for either 4 h or 24 h. Cell lysates were collected and RNA extracted for qPCR analysis. The expression *of HMGCR, DHCR24, SQLE* and *ABCG1* were determined, and normalised to the housekeeper genes *18S* and *HPRT1*. Data presented as mean ± SEM from 5 biological replicates, and analysed by a two-way ANOVA followed by sidak's post-hoc analysis (*P<0.05, **P<0.01, ****P<0.0001).

5.2.3 Both 25HC and IFNβ alter sterol gene expression in human MDMs

To the best of our knowledge, this study is the first to investigate alterations in lipid metabolism through the actions of the type I IFN pathway, specifically in brain endothelial cells. Previous literature has focused on immune cells for this characterisation, and observed significant changes within the sterol biosynthesis pathways following IFNβ treatment, which widely differs from the expression levels we measured in hCMEC/D3 cells (York et al., 2015). Therefore, we treated human MDMs with IFNβ and 25HC to verify their effect in immune cells, which we hypothesised would corroborate with the existing literature.

MDMs were treated for 24 h, where a significant ~20 and ~16 fold increase in ISG expression was identified in IFNβ treated cells, for both *RSAD2* ($P<0.0001$) and *ISG15* ($P<0.0001$) (Fig 5.5a-b). This corroborated with the ISG expression levels previously determined in hCMEC/D3 cells treated with IFNβ. The exception was *CH25H*, which, whilst upregulated compared to the Ctrl group, did not reach significance (Fig 5.5c). This suggested that sterol gene expression would also remain unchanged. However, *HMGCR, DHCR24* and *SQLE* all demonstrated a small, but persistent downregulation, reaching significance in *DHCR24* which presented with ~3 fold decrease in gene expression ($P<0.05$) (Fig 5.6a-c). *ABCG1* expression was not altered, potentially as a result of the small sample size, coupled with the variation between the samples (Fig 5.6d).

Moreover, 25HC treatment elicited similar expression profiles as observed within hCMEC/D3 cells: a lack of effect with ISG expression (Fig 5.5), coupled with a significant ~4 fold decrease in *HMGCR* ($P<0.01$)*, DHCR24* ($P<0.05$) and *SQLE* ($P<0.01$). This was followed by a significant upregulation in *ABCG1*, equating to ~8 fold increase in expression ($P<0.05$) (Fig 5.6). Thus, these data demonstrate that IFNβ and 25HC treatment in immune cells corroborates with expression patterns observed previously within the literature, and further highlight the presence of cell type specific differences, as identified between MDMs and hCMEC/D3 cells, in particular with sterol gene expression following IFNβ treatment.

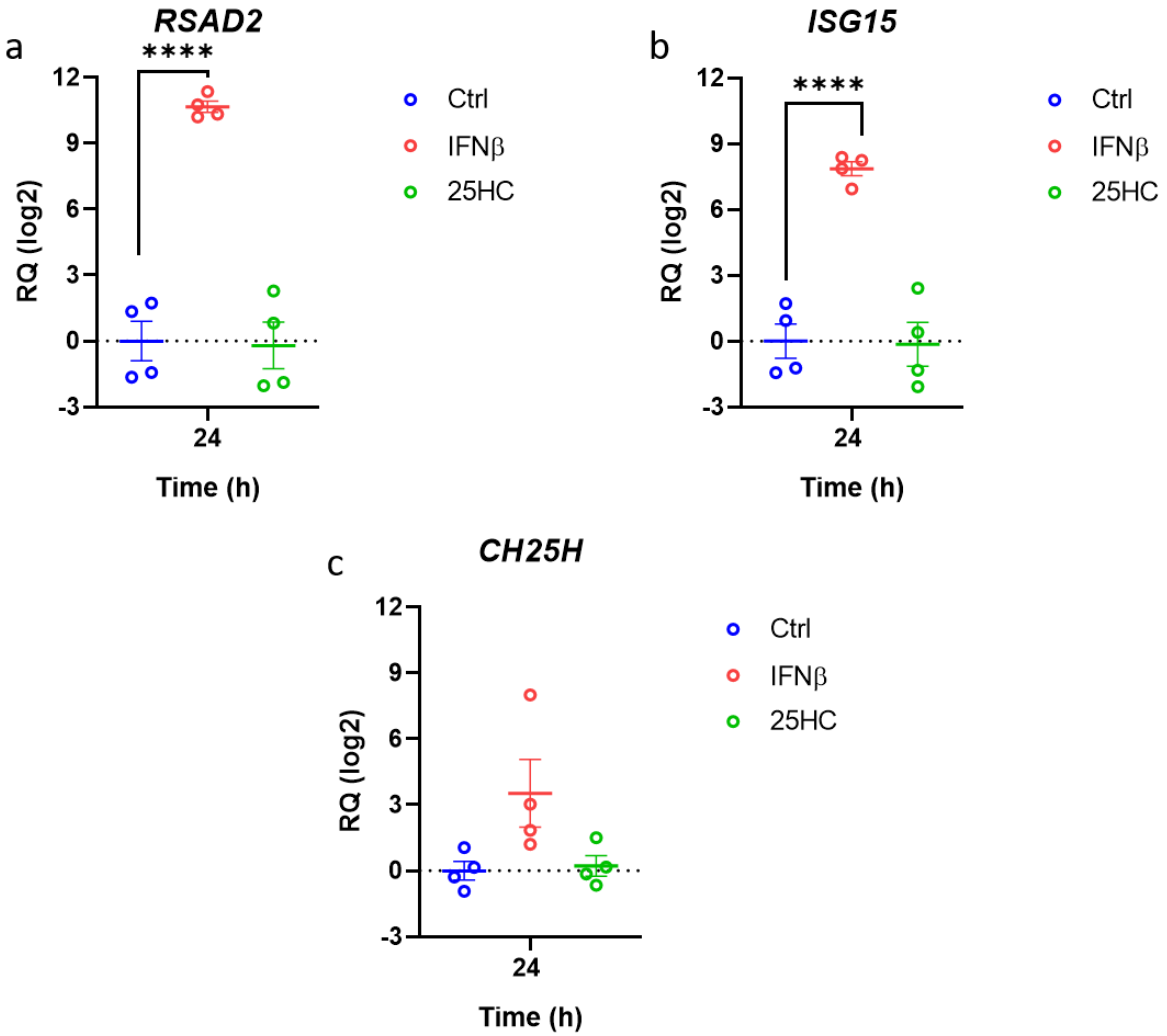

Figure 5.5- IFNβ treatment of MDMs results in a strong antiviral response through ISG upregulation

Human MDMs were seeded at a density of 214285 cells/cm^2 in a 12 well plate and left for 7 days to differentiate prior to treatment of either IFNβ or 25HC at a final concentration of 20 ng/ml or 5 μM for 24 h, a Ctrl group treated with ethanol and 0.1% BSA in PBS was also used. Cell lysates were collected and RNA extracted for qPCR analysis. The expression of *RSAD2, ISG15* and *CH25H* were determined, and normalised to the housekeeper genes *18S* and *HPRT1*. Data presented as mean ± SEM from 4 biological replicates, and analysed by a one-way ANOVA followed by Dunnett's multiple comparisons test (****P<0.0001).

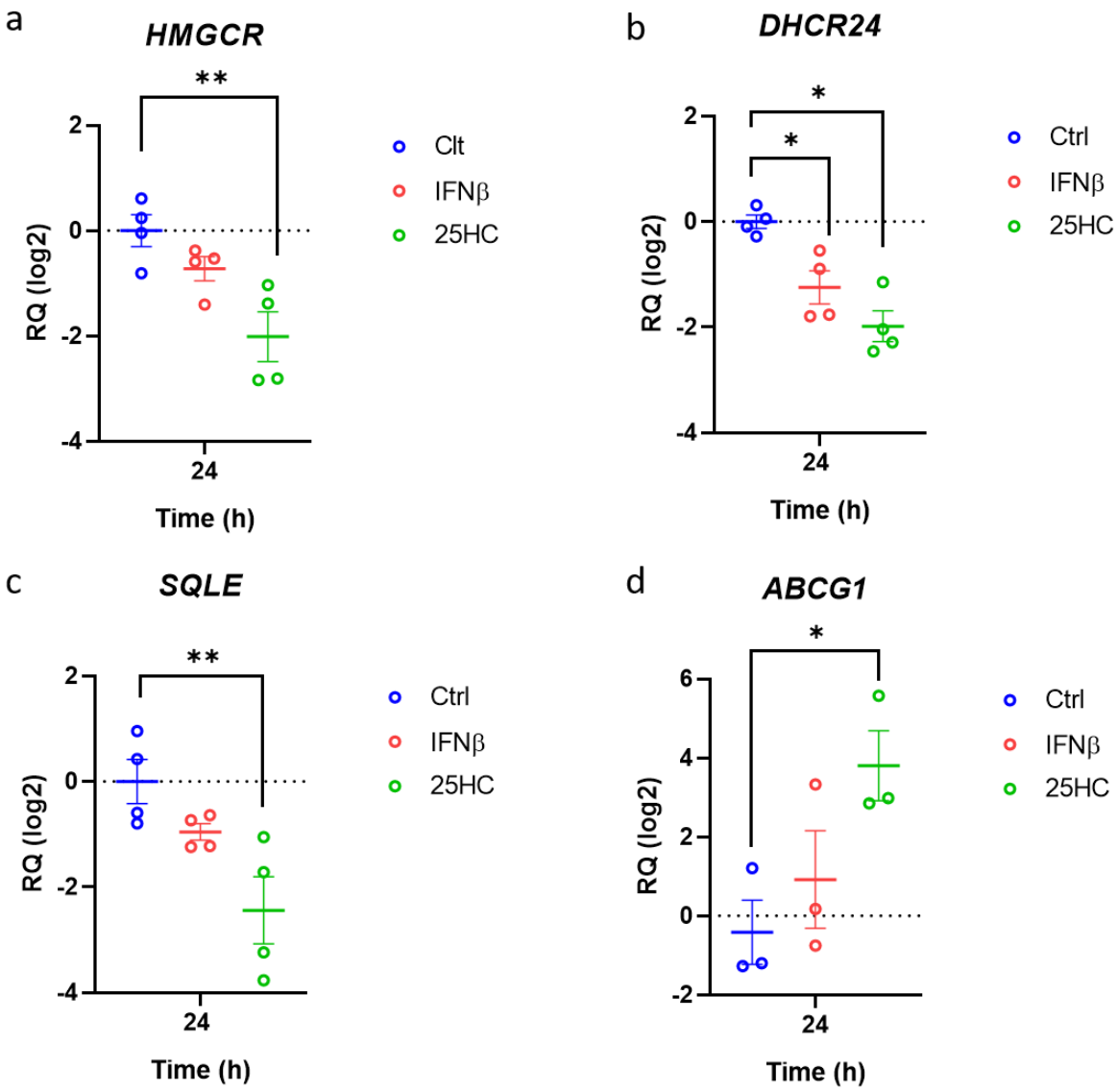

Figure 5.6- IFNβ and 25HC treatment of MDMs alters sterol related gene expression

Human MDMs were seeded at a density of 214285 cells/cm^2 in a 12 well plate and left for 7 days to differentiate prior to treatment of either IFNβ or 25HC at a final concentration of 20 ng/ml or 5 µM for 24 h, a Ctrl group treated with ethanol and 0.1% BSA in PBS was also used. Cell lysates were collected and RNA extracted for qPCR analysis. The expression of *HMGCR, DHCR24, SQLE* and *ABCG1* were determined, and normalised to the housekeeper genes *18S* and *HPRT1*. Data presented as mean ± SEM from 3/4 biological replicates, and analysed by a one-way ANOVA followed by Dunnett's multiple comparisons test (*P<0.05, **P<0.01).

5.2.4 25HC treatment is protective against SLO induced cell death in hCMEC/D3 cells

Following the discovery that IFNβ treatment does not generate a sufficient sterol response in hCMEC/D3 cells, we continued to investigate the relationship between antiviral signalling and cholesterol by focusing solely on 25HC treatment. A reduction in *de novo* cholesterol biosynthesis suggests that intracellular cholesterol levels may also be reduced, although a previous study

observed a modest increase in total cholesterol following IFNβ treatment in macrophages, proposed to be due to the actions of CH25H and 25HC (Zhou et al., 2020).

Measuring total cholesterol levels in hCMEC/D3 cells treated with 25HC, revealed no significant change (Fig 5.7a). However, this lack of overall effect may be due to a variable response to 25HC, as we detected the presence of two distinct groups, with both higher and lower cholesterol levels than the Ctrl values, thus making it difficult to draw any conclusions regarding total cholesterol within the cells, without further investigation with more sensitive lipid measuring approaches.

Whilst the total intracellular cholesterol levels produced an inconclusive result, previous studies have shown that 25HC changes the accessibility and trafficking of cholesterol in the plasma membrane to the ER and even acts to remove an accessible pool of cholesterol, thought to be targeted by pathogens to enter cells (Abrams et al., 2020; S. Wang et al., 2020; Zhou et al., 2020). Thus, we next wanted to determine if 25HC could deplete accessible cholesterol on the plasma membrane of hCMEC/D3 cells, as these small perturbations would not be identified by measuring total intracellular cholesterol levels.

Following a 4 h or 24 h treatment with 25HC, cells were incubated with SLO, a cholesterol-dependent cytolysin (CDC) class of toxin. SLO exerts its effects through binding to free ‘accessible’ cholesterol which is not tightly associated with sphinogmyelins and other phospholipids within the cell membrane. Once bound, SLO oligomerizes and form pores, resulting in cell death (Zhou et al., 2020). CDC toxins have commonly been utilised to identify free cholesterol within the plasma membrane of cells, thus are an indirect measure of free cholesterol levels within the plasma membrane. Following 4 h of 25HC treatment, there was a 24% reduction in the percentage of SLO induced cell death, although this has only been repeated twice, and thus requires additional replicates. Moreover, a 24 h stimulation generated a 68% reduction in SLO induced cell death ($P<0.0001$) (Fig 5.7b-d). This has previously been hypothesised to be a result of 25HC altering the distribution of cholesterol within the membrane to prevent SLO from binding to accessible cholesterol and forming pores (Abrams et al., 2020; S. Wang et al., 2020; Zhou et al., 2020).

An interaction between the cholesterol storage pathway and 25HC has been described previously, and suggested to be a mechanism by which 25HC reduces the accessible cholesterol pools within the plasma membrane (Abrams et al., 2020). This pathway is mediated by the ACAT enzymes, responsible for converting free cholesterol in the ER membrane to cholesterol esters which are stored in lipid droplets. It is hypothesised this esterification triggers rapid cholesterol remodelling on the plasma membrane (Abrams et al., 2020). To determine whether 25HC redistributes intracellular cholesterol, we measured the amount of free cholesterol and cholesterol esters in hCMEC/D3 cells. As observed with total cholesterol levels, there was too much variation between the free cholesterol amounts. However, there did appear to be a slight trend towards an increase in intracellular cholesterol ester levels (Fig 5.7e-f). Taken together, these data confirms that 25HC successfully inhibits SLO induced cell death, although we have not been able to precisely determine the downstream effects on intracellular cholesterol fractions following 25HC treatment, thus cannot fully

state this rescue of cell death is attributed to a loss of free cholesterol within the cell membrane. However, given the mechanism by which the SLO toxin exerts its effects, this hypothesised mechanism is likely to have occurred, and through further experimentation on specific lipid fractions, will confirm the membrane cholesterol altering effects of 25HC.

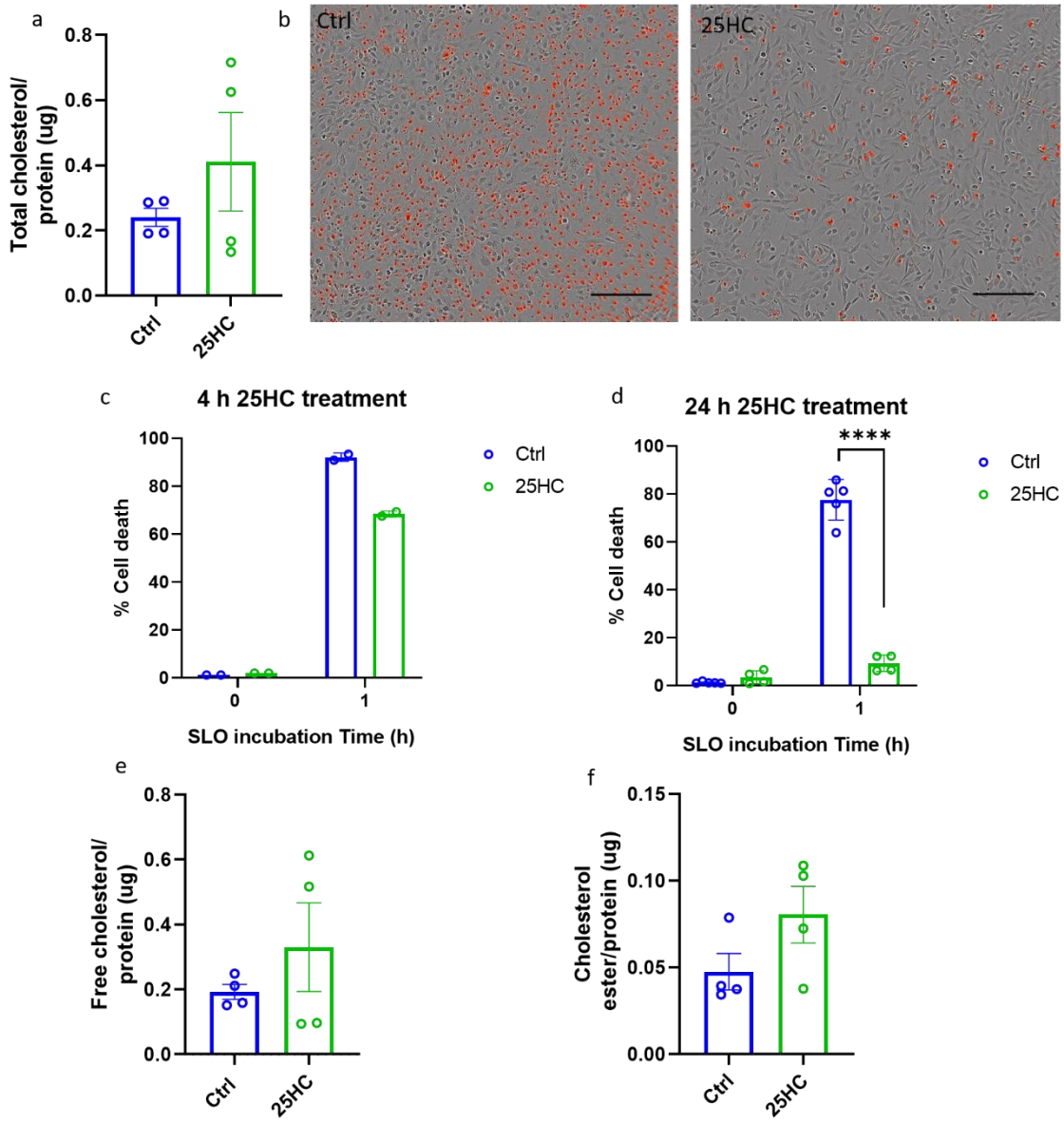

Figure 5.7- 25HC treatment is protective against SLO induced cell death

To measure the different cholesterol fractions within hCMEC/D3 cells following 25HC treatment (a,e-f) cells were seeded at a density of 41666 cells/cm^2 in a 6 well plate and left overnight, prior to a 48 h treatment with 25HC at a final concentration of 5 µM, or ethanol Ctrl. Cell lysates were taken for different cholesterol measurements using a cholesterol/cholesterol ester detection kit from Abcam according to instruction. Data presented as mean ± SEM from 4 biological replicates, and analysed by an unpaired t test. b-d) To determine the effect 25HC has on plasma membrane cholesterol, hCMEC/D3 cells were seeded at 93750 cells/ cm^2 (4 h treatment) or 78125 cells/ cm^2 (24 h treatment) in a black bottom 96 well plate, and left overnight, prior to the addition of 25HC at 5 µM for the required time, or ethanol Ctrl. Before imaging, media was replaced with TO-PRO-3 and Opti-MEM, in order to visualise the dead cells. Following a base line image at time 0, SLO (2 U/µl) was added and the cells imaged 1 h later. Images were taken on the Incucyte zoom live cell analysis system using a 120 10x/3.05 plan Apo OFN25 objective. b) Representative images of cell death following 1 h incubation with SLO in Ctrl vs 25HC. Scale bar is 200 µm c-d) Percentage cell death was determined using the incucyte basic analysis software, and was a percentage of the cell death established following 10% triton addition to the wells after 1 h incubation with SLO, which produced 100% cell death. Data presented as mean ± SEM from either 2 or 4 biological replicates, and the 24 h treatment (n=4) was analysed using a 2 way ANOVA with sidak's post hoc analysis. (P****<0.0001).

5.2.5 The cholesterol altering effects of 25HC reduce brain endothelial cell migration

As already discussed, the intracellular cholesterol altering properties of 25HC are utilised as defence mechanisms against pathogen entry. However, sterol metabolism is closely regulated within healthy cells, thus any disruption to the homeostatic state is likely to have consequences on the normal functioning of the affected cells (Tan et al., 2020). In endothelial cells, angiogenesis is one of the primary physiological processes, required to establish new blood vessels. We therefore treated hCMEC/D3 cells with 25HC to investigate any changes in cell migration, an essential component of angiogenesis, following the resulting disturbances to intracellular cholesterol.

The scratch wound assay was implemented as a method to measure cell migration on hCMEC/D3 cells treated with 25HC either 3 h or 24 h prior to generation of the wound (Goodwin, 2007; Lampugnani, 1999). Cell migration is characterised by the relative wound density, and a higher cell migration equates to increased cell counts in the scratched zone of the well. Both incubation times of 25HC resulted in a significant reduction in the relative wound density compared to control. This was apparent from 10 h post scratch from the 4 h 25HC treatment, causing ~20% reduction in relative wound density, which remained consistent until the end of the 24 h period ($P<0.05$, $P<0.01$). The 24 h pre-treatment resulted in a further reduction, manifesting first at 6 h post scratch, with a 20% reduction in relative wound density, which increased to a 35% reduction compared to the Ctrl group by the end of the 24 h period ($P<0.05$, $P<0.0001$) (Fig 5.8a-c). From this, we have revealed that 25HC treatment significantly reduces cell migration in brain endothelial cells.

Understandably, cell migration results can be affected by changes in cell proliferation rate, and previous studies have presented with conflicting findings regarding the effect of 25HC on cell proliferation. Treatment of 25HC has been found to reduce cell proliferation, thought to be attributed to cholesterol altering properties, given the important role cholesterol plays in cell division (Wen et al., 2018; Wu et al., 2018). Whilst another study found no effect on cell proliferation and apoptosis following 25HC treatment (Wang et al., 2019). A reduction in the number of cells, in response to 25HC treatment (e.g. anti-proliferative), compared to Ctrl groups could manipulate the cell migration result, as there would be less cells to migrate onto the scratched area, and thus the relative wound density would remain lower for treated cells. In order to determine the effect of 25HC on hCMEC/D3 cell density, cell counts were established following 20 h 25HC pre-treatment. Whilst a small reduction between Ctrl cells and 25HC treated cell densities was found, this was not significant. The groups were then seeded at the same density prior to generation of the scratch, which acted to ensure the reduction in cell migration was not a direct effect of reduced cell proliferation (Fig 5.8d). Therefore, although we cannot rule out that the small decrease in cell proliferation affects our final results, it is unlikely that the decrease in migration is only due to a decrease in cell proliferation, as cell migration is reduced from as little as 6 h post-scratch.

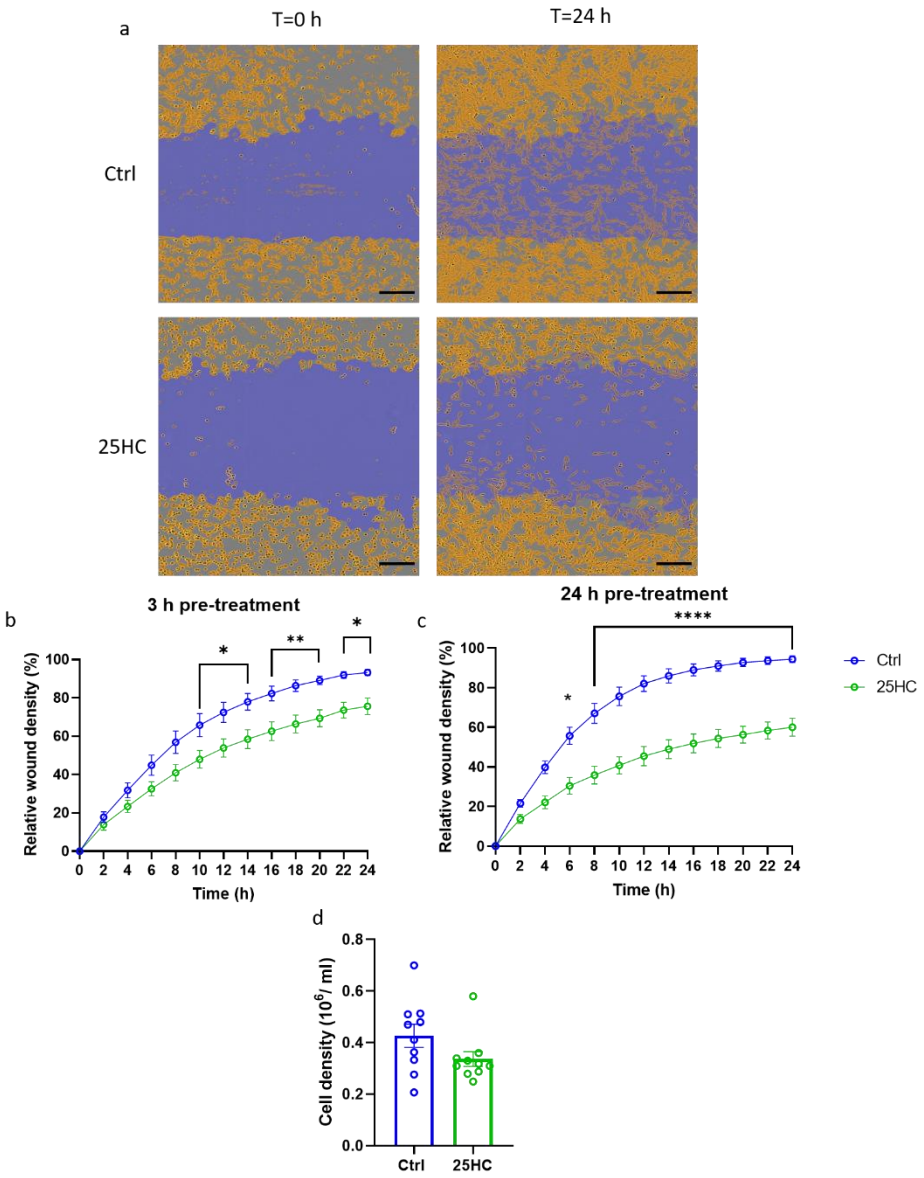

Figure 5.8- 25HC treatment of hCMEC/D3 cells reduces endothelial cell migration

To measure cell migration, hCMEC/D3 cells were seeded at a density of 78125 cells/ cm^2 in a 24 well plate and left overnight prior to treatment with 25HC at a final concentration of 5 µM, or ethanol Ctrl for 20 h. Following treatment, cells were re-suspended and re-seeded at a density of 125000 cells/ cm^2 in a 96-well Essen ImageLock plate before being left to adhere for 1 h prior to re-treatment with 5 µM 25HC, or ethanol Ctrl. For 3 h pre-treatment, cells were seeded directly into the 96-well plate. The cells were left to adhere for 1 h and treated with the above treatments. The 96-pin IncuCyte WoundMaker Tool was used to create uniform cell-free zones. Phase contrast images were acquired every 2 h on an IncuCyte Zoom Live Cell Analysis system using a 123 4x/3.05 Plan Apo OFN25 objective. a) Representative images of scratch wound at t=0 and t=24 for Ctrl and 25HC treated cells. Blue indicates the initial scratch wound, and yellow denotes cells, scale bar is 200 µm. b+c) The Incucyte scratch wound assay analysis software was used to calculate relative wound density, presented as a time course (b+c) from 0-24 h post scratch for the 4 h and 24 h pre-treatment of 25HC, analysed by a two-way ANOVA repeated measures with Sidak's post hoc analysis (*P<0.05, **P<0.01, ****P<0.0001). All data presented as mean ± SEM, from 6 biological replicates d) prior to the re-seeding of 25HC treated cells, cell counts were established to determine any antiproliferative effects of 25HC. An unpaired t test was used to analyse differences between Ctrl and 25HC cells. Data presented as mean ± SEM, from 10 biological replicates.

5.2.6 Cholesterol supplementation restores cell migration in 25HC treated hCMEC/D3 cells

It has been suggested that a disruption in membrane cholesterol acts to alter the actin cytoskeletal organisation which reduces cell migration (Kumar et al., 2018). If 25HC decreases cell migration via a reduction of membrane cholesterol, we hypothesised that supplementing 25HC treatment with cholesterol would improve cell migration. Additionally, the cholesterol precursor desmosterol was added as a co-treatment. Desmosterol has been shown previously to act as a replacement for cholesterol in J774 cells (a cell line unable to produce the enzyme DHCR24, which is responsible for converting desmosterol into cholesterol) (Rodriguez-Acebes et al., 2009). Therefore, we hypothesised that desmosterol may also rescue cell migration alongside cholesterol in 25HC treated cells. Finally, 25HC treated hCMEC/D3 cells were co-treated with the ACAT inhibitor SZ 58-035, in order to inhibit the esterification of free cholesterol induced by 25HC within the cells. SZ 58-035 has previously been shown to increase cholesterol levels within the plasma membrane of 25HC treated cells (Abrams et al., 2020; S. Wang et al., 2020; Zhou et al., 2020), therefore we hypothesised this would also increase cell migration.

Co-treatment of 25HC with cholesterol partially rescued the relative wound density, compared to the no supplementation group, and resulted in ~19% increase in relative wound density ($P<0.01$), suggesting that sufficient intracellular cholesterol levels are necessary for cell migration (Fig 5.9a). Co-treatments of 25HC with both desmosterol and SZ 58-035 were unable to undergo statistical analysis, due to the small N numbers associated with the no supplementation groups, thus no comparisons could be performed. However, despite the small sample size, it appears that 25HC treatment supplemented with desmosterol acts to increase the relative wound density, similar to what was observed following cholesterol supplementation (Fig 5.9b). Interestingly, there was no difference between 25HC treatment, and supplementation with SZ 58-035 (Fig 5.9c).

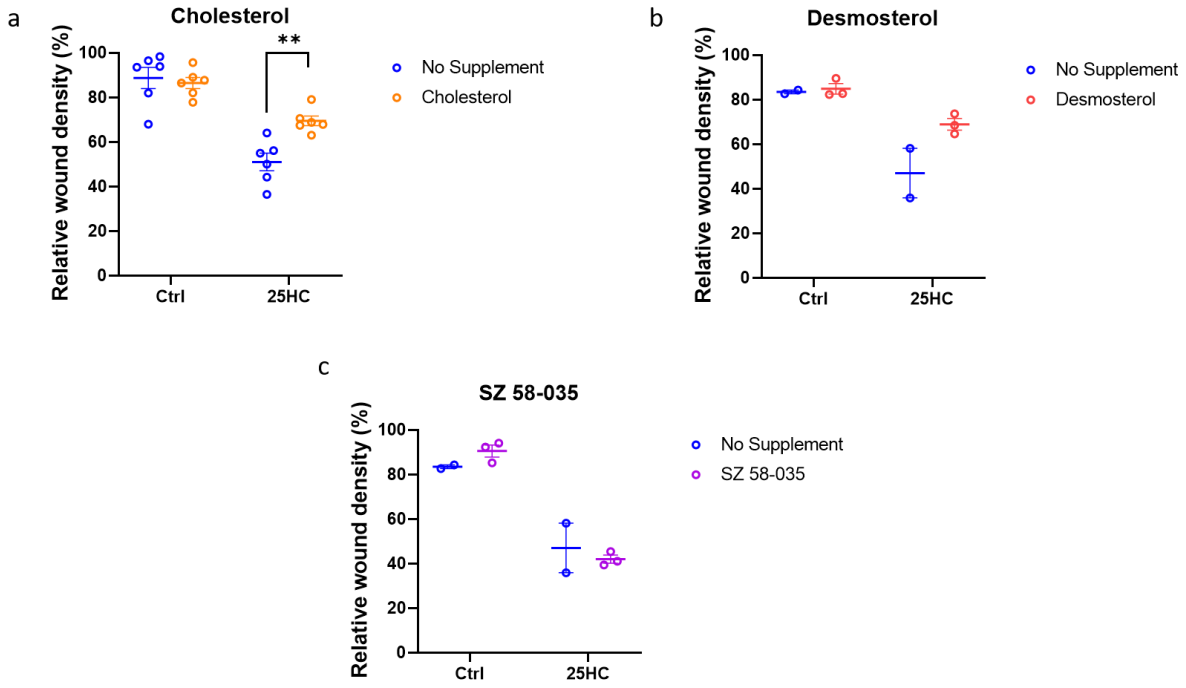

Figure 5.9- Cholesterol supplementation restores cell migration in 25HC treated hCMEC/D3 cells

a-c) hCMEC/D3 cells were seeded at a density of 78125 cells/ cm^2 and left overnight prior to treatment with 25HC at a final concentration of 5 uM for 24 h. Alongside 25HC treatment cholesterol (50 µM), desmosterol (10 µM) or SZ 58-035 (10 µM) were also added to the wells as a co-treatment. The no supplement Ctrl groups, were treated with ethanol as a Ctrl for cholesterol, and DMSO with DMF for Desmosterol and SZ 58-035 treatment. After 20 h, the cells were re-suspended and re-seeded at a density of 125000 cells/ cm^2 into a 96-well Essen ImageLock plate, before being left to adhere for 1 h prior to re-treatment with 25HC and the corresponding co-treatment. After 3 h following re-treatment, the 96-pin IncuCyte WoundMaker Tool was used to create uniform cell-free zones. Phase contrast images were acquired every 2 h on an IncuCyte Zoom Live Cell Analysis system using a 123 4x/3.05 Plan Apo OFN25 objective. The IncuCyte scratch wound assay analysis software was used to calculate relative wound confluence. This is shown as the final wound density value at the 24 h time point. All data is presented as mean ± SEM with 6 biological replicates for 50 µM cholesterol data, which was analysed by a two-way ANOVA with sidak's post hoc analysis (*P<0.05). The other data sets did not contain enough N numbers for statistical analysis.

5.2.7 Sterol supplementation of 25HC treated cells has no effect on SLO induced cell death

Following the improvement in cell migration after cholesterol supplementation of 25HC treated hCMEC/D3 cells, we hypothesised the addition of exogenous cholesterol may replenish the proposed depleted free cholesterol within the plasma membrane of hCMEC/D3 cells treated with 25HC, and would further provide evidence that protection from the SLO assay is a result of altered cholesterol within the plasma membrane. Exogenous cholesterol would provide adequate levels of cholesterol for the SLO toxin to bind to and thus largely increase cell death, reversing the protection gained by 25HC. The same co-treatments were utilised for the functional cholesterol rescue experiment.

Interestingly, none of the co-treatments exhibited any significant effect on the 25HC treated cells (Fig 5.10). Cholesterol and desmosterol treatment generated a large variation across replicates, either increasing cell death, or having no effect. Therefore, no conclusions can be made regarding supplementation of cholesterol or its precursor desmosterol in exacerbating SLO induced cell death in hCMEC/D3 cells (Fig 5.10a-b). Similarly SZ 58-035 exerted no effect on 25HC treated cells (Fig 5.10c). This was unexpected, as in macrophages, ACAT inhibition increases susceptibility to cell death of cells treated with 25HC, following CDC mediated membrane damage (Zhou et al., 2020). This potentially alludes to a cell type specific effect, whereby ACAT is not as widely utilised in brain endothelial cells. However, further experimentation is required before this can be determined.

An important consideration regarding the *in vitro* experimentation with 25HC is the concentration of exogenous oxysterol used. Whilst 5 µM and higher concentrations are widely described within the literature, these are arguably supraphysiological. Moreover, the nanomolar range of 25HC also generates profound effects in macrophages (Blanc et al., 2013; Robertson and Ghazal, 2016). Given the lack of response with any of the co-treatments, we hypothesised that the 25HC concentration may be too high, thus preventing any of the co-treatments from interfering with the 25HC response. Therefore, we performed a dose-response experiment with the SLO toxin, to determine which concentration of 25HC should be utilised in future experiments (Fig 5.10d). The lowest concentration of 25HC (0.2 µM) halved the number of TO-PRO-3 cells compared to Ctrl ($P < 0.01$), which suggests an adequate 25HC response can be attained with a much lower concentration than used in this present study. Concentrations of 1, 5 and 25 µM also provided significant protection against cell death ($P < 0.0001$). In future studies, the SLO assay will be repeated with the co-treatments at the lower dose of either 0.2-1 µM.

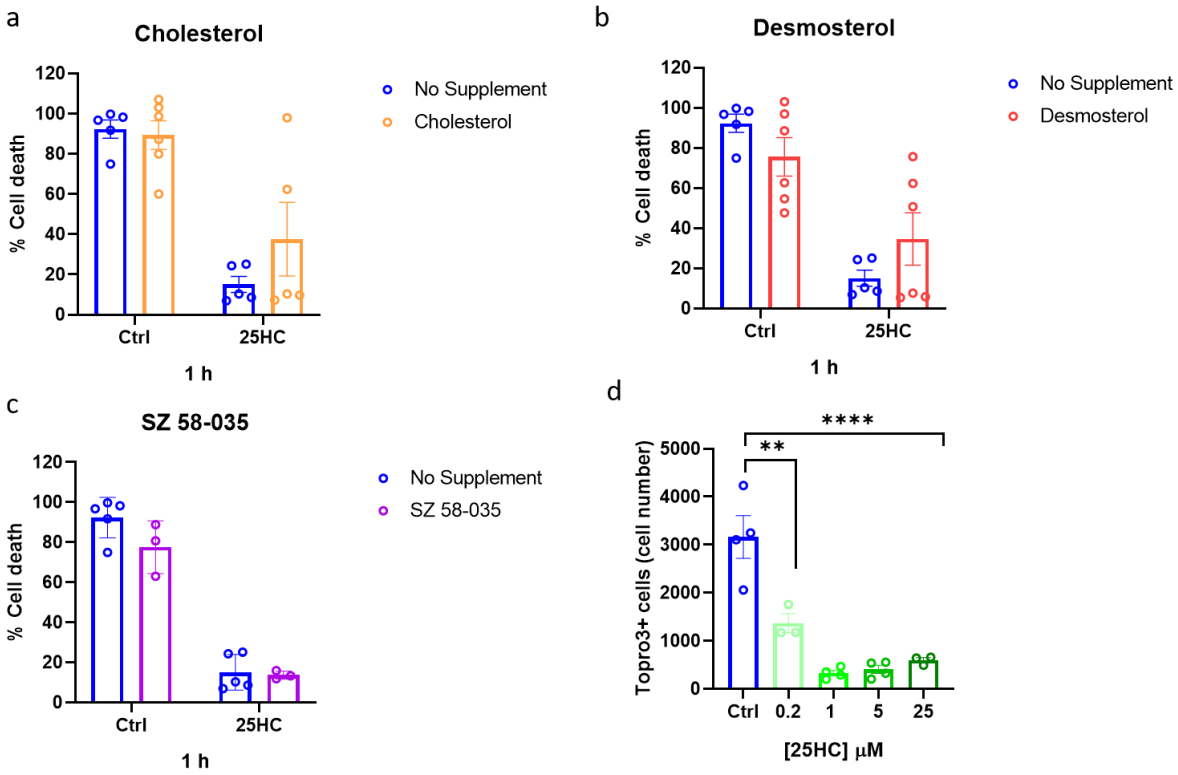

Figure 5.10- Sterol supplementation with 25HC has no effect on SLO induced cell death

a-c) hCMEC/D3 cells were seeded at 78125 cells/cm^2 in a 96 black bottomed well plate and left overnight, prior to treatment with 25HC at 5 µM. Alongside 25HC treatment cholesterol (10 µM), desmosterol (10 µM) or SZ 58-035 (10 µM) were also added to the wells as a co-treatment for 24 h. The no supplement Ctrl groups were treated with ethanol, DMSO and DMF. Prior to imaging, media was replaced with TO-PRO-3 and Opti-MEM, in order to visualise the dead cells. Following a baseline image at time 0, SLO (2 U/µl) was added and cells imaged 1 h later. Images were taken on the IncuCyte zoom live cell analysis system using a 123 10x/3.05 Plan Apo OFN25 objective. Percentage cell death was determined using the IncuCyte basic analysis software, and was a percentage of the cell death established following 10% triton addition to the wells following the 1 h incubation with SLO, to produce 100% cell death. Data analysed by a two-way ANOVA with sidak's post hoc analysis. Data presented as mean ±SEM, with 3-6 biological replicates d) Dose response for 25HC. 0.2, 1, 5 and 25 µM 25HC was added for 24 h, prior to SLO assay. Cell death was quantified by the number of TO-PRO-3 cells, determined using the IncuCyte basic analysis software, and was analysed by a one-way ANOVA with Dunnetts multiple comparisons, compared to the control (**P<0.01, ****P<0.0001). Data presented as mean ± SEM with 4 biological replicates.

5.3 Discussion

The relationship between type I IFN and cholesterol has been discussed in chapter 4, looking specifically in the context of AGS. This chapter aimed to increase understanding of this association by utilising both IFNβ and 25HC which bridges the link between cholesterol and immunity. Through *in vitro* modelling of hCMEC/D3 cells, we sought to investigate the effects of inflammation on intracellular cholesterol distribution, and how modifications to cholesterol can act to alter endothelial cell function, which we propose may play a role in cerebrovascular instability leading to ICH.

IFNβ treatment of hCMEC/D3 cells resulted in the characteristic upregulation of a number of ISGs observed after 4 h of stimulation, and maintained up to 24 h treatment. Although there are limited reports in the literature, type I IFN has previously been shown to induce ISG expression in a human aortic endothelial cell line, and in hCMEC/D3 cells following Poly I:C treatment (J. Li et al., 2013; Reynolds et al., 2014). Whilst all four genes measured: *ISG15, RSAD2, CH25H* and *IFITM3* are canonical ISGs and act to exert antiviral effects following transcription, *CH25H* and *IFITM3* perform these effects through a relationship with intracellular cholesterol (Amini-Bavil-Olyaee et al., 2013; Cyster et al., 2014).

CH25H is the enzyme responsible for producing 25HC, and was only found to be significantly upregulated in hCMEC/D3 cells following IFNβ treatment at 24 h. Interestingly, the expression of *CH25H* has previously been shown to be rapidly upregulated within 30 minutes of IFN stimulation in murine BMDMs (Blanc et al., 2013; Lu et al., 2015). This rapid upregulation corresponds to an immediate proteosomal degradation of HMGCR, coupled with inhibition of the transcription factor SREBP2, preventing its translocation to the nucleus (Robertson and Ghazal, 2016). These acute effects downstream from CH25H in murine BMDMs, suggests individual cell types have different response times following IFNβ stimulation. We suggest it may be more efficient for a rapid immune cell response to ensure sufficient production of 25HC, which is then released as a paracrine factor to exert effects on sterol biosynthesis on neighbouring cells. This aligns with previous studies which demonstrated the secretion of 25HC from immune cells following viral infection and IFN treatment (IFNβ and IFNγ) (Blanc et al., 2013).

Upregulation of *CH25H* following IFNβ treatment in hCMEC/D3 cells did not equate to a reduction in cholesterol biosynthesis gene expression. Furthermore, the expression levels of the cholesterol efflux transporter *ABCG1* was unaffected. *ABCG1* is associated with the LXR family of receptors, an additional mechanism by which 25HC can exert an antiviral response (Liu et al., 2018b). We hypothesised the transporter would be upregulated following *CH25H* expression, as observed with the cholesterol efflux transporter *ABCA1* following HIV-1 infection (Cui et al., 2012).

In an attempt to elucidate the cause of discrepancies following IFNβ treatment in brain endothelial cells compared to the existing literature, we treated human MDMs with IFNβ for 24 h. Interestingly, *CH25H* was not significantly upregulated, whilst the other ISGs were. This could be attributed to the rapid upregulation of *CH25H*, as previously described in murine BMDMs and we may have missed

the time frame where the enzyme is upregulated acutely following type I IFN stimulation (Blanc et al., 2013; Lu et al., 2015). Interestingly, despite this, a larger decrease in sterol related genes was observed than found in hCMEC/D3 cells, with *DHCR24* being significantly downregulated. This suggested there was an additional mechanism capable of reducing biosynthesis gene expression following IFN treatment. Alternatively the CH25H protein, but not the transcript, is still present and able to catalyse the conversion of cholesterol to 25HC. Therefore, it would have been useful to measure CH25H at the protein level by western blot, and not just at the transcriptional level.

Robertson and colleagues previously identified a reduction in cholesterol biosynthesis genes following IFN-γ treatment in *Ch25h*$^{-/-}$ murine BMDMs. They further discovered a mi-RNA (miR-342-5p) was upregulated following both IFNγ and IFNβ treatment, which exerted antiviral effects through SREBP-dependent and independent mechanisms. It has been proposed this miRNA is activated following the acute response of *CH25H*, whereby it generates a more sustained response. As the MDMs in this study were treated for 24 h, this suggests *CH25H* could have been upregulated at a much earlier time point, and the effects on sterol biosynthesis observed are a result of an alternative pathway, involving miR-342-5p (Robertson et al., 2016).

Notably, this further demonstrates the presence of cell type specific effects. There is a lack of literature confirming the presence of miR-342-5p in the endothelium. Instead, this miRNA has mainly been identified in macrophages (Wei et al., 2013). This may provide an explanation for why no changes in sterol biosynthesis or efflux were observed in hCMEC/D3 cells. For example, 25HC levels are too low, following insufficient *CH25H* expression, and coupled with a lack of miRNA activation could explain why no effect on sterol synthesis or efflux was observed. This hypothesis needs to be confirmed by identifying the presence of miR-342-5p within the brain endothelium.

Based on the lack of effect on cholesterol metabolism observed following IFNβ treatment on hCMEC/D3 cells, we chose to focus on 25HC treatment, introduced as a paracrine factor, downstream of type I IFN signalling. 25HC treatment did produce profound effects on hCMEC/D3 cells, implying that brain endothelial cells can be targeted by the oxysterol in order to prevent viral entry into the vasculature. We observed a significant downregulation in all of the sterol biosynthesis genes measured, confirming the known functions of 25HC on reducing expression of cholesterol biosynthesis genes. This was coupled with an increase in *ABCG1* expression, which may equate to higher cholesterol efflux in the endothelial cells. Together, this revealed a dual pathway of activation, with 25HC acting on both SREBP and the LXR pathways as previously described (Robertson and Ghazal, 2016). An important future experiment would involve measuring the precursor and mature forms of SREBP. From the literature, 25HC treatment reduces both forms of SREBP2, correlating to a reduction of HGMCR at the protein level, alongside a loss in gene expression of *HMGCR* and other cholesterol biosynthesis genes. Therefore it would be important to confirm this mechanism in brain endothelial cells (Liu et al., 2018a; Wen et al., 2018).

Treating human MDMs with 25HC produced a similar pattern in sterol gene expression, as identified in hCMEC/D3 cells. This finding confirms the ability of 25HC to directly affect sterol expression in

brain endothelial cells, akin to what has been previously demonstrated other cell types (Nishimura et al., 2005) . Whilst the apparent lack of 25HC production following IFNβ treatment suggests brain endothelial cells do not make large endogenous quantities of 25HC, these cells are still capable of responding to the oxysterol, most likely attributed to paracrine signalling, whereby 25HC is secreted from immune cells. To confirm this paracrine signalling, MDMs treated with type I IFN or a virus should be co-cultured with hCMEC/D3 cells, and the sterol gene expression measured, which would determine whether the amount of 25HC released is sufficient to exert effects on endothelial cells.

Alongside altering *de novo* cholesterol biosynthesis, 25HC has been strongly implicated in inhibiting viral entry, alluding to a functional role within the structure and organisation of the plasma membrane. (Liu et al., 2013). Previous studies have identified an accessible pool of free cholesterol utilised by pathogens to facilitate entry into cells. 25HC acts to removes that pool (Abrams et al., 2020). This hypothesis has already been shown in the context of the virus SARS-CoV-2, and also the bacteria *L.monocytogenes* and *S.flexneri* (Abrams et al., 2020; S. Wang et al., 2020). Similarly, we too, demonstrated the protective properties of 25HC against the bacterial toxin, SLO, which binds to this free accessible pool of cholesterol within the plasma membrane and causes cell death through the pore forming properties of the toxin.

Upon 25HC treatment, there was a significant reduction in cell death, and whilst we hypothesised that the protective properties of the oxysterol arise from removing the free accessible cholesterol pool within brain endothelial cells, issues with accurately measuring the intracellular cholesterol fractions made this difficult to conclude. However, a previous study observing the effects of IFN treatment on protection from different CDCs, including SLO, also saw no difference in the total cholesterol within the cell, but instead identified a significant downregulation in cholesterol biosynthesis genes expression, and also a small increase in cholesterol esters, thought to be attributed to the actions of CH25H and 25HC (Zhou et al., 2020). This mimics what we observed in this study, and as the SLO assay is considered an indirect measure of free membrane cholesterol, it does suggest that 25HC is reducing the free accessible cholesterol within the cell membrane, to prevent the toxin from binding and forming pores to result in cell death. More specific lipid detecting methods within the plasma membrane, such as distinguishing between free cholesterol, and cholesterol bound to sphingomyelin/other phospholipids would help to confirm this mechanism. Moreover, to provide further clarity, a positive cell death control should be implemented that results in cell death independent of cholesterol. If 25HC treatment with the positive control also inhibits cell death, it would indicate that 25HC is acting via a different mechanism to protect the cells.

One additional mechanism which may be utilised by 25HC to protect against SLO induced cell death is related to glycans. A number of CDCs, including SLO, can recognise and bind to multiple glycans on the host cell membrane to also allow pore formation, independent of cholesterol (Shewell et al., 2020). Similarly, 25HC has been shown to cause aberrant glycosylation of a viral glycoprotein from the lassa virus, preventing host cell surface attachment and entry, thus indicating that 25HC can also alter glycans, although it is not known whether the oxysterol can alter glycosylation within the host cell membrane (Shrivastava-Ranjan et al., 2016).

This potential decrease of plasma membrane free cholesterol within brain endothelial cells could provide rationale for the relationship between viral infections and ICH. The actions of 25HC altering the lipid composition of the cell membrane, could act to increase the fluidity, and reduce the structural integrity of the endothelium, making it more susceptible to rupturing and causing a haemorrhagic stroke. We hypothesise this antiviral mechanism induced by 25HC may partially explain the development of ICH following certain viral infections, which could lead to the production of 25HC downstream of type I IFN signalling (Nagel et al., 2010). Moreover, the degradation of HMGCR by the actions of 25HC may induce ICH through a similar mechanism as examined in the ATV model of haemorrhagic stroke used in zebrafish disease modelling (see chapter 4). However, we do hypothesise this is unlikely to be a sole risk factor, and will most probably occur in combination with other co-morbidities, such as hypertension.

We then hypothesised that supplementing 25HC treated cells with cholesterol would increase the SLO-induced cell death, as observed in a Calu-3 cell line treated with SARS-CoV-2 (S. Wang et al., 2020). No differences were detected, due to the large levels of variation observed between replicates. This was also apparent for co-treatment with the cholesterol precursor desmosterol. Ongoing studies will aim to determine why no effect was observed following sterol rescue. One suggestion is that the concentration of 25HC is too high for the sterols to have any effect, due to the strong response produced by 25HC not being reversed. Following a dose-response SLO experiment, a significant reduction in cell death was observed from 0.2 µM 25HC, and as a result, future studies will focus on utilising the lower concentrations to see if an effect can be established.

Interestingly, the ACAT inhibitor SZ 58-035 also exhibited no effect on SLO induced cell death. This was more surprising, given the enzymatic properties of ACAT are suggested to be the primary mechanism by which 25HC causes a reduction in accessible cholesterol within the plasma membrane. ACAT converts free cholesterol into cholesterol esters, which are stored in cytoplasmic lipid droplets, inaccessible for viruses. This loss of free cholesterol results in a re-distribution of cholesterol on the plasma membrane (Abrams et al., 2020; S. Wang et al., 2020). SZ 58-035 is widely used throughout the literature, for similar experiments with 25HC treatment. One difference between this study and others is pre-treatment of the inhibitor, prior to the addition of 25HC, which appears to generate the expected effects (Ormsby et al., 2022; S. Wang et al., 2020). This method will be utilised in the future to determine whether ACAT inhibitors do rescue SLO induced cell death.

The relationship between ACAT and 25HC indicated that 25HC treated cells should exhibit higher concentrations of cholesterol esters. Whilst a trend towards an increase in cholesterol esters was detected following 25HC treatment, there was considerable variation within the free cholesterol levels. As a result, no conclusions could be established, and further experimentation is required, potentially utilising a more sensitive lipid measuring approach, such as mass-spectrometry. Moreover, the activity of ACAT should have been established, through measuring the number of lipid droplets found in cells following 25HC treatment, as we did not determine the activation of ACAT within brain endothelial cells (S. Wang et al., 2020).

A reduction in plasma membrane cholesterol in brain endothelial cells could be a contributing factor for haemorrhagic stroke, as previously discussed. Furthermore, subtle changes may be apparent within the homeostatic functions of these cells, which led us to measure aspects of brain endothelial cell function, in particular, cell migration. Following 25HC treatment, there was a significant reduction in cell migration, hypothesised to be a result of disruption in membrane cholesterol, which acts to alter the actin cytoskeletal organisation (Kumar et al., 2018). A previous study also treated endothelial cells with 25HC, and observed reduced cell migration, which they attributed to dysfunction of the nitric oxide pathway, and the subsequent production of superoxide acting to inhibit endothelial cell proliferation, migration, tube formation and vasodilation (Ou et al., 2016). Whilst this pathway does possess a role in endothelial cell function, we also suggest that the alterations in lipid metabolism, and the intracellular organisation of lipids induced by 25HC plays a role in disrupting the functioning of endothelial cells.

To confirm this, we supplemented the 25HC treated cells with cholesterol in an attempt to rescue the cell migration phenotype. Cholesterol co-treatment did significantly increase cell migration, thus reinforcing the importance of intracellular cholesterol homeostasis for the normal functioning of brain endothelial cells. The cholesterol precursor desmosterol also improved cell migration, although more replicates are required to confirm this. Surprisingly, the ACAT inhibitor SZ 58-035 had no effect on cell migration, akin to the lack of effect on SLO induced cell death. We hypothesised inhibiting ACAT would retain free cholesterol in the plasma membrane and thus be used to aid cell migration. As this wasn't observed, it suggests cholesterol leaves the membrane via other mechanisms independent of esterification. There are several other proteins which interact with 25HC, and the oxysterol can affect the properties of the plasma membrane independent of ACAT induction, through altering the position, orientation and solvent accessibility of cholesterol (Olsen et al., 2011). Alternatively, a reduction in membrane cholesterol may not be the sole reason why cells stop migrating, as observed following nitric oxide pathway dysfunction (Ou et al., 2016). To further understand this mechanism, it would be useful to fluorescently label the supplemented cholesterol and identify its intracellular location. If the exogenous cholesterol does not affect the plasma membrane free cholesterol levels, it would indicate that cholesterol is utilised in a different manner to facilitate cell migration.

Current work is focusing on other functional properties of brain endothelial cells, with particular emphasis on tube formation, as a readout of angiogenesis. Furthermore, the effect of shear stress is also being researched as levels of plasma membrane free cholesterol are relevant for shear stress response, which is a highly relevant output that may help to provide additional insight into the development of ICH, in response to low cholesterol levels (Yamamoto et al., 2020). Whilst beyond the scope of this study, it would be interesting to examine the other roles of 25HC, independent from the cholesterol altering antiviral properties, as the oxysterol has been implicated in both pro and anti-inflammatory mechanisms (Dang et al., 2017; Jang et al., 2016; Liu et al., 1997; Reboldi et al., 2014; Zhao et al., 2020). Thus this would enable further characterisation of the actions of 25HC on brain endothelial cells, and begin to elucidate whether enhanced inflammation via 25HC can act to further

damage the cerebrovascular endothelium, potentially underpinning different mechanisms for the development of cerebrovascular disease.

This chapter aimed to increase understanding of the immune-cholesterol axis in a previously undescribed cell type: brain endothelial cells. Whilst inflammation from IFNβ treatment did not produce a 25HC response, utilising 25HC as a paracrine signalling factor exhibited comparable effects to those identified in immune cells. We highlighted the protective properties of 25HC against SLO induced cell death, likely through remodelling of cellular cholesterol by reducing the accessible cholesterol pool within the plasma membrane, and additionally, via actions on reducing *de novo* biosynthesis. Both methods are implemented as antiviral mechanisms and have been identified previously in a number of other cell types, but this study was the first to demonstrate this relationship in brain endothelial cells. Cholesterol dysregulation affected normal functional properties of endothelial cells, such as cell migration. We suspect alterations to the endothelial plasma membrane could have deleterious effects on the integrity of the endothelium, and result in vessel rupture and haemorrhagic stroke. This may occur following inflammation, and be attributed to viral infection of the cerebrovasculature, which leads to the involvement of 25HC on the endothelium. Further experimentation, with regards to shear stress and other angiogenic processes will help to solidify this hypothesis and further our understanding of viral-induced inflammation as a risk factor for ICH.

Chapter 6: General Discussion

6.1 Main Findings

The work presented throughout this thesis has addressed three primary aims:

1) To validate and further demonstrate zebrafish as a viable pre-clinical organism to model AGS

2) To characterise the cerebrovascular complications which arise in AGS5

3) To study the role of type I IFN signalling and cholesterol in human brain endothelial cells.

Through this work we have shown that a stable mutant zebrafish line (*samhd1*$^{\Delta 23/\Delta 23}$) phenocopies specific symptoms of AGS patients, which have not been identified in previous pre-clinical rodent models, including neurological phenotypes, such as microcephaly, enhanced brain cell death and locomotion deficits. As such, these data further emphasises the usefulness of zebrafish as a model organism to study AGS. Moreover, the quantifiable and reproducible phenotypes highlights the potential for the *samhd1*$^{\Delta 23/\Delta 23}$ model to be utilised for pre-clinical drug screens, as observed following JAK inhibitor (ruxolitinib) treatment. Whilst the treatment was unsuccessful at ameliorating the microcephaly and brain cell death phenotypes, there will be additional opportunities to test treatments for AGS and other type I interferonopathies in the *samhd1*$^{\Delta 23/\Delta 23}$ model, to complement clinical studies.

Modelling a mutation in *samhd1* provided a unique opportunity to investigate a monogenic form of cerebrovascular disease, commonly identified in AGS5 patients. We identified a subtle pre-disposition to both ischaemic and haemorrhagic events at baseline conditions, whilst the mutant embryos possessed an increased susceptibility to cerebral haemorrhaging following ATV treatment. The mechanism by which ATV causes brain haemorrhage in embryonic zebrafish led us to identify a cholesterol dysregulation in the *samhd1*$^{\Delta 23/\Delta 23}$ model, whereby reduced cholesterol biosynthesis gene expression was hypothesised to result in cerebrovascular weakness, and increase the risk of vessel rupture and haemorrhage. This finding generated interest in the type I IFN and cholesterol signalling axis within AGS patients. We observed a dysregulation of cholesterol biosynthesis genes across the majority of AGS sub-types, although the genes were upregulated, rather than downregulated as observed in the *samhd1*$^{\Delta 23/\Delta 23}$ model. Irrespective of the direction, we have shown that AGS patients possess cholesterol dysregulation at the genetic level, and we propose that this may help provide new mechanistic insight into the more ubiquitous phenotypes found across all AGS sub-types.

The relationship between IFN signalling and cholesterol dysregulation was then examined in the context of cerebrovascular disease in general. Human brain endothelial cells were used to identify a relationship between the inflammatory modulator produced downstream of type I IFN signalling (25HC), and intracellular cholesterol dysregulation. To our knowledge, it is the first time this relationship has been observed in brain endothelial cells, and may begin to explain a link between a complex mechanism involving viral infection, type I IFN signalling, hypocholesterolaemia and risk of ICH.

6.2 Zebrafish as a useful pre-clinical model organism to research AGS

Throughout this study, we have highlighted the lack of appropriate pre-clinical models of AGS, with all rodent models of AGS1-7 failing to accurately recapitulate the many complex phenotypes which arise in AGS patients, specifically the neurological phenotypes which are one of the hallmarks of the condition (Rutherford et al., 2020). Previous generation of a transient *samhd1* model in zebrafish larvae (*samhd1* MO) managed to replicate a number of clinically relevant phenotypes, including neurological involvement, with the generation of spontaneous ICH (Kasher et al., 2015). This model provided rationale to further investigate the ability of zebrafish to be a useful and accurate pre-clinical model of AGS, by generating a stable mutant via CRISPR-Cas9 technology. In this study, we aimed to characterise and validate the *samhd1*$^{\Delta 23/\Delta 23}$ model, which was achieved via identification of a number of classical symptoms associated with AGS.

The variable ISG expression was an interesting finding, as we had anticipated a significant increase across all ISGs measured, as previously identified in the *samhd1* MO model (Kasher et al., 2015). However, as previously alluded to, measuring ISGs and antiviral responses may be complicated in zebrafish models by environmental factors, such as the presence of viruses within the aquaria housing adult zebrafish. Recently, a novel picornavirus has been discovered, found to infect zebrafish in multiple research facilities around the world (Altan et al., 2019; Balla et al., 2020). Whilst the viral infection appeared to be relatively asymptomatic, RNA sequencing data revealed a large upregulation of a number of ISGs, including *stat1b*, *mxa*, *rsad2* and *isg15*. Moreover, the generation of a Tg(*isg15:*GFP) zebrafish line further highlighted the heightened antiviral response in WT larvae infected with picornavirus (Balla et al., 2020).

Interestingly, a similar panel of ISGs that were found upregulated in the picornavirus study were also measured in the *samhd1*$^{\Delta 23/\Delta 23}$ model, and the large variation between replicates could indicate that some clutches of larvae were infected with picornavirus, and others were not, resulting in differential ISG expression. In addition, this could also provide rationale for the increased ISG expression identified in a number of WT larval replicates. However, no firm conclusions can be established, as despite picornavirus being confirmed within the aquaria in the Manchester Biological Services Unit, it remains unclear whether the *samhd1*$^{\Delta 23/\Delta 23}$ and WT stains have been affected. Furthermore, the induction of the Tg(*isg15:*GFP) reporter line was not observed until 8 dpf, the same time point used for RNAseq data (Balla et al., 2020). This suggests that if picornavirus is present in Manchester, it may not have affected the larvae at the time point they were taken for ISG expression (5 dpf). To combat this confounding factor, it has been suggested that bleaching embryos prior to hatching is an effective way to remove the virus (Balla et al., 2020). Therefore, such an approach should be repeated in the *samhd1*$^{\Delta 23/\Delta 23}$ model to remove any form of environmental exposure to viruses, and to confirm that increased ISG response is primarily a result of a mutated *samhd1* gene.

However, there are also drawbacks associated with the bleaching method. A ‘dirty’ environment within zebrafish aquaria is more representative of the environment that humans live in, and it has been proposed that infection and initiation of an antiviral response may act as a trigger for the

generation of AGS symptoms, previously shown in *ADAR1* patients (Crow and Stetson, 2021; Livingston et al., 2014a). Rutherford and colleagues also proposed that a non-sterile aquaria environment may offer an explanation as to why zebrafish models of type I interferonopathies have been more successful at recapitulating phenotypes over rodent models, which are commonly placed in sterile, pathogen free environments (Rutherford et al., 2020).

One aspect of the immune system not translated from humans to the developing zebrafish is the adaptive immune system, which needs to be taken into consideration when characterising AGS. The innate immune system is detectable and active in zebrafish embryos from 1 dpf, whilst the adaptive is only morphologically and functionally mature from 4-6 weeks post fertilisation (Herbomel et al., 1999; Herbomel et al., 2001; Lam et al., 2004). Therefore, all characterisation of the *samhd1*$^{\Delta 23/\Delta 23}$ model was performed based on the response of an exclusively innate immune system. The antiviral type I IFN response generated by mutations in the AGS causing genes are most likely initiated by the innate immune system. However, the type I IFN producing cells in AGS within the periphery have been poorly described in the literature, whilst the type I IFN produced within the CSF has been suggested to be largely attributed to astrocytes (Cuadrado et al., 2013). Irrespective of the cells producing type I IFN, specific adaptive immune responses have been identified in the disease. For example, the presence of auto-antibodies in AGS patient brain tissue. It is unknown whether these auto-antibodies play a causal role in disease pathology, or have a role in the more general process of the immune dysregulation found across the disease (Cuadrado et al., 2015b). Moreover, lymphocytosis within the CSF is a common diagnostic feature for AGS, and the resulting lymphocytes have been shown to exhibit an upregulation in a proteolytic enzyme cathepsin D, which has been identified as a myelin-degrading protease and may contribute to the generation of white matter disease found in AGS patients (Cuadrado et al., 2013; Izzotti et al., 2009). Therefore, through modelling AGS in zebrafish, we are missing a proportion of the combined immune response, thus not completely mimicking the human condition.

There are advantages and disadvantages between modelling AGS in older and younger zebrafish (i.e. juveniles versus embryos/larvae). The main advantage of the older ages is the presence of a full immune system, whist one advantage of the younger ages is using a more pathologically relevant time period for AGS, to more accurately mimic the development of symptoms. As previously highlighted, a large proportion of AGS patients develop symptoms prenatally, or within the first few months of life (Crow et al., 2015). Moreover, modelling AGS at earlier time points may be a more effective way to identify AGS phenotypes, prior to any regenerative capabilities of the zebrafish reversing existing phenotypes. We hypothesised this may have occurred following the locomotion studies in the *samhd1*$^{\Delta 23/\Delta 23}$ model. A significant motor deficit was observed at 4 dpf, which was quickly resolved by 5 dpf, indicating an intrinsic rescue mechanism present in the zebrafish. To confirm this effect, a future experiment would include attempting to phenocopy the other neurological effects, such as microcephaly and brain cell death in 5 dpf larvae to determine whether these phenotypes persist in the older animals. The regenerative capabilities of zebrafish larvae has already been demonstrated in zebrafish models of ICH, whereby loss of motility is improved from three days

post injury, suggesting effective recovery processes are responding to brain cell death following ICH, and we may be observing a similar mechanism with the *samhd1*$^{\Delta 23/\Delta 23}$ model (Crilly et al., 2018).

The identification of neurological phenotypes in the *samhd1*$^{\Delta 23/\Delta 23}$ strain demonstrated the effectiveness of the model at recapitulating clinically relevant AGS phenotypes and also provides exciting new avenues for future study. As this thesis focussed mainly on broad characterisation of the *samhd1*$^{\Delta 23/\Delta 23}$ model, we were unable to identify mechanisms by which these neurological phenotypes manifested. As such, future studies would involve utilising various transgenic reporter lines to understand the cell types involved in the formation of these phenotypes. For example, the Tg(*ifnphi1:*mCherry) reporter line, previously discussed in chapter 3, should be crossed onto the *samhd1*$^{\Delta 23/\Delta 23}$ line to identify the number and location of *ifnphi1* positive cells, to determine whether a higher concentration of cells are observed within the CNS compared to the periphery (Kasher et al., 2015; Palha et al., 2013). The *ifnphi1* positive cells could be FACS sorted, followed by analysis of their mRNA expression profile, by using specific cell markers, allowing the identity of the main cell types involved in type I IFN production to be determined, as previously performed using the Tg(ifphi1:mCherry) line infected with chikungunya virus (Palha et al., 2013). Moreover, it would be useful to co-stain TUNEL (which identified enhanced brain cell death) with brain cell specific markers, to identify the exact cell types affected. Similarly, the TUNEL stain should be co-stained with the znp-1 antibody, to elucidate whether the cause of the motor deficits in the *samhd1*$^{\Delta 23/\Delta 23}$ model is due to enhanced motor neuron death.

The presence of classical AGS phenotypes, and subtle subtype specific phenotypes found in the *samhd1*$^{\Delta 23/\Delta 23}$ line, presents zebrafish as an advantageous alternative to AGS disease modelling in rodents. Alternatively, zebrafish modelling could be utilised in conjunction with the more recent CNS specific conditional knock-out rodent models which have been generated, and have been found to present with similar neurological phenotypes as AGS patients (Aditi et al., 2021).

We suggest that the additional AGS sub-types could also be modelled in zebrafish. An *adar1* MO model was used alongside the *samhd1* MO model, and produced similar phenotypes, with regards to ISG expression and developmental delay (Kasher et al., 2015). Therefore, we hypothesise that a stable *adar1* mutant should be generated, alongside a gain of function *ifih1* model (a loss of function model exists, but was not used to model AGS7) (Rajshekar et al., 2018).

There were a number of limitations associated with the generation and characterisation of the *samhd1*$^{\Delta 23/\Delta 23}$ model. Firstly, we were unable to confirm that knock-down of *samhd1* following CRISPR-Cas9 equated to a loss in protein levels, due to the lack of a reliable antibody. Therefore, we had to make an assumption that a significant loss in gene expression would also lead to a reduction in protein production. This may in part be confirmed by the presence of AGS specific phenotypes in the *samhd1*$^{\Delta 23/\Delta 23}$ model which does suggest a link to loss of samhd1 function. However, it should also be confirmed that a mutation in *samhd1* is the reason behind the phenotypes observed, which could be achieved by injecting full length *samhd1* mRNA into fertilised *samhd1*$^{\Delta 23/\Delta 23}$ eggs to determine whether the phenotypes are rescued. Additionally, the uncertainty regarding

picornavirus infection within the aquaria is another limitation, as an infection could mask the true effect of the *samhd1*$^{\Delta 23/\Delta 23}$ model, when compared to WT fish that are also infected with a virus. Care should be taken in the future to establish ISG expressions between bleached and non-bleached larvae to determine any differences.

6.3 The role of samhd1 in cerebrovascular disease

The literature suggests that AGS5 patients suffer from cerebrovascular disease because SAMHD1 possesses an as yet undescribed role relating to neurovascular stability, distinct from the established dNTPase activity of SAMHD1 (Ramesh et al., 2010). We attempted to elucidate this role in the *samhd1*$^{\Delta 23/\Delta 23}$ model, however, this proved challenging as the fish possessed only a subtle cerebrovascular disease phenotype, with a small percentage demonstrating a spontaneous ischaemic or haemorrhagic stroke phenotype under baseline conditions. However, the *samhd1*$^{\Delta 23/\Delta 23}$ embryos did possess an increased susceptibility to brain haemorrhaging upon low dose ATV treatment. As discussed in previous chapters, ATV results in ICH by causing cerebrovascular weakness through the actions of reduced cholesterol on the structural components of the endothelium, leading to vessel weakness and rupture (Eisa-Beygi et al., 2013). The findings that *samhd1*$^{\Delta 23/\Delta 23}$ embryos were more susceptible to the vessel rupture indicated a pre-existing cerebrovascular weakness, prior to the addition of ATV. Due to the mechanism by which ATV exerts its effects, we hypothesised the weakness observed in the *samhd1*$^{\Delta 23/\Delta 23}$ embryos was a result of a cholesterol dysregulation, alluding to a functional role of samhd1 within the cholesterol biosynthesis pathway. Such a link would also fit with the presence of both ischaemic and haemorrhagic stroke in AGS5 patients, as both high and low cholesterol are risk factors for both stroke sub-types within the general population (Prospective Studies et al., 2007). Analysis of cholesterol biosynthesis gene expression revealed a downregulation in *samhd1*$^{\Delta 23/\Delta 23}$ larval heads, furthering our hypothesis of samhd1 involvement with cholesterol.

However, we then suspected a different relationship may have confounded this result. Over recent years, an immune-cholesterol axis has been established, with particular focus on the interaction between type I IFN signalling and intracellular cholesterol, as an antiviral response mechanism. Therefore, this suggested that what we observed in the *samhd1*$^{\Delta 23/\Delta 23}$ model, may not be specifically attributed to samhd1, rather a general type I IFN effect. This was reinforced by clinical studies observing a reduction in total cholesterol and other lipid fractions following IFN treatment for a number of different conditions, including cancer, HCV and MS (Borden et al., 1990; Coppola et al., 2006; Shinohara et al., 1997). RNA sequencing data of whole blood from AGS1-7 patients confirmed that cholesterol dysregulation was not a SAMHD1 specific event, as a significant upregulation of a number of cholesterol biosynthesis genes was identified across all sub-types (excluding *TREX1* patients). This finding was interesting, and opposed our original hypothesis, from a directional perspective at least. However, there is one key difference between the results obtained in this study and the IFN treatment studies. As previously mentioned, we measured cholesterol biosynthesis gene

expression in whole blood, whilst the other studies measured cholesterol and other lipids fractions at the lipid level, to more accurately determine the concentrations of cholesterol within the plasma. Gene expression does not necessarily equate to lipid levels, therefore, we are unable to make full comparisons between the studies. However, we have suggested that the discrepancies observed within cholesterol upregulation (patient blood) and downregulation (zebrafish model) may be accounted for by a negative feedback loop in AGS patients. Due to the chronic activation of the type I IFN pathway in AGS patients, there may be a mechanism to override the consistent downregulation of *de novo* cholesterol biosynthesis. This could include suppression of particular ISGs, such as *CH25H*, by the actions of ATF3 (Gold et al., 2012). *CH25H* encodes the enzyme responsible generating 25HC, the oxysterol that acts to specifically reduce *de novo* cholesterol biosynthesis as an antiviral mechanism.

Therefore, we believe that the RNA sequencing data set should be more widely utilised in future studies to look more in depth at interactions between other pathways affected by excessive type I IFN production. It would also be interesting to compare gene expression between chronic type I IFN exposure, and more acute exposure, as occurs following viral infection. This would further help to elucidate feedback mechanisms that may be in place depending on the exposure time for type I IFN. One caveat with this data set was the lack of additional information regarding the AGS patients. Most importantly, we did not possess knowledge of external factors that may contribute to cholesterol dysregulation at the genetic level, for example any drug treatment which could interfere with cholesterol biosynthesis.

Moreover, in the future, it would be useful to measure cholesterol and other lipid concentrations in both the periphery and the CSF. This would be to first determine the relationship between cholesterol biosynthesis gene expression and total cholesterol concentrations. Secondly, we hypothesise that a cholesterol dysregulation is also apparent within the CSF, as a result of the CSF being the primary site of type I IFN production in AGS patients (Lodi et al., 2021). As brain cholesterol is synthesised locally, peripheral samples do not directly indicate the levels within the brain and CNS, thus separate measurements should be produced (Bjorkhem and Meaney, 2004). However, this is not to discredit the usefulness of peripheral measurements, which are much easier to obtain than CSF. The literature has previously identified direct correlative relationships between plasma cholesterol levels and stroke (both ischaemic and haemorrhagic). Moreover, there are associations between increased plasma LDL levels, resulting in intracranial calcifications, and also dysregulated cholesterol homeostasis leading to chronic neurodegenerative disorders (Vance, 2012; Yao et al., 2020). Therefore, by identifying this novel dysregulation of cholesterol biosynthesis genes, it could lead to greater understanding regarding a number of the more common classical symptoms found in AGS, such as intracranial calcifications, white matter disease and brain atrophy, where cholesterol may be a key contributing factor (La Piana et al., 2016).

Limitations associated with chapter 4 are similar to those discussed regarding chapter 3. Additionally, the identification of cerebrovascular abnormalities could be greatly improved, as described in chapter 4. Technical limitations made it difficult to identify any gross structural issues within the

cerebrovasculature. Given the subtle nature of a number of phenotypes observed in the *samhd1*$^{\Delta 23/\Delta 23}$ model, there is a chance that any subtle differences between the WT and *samhd1*$^{\Delta 23/\Delta 23}$ vessels were missed. Thus, this experiment should be revisited again following future optimisation of the imaging techniques, to more accurately depict abnormalities within the cerebrovasculature. Moreover, time also limited further evaluation of the cholesterol dysregulation identified in the *samhd1*$^{\Delta 23/\Delta 23}$ model. As discussed, cholesterol biosynthesis gene expression was measured in larval brains, and it would have been useful to also measure cholesterol lipid levels within the larval brains to further support the hypothesis regarding cerebrovascular weakness as a result of reduced cholesterol. We have also discussed the need to measure cholesterol levels in AGS patients, following the finding of cholesterol biosynthesis dysregulation in whole blood, which may improve our understanding of the disease pathology.

6.4 Type I IFN and cholesterol relationship within the brain endothelium

The immune-cholesterol axis previously described, has been identified in a number of different immune cells and other cell types, highlighting the ability of type I IFN signalling to directly alter intracellular cholesterol, as an antiviral response (Lee and Bensinger, 2022; York et al., 2015; Zhou et al., 2020). This has been shown to occur predominantly through the actions of CH25H/25HC (Abrams et al., 2020; Cyster et al., 2014; Liu et al., 2013; Liu et al., 2018a). One cell type where this response had not been elucidated was in brain endothelial cells, leading us to investigate the effect of type I IFN on intracellular cholesterol, and the downstream effect on brain endothelial cell function, which we aimed to relate to cerebrovascular disease.

Whilst IFNβ treatment in brain endothelial cells highlighted the ability of the endothelium to respond to type I IFN by upregulating a number of ISGs, there was no effect on cholesterol biosynthesis gene expression. This suggested the presence of cell type specific effects, whereby the levels of 25HC produced by CH25H were not sufficient to reduce cholesterol biosynthesis gene expression in brain endothelial cells. As a result, we focussed on direct 25HC treatment in brain endothelial cells, which we hypothesised would represent a paracrine signalling factor produced downstream of type I IFN. This is more likely to mimic the situation *in vivo*, as immune cells are capable of secreting 25HC which then act on neighbouring cells (Blanc et al., 2013).

25HC treatment on brain endothelial cells correlated with 25HC treatment in other cell types that highlighted a significant reduction in cholesterol biosynthesis gene expression, coupled with a loss of free cholesterol from the plasma membrane (Abrams et al., 2020; Liu et al., 2018a; Zhou et al., 2020). As described previously, there are other important mechanisms by which 25HC exerts its effects, and thus should also be established in future studies, to determine the full effect of 25HC in brain endothelial cells. These include measuring levels of the precursor and mature SREBP2 protein, as both forms have been shown to be reduced following 25HC treatment. Moreover, the protein levels of HMGCR and other enzymes involved in cholesterol biosynthesis should be established, given the role 25HC plays in facilitating proteasomal degradation of HMGCR (Liu et al., 2018a; Wen et al., 2018).

We proposed that the protection against SLO induced cell in 25HC treated cells was a result of the loss of free unesterified cholesterol within the plasma membrane of brain endothelial cells. We hypothesised that this loss of membrane cholesterol was responsible for a reduction in cell migration, subsequently rescued upon the addition of exogenous cholesterol administration (Kumar et al., 2018). We also suggest intracellular cholesterol dysregulation may be responsible for altering other functional properties of brain endothelial cells, such as tube formation and shear stress, which future experiments will determine. Moreover, the alteration to membrane cholesterol has allowed us to propose a potential mechanism for the development of ICH.

A small number of viral infections have been associated with an increased ICH risk (VZV, HSV, HCV and HIV) (Behrouz et al., 2016; Hauer et al., 2019; Nagel and Gilden, 2014; Nagel et al., 2010; Tseng et al., 2015). Recent preliminary studies now also indicate a potential association with COVID-19 and risks of ICH (Varatharaj et al., 2020; H. Wang et al., 2020). The resulting mechanism behind infection leading to vessel rupture remains poorly understood, but has been suggested to occur due to infection of the cerebrovasculature causing inflammation of the endothelium and vasculopathy. As described in chapter 5, this manifests as a weakness of the cerebrovasculature, making it more susceptible to rupturing (Nagel et al., 2010). It has been proposed that a number of cytokines (including IFN-γ), chemokines and proteases all released as a result of the inflammation can reduce cerebrovascular integrity, as observed in HSV patients (Hauer et al., 2019; Kamei et al., 2009). We suggest that following infection, IFNs (type I and II) are produced and initiate the downstream transcription of *CH25H*, which acts to generate 25HC. If viruses are directly infecting the cerebrovasculature, then 25HC may exert effects on the brain endothelium to try and prevent viral entry and replication. As we hypothesised that 25HC reduces free cholesterol from the plasma membrane, this could act to weaken the structural integrity of the endothelium, and when coupled with additional inflammatory insults targeting the endothelium, may result in vessel rupture. Indeed, we hypothesise that the sole actions of 25HC on the plasma membrane are not sufficient to cause ICH, as this would suggest a much larger proportion of the public would suffer from ICH following viral infection than has been identified. However, when coupled with additional risk factors and/or co-morbidities (such as hypertension), this could create the ideal environment for vessel rupture and the generation of an ICH.

Moreover, this may provide additional links with another risk factor for ICH: hypocholesterolaemia. A reduction in serum cholesterol and corresponding lipids has been associated with increased ICH risk (Phuah et al., 2016; Valappil et al., 2012; Wang et al., 2013). Hypocholesterolaemia can occur due to a plethora of reasons (Olsson et al., 2017), however of greatest interest to us is a systemic inflammatory event prior to the generation of the ICH (Phuah et al., 2016). However, as with AGS patient data, we cannot confirm that a reduction in plasma cholesterol equates to the cholesterol levels within the brain. Nevertheless, direct correlations have been established between these measurable cholesterol levels, and the onset of ICH.

The mechanisms that explain how hypocholesterolaemia can cause ICH are not well understand, but have been hypothesised to relate to the important structural role cholesterol plays within the

plasma membrane of the endothelium (Valappil et al., 2012). We hypothesise this would work mechanistically in a similar way as to how ATV causes ICH in zebrafish embryos (Eisa-Beygi et al., 2013). Alternatively, if hypocholesterolaemia occurs as a result of viral infection, then we propose the 25HC driven mechanism described above could effectively result in ICH, similarly based on the structural integrity of the plasma membrane.

The link between viral infections and hypocholesterolaemia is yet to be fully explored, and as aforementioned, we believe vessel weakness itself is not capable of directly causing a haemorrhagic event. Hypertension was present in >80% of hypocholesterolamic patients who went on to develop an ICH, and is also commonly identified in HIV patients, thus may provide an additional risk factor necessary to generate a vessel rupture (Fahme et al., 2018; Phuah et al., 2016; Wang et al., 2013). A weakened cerebrovasculature, coupled with increased blood pressure, could produce the right environment to result in ICH. Understandably, research into hypocholesterolaemia and viral infections as risk factors for ICH are in their infancy, hence there are a large number of unanswered questions and hypotheses which need to be addressed. As such, it would be useful for future clinical ICH studies to obtain information on cholesterol levels of the patient, and also establish any recent infection, similar to what was described in a study that identified an increased risk of ICH 24 h following flu-like disease or fever (van Etten et al., 2021).

The primary limitation associated with the *in vitro* experimentation in Chapter 5 was the concentration of 25HC used to treat the brain endothelial cells. Whilst 5 µM has commonly been implemented in the literature, other studies argue that using supraphysiological concentrations is not an accurate representation of the *in vivo* environment (Robertson and Ghazal, 2016). Additionally, 25HC may have altering pro or anti-inflammatory effects, depending on the dosage used (Zhao et al., 2020). We suggested that the high concentrations may provide an explanation for why the cholesterol rescue experiment was not successful following the SLO assay. As a result, lower concentrations are currently being tested in the lab, as discussed in chapter 5.

Moreover, we have suggested that the SLO assay revealed a reduction in free cholesterol within the plasma membrane of 25HC treated cells, and upon cholesterol supplementation (for both the SLO assay and cell migration assays) it would have been useful to have fluorescently tagged the exogenous cholesterol, to observe its location within the cell, to confirm that cholesterol entered the plasma membrane. Additionally, a more specific technique should have been utilised to measure the cholesterol fractions within the cell. The results obtained were largely variable, and we did not use a method sensitive enough to directly measure free cholesterol specifically from the plasma membrane, thus the SLO assay was utilised as an indirect measure of the free membrane cholesterol. It would also be important to confirm that 25HC reduces free cholesterol, and also increases cholesterol esters, via the actions of ACAT. These actions of ACAT were not established in the brain endothelial cells, but we had anticipated that the enzyme was responsible for converting free cholesterol into cholesterol esters, as had been identified in other cell types (Abrams et al., 2020; Zang et al., 2020). Therefore, it is apparent that a number of these limitations throughout chapter 5 were based on making assumptions that brain endothelial cells would act in a similar manner to other

cell types previously described in the literature, and it is necessary to confirm the mechanism by which 25HC exerts its effects within brain endothelial cells specifically, as they could differ between cell types.

6.5 Future directions

With regards to the *samhd1*$^{\Delta 23/\Delta 23}$ model, we have attempted to thoroughly characterise the presence of clinically relevant phenotypes. However, we have not elucidated the mechanism by which these phenotypes arise, and as discussed, for future studies, we aim to utilise a number of cell-specific transgenic reporter lines to try and understand the cell types involved in the generation of these phenotypes, and whether this correlates with AGS patients. Excessive type I IFN production within the CNS has long been proposed to be responsible for the neurological phenotypes found in AGS, corroborated by rodents treated with IFN within the CSF which generated similar neurological manifestations as found in AGS patients (Akwa et al., 1998; Campbell et al., 1999). However, a recent brain specific conditional knock-out of the *Rnaseh2* gene in mice proposed that DNA damage may explain the presence of the neurological phenotypes (Aditi et al., 2021). Furthermore, we suggest the *samhd1*$^{\Delta 23/\Delta 23}$ model can also be used to determine the cause of the neurological phenotypes, by crossing the line onto a *ifnphi1-3* knockout, which has recently been obtained from Dr Jean-Pierre Levraud's research group.

Moreover, we anticipate that due to the presence of neurological phenotypes in the *samhd1*$^{\Delta 23/\Delta 23}$ model, multiple drug screens can be performed, with phenotypic rescue as a favourable outcome. Whilst ruxolitinib was not successful at preventing microcephaly, or brain cell death, there are other drugs, such as RTIs, which have been found to be effective in a small clinical trial involving AGS patients that could be tested in the *samhd1*$^{\Delta 23/\Delta 23}$ model (Rice et al., 2018).

The *in vitro* aspect of the project researching the immune-cholesterol axis in brain endothelial cells is largely ongoing, and as such there are a number of exciting experiments in the pipeline which will hopefully increase our understanding of the relationship between type I IFN and intracellular cholesterol within brain endothelial cells. As alluded to, we have shown that through the actions of 25HC, a reduction in cholesterol biosynthesis expression and also a reduction in free cholesterol in the plasma membrane is observed. This reduction in free cholesterol has been shown to alter the functional properties of brain endothelial cells, by reducing cell migration, an essential part of angiogenesis. We also hypothesise that this reduction in cholesterol may affect further properties, such as tube formation, and how the cells respond to shear stress. If shown that these properties are affected by 25HC treatment, and rescued upon the addition of exogenous cholesterol, it would be a novel discovery, and highlight the importance of intracellular cholesterol homeostasis within brain endothelial cells, in particular within the plasma membrane. This may also lend previously unknown insight into a potential mechanism for the generation of ICH following viral infection, hypocholesterolaemia, and also AGS5, as previously described.

Further characterisation is also required to accurately measure the different intracellular lipid fractions, which was not successfully determined previously. Gas chromatography- mass spectrometry has previously been used to specifically measure total cholesterol and plasma membrane cholesterol levels previously, and could be utilised in the future (Zhou et al., 2020). Moreover, the brain endothelial cells should be imaged and the effect of 25HC treatment on the formation of adheren junctions, which contribute towards endothelial integrity can be determined, as has been identified in HUVEC cells overexpressing SQLE (Tan et al., 2020). Together this will help increase understanding of the intracellular lipid composition and how it affects the structural properties of brain endothelial cells.

Additionally, future studies should include experimentation in a transwell, co-culture system of brain endothelial cells and immune cells, as have been utilised in other studies (Noonan et al., 2019). This would more accurately depict an *in vivo* environment, allowing for the complex interplay between immune cell stimulation with a virus, and the downstream type I IFN response on brain endothelial cells to be established. Importantly, it would help to determine the physiological concentrations of 25HC produced from the immune cells, and the resulting effects on brain endothelial cells.

Aside from *in vitro* studies, *in vivo* work should also be implemented to increase understanding of hypocholesterolaemia, viral infections and ICH. One avenue of this PhD project which was halted due to COVID-19, was the effect of hypocholesterolamia on haematoma volumes. Mice lacking the enzyme proprotein convertase subtilisin/kenin type 9 (PCSK9) possess a significant reduction in circulating lipoproteins and plasma cholesterol levels. PCSK9 acts to enhance degradation of LDL receptors (LDLR) on cell surfaces, and upon mutation, increased LDLR presence leads to increased clearance of the lipoproteins and cholesterol, reducing lipid levels in the plasma (Rashid et al., 2005). We hypothesised that *Pcsk9*$^{-/-}$ mice would produce higher haematoma volumes with low dose collagenase injection, due to increased fragility of the cerebrovasculature. However, whilst we were unable to answer this question, another group performed a similar study, and observed no difference in haematoma volume (Schlunk et al., 2020). Understandably, collagenase injection is not an accurate representation of ICH generation in patients. Therefore, we propose crossing *Pcsk9*$^{-/-}$ mice with a hypertensive strain, and using MRI imaging to determine the presence of spontaneous haemorrhages within the cerebrovasculature. Moreover, a similar method could be implemented whereby hypertensive mice could be infected with a virus, to see if similar effects are observed, which would indicate a similar mechanism of action.

6.6 Conclusion

In conclusion, a new pre-clinical model of AGS5 in zebrafish larvae validated the use of zebrafish to model type I interferonopathies more successfully than existing rodent pre-clinical models. Through characterisation of the model, we identified a novel relationship between excessive type I IFN signalling and cholesterol dysregulation in AGS patients, which lead to more general understanding regarding the antiviral response from type I IFN signalling, cholesterol dysregulation and the development of cerebrovascular disease in an *in vitro* setting. We have demonstrated that studying

the cause of monogenic cerebrovascular disease, such as AGS5, can facilitate understanding of more common forms of cerebrovascular disease, such as ICH associated with viral infections and hypocholesterolaemia, which will help to direct future research and potential treatment strategies for patients.

Bibliography

Abrams, M. E., Johnson, K. A., Perelman, S. S., Zhang, L. S., Endapally, S., Mar, K. B., Thompson, B. M., McDonald, J. G., Schoggins, J. W., Radhakrishnan, A. & Alto, N. M. (2020). 'Oxysterols provide innate immunity to bacterial infection by mobilizing cell surface accessible cholesterol', *Nature Microbiology,* 5(7), pp. 929-942.

Adams, C. M., Reitz, J., De Brabander, J. K., Feramisco, J. D., Li, L., Brown, M. S. & Goldstein, J. L. (2004). 'Cholesterol and 25-hydroxycholesterol inhibit activation of SREBPs by different mechanisms, both involving SCAP and Insigs', *Journal of Biological Chemistry,* 279(50), pp. 52772-80.

Adams, H. P., Jr., Bendixen, B. H., Kappelle, L. J., Biller, J., Love, B. B., Gordon, D. L. & Marsh, E. E., 3rd (1993). 'Classification of subtype of acute ischemic stroke. Definitions for use in a multicenter clinical trial. TOAST. Trial of Org 10172 in Acute Stroke Treatment', *Stroke,* 24(1), pp. 35-41.

Adamson, K. I., Sheridan, E. & Grierson, A. J. (2018). 'Use of zebrafish models to investigate rare human disease', *Journal of Medical Genetics,* 55(10), pp. 641-649.

Adang, L., Gavazzi, F., De Simone, M., Fazzi, E., Galli, J., Koh, J., Kramer-Golinkoff, J., De Giorgis, V., Orcesi, S., Peer, K., Ulrick, N., Woidill, S., Shults, J. & Vanderver, A. (2020). 'Developmental Outcomes of Aicardi Goutieres Syndrome', *Journal of Child Neurology,* 35(1), pp. 7-16.

Adinolfi, L. E., Restivo, L., Guerrera, B., Sellitto, A., Ciervo, A., Iuliano, N., Rinaldi, L., Santoro, A., Li Vigni, G. & Marrone, A. (2013). 'Chronic HCV infection is a risk factor of ischemic stroke', *Atherosclerosis,* 231(1), pp. 22-6.

Aditi, Downing, S. M., Schreiner, P. A., Kwak, Y. D., Li, Y., Shaw, T. I., Russell, H. R. & McKinnon, P. J. (2021). 'Genome instability independent of type I interferon signaling drives neuropathology caused by impaired ribonucleotide excision repair', *Neuron,* 109(24), pp. 3962-3979 e6.

Aggad, D., Mazel, M., Boudinot, P., Mogensen, K. E., Hamming, O. J., Hartmann, R., Kotenko, S., Herbomel, P., Lutfalla, G. & Levraud, J. P. (2009). 'The two groups of zebrafish virus-induced interferons signal via distinct receptors with specific and shared chains', *Journal of Immunology,* 183(6), pp. 3924-31.

Aicardi, J. & Goutieres, F. (1984). 'A progressive familial encephalopathy in infancy with calcifications of the basal ganglia and chronic cerebrospinal fluid lymphocytosis', *Annals of Neurology,* 15(1), pp. 49-54.

Akiyama, H., Ikeda, K., Katoh, M., McGeer, E. G. & McGeer, P. L. (1994). 'Expression of MRP14, 27E10, interferon-alpha and leukocyte common antigen by reactive microglia in postmortem human brain tissue', *Journal of Neuroimmunology,* 50(2), pp. 195-201.

Akwa, Y., Hassett, D. E., Eloranta, M. L., Sandberg, K., Masliah, E., Powell, H., Whitton, J. L., Bloom, F. E. & Campbell, I. L. (1998). 'Transgenic expression of IFN-alpha in the central nervous system of mice protects against lethal neurotropic viral infection but induces inflammation and neurodegeneration', *Journal of Immunology,* 161(9), pp. 5016-26.

Altan, E., Kubiski, S. V., Boros, A., Reuter, G., Sadeghi, M., Deng, X., Creighton, E. K., Crim, M. J. & Delwart, E. (2019). 'A Highly Divergent Picornavirus Infecting the Gut Epithelia of Zebrafish (Danio rerio) in Research Institutions Worldwide', *Zebrafish,* 16(3), pp. 291-299.

Amini-Bavil-Olyaee, S., Choi, Y. J., Lee, J. H., Shi, M., Huang, I. C., Farzan, M. & Jung, J. U. (2013). 'The antiviral effector IFITM3 disrupts intracellular cholesterol homeostasis to block viral entry', *Cell Host & Microbe,* 13(4), pp. 452-64.

An, S. J., Kim, T. J. & Yoon, B. W. (2017). 'Epidemiology, Risk Factors, and Clinical Features of Intracerebral Hemorrhage: An Update', *Journal of Stroke,* 19(1), pp. 3-10.

Andersen, K. K., Olsen, T. S., Dehlendorff, C. & Kammersgaard, L. P. (2009). 'Hemorrhagic and ischemic strokes compared: stroke severity, mortality, and risk factors', *Stroke,* 40(6), pp. 2068-72.

Apschner, A., Huitema, L. F., Ponsioen, B., Peterson-Maduro, J. & Schulte-Merker, S. (2014). 'Zebrafish enpp1 mutants exhibit pathological mineralization, mimicking features of generalized arterial calcification of infancy (GACI) and pseudoxanthoma elasticum (PXE)', *Disease Models & Mechanisms,* 7(7), pp. 811-22.

Assinger, A., Kral, J. B., Yaiw, K. C., Schrottmaier, W. C., Kurzejamska, E., Wang, Y., Mohammad, A. A., Religa, P., Rahbar, A., Schabbauer, G., Butler, L. M. & Soderberg-Naucler, C. (2014). 'Human cytomegalovirus-platelet interaction triggers toll-like receptor 2-dependent proinflammatory and proangiogenic responses', *Arteriosclerosis, Thrombosis, and Vascular Biology,* 34(4), pp. 801-9.

Badrock, A. P., Uggenti, C., Wacheul, L., Crilly, S., Jenkinson, E. M., Rice, G. I., Kasher, P. R., Lafontaine, D. L. J., Crow, Y. J. & O'Keefe, R. T. (2020). 'Analysis of U8 snoRNA Variants in Zebrafish Reveals How Bi-allelic Variants Cause Leukoencephalopathy with Calcifications and Cysts', *American Journal of Human Genetics,* 106(5), pp. 694-706.

Balla, K. M., Rice, M. C., Gagnon, J. A. & Elde, N. C. (2020). 'Linking Virus Discovery to Immune Responses Visualized during Zebrafish Infections', *Current Biology,* 30(11), pp. 2092-2103 e5.

Bartsch, K., Damme, M., Regen, T., Becker, L., Garrett, L., Holter, S. M., Knittler, K., Borowski, C., Waisman, A., Glatzel, M., Fuchs, H., Gailus-Durner, V., Hrabe de Angelis, M. & Rabe, B. (2018). 'RNase H2 Loss in Murine Astrocytes Results in Cellular Defects Reminiscent of Nucleic Acid-Mediated Autoinflammation', *Frontiers in Immunology,* 9, p. 587.

Bedell, V. M., Westcot, S. E. & Ekker, S. C. (2011). 'Lessons from morpholino-based screening in zebrafish', *Briefings in Functional Genomics,* 10(4), pp. 181-8.

Behrendt, R., Schumann, T., Gerbaulet, A., Nguyen, L. A., Schubert, N., Alexopoulou, D., Berka, U., Lienenklaus, S., Peschke, K., Gibbert, K., Wittmann, S., Lindemann, D., Weiss, S., Dahl, A., Naumann, R., Dittmer, U., Kim, B., Mueller, W., Gramberg, T. & Roers, A. (2013). 'Mouse SAMHD1 has antiretroviral activity and suppresses a spontaneous cell-intrinsic antiviral response', *Cell Reports,* 4(4), pp. 689-96.

Behrouz, R., Topel, C. H., Seifi, A., Birnbaum, L. A., Brey, R. L., Misra, V. & Di Napoli, M. (2016). 'Risk of intracerebral hemorrhage in HIV/AIDS: a systematic review and meta-analysis', *Journal of Neurovirology,* 22(5), pp. 634-640.

Beloglazova, N., Flick, R., Tchigvintsev, A., Brown, G., Popovic, A., Nocek, B. & Yakunin, A. F. (2013). 'Nuclease activity of the human SAMHD1 protein implicated in the Aicardi-Goutieres syndrome and HIV-1 restriction', *Journal of Biological Chemistry,* 288(12), pp. 8101-10.

Bennett, C. M., Kanki, J. P., Rhodes, J., Liu, T. X., Paw, B. H., Kieran, M. W., Langenau, D. M., Delahaye-Brown, A., Zon, L. I., Fleming, M. D. & Look, A. T. (2001). 'Myelopoiesis in the zebrafish, Danio rerio', *Blood,* 98(3), pp. 643-51.

Bjorkhem, I. & Meaney, S. (2004). 'Brain cholesterol: long secret life behind a barrier', *Arteriosclerosis, Thrombosis, and Vascular Biology,* 24(5), pp. 806-15.

Blanc, M., Hsieh, W. Y., Robertson, K. A., Kropp, K. A., Forster, T., Shui, G., Lacaze, P., Watterson, S., Griffiths, S. J., Spann, N. J., Meljon, A., Talbot, S., Krishnan, K., Covey, D. F., Wenk, M. R., Craigon, M., Ruzsics, Z., Haas, J., Angulo, A., Griffiths, W. J., Glass, C. K., Wang, Y. & Ghazal, P. (2013). 'The transcription factor STAT-1 couples macrophage synthesis of 25-hydroxycholesterol to the interferon antiviral response', *Immunity,* 38(1), pp. 106-18.

Blanc, M., Hsieh, W. Y., Robertson, K. A., Watterson, S., Shui, G., Lacaze, P., Khondoker, M., Dickinson, P., Sing, G., Rodriguez-Martin, S., Phelan, P., Forster, T., Strobl, B., Muller, M., Riemersma, R., Osborne, T., Wenk, M. R., Angulo, A. & Ghazal, P. (2011). 'Host defense against viral infection involves interferon mediated down-regulation of sterol biosynthesis', *PLoS Biology,* 9(3), p. e1000598.

Boehme, A. K., Esenwa, C. & Elkind, M. S. (2017). 'Stroke Risk Factors, Genetics, and Prevention', *Circulation Research,* 120(3), pp. 472-495.

Borden, E. C., Rinehart, J. J., Storer, B. E., Trump, D. L., Paulnock, D. M. & Teitelbaum, A. P. (1990). 'Biological and clinical effects of interferon-beta ser at two doses', *Journal of Interferon Research,* 10(6), pp. 559-70.

Boren, J., Chapman, M. J., Krauss, R. M., Packard, C. J., Bentzon, J. F., Binder, C. J., Daemen, M. J., Demer, L. L., Hegele, R. A., Nicholls, S. J., Nordestgaard, B. G., Watts, G. F., Bruckert, E., Fazio, S., Ference, B. A., Graham, I., Horton, J. D., Landmesser, U., Laufs, U., Masana, L., Pasterkamp, G., Raal, F. J., Ray, K. K., Schunkert, H., Taskinen, M. R., van de Sluis, B., Wiklund, O., Tokgozoglu, L., Catapano, A. L. & Ginsberg, H. N. (2020). 'Low-density lipoproteins cause atherosclerotic cardiovascular disease: pathophysiological, genetic, and therapeutic insights: a consensus statement from the European Atherosclerosis Society Consensus Panel', *European Heart Journal,* 41(24), pp. 2313-2330.

Briolat, V., Jouneau, L., Carvalho, R., Palha, N., Langevin, C., Herbomel, P., Schwartz, O., Spaink, H. P., Levraud, J. P. & Boudinot, P. (2014). 'Contrasted innate responses to two viruses in zebrafish: insights into the ancestral repertoire of vertebrate IFN-stimulated genes', *Journal of Immunology,* 192(9), pp. 4328-41.

Butler, R., Wood, J. D., Landers, J. A. & Cunliffe, V. T. (2010). 'Genetic and chemical modulation of spastin-dependent axon outgrowth in zebrafish embryos indicates a role for impaired microtubule dynamics in hereditary spastic paraplegia', *Disease Models & Mechanisms,* 3(11-12), pp. 743-51.

Campbell, I. L., Krucker, T., Steffensen, S., Akwa, Y., Powell, H. C., Lane, T., Carr, D. J., Gold, L. H., Henriksen, S. J. & Siggins, G. R. (1999). 'Structural and functional neuropathology in transgenic mice with CNS expression of IFN-alpha', *Brain Research,* 835(1), pp. 46-61.

Cerritelli, S. M. & Crouch, R. J. (2009). 'Ribonuclease H: the enzymes in eukaryotes', *FEBS Journal,* 276(6), pp. 1494-505.

Chandra, A., Li, W. A., Stone, C. R., Geng, X. & Ding, Y. (2017a). 'The cerebral circulation and cerebrovascular disease I: Anatomy', *Brain Circulation,* 3(2), pp. 45-56.

Chandra, A., Stone, C. R., Li, W. A., Geng, X. & Ding, Y. (2017b). 'The cerebral circulation and cerebrovascular disease II: Pathogenesis of cerebrovascular disease', *Brain Circulation,* 3(2), pp. 57-65.

Chang, J. J., Katsanos, A. H., Khorchid, Y., Dillard, K., Kerro, A., Burgess, L. G., Goyal, N., Alexandrov, A. W., Alexandrov, A. V. & Tsivgoulis, G. (2018). 'Higher low-density lipoprotein cholesterol levels are associated with decreased mortality in patients with intracerebral hemorrhage', *Atherosclerosis,* 269, pp. 14-20.

Chen, J., Poskanzer, K. E., Freeman, M. R. & Monk, K. R. (2020). 'Live-imaging of astrocyte morphogenesis and function in zebrafish neural circuits', *Nature Neuroscience,* 23(10), pp. 1297-1306.

Chen, Y. W., Li, C. H., Yang, C. D., Liu, C. H., Chen, C. H., Sheu, J. J., Lin, S. K., Chen, A. C., Chen, P. K., Chen, P. L., Yeh, C. H., Chen, J. R., Hsiao, Y. J., Lin, C. H., Hsu, S. P., Chen, T. S., Sung, S. F., Yu, S. C., Muo, C. H., Wen, C. P., Sung, F. C., Jeng, J. S., Hsu, C. Y. & Taiwan Stroke Registry, I. (2017). 'Low cholesterol level associated with severity and outcome of spontaneous intracerebral hemorrhage: Results from Taiwan Stroke Registry', *PloS One,* 12(4), p. e0171379.

Choe, C. P., Choi, S. Y., Kee, Y., Kim, M. J., Kim, S. H., Lee, Y., Park, H. C. & Ro, H. (2021). 'Transgenic fluorescent zebrafish lines that have revolutionized biomedical research', *Lab Anim Res,* 37(1), p. 26.

Clifford, R., Louis, T., Robbe, P., Ackroyd, S., Burns, A., Timbs, A. T., Colopy, G. W., Dreau, H., Sigaux, F., Judde, J. G., Rotger, M., Telenti, A., Lin, Y. L., Pasero, P., Maelfait, J., Titsias, M., Cohen, D. R., Henderson, S. J., Ross, M. T., Bentley, D., Hillmen, P., Pettitt, A., Rehwinkel, J., Knight, S. J. L., Taylor, J. C., Crow, Y. J., Benkirane, M. & Schuh, A. (2014). 'SAMHD1 is mutated recurrently in chronic lymphocytic leukemia and is involved in response to DNA damage', *Blood,* 123(7), pp. 1021-1031.

Coggins, S. A., Mahboubi, B., Schinazi, R. F. & Kim, B. (2020). 'SAMHD1 Functions and Human Diseases', *Viruses,* 12(4), p. 382.

Collaborators, G. B. D. S. (2019). 'Global, regional, and national burden of stroke, 1990-2016: a systematic analysis for the Global Burden of Disease Study 2016', *Lancet Neurology,* 18(5), pp. 439-458.

Coppola, G., Lanzillo, R., Florio, C., Orefice, G., Vivo, P., Ascione, S., Schiavone, V., Pagano, A., Vacca, G., De Michele, G. & Morra, V. B. (2006). 'Long-term clinical experience with weekly interferon beta-1a in relapsing multiple sclerosis', *European Journal of Neurology,* 13(9), pp. 1014-21.

Coquel, F., Neumayer, C., Lin, Y. L. & Pasero, P. (2019). 'SAMHD1 and the innate immune response to cytosolic DNA during DNA replication', *Current Opinion in Immunology,* 56, pp. 24-30.

Coquel, F., Silva, M. J., Techer, H., Zadorozhny, K., Sharma, S., Nieminuszczy, J., Mettling, C., Dardillac, E., Barthe, A., Schmitz, A. L., Promonet, A., Cribier, A., Sarrazin, A., Niedzwiedz, W., Lopez, B., Costanzo, V., Krejci, L., Chabes, A., Benkirane, M., Lin, Y. L. & Pasero, P. (2018). 'SAMHD1 acts at stalled replication forks to prevent interferon induction', *Nature,* 557(7703), pp. 57-61.

Corvera, S., DiBonaventura, C. & Shpetner, H. S. (2000). 'Cell confluence-dependent remodeling of endothelial membranes mediated by cholesterol', *Journal of Biological Chemistry,* 275(40), pp. 31414-31421.

Crilly, S., Njegic, A., Laurie, S. E., Fotiou, E., Hudson, G., Barrington, J., Webb, K., Young, H. L., Badrock, A. P., Hurlstone, A., Rivers-Auty, J., Parry-Jones, A. R., Allan, S. M. & Kasher, P. R. (2018). 'Using zebrafish larval models to study brain injury, locomotor and neuroinflammatory outcomes following intracerebral haemorrhage', *F1000 Research,* 7, p. 1617.

Crosse, K. M., Monson, E. A., Beard, M. R. & Helbig, K. J. (2018). 'Interferon-Stimulated Genes as Enhancers of Antiviral Innate Immune Signaling', *Journal of Innate Immunity,* 10(2), pp. 85-93.

Crow, Y. J. (2011). 'Type I interferonopathies: a novel set of inborn errors of immunity', *Annals of the New York Academy of Sciences,* 1238, pp. 91-8.

Crow, Y. J., Chase, D. S., Lowenstein Schmidt, J., Szynkiewicz, M., Forte, G. M., Gornall, H. L., Oojageer, A., Anderson, B., Pizzino, A., Helman, G., Abdel-Hamid, M. S., Abdel-Salam, G. M., Ackroyd, S., Aeby, A., Agosta, G., Albin, C., Allon-Shalev, S., Arellano, M., Ariaudo, G., Aswani, V., Babul-Hirji, R., Baildam, E. M., Bahi-Buisson, N., Bailey, K. M., Barnerias, C., Barth, M., Battini, R., Beresford, M. W., Bernard, G., Bianchi, M., Billette de Villemeur, T., Blair, E. M., Bloom, M., Burlina, A. B., Carpanelli, M. L., Carvalho, D. R., Castro-Gago, M., Cavallini, A., Cereda, C., Chandler, K. E., Chitayat, D. A., Collins, A. E., Sierra Corcoles, C., Cordeiro, N. J., Crichiutti, G., Dabydeen, L., Dale, R. C., D'Arrigo, S., De Goede, C. G., De Laet, C., De Waele, L. M., Denzler, I., Desguerre, I., Devriendt, K., Di Rocco, M., Fahey, M. C., Fazzi, E., Ferrie, C. D., Figueiredo, A., Gener, B., Goizet, C., Gowrinathan, N. R., Gowrishankar, K., Hanrahan, D., Isidor, B., Kara, B., Khan, N., King, M. D., Kirk, E. P., Kumar, R., Lagae, L., Landrieu, P., Lauffer, H., Laugel, V., La Piana, R., Lim, M. J., Lin, J. P., Linnankivi, T., Mackay, M. T., Marom, D. R., Marques Lourenco, C., McKee, S. A., Moroni, I., Morton, J. E., Moutard, M. L., Murray, K., Nabbout, R., Nampoothiri, S., Nunez-Enamorado, N., Oades, P. J., Olivieri, I., Ostergaard, J. R., Perez-Duenas, B., Prendiville, J. S., Ramesh, V., Rasmussen, M., Regal, L., Ricci, F., Rio, M., Rodriguez, D., et al. (2015). 'Characterization of human disease phenotypes associated with mutations in TREX1, RNASEH2A, RNASEH2B, RNASEH2C, SAMHD1, ADAR, and IFIH1', *American Journal of Medical Genetics Part A,* 167A(2), pp. 296-312.

Crow, Y. J., Hayward, B. E., Parmar, R., Robins, P., Leitch, A., Ali, M., Black, D. N., van Bokhoven, H., Brunner, H. G., Hamel, B. C., Corry, P. C., Cowan, F. M., Frints, S. G., Klepper, J., Livingston, J. H., Lynch, S. A., Massey, R. F., Meritet, J. F., Michaud, J. L., Ponsot, G., Voit, T., Lebon, P.,

Bonthron, D. T., Jackson, A. P., Barnes, D. E. & Lindahl, T. (2006a). 'Mutations in the gene encoding the 3'-5' DNA exonuclease TREX1 cause Aicardi-Goutieres syndrome at the AGS1 locus', *Nature Genetics,* 38(8), pp. 917-20.

Crow, Y. J., Leitch, A., Hayward, B. E., Garner, A., Parmar, R., Griffith, E., Ali, M., Semple, C., Aicardi, J., Babul-Hirji, R., Baumann, C., Baxter, P., Bertini, E., Chandler, K. E., Chitayat, D., Cau, D., Dery, C., Fazzi, E., Goizet, C., King, M. D., Klepper, J., Lacombe, D., Lanzi, G., Lyall, H., Martinez-Frias, M. L., Mathieu, M., McKeown, C., Monier, A., Oade, Y., Quarrell, O. W., Rittey, C. D., Rogers, R. C., Sanchis, A., Stephenson, J. B., Tacke, U., Till, M., Tolmie, J. L., Tomlin, P., Voit, T., Weschke, B., Woods, C. G., Lebon, P., Bonthron, D. T., Ponting, C. P. & Jackson, A. P. (2006b). 'Mutations in genes encoding ribonuclease H2 subunits cause Aicardi-Goutieres syndrome and mimic congenital viral brain infection', *Nature Genetics,* 38(8), pp. 910-6.

Crow, Y. J. & Livingston, J. H. (2008). 'Aicardi-Goutieres syndrome: an important Mendelian mimic of congenital infection', *Developmental Medicine and Child Neurology,* 50(6), pp. 410-6.

Crow, Y. J. & Manel, N. (2015). 'Aicardi-Goutieres syndrome and the type I interferonopathies', *Nature Reviews: Immunology,* 15(7), pp. 429-40.

Crow, Y. J., Shetty, J. & Livingston, J. H. (2020). 'Treatments in Aicardi-Goutieres syndrome', *Developmental Medicine and Child Neurology,* 62(1), pp. 42-47.

Crow, Y. J. & Stetson, D. B. (2021). 'The type I interferonopathies: 10 years on', *Nature Reviews: Immunology*.

Crow, Y. J., Zaki, M. S., Abdel-Hamid, M. S., Abdel-Salam, G., Boespflug-Tanguy, O., Cordeiro, N. J., Gleeson, J. G., Gowrinathan, N. R., Laugel, V., Renaldo, F., Rodriguez, D., Livingston, J. H. & Rice, G. I. (2014). 'Mutations in ADAR1, IFIH1, and RNASEH2B presenting as spastic paraplegia', *Neuropediatrics,* 45(6), pp. 386-93.

Crowl, J. T., Gray, E. E., Pestal, K., Volkman, H. E. & Stetson, D. B. (2017). 'Intracellular Nucleic Acid Detection in Autoimmunity', *Annual Review of Immunology,* 35, pp. 313-336.

Cuadrado, E., Jansen, M. H., Anink, J., De Filippis, L., Vescovi, A. L., Watts, C., Aronica, E., Hol, E. M. & Kuijpers, T. W. (2013). 'Chronic exposure of astrocytes to interferon-alpha reveals molecular changes related to Aicardi-Goutieres syndrome', *Brain,* 136(Pt 1), pp. 245-58.

Cuadrado, E., Michailidou, I., van Bodegraven, E. J., Jansen, M. H., Sluijs, J. A., Geerts, D., Couraud, P. O., De Filippis, L., Vescovi, A. L., Kuijpers, T. W. & Hol, E. M. (2015a). 'Phenotypic variation in Aicardi-Goutieres syndrome explained by cell-specific IFN-stimulated gene response and cytokine release', *Journal of Immunology,* 194(8), pp. 3623-33.

Cuadrado, E., Vanderver, A., Brown, K. J., Sandza, A., Takanohashi, A., Jansen, M. H., Anink, J., Herron, B., Orcesi, S., Olivieri, I., Rice, G. I., Aronica, E., Lebon, P., Crow, Y. J., Hol, E. M. & Kuijpers, T. W. (2015b). 'Aicardi-Goutieres syndrome harbours abundant systemic and brain-reactive autoantibodies', *Annals of the Rheumatic Diseases,* 74(10), pp. 1931-9.

Cui, H. L., Grant, A., Mukhamedova, N., Pushkarsky, T., Jennelle, L., Dubrovsky, L., Gaus, K., Fitzgerald, M. L., Sviridov, D. & Bukrinsky, M. (2012). 'HIV-1 Nef mobilizes lipid rafts in macrophages through a pathway that competes with ABCA1-dependent cholesterol efflux', *Journal of Lipid Research,* 53(4), pp. 696-708.

Cully, M. (2019). 'Zebrafish earn their drug discovery stripes', *Nature Reviews: Drug Discovery,* 18(11), pp. 811-813.

Cunningham, F., Allen, J. E., Allen, J., Alvarez-Jarreta, J., Amode, M. R., Armean, I. M., Austine-Orimoloye, O., Azov, A. G., Barnes, I., Bennett, R., Berry, A., Bhai, J., Bignell, A., Billis, K., Boddu, S., Brooks, L., Charkhchi, M., Cummins, C., Da Rin Fioretto, L., Davidson, C., Dodiya, K., Donaldson, S., El Houdaigui, B., El Naboulsi, T., Fatima, R., Giron, C. G., Genez, T., Martinez, J. G., Guijarro-Clarke, C., Gymer, A., Hardy, M., Hollis, Z., Hourlier, T., Hunt, T., Juettemann, T., Kaikala, V., Kay, M., Lavidas, I., Le, T., Lemos, D., Marugan, J. C., Mohanan, S., Mushtaq, A., Naven, M., Ogeh, D. N., Parker, A., Parton, A., Perry, M., Pilizota, I., Prosovetskaia, I., Sakthivel, M. P., Salam, A. I. A., Schmitt, B. M., Schuilenburg, H.,

Sheppard, D., Perez-Silva, J. G., Stark, W., Steed, E., Sutinen, K., Sukumaran, R., Sumathipala, D., Suner, M. M., Szpak, M., Thormann, A., Tricomi, F. F., Urbina-Gomez, D., Veidenberg, A., Walsh, T. A., Walts, B., Willhoft, N., Winterbottom, A., Wass, E., Chakiachvili, M., Flint, B., Frankish, A., Giorgetti, S., Haggerty, L., Hunt, S. E., GR, I. I., Loveland, J. E., Martin, F. J., Moore, B., Mudge, J. M., Muffato, M., Perry, E., Ruffier, M., Tate, J., Thybert, D., Trevanion, S. J., Dyer, S., Harrison, P. W., Howe, K. L., Yates, A. D., Zerbino, D. R. & Flicek, P. (2022). 'Ensembl 2022', *Nucleic Acids Research,* 50(D1), pp. D988-D995.

Cyster, J. G., Dang, E. V., Reboldi, A. & Yi, T. (2014). '25-Hydroxycholesterols in innate and adaptive immunity', *Nature Reviews: Immunology,* 14(11), pp. 731-43.

d'Angelo, D. M., Di Filippo, P., Breda, L. & Chiarelli, F. (2021). 'Type I Interferonopathies in Children: An Overview', *Frontiers in Pediatrics,* 9, p. 631329.

D'Arrigo, S., Riva, D., Bulgheroni, S., Chiapparini, L., Lebon, P., Rice, G., Crow, Y. J. & Pantaleoni, C. (2008). 'Aicardi-Goutieres syndrome: description of a late onset case', *Developmental Medicine and Child Neurology,* 50(8), pp. 631-4.

D'Ascenzo, F., Quadri, G., Cerrato, E., Calcagno, A., Omede, P., Grosso Marra, W., Abbate, A., Bonora, S., Biondi Zoccai, G., Moretti, C. & Gaita, F. (2015). 'A meta-analysis investigating incidence and features of stroke in HIV-infected patients in the highly active antiretroviral therapy era', *Journal of Cardiovascular Medicine (Hagerstown, Md.),* 16(12), pp. 839-43.

Dang, E. V., McDonald, J. G., Russell, D. W. & Cyster, J. G. (2017). 'Oxysterol Restraint of Cholesterol Synthesis Prevents AIM2 Inflammasome Activation', *Cell,* 171(5), pp. 1057-1071 e11.

Davidson, S., Crotta, S., McCabe, T. M. & Wack, A. (2014). 'Pathogenic potential of interferon alphabeta in acute influenza infection', *Nature Communications,* 5, p. 3864.

Diczfalusy, U., Olofsson, K. E., Carlsson, A. M., Gong, M., Golenbock, D. T., Rooyackers, O., Flaring, U. & Bjorkbacka, H. (2009). 'Marked upregulation of cholesterol 25-hydroxylase expression by lipopolysaccharide', *Journal of Lipid Research,* 50(11), pp. 2258-64.

Donkor, E. S. (2018). 'Stroke in the 21(st) Century: A Snapshot of the Burden, Epidemiology, and Quality of Life', *Stroke Research and Treatment,* 2018, p. 3238165.

Doyon, Y., McCammon, J. M., Miller, J. C., Faraji, F., Ngo, C., Katibah, G. E., Amora, R., Hocking, T. D., Zhang, L., Rebar, E. J., Gregory, P. D., Urnov, F. D. & Amacher, S. L. (2008). 'Heritable targeted gene disruption in zebrafish using designed zinc-finger nucleases', *Nature Biotechnology,* 26(6), pp. 702-8.

du Moulin, M., Nurnberg, P., Crow, Y. J. & Rutsch, F. (2011). 'Cerebral vasculopathy is a common feature in Aicardi-Goutieres syndrome associated with SAMHD1 mutations', *Proceedings of the National Academy of Sciences of the United States of America,* 108(26), p. E232; author reply E233.

Du, S. J., Frenkel, V., Kindschi, G. & Zohar, Y. (2001). 'Visualizing normal and defective bone development in zebrafish embryos using the fluorescent chromophore calcein', *Developmental Biology,* 238(2), pp. 239-46.

Duncan, C. J. A., Randall, R. E. & Hambleton, S. (2021). 'Genetic Lesions of Type I Interferon Signalling in Human Antiviral Immunity', *Trends in Genetics,* 37(1), pp. 46-58.

Duncan, C. J. A., Thompson, B. J., Chen, R., Rice, G. I., Gothe, F., Young, D. F., Lovell, S. C., Shuttleworth, V. G., Brocklebank, V., Corner, B., Skelton, A. J., Bondet, V., Coxhead, J., Duffy, D., Fourrage, C., Livingston, J. H., Pavaine, J., Cheesman, E., Bitetti, S., Grainger, A., Acres, M., Innes, B. A., Mikulasova, A., Sun, R., Hussain, R., Wright, R., Wynn, R., Zarhrate, M., Zeef, L. A. H., Wood, K., Hughes, S. M., Harris, C. L., Engelhardt, K. R., Crow, Y. J., Randall, R. E., Kavanagh, D., Hambleton, S. & Briggs, T. A. (2019). 'Severe type I interferonopathy and unrestrained interferon signaling due to a homozygous germline mutation in STAT2', *Science Immunology,* 4(42), p. eaav7501.

Duntas, L. H. & Brenta, G. (2018). 'A Renewed Focus on the Association Between Thyroid Hormones and Lipid Metabolism', *Frontiers in Endocrinology,* 9, p. 511.
Eisa-Beygi, S., Hatch, G., Noble, S., Ekker, M. & Moon, T. W. (2013). 'The 3-hydroxy-3-methylglutaryl-CoA reductase (HMGCR) pathway regulates developmental cerebral-vascular stability via prenylation-dependent signalling pathway', *Developmental Biology,* 373(2), pp. 258-66.
Eisen, J. S. (1996). 'Zebrafish make a big splash', *Cell,* 87(6), pp. 969-77.
Eisen, J. S. & Smith, J. C. (2008). 'Controlling morpholino experiments: don't stop making antisense', *Development,* 135(10), pp. 1735-43.
Elkind, M. S. V., Boehme, A. K., Smith, C. J., Meisel, A. & Buckwalter, M. S. (2020). 'Infection as a Stroke Risk Factor and Determinant of Outcome After Stroke', *Stroke,* 51(10), pp. 3156-3168.
Fahme, S. A., Bloomfield, G. S. & Peck, R. (2018). 'Hypertension in HIV-Infected Adults: Novel Pathophysiologic Mechanisms', *Hypertension,* 72(1), pp. 44-55.
Fan, T. H., Khoury, J., Cho, S. M., Bhimraj, A., Shoskes, A. & Uchino, K. (2020). 'Cerebrovascular complications and vasculopathy in patients with herpes simplex virus central nervous system infection', *Journal of the Neurological Sciences,* 419, p. 117200.
Faundes, V., Jennings, M. D., Crilly, S., Legraie, S., Withers, S. E., Cuvertino, S., Davies, S. J., Douglas, A. G. L., Fry, A. E., Harrison, V., Amiel, J., Lehalle, D., Newman, W. G., Newkirk, P., Ranells, J., Splitt, M., Cross, L. A., Saunders, C. J., Sullivan, B. R., Granadillo, J. L., Gordon, C. T., Kasher, P. R., Pavitt, G. D. & Banka, S. (2021). 'Impaired eIF5A function causes a Mendelian disorder that is partially rescued in model systems by spermidine', *Nature Communications,* 12(1), p. 833.
Filippas-Ntekouan, S., Liberopoulos, E. & Elisaf, M. (2017). 'Lipid testing in infectious diseases: possible role in diagnosis and prognosis', *Infection,* 45(5), pp. 575-588.
Funabiki, M., Kato, H., Miyachi, Y., Toki, H., Motegi, H., Inoue, M., Minowa, O., Yoshida, A., Deguchi, K., Sato, H., Ito, S., Shiroishi, T., Takeyasu, K., Noda, T. & Fujita, T. (2014). 'Autoimmune disorders associated with gain of function of the intracellular sensor MDA5', *Immunity,* 40(2), pp. 199-212.
Gale, S. E., Westover, E. J., Dudley, N., Krishnan, K., Merlin, S., Scherrer, D. E., Han, X., Zhai, X., Brockman, H. L., Brown, R. E., Covey, D. F., Schaffer, J. E., Schlesinger, P. & Ory, D. S. (2009). 'Side chain oxygenated cholesterol regulates cellular cholesterol homeostasis through direct sterol-membrane interactions', *Journal of Biological Chemistry,* 284(3), pp. 1755-64.
Gall, A., Treuting, P., Elkon, K. B., Loo, Y. M., Gale, M., Jr., Barber, G. N. & Stetson, D. B. (2012). 'Autoimmunity initiates in nonhematopoietic cells and progresses via lymphocytes in an interferon-dependent autoimmune disease', *Immunity,* 36(1), pp. 120-31.
Gao, D., Li, T., Li, X. D., Chen, X., Li, Q. Z., Wight-Carter, M. & Chen, Z. J. (2015). 'Activation of cyclic GMP-AMP synthase by self-DNA causes autoimmune diseases', *Proceedings of the National Academy of Sciences of the United States of America,* 112(42), pp. E5699-705.
Garau, J., Cavallera, V., Valente, M., Tonduti, D., Sproviero, D., Zucca, S., Battaglia, D., Battini, R., Bertini, E., Cappanera, S., Chiapparini, L., Crasa, C., Crichiutti, G., Dalla Giustina, E., D'Arrigo, S., De Giorgis, V., De Simone, M., Galli, J., La Piana, R., Messana, T., Moroni, I., Nardocci, N., Panteghini, C., Parazzini, C., Pichiecchio, A., Pini, A., Ricci, F., Saletti, V., Salvatici, E., Santorelli, F. M., Sartori, S., Tinelli, F., Uggetti, C., Veneselli, E., Zorzi, G., Garavaglia, B., Fazzi, E., Orcesi, S. & Cereda, C. (2019). 'Molecular Genetics and Interferon Signature in the Italian Aicardi Goutieres Syndrome Cohort: Report of 12 New Cases and Literature Review', *Journal of Clinical Medicine,* 8(5), p. 750.
Gasteiger, E., Gattiker, A., Hoogland, C., Ivanyi, I., Appel, R. D. & Bairoch, A. (2003). 'ExPASy: The proteomics server for in-depth protein knowledge and analysis', *Nucleic Acids Research,* 31(13), pp. 3784-8.

Genovese, M. C., Kremer, J., Zamani, O., Ludivico, C., Krogulec, M., Xie, L., Beattie, S. D., Koch, A. E., Cardillo, T. E., Rooney, T. P., Macias, W. L., de Bono, S., Schlichting, D. E. & Smolen, J. S. (2016). 'Baricitinib in Patients with Refractory Rheumatoid Arthritis', *New England Journal of Medicine,* 374(13), pp. 1243-52.

Gold, E. S., Ramsey, S. A., Sartain, M. J., Selinummi, J., Podolsky, I., Rodriguez, D. J., Moritz, R. L. & Aderem, A. (2012). 'ATF3 protects against atherosclerosis by suppressing 25-hydroxycholesterol-induced lipid body formation', *Journal of Experimental Medicine,* 209(4), pp. 807-17.

Goldstone, D. C., Ennis-Adeniran, V., Hedden, J. J., Groom, H. C., Rice, G. I., Christodoulou, E., Walker, P. A., Kelly, G., Haire, L. F., Yap, M. W., de Carvalho, L. P., Stoye, J. P., Crow, Y. J., Taylor, I. A. & Webb, M. (2011). 'HIV-1 restriction factor SAMHD1 is a deoxynucleoside triphosphate triphosphohydrolase', *Nature,* 480(7377), pp. 379-82.

Gomez-Arias, P. J., Gomez-Garcia, F., Hernandez-Parada, J., Montilla-Lopez, A. M., Ruano, J. & Parra-Peralbo, E. (2021). 'Efficacy and Safety of Janus Kinase Inhibitors in Type I Interferon-Mediated Monogenic Autoinflammatory Disorders: A Scoping Review', *Dermatology and Therapy (Heidelb),* 11(3), pp. 733-750.

Goodwin, A. M. (2007). 'In vitro assays of angiogenesis for assessment of angiogenic and anti-angiogenic agents', *Microvascular Research,* 74(2-3), pp. 172-83.

Gresser, I., Morel-Maroger, L., Riviere, Y., Guillon, J. C., Tovey, M. G., Woodrow, D., Sloper, J. C. & Moss, J. (1980). 'Interferon-induced disease in mice and rats', *Annals of the New York Academy of Sciences,* 350, pp. 12-20.

Gritsenko, A., Yu, S., Martin-Sanchez, F., Diaz-Del-Olmo, I., Nichols, E. M., Davis, D. M., Brough, D. & Lopez-Castejon, G. (2020). 'Priming Is Dispensable for NLRP3 Inflammasome Activation in Human Monocytes In Vitro', *Frontiers in Immunology,* 11, p. 565924.

Grouleff, J., Irudayam, S. J., Skeby, K. K. & Schiott, B. (2015). 'The influence of cholesterol on membrane protein structure, function, and dynamics studied by molecular dynamics simulations', *Biochimica Et Biophysica Acta-Biomembranes,* 1848(9), pp. 1783-1795.

Gutierrez, J., Goldman, J., Dwork, A. J., Elkind, M. S., Marshall, R. S. & Morgello, S. (2015). 'Brain arterial remodeling contribution to nonembolic brain infarcts in patients with HIV', *Neurology,* 85(13), pp. 1139-45.

Gutierrez, J., Menshawy, K., Gonzalez, M., Goldman, J., Elkind, M. S., Marshall, R. & Morgello, S. (2016). 'Brain large artery inflammation associated with HIV and large artery remodeling', *AIDS,* 30(3), pp. 415-23.

Hackam, D. G. & Hegele, R. A. (2019). 'Cholesterol Lowering and Prevention of Stroke', *Stroke,* 50(2), pp. 537-541.

Hadjadj, J., Fremond, M. L. & Neven, B. (2021). 'Emerging Place of JAK Inhibitors in the Treatment of Inborn Errors of Immunity', *Frontiers in Immunology,* 12, p. 717388.

Haller, O., Arnheiter, H., Gresser, I. & Lindenmann, J. (1979). 'Genetically determined, interferon-dependent resistance to influenza virus in mice', *Journal of Experimental Medicine,* 149(3), pp. 601-12.

Hamilton, N., Rutherford, H. A., Petts, J. J., Isles, H. M., Weber, T., Henneke, M., Gartner, J., Dunning, M. J. & Renshaw, S. A. (2020). 'The failure of microglia to digest developmental apoptotic cells contributes to the pathology of RNASET2-deficient leukoencephalopathy', *Glia,* 68(7), pp. 1531-1545.

Hamming, O. J., Lutfalla, G., Levraud, J. P. & Hartmann, R. (2011). 'Crystal structure of Zebrafish interferons I and II reveals conservation of type I interferon structure in vertebrates', *Journal of Virology,* 85(16), pp. 8181-7.

Hartner, J. C., Schmittwolf, C., Kispert, A., Muller, A. M., Higuchi, M. & Seeburg, P. H. (2004). 'Liver disintegration in the mouse embryo caused by deficiency in the RNA-editing enzyme ADAR1', *Journal of Biological Chemistry,* 279(6), pp. 4894-902.

Hartner, J. C., Walkley, C. R., Lu, J. & Orkin, S. H. (2009). 'ADAR1 is essential for the maintenance of hematopoiesis and suppression of interferon signaling', *Nature Immunology,* 10(1), pp. 109-15.

Haud, N., Kara, F., Diekmann, S., Henneke, M., Willer, J. R., Hillwig, M. S., Gregg, R. G., Macintosh, G. C., Gartner, J., Alia, A. & Hurlstone, A. F. (2011). 'rnaset2 mutant zebrafish model familial cystic leukoencephalopathy and reveal a role for RNase T2 in degrading ribosomal RNA', *Proceedings of the National Academy of Sciences of the United States of America,* 108(3), pp. 1099-103.

Hauer, L., Pikija, S., Schulte, E. C., Sztriha, L. K., Nardone, R. & Sellner, J. (2019). 'Cerebrovascular manifestations of herpes simplex virus infection of the central nervous system: a systematic review', *Journal of Neuroinflammation,* 16(1), p. 19.

Herbomel, P., Thisse, B. & Thisse, C. (1999). 'Ontogeny and behaviour of early macrophages in the zebrafish embryo', *Development,* 126(17), pp. 3735-45.

Herbomel, P., Thisse, B. & Thisse, C. (2001). 'Zebrafish early macrophages colonize cephalic mesenchyme and developing brain, retina, and epidermis through a M-CSF receptor-dependent invasive process', *Developmental Biology,* 238(2), pp. 274-88.

Hiller, B., Achleitner, M., Glage, S., Naumann, R., Behrendt, R. & Roers, A. (2012). 'Mammalian RNase H2 removes ribonucleotides from DNA to maintain genome integrity', *Journal of Experimental Medicine,* 209(8), pp. 1419-26.

Hogg, M., Paro, S., Keegan, L. P. & O'Connell, M. A. (2011). 'RNA editing by mammalian ADARs', *Advances in Genetics,* 73, pp. 87-120.

Hosen, M. J., Vanakker, O. M., Willaert, A., Huysseune, A., Coucke, P. & De Paepe, A. (2013). 'Zebrafish models for ectopic mineralization disorders: practical issues from morpholino design to post-injection observations', *Frontiers in Genetics,* 4, p. 74.

Howe, K., Clark, M. D., Torroja, C. F., Torrance, J., Berthelot, C., Muffato, M., Collins, J. E., Humphray, S., McLaren, K., Matthews, L., McLaren, S., Sealy, I., Caccamo, M., Churcher, C., Scott, C., Barrett, J. C., Koch, R., Rauch, G. J., White, S., Chow, W., Kilian, B., Quintais, L. T., Guerra-Assuncao, J. A., Zhou, Y., Gu, Y., Yen, J., Vogel, J. H., Eyre, T., Redmond, S., Banerjee, R., Chi, J., Fu, B., Langley, E., Maguire, S. F., Laird, G. K., Lloyd, D., Kenyon, E., Donaldson, S., Sehra, H., Almeida-King, J., Loveland, J., Trevanion, S., Jones, M., Quail, M., Willey, D., Hunt, A., Burton, J., Sims, S., McLay, K., Plumb, B., Davis, J., Clee, C., Oliver, K., Clark, R., Riddle, C., Elliot, D., Threadgold, G., Harden, G., Ware, D., Begum, S., Mortimore, B., Kerry, G., Heath, P., Phillimore, B., Tracey, A., Corby, N., Dunn, M., Johnson, C., Wood, J., Clark, S., Pelan, S., Griffiths, G., Smith, M., Glithero, R., Howden, P., Barker, N., Lloyd, C., Stevens, C., Harley, J., Holt, K., Panagiotidis, G., Lovell, J., Beasley, H., Henderson, C., Gordon, D., Auger, K., Wright, D., Collins, J., Raisen, C., Dyer, L., Leung, K., Robertson, L., Ambridge, K., Leongamornlert, D., McGuire, S., Gilderthorp, R., Griffiths, C., Manthravadi, D., Nichol, S., Barker, G., et al. (2013). 'The zebrafish reference genome sequence and its relationship to the human genome', *Nature,* 496(7446), pp. 498-503.

Hwang, W. Y., Fu, Y., Reyon, D., Maeder, M. L., Tsai, S. Q., Sander, J. D., Peterson, R. T., Yeh, J. R. & Joung, J. K. (2013). 'Efficient genome editing in zebrafish using a CRISPR-Cas system', *Nature Biotechnology,* 31(3), pp. 227-9.

Isaacs, A. & Hitchcock, G. (1960). 'Role of interferon in recovery from virus infections', *Lancet,* 2(7141), pp. 69-71.

Ismael, S., Moshahid Khan, M., Kumar, P., Kodidela, S., Mirzahosseini, G., Kumar, S. & Ishrat, T. (2020). 'HIV Associated Risk Factors for Ischemic Stroke and Future Perspectives', *International Journal of Molecular Sciences,* 21(15).

Isogai, S., Horiguchi, M. & Weinstein, B. M. (2001). 'The vascular anatomy of the developing zebrafish: an atlas of embryonic and early larval development', *Developmental Biology,* 230(2), pp. 278-301.

Ivashkiv, L. B. & Donlin, L. T. (2014). 'Regulation of type I interferon responses', *Nature Reviews: Immunology,* 14(1), pp. 36-49.

Izzotti, A., Pulliero, A., Orcesi, S., Cartiglia, C., Longobardi, M. G., Capra, V., Lebon, P., Cama, A., La Piana, R., Lanzi, G. & Fazzi, E. (2009). 'Interferon-related transcriptome alterations in the cerebrospinal fluid cells of Aicardi-Goutieres patients', *Brain Pathology,* 19(4), pp. 650-60.

Jang, J., Park, S., Jin Hur, H., Cho, H. J., Hwang, I., Pyo Kang, Y., Im, I., Lee, H., Lee, E., Yang, W., Kang, H. C., Won Kwon, S., Yu, J. W. & Kim, D. W. (2016). '25-hydroxycholesterol contributes to cerebral inflammation of X-linked adrenoleukodystrophy through activation of the NLRP3 inflammasome', *Nat Commun,* 7, p. 13129.

Ji, Y. N., An, L., Zhan, P. & Chen, X. H. (2012). 'Cytomegalovirus infection and coronary heart disease risk: a meta-analysis', *Molecular Biology Reports,* 39(6), pp. 6537-46.

Jia, H., Thelwell, C., Dilger, P., Bird, C., Daniels, S. & Wadhwa, M. (2018). 'Endothelial cell functions impaired by interferon in vitro: Insights into the molecular mechanism of thrombotic microangiopathy associated with interferon therapy', *Thrombosis Research,* 163, pp. 105-116.

Jobst-Schwan, T., Schmidt, J. M., Schneider, R., Hoogstraten, C. A., Ullmann, J. F. P., Schapiro, D., Majmundar, A. J., Kolb, A., Eddy, K., Shril, S., Braun, D. A., Poduri, A. & Hildebrandt, F. (2018). 'Acute multi-sgRNA knockdown of KEOPS complex genes reproduces the microcephaly phenotype of the stable knockout zebrafish model', *PloS One,* 13(1), p. e0191503.

Kamei, S., Taira, N., Ishihara, M., Sekizawa, T., Morita, A., Miki, K., Shiota, H., Kanno, A., Suzuki, Y., Mizutani, T., Itoyama, Y., Morishima, T. & Hirayanagi, K. (2009). 'Prognostic value of cerebrospinal fluid cytokine changes in herpes simplex virus encephalitis', *Cytokine,* 46(2), pp. 187-93.

Kasher, P. R., Jenkinson, E. M., Briolat, V., Gent, D., Morrissey, C., Zeef, L. A., Rice, G. I., Levraud, J. P. & Crow, Y. J. (2015). 'Characterization of samhd1 morphant zebrafish recapitulates features of the human type I interferonopathy Aicardi-Goutieres syndrome', *Journal of Immunology,* 194(6), pp. 2819-25.

Kato, H., Takeuchi, O., Sato, S., Yoneyama, M., Yamamoto, M., Matsui, K., Uematsu, S., Jung, A., Kawai, T., Ishii, K. J., Yamaguchi, O., Otsu, K., Tsujimura, T., Koh, C. S., Reis e Sousa, C., Matsuura, Y., Fujita, T. & Akira, S. (2006). 'Differential roles of MDA5 and RIG-I helicases in the recognition of RNA viruses', *Nature,* 441(7089), pp. 101-5.

Ketter, E. & Randall, G. (2019). 'Virus Impact on Lipids and Membranes', *Annu Rev Virol,* 6(1), pp. 319-340.

Kettleborough, R. N., Busch-Nentwich, E. M., Harvey, S. A., Dooley, C. M., de Bruijn, E., van Eeden, F., Sealy, I., White, R. J., Herd, C., Nijman, I. J., Fenyes, F., Mehroke, S., Scahill, C., Gibbons, R., Wali, N., Carruthers, S., Hall, A., Yen, J., Cuppen, E. & Stemple, D. L. (2013). 'A systematic genome-wide analysis of zebrafish protein-coding gene function', *Nature,* 496(7446), pp. 494-7.

Kimmel, C. B., Ballard, W. W., Kimmel, S. R., Ullmann, B. & Schilling, T. F. (1995). 'Stages of embryonic development of the zebrafish', *Developmental Dynamics,* 203(3), pp. 253-310.

Kossorotoff, M., Touze, E., Godon-Hardy, S., Serre, I., Mateus, C., Mas, J. L. & Zuber, M. (2006). 'Cerebral vasculopathy with aneurysm formation in HIV-infected young adults', *Neurology,* 66(7), pp. 1121-2.

Kretschmer, S., Wolf, C., Konig, N., Staroske, W., Guck, J., Hausler, M., Luksch, H., Nguyen, L. A., Kim, B., Alexopoulou, D., Dahl, A., Rapp, A., Cardoso, M. C., Shevchenko, A. & Lee-Kirsch, M. A. (2015). 'SAMHD1 prevents autoimmunity by maintaining genome stability', *Annals of the Rheumatic Diseases,* 74(3), p. e17.

Kumar, M., Irungbam, K. & Kataria, M. (2018). 'Depletion of membrane cholesterol compromised caspase-8 imparts in autophagy induction and inhibition of cell migration in cancer cells', *Cancer Cell International,* 18, p. 23.

La Piana, R., Uggetti, C., Olivieri, I., Tonduti, D., Balottin, U., Fazzi, E. & Orcesi, S. (2014). 'Bilateral striatal necrosis in two subjects with Aicardi-Goutieres syndrome due to mutations in ADAR1 (AGS6)', *American Journal of Medical Genetics Part A,* 164A(3), pp. 815-9.

La Piana, R., Uggetti, C., Roncarolo, F., Vanderver, A., Olivieri, I., Tonduti, D., Helman, G., Balottin, U., Fazzi, E., Crow, Y. J., Livingston, J. & Orcesi, S. (2016). 'Neuroradiologic patterns and novel imaging findings in Aicardi-Goutieres syndrome', *Neurology,* 86(1), pp. 28-35.

Lai, J. K. H., Gagalova, K. K., Kuenne, C., El-Brolosy, M. A. & Stainier, D. Y. R. (2019). 'Induction of interferon-stimulated genes and cellular stress pathways by morpholinos in zebrafish', *Developmental Biology,* 454(1), pp. 21-28.

Lam, S. H., Chua, H. L., Gong, Z., Lam, T. J. & Sin, Y. M. (2004). 'Development and maturation of the immune system in zebrafish, Danio rerio: a gene expression profiling, in situ hybridization and immunological study', *Developmental & Comparative Immunology,* 28(1), pp. 9-28.

Lampugnani, M. G. (1999). 'Cell migration into a wounded area in vitro', *Methods in Molecular Biology,* 96, pp. 177-82.

Langevin, C., Aleksejeva, E., Passoni, G., Palha, N., Levraud, J. P. & Boudinot, P. (2013). 'The antiviral innate immune response in fish: evolution and conservation of the IFN system', *Journal of Molecular Biology,* 425(24), pp. 4904-20.

Lanzi, G., Fazzi, E. & D'Arrigo, S. (2002). 'Aicardi-Goutieres syndrome: a description of 21 new cases and a comparison with the literature', *European Journal of Paediatric Neurology,* 6 Suppl A, pp. A9-22; discussion A23-5, A77-86.

Lavin, M. F. & Yeo, A. J. (2021). 'DNA damage rather than type I IFN signaling is the primary mediator of neural dysfunction in Aicardi-Goutieres syndrome after RNASEH2 disruption', *Neuron,* 109(24), pp. 3897-3900.

Lawson, N. D. & Weinstein, B. M. (2002). 'In vivo imaging of embryonic vascular development using transgenic zebrafish', *Developmental Biology,* 248(2), pp. 307-18.

Lebon, P., Badoual, J., Ponsot, G., Goutieres, F., Hemeury-Cukier, F. & Aicardi, J. (1988). 'Intrathecal synthesis of interferon-alpha in infants with progressive familial encephalopathy', *Journal of the Neurological Sciences,* 84(2-3), pp. 201-8.

Lee, A. J. & Ashkar, A. A. (2018). 'The Dual Nature of Type I and Type II Interferons', *Frontiers in Immunology,* 9, p. 2061.

Lee, M. S. & Bensinger, S. J. (2022). 'Reprogramming cholesterol metabolism in macrophages and its role in host defense against cholesterol-dependent cytolysins', *Cellular & Molecular Immunology,* 19(3), pp. 327-336.

Lehmann, J. M., Kliewer, S. A., Moore, L. B., Smith-Oliver, T. A., Oliver, B. B., Su, J. L., Sundseth, S. S., Winegar, D. A., Blanchard, D. E., Spencer, T. A. & Willson, T. M. (1997). 'Activation of the nuclear receptor LXR by oxysterols defines a new hormone response pathway', *Journal of Biological Chemistry,* 272(6), pp. 3137-40.

Levraud, J. P., Boudinot, P., Colin, I., Benmansour, A., Peyrieras, N., Herbomel, P. & Lutfalla, G. (2007). 'Identification of the zebrafish IFN receptor: implications for the origin of the vertebrate IFN system', *Journal of Immunology,* 178(7), pp. 4385-94.

Levraud, J. P., Jouneau, L., Briolat, V., Laghi, V. & Boudinot, P. (2019). 'IFN-Stimulated Genes in Zebrafish and Humans Define an Ancient Arsenal of Antiviral Immunity', *Journal of Immunology,* 203(12), pp. 3361-3373.

Li, J., Wang, Y., Wang, X., Ye, L., Zhou, Y., Persidsky, Y. & Ho, W. (2013). 'Immune activation of human brain microvascular endothelial cells inhibits HIV replication in macrophages', *Blood,* 121(15), pp. 2934-42.

Li, K., Markosyan, R. M., Zheng, Y. M., Golfetto, O., Bungart, B., Li, M., Ding, S., He, Y., Liang, C., Lee, J. C., Gratton, E., Cohen, F. S. & Liu, S. L. (2013). 'IFITM proteins restrict viral membrane hemifusion', *PLoS Pathogens,* 9(1), p. e1003124.

Liddicoat, B. J., Piskol, R., Chalk, A. M., Ramaswami, G., Higuchi, M., Hartner, J. C., Li, J. B., Seeburg, P. H. & Walkley, C. R. (2015). 'RNA editing by ADAR1 prevents MDA5 sensing of endogenous dsRNA as nonself', *Science,* 349(6252), pp. 1115-20.

Lieberman, A. P., Pitha, P. M., Shin, H. S. & Shin, M. L. (1989). 'Production of tumor necrosis factor and other cytokines by astrocytes stimulated with lipopolysaccharide or a neurotropic virus', *Proceedings of the National Academy of Sciences of the United States of America,* 86(16), pp. 6348-52.

Lieschke, G. J. & Currie, P. D. (2007). 'Animal models of human disease: zebrafish swim into view', *Nature Reviews: Genetics,* 8(5), pp. 353-67.

Lieschke, G. J., Oates, A. C., Crowhurst, M. O., Ward, A. C. & Layton, J. E. (2001). 'Morphologic and functional characterization of granulocytes and macrophages in embryonic and adult zebrafish', *Blood,* 98(10), pp. 3087-96.

Lim, K. H., Chang, Y. C., Chiang, Y. H., Lin, H. C., Chang, C. Y., Lin, C. S., Huang, L., Wang, W. T., Gon-Shen Chen, C., Chou, W. C. & Kuo, Y. Y. (2016). 'Expression of CALR mutants causes mpl-dependent thrombocytosis in zebrafish', *Blood Cancer Journal,* 6(10), p. e481.

Lin, S. J., Vona, B., Barbalho, P. G., Kaiyrzhanov, R., Maroofian, R., Petree, C., Severino, M., Stanley, V., Varshney, P., Bahena, P., Alzahrani, F., Alhashem, A., Pagnamenta, A. T., Aubertin, G., Estrada-Veras, J. I., Hernandez, H. A. D., Mazaheri, N., Oza, A., Thies, J., Renaud, D. L., Dugad, S., McEvoy, J., Sultan, T., Pais, L. S., Tabarki, B., Villalobos-Ramirez, D., Rad, A., Genomics England Research, C., Galehdari, H., Ashrafzadeh, F., Sahebzamani, A., Saeidi, K., Torti, E., Elloumi, H. Z., Mora, S., Palculict, T. B., Yang, H., Wren, J. D., Ben, F., Joshi, M., Behra, M., Burgess, S. M., Nath, S. K., Hanna, M. G., Kenna, M., Merritt, J. L., 2nd, Houlden, H., Karimiani, E. G., Zaki, M. S., Haaf, T., Alkuraya, F. S., Gleeson, J. G. & Varshney, G. K. (2021). 'Biallelic variants in KARS1 are associated with neurodevelopmental disorders and hearing loss recapitulated by the knockout zebrafish', *Genetics in Medicine,* 23(10), pp. 1933-1943.

Liu, J., Fraser, S. D., Faloon, P. W., Rollins, E. L., Vom Berg, J., Starovic-Subota, O., Laliberte, A. L., Chen, J. N., Serluca, F. C. & Childs, S. J. (2007). 'A betaPix Pak2a signaling pathway regulates cerebral vascular stability in zebrafish', *Proceedings of the National Academy of Sciences of the United States of America,* 104(35), pp. 13990-5.

Liu, S. Y., Aliyari, R., Chikere, K., Li, G., Marsden, M. D., Smith, J. K., Pernet, O., Guo, H., Nusbaum, R., Zack, J. A., Freiberg, A. N., Su, L., Lee, B. & Cheng, G. (2013). 'Interferon-inducible cholesterol-25-hydroxylase broadly inhibits viral entry by production of 25-hydroxycholesterol', *Immunity,* 38(1), pp. 92-105.

Liu, Y., Hulten, L. M. & Wiklund, O. (1997). 'Macrophages isolated from human atherosclerotic plaques produce IL-8, and oxysterols may have a regulatory function for IL-8 production', *Arteriosclerosis, Thrombosis, and Vascular Biology,* 17(2), pp. 317-23.

Liu, Y., Wei, Z., Ma, X., Yang, X., Chen, Y., Sun, L., Ma, C., Miao, Q. R., Hajjar, D. P., Han, J. & Duan, Y. (2018a). '25-Hydroxycholesterol activates the expression of cholesterol 25-hydroxylase in an LXR-dependent mechanism', *Journal of Lipid Research,* 59(3), pp. 439-451.

Liu, Y., Wei, Z., Zhang, Y., Ma, X., Chen, Y., Yu, M., Ma, C., Li, X., Cao, Y., Liu, J., Han, J., Yang, X. & Duan, Y. (2018b). 'Activation of liver X receptor plays a central role in antiviral actions of 25-hydroxycholesterol', *Journal of Lipid Research,* 59(12), pp. 2287-2296.

Livingston, J. H. & Crow, Y. J. (2016). 'Neurologic Phenotypes Associated with Mutations in TREX1, RNASEH2A, RNASEH2B, RNASEH2C, SAMHD1, ADAR1, and IFIH1: Aicardi-Goutieres Syndrome and Beyond', *Neuropediatrics,* 47(6), pp. 355-360.

Livingston, J. H., Lin, J. P., Dale, R. C., Gill, D., Brogan, P., Munnich, A., Kurian, M. A., Gonzalez-Martinez, V., De Goede, C. G., Falconer, A., Forte, G., Jenkinson, E. M., Kasher, P. R., Szynkiewicz, M., Rice, G. I. & Crow, Y. J. (2014a). 'A type I interferon signature identifies bilateral striatal necrosis due to mutations in ADAR1', *Journal of Medical Genetics,* 51(2), pp. 76-82.

Livingston, J. H., Stivaros, S., Warren, D. & Crow, Y. J. (2014b). 'Intracranial calcification in childhood: a review of aetiologies and recognizable phenotypes', *Developmental Medicine and Child Neurology,* 56(7), pp. 612-26.

Lodi, L., Melki, I., Bondet, V., Seabra, L., Rice, G. I., Carter, E., Lepelley, A., Martin-Niclos, M. J., Al Adba, B., Bader-Meunier, B., Barth, M., Blauwblomme, T., Bodemer, C., Boespflug-Tanguy, O., Dale, R. C., Desguerre, I., Ducrocq, C., Dulieu, F., Dumaine, C., Ellul, P., Hadchouel, A., Hentgen, V., Hie, M., Hully, M., Jeziorski, E., Levy, R., Mochel, F., Orcesi, S., Passemard, S., Pouletty, M., Quartier, P., Renaldo, F., Seidl, R., Shetty, J., Neven, B., Blanche, S., Duffy, D., Crow, Y. J. & Fremond, M. L. (2021). 'Differential Expression of Interferon-Alpha Protein Provides Clues to Tissue Specificity Across Type I Interferonopathies', *Journal of Clinical Immunology,* 41(3), pp. 603-609.

Lu, H., Talbot, S., Robertson, K. A., Watterson, S., Forster, T., Roy, D. & Ghazal, P. (2015). 'Rapid proteasomal elimination of 3-hydroxy-3-methylglutaryl-CoA reductase by interferon-gamma in primary macrophages requires endogenous 25-hydroxycholesterol synthesis', *Steroids,* 99(Pt B), pp. 219-29.

Mackenzie, K. J., Carroll, P., Lettice, L., Tarnauskaite, Z., Reddy, K., Dix, F., Revuelta, A., Abbondati, E., Rigby, R. E., Rabe, B., Kilanowski, F., Grimes, G., Fluteau, A., Devenney, P. S., Hill, R. E., Reijns, M. A. & Jackson, A. P. (2016). 'Ribonuclease H2 mutations induce a cGAS/STING-dependent innate immune response', *EMBO Journal,* 35(8), pp. 831-44.

MacRae, C. A. & Peterson, R. T. (2015). 'Zebrafish as tools for drug discovery', *Nature Reviews: Drug Discovery,* 14(10), pp. 721-31.

Majdoul, S. & Compton, A. A. (2021). 'Lessons in self-defence: inhibition of virus entry by intrinsic immunity', *Nature Reviews: Immunology*.

Mannion, N. M., Greenwood, S. M., Young, R., Cox, S., Brindle, J., Read, D., Nellaker, C., Vesely, C., Ponting, C. P., McLaughlin, P. J., Jantsch, M. F., Dorin, J., Adams, I. R., Scadden, A. D., Ohman, M., Keegan, L. P. & O'Connell, M. A. (2014). 'The RNA-editing enzyme ADAR1 controls innate immune responses to RNA', *Cell Reports,* 9(4), pp. 1482-94.

Mazur, D. J. & Perrino, F. W. (1999). 'Identification and expression of the TREX1 and TREX2 cDNA sequences encoding mammalian 3'-->5' exonucleases', *Journal of Biological Chemistry,* 274(28), pp. 19655-60.

McNab, F., Mayer-Barber, K., Sher, A., Wack, A. & O'Garra, A. (2015). 'Type I interferons in infectious disease', *Nature Reviews: Immunology,* 15(2), pp. 87-103.

Meuwissen, M. E., Schot, R., Buta, S., Oudesluijs, G., Tinschert, S., Speer, S. D., Li, Z., van Unen, L., Heijsman, D., Goldmann, T., Lequin, M. H., Kros, J. M., Stam, W., Hermann, M., Willemsen, R., Brouwer, R. W., Van, I. W. F., Martin-Fernandez, M., de Coo, I., Dudink, J., de Vries, F. A., Bertoli Avella, A., Prinz, M., Crow, Y. J., Verheijen, F. W., Pellegrini, S., Bogunovic, D. & Mancini, G. M. (2016). 'Human USP18 deficiency underlies type 1 interferonopathy leading to severe pseudo-TORCH syndrome', *Journal of Experimental Medicine,* 213(7), pp. 1163-74.

Miller, E. C. & Elkind, M. S. (2016). 'Infection and Stroke: an Update on Recent Progress', *Current Neurology and Neuroscience Reports,* 16(1), p. 2.

Mitsche, M. A., McDonald, J. G., Hobbs, H. H. & Cohen, J. C. (2015). 'Flux analysis of cholesterol biosynthesis in vivo reveals multiple tissue and cell-type specific pathways', *Elife,* 4, p. e07999.

Montague, T. G., Cruz, J. M., Gagnon, J. A., Church, G. M. & Valen, E. (2014). 'CHOPCHOP: a CRISPR/Cas9 and TALEN web tool for genome editing', *Nucleic Acids Research,* 42(Web Server issue), pp. W401-7.

Morita, M., Stamp, G., Robins, P., Dulic, A., Rosewell, I., Hrivnak, G., Daly, G., Lindahl, T. & Barnes, D. E. (2004). 'Gene-targeted mice lacking the Trex1 (DNase III) 3'-->5' DNA exonuclease develop inflammatory myocarditis', *Molecular and Cellular Biology,* 24(15), pp. 6719-27.

Moulton, J. D. (2017). 'Using Morpholinos to Control Gene Expression', *Current Protocols in Nucleic Acid Chemistry,* 68, pp. 4 30 1-4 30 29.

Mowry, K. L. & Steitz, J. A. (1987). 'Identification of the human U7 snRNP as one of several factors involved in the 3' end maturation of histone premessenger RNA's', *Science,* 238(4834), pp. 1682-7.

Mu, X., Ahmad, S. & Hur, S. (2016). 'Endogenous Retroelements and the Host Innate Immune Sensors', *Advances in Immunology,* 132, pp. 47-69.

Mustanoja, S., Strbian, D., Putaala, J., Meretoja, A., Curtze, S., Haapaniemi, E., Sairanen, T., Hietikko, R., Siren, J., Kaste, M. & Tatlisumak, T. (2013). 'Association of prestroke statin use and lipid levels with outcome of intracerebral hemorrhage', *Stroke,* 44(8), pp. 2330-2.

Nagel, M. A. & Bubak, A. N. (2018). 'Varicella Zoster Virus Vasculopathy', *Journal of Infectious Diseases,* 218(suppl_2), pp. S107-S112.

Nagel, M. A. & Gilden, D. (2014). 'Update on varicella zoster virus vasculopathy', *Current Infectious Disease Reports,* 16(6), p. 407.

Nagel, M. A. & Gilden, D. (2015). 'The relationship between herpes zoster and stroke', *Current Neurology and Neuroscience Reports,* 15(4), p. 16.

Nagel, M. A., Mahalingam, R., Cohrs, R. J. & Gilden, D. (2010). 'Virus vasculopathy and stroke: an under-recognized cause and treatment target', *Infectious Disorders-Drug Targets,* 10(2), pp. 105-11.

Neven, B., Al Adba, B., Hully, M., Desguerre, I., Pressiat, C., Boddaert, N., Duffy, D., Rice, G. I., Seabra, L., Fremond, M. L., Blanche, S. & Crow, Y. J. (2020). 'JAK Inhibition in the Aicardi-Goutieres Syndrome', *New England Journal of Medicine,* 383(22), pp. 2190-2191.

Nishimura, T., Inoue, T., Shibata, N., Sekine, A., Takabe, W., Noguchi, N. & Arai, H. (2005). 'Inhibition of cholesterol biosynthesis by 25-hydroxycholesterol is independent of OSBP', *Genes to Cells,* 10(8), pp. 793-801.

Noonan, J., Grassia, G., MacRitchie, N., Garside, P., Guzik, T. J., Bradshaw, A. C. & Maffia, P. (2019). 'A Novel Triple-Cell Two-Dimensional Model to Study Immune-Vascular Interplay in Atherosclerosis', *Frontiers in Immunology,* 10, p. 849.

O'Donnell, M., Xavier, D., Diener, C., Sacco, R., Lisheng, L., Zhang, H., Pias, P., Truelsen, T., Chin, S. L., Rangarajan, S., Devilliers, L., Damasceno, A., Mondo, C., Lanas, F., Avezum, A., Diaz, R., Varigos, J., Hankey, G., Teal, P., Kapral, M., Ryglewicz, D., Czlonkowska, A., Skowronska, M., Lopez-Jaramillo, P., Dans, T., Langhorne, P., Yusuf, S. & investigators, I. (2010). 'Rationale and design of INTERSTROKE: a global case-control study of risk factors for stroke', *Neuroepidemiology,* 35(1), pp. 36-44.

Olsen, B. N., Schlesinger, P. H., Ory, D. S. & Baker, N. A. (2011). '25-Hydroxycholesterol increases the availability of cholesterol in phospholipid membranes', *Biophysical Journal,* 100(4), pp. 948-56.

Olsson, A. G., Angelin, B., Assmann, G., Binder, C. J., Bjorkhem, I., Cedazo-Minguez, A., Cohen, J., von Eckardstein, A., Farinaro, E., Muller-Wieland, D., Parhofer, K. G., Parini, P., Rosenson, R. S., Starup-Linde, J., Tikkanen, M. J. & Yvan-Charvet, L. (2017). 'Can LDL cholesterol be too low? Possible risks of extremely low levels', *Journal of Internal Medicine,* 281(6), pp. 534-553.

Orcesi, S., La Piana, R. & Fazzi, E. (2009). 'Aicardi-Goutieres syndrome', *British Medical Bulletin,* 89, pp. 183-201.

Ormsby, T. J. R., Owens, S. E., Clement, L., Mills, T. J., Cronin, J. G., Bromfield, J. J. & Sheldon, I. M. (2022). 'Oxysterols Protect Epithelial Cells Against Pore-Forming Toxins', *Frontiers in Immunology,* 13, p. 815775.

Otsuki, N., Sakata, M., Saito, K., Okamoto, K., Mori, Y., Hanada, K. & Takeda, M. (2018). 'Both Sphingomyelin and Cholesterol in the Host Cell Membrane Are Essential for Rubella Virus Entry', *Journal of Virology,* 92(1).

Ou, Z. J., Chen, J., Dai, W. P., Liu, X., Yang, Y. K., Li, Y., Lin, Z. B., Wang, T. T., Wu, Y. Y., Su, D. H., Cheng, T. P., Wang, Z. P., Tao, J. & Ou, J. S. (2016). '25-Hydroxycholesterol impairs endothelial function and vasodilation by uncoupling and inhibiting endothelial nitric oxide synthase', *American Journal of Physiology: Endocrinology and Metabolism,* 311(4), pp. E781-E790.

Palha, N., Guivel-Benhassine, F., Briolat, V., Lutfalla, G., Sourisseau, M., Ellett, F., Wang, C. H., Lieschke, G. J., Herbomel, P., Schwartz, O. & Levraud, J. P. (2013). 'Real-time whole-body visualization of Chikungunya Virus infection and host interferon response in zebrafish', *PLoS Pathogens,* 9(9), p. e1003619.

Parng, C., Seng, W. L., Semino, C. & McGrath, P. (2002). 'Zebrafish: a preclinical model for drug screening', *Assay and Drug Development Technologies,* 1(1 Pt 1), pp. 41-8.

Pestka, S., Krause, C. D. & Walter, M. R. (2004). 'Interferons, interferon-like cytokines, and their receptors', *Immunological Reviews,* 202, pp. 8-32.

Phuah, C. L., Raffeld, M. R., Ayres, A. M., Viswanathan, A., Greenberg, S. M., Biffi, A., Rosand, J. & Anderson, C. D. (2016). 'Subacute decline in serum lipids precedes the occurrence of primary intracerebral hemorrhage', *Neurology,* 86(22), pp. 2034-41.

Piccoli, C., Bronner, N., Gavazzi, F., Dubbs, H., De Simone, M., De Giorgis, V., Orcesi, S., Fazzi, E., Galli, J., Masnada, S., Tonduti, D., Varesio, C., Vanderver, A., Vossough, A. & Adang, L. (2021). 'Late-Onset Aicardi-Goutieres Syndrome: A Characterization of Presenting Clinical Features', *Pediatric Neurology,* 115, pp. 1-6.

Pillai, R. S., Grimmler, M., Meister, G., Will, C. L., Luhrmann, R., Fischer, U. & Schumperli, D. (2003). 'Unique Sm core structure of U7 snRNPs: assembly by a specialized SMN complex and the role of a new component, Lsm11, in histone RNA processing', *Genes & Development,* 17(18), pp. 2321-33.

Place, E. S. & Smith, J. C. (2017). 'Zebrafish atoh8 mutants do not recapitulate morpholino phenotypes', *PloS One,* 12(2), p. e0171143.

Pokatayev, V., Hasin, N., Chon, H., Cerritelli, S. M., Sakhuja, K., Ward, J. M., Morris, H. D., Yan, N. & Crouch, R. J. (2016). 'RNase H2 catalytic core Aicardi-Goutieres syndrome-related mutant invokes cGAS-STING innate immune-sensing pathway in mice', *Journal of Experimental Medicine,* 213(3), pp. 329-36.

Prospective Studies, C., Lewington, S., Whitlock, G., Clarke, R., Sherliker, P., Emberson, J., Halsey, J., Qizilbash, N., Peto, R. & Collins, R. (2007). 'Blood cholesterol and vascular mortality by age, sex, and blood pressure: a meta-analysis of individual data from 61 prospective studies with 55,000 vascular deaths', *Lancet,* 370(9602), pp. 1829-39.

Rajshekar, S., Yao, J., Arnold, P. K., Payne, S. G., Zhang, Y., Bowman, T. V., Schmitz, R. J., Edwards, J. R. & Goll, M. (2018). 'Pericentromeric hypomethylation elicits an interferon response in an animal model of ICF syndrome', *Elife,* 7, p. e39658.

Ramesh, V., Bernardi, B., Stafa, A., Garone, C., Franzoni, E., Abinun, M., Mitchell, P., Mitra, D., Friswell, M., Nelson, J., Shalev, S. A., Rice, G. I., Gornall, H., Szynkiewicz, M., Aymard, F., Ganesan, V., Prendiville, J., Livingston, J. H. & Crow, Y. J. (2010). 'Intracerebral large artery disease in Aicardi-Goutieres syndrome implicates SAMHD1 in vascular homeostasis', *Developmental Medicine and Child Neurology,* 52(8), pp. 725-32.

Rashid, S., Curtis, D. E., Garuti, R., Anderson, N. N., Bashmakov, Y., Ho, Y. K., Hammer, R. E., Moon, Y. A. & Horton, J. D. (2005). 'Decreased plasma cholesterol and hypersensitivity to statins in mice lacking Pcsk9', *Proceedings of the National Academy of Sciences of the United States of America,* 102(15), pp. 5374-9.

Reboldi, A., Dang, E. V., McDonald, J. G., Liang, G., Russell, D. W. & Cyster, J. G. (2014). 'Inflammation. 25-Hydroxycholesterol suppresses interleukin-1-driven inflammation downstream of type I interferon', *Science,* 345(6197), pp. 679-84.

Rehwinkel, J., Maelfait, J., Bridgeman, A., Rigby, R., Hayward, B., Liberatore, R. A., Bieniasz, P. D., Towers, G. J., Moita, L. F., Crow, Y. J., Bonthron, D. T. & Reis e Sousa, C. (2013). 'SAMHD1-dependent retroviral control and escape in mice', *EMBO Journal,* 32(18), pp. 2454-62.

Reijns, M. A., Rabe, B., Rigby, R. E., Mill, P., Astell, K. R., Lettice, L. A., Boyle, S., Leitch, A., Keighren, M., Kilanowski, F., Devenney, P. S., Sexton, D., Grimes, G., Holt, I. J., Hill, R. E., Taylor, M. S., Lawson, K. A., Dorin, J. R. & Jackson, A. P. (2012). 'Enzymatic removal of ribonucleotides from DNA is essential for mammalian genome integrity and development', *Cell,* 149(5), pp. 1008-22.

Reynolds, J. A., Ray, D. W., Zeef, L. A., O'Neill, T., Bruce, I. N. & Alexander, M. Y. (2014). 'The effect of type 1 IFN on human aortic endothelial cell function in vitro: relevance to systemic lupus erythematosus', *Journal of Interferon & Cytokine Research,* 34(5), pp. 404-12.

Rice, G. I., Bond, J., Asipu, A., Brunette, R. L., Manfield, I. W., Carr, I. M., Fuller, J. C., Jackson, R. M., Lamb, T., Briggs, T. A., Ali, M., Gornall, H., Couthard, L. R., Aeby, A., Attard-Montalto, S. P., Bertini, E., Bodemer, C., Brockmann, K., Brueton, L. A., Corry, P. C., Desguerre, I., Fazzi, E., Cazorla, A. G., Gener, B., Hamel, B. C., Heiberg, A., Hunter, M., van der Knaap, M. S., Kumar, R., Lagae, L., Landrieu, P. G., Lourenco, C. M., Marom, D., McDermott, M. F., van der Merwe, W., Orcesi, S., Prendiville, J. S., Rasmussen, M., Shalev, S. A., Soler, D. M., Shinawi, M., Spiegel, R., Tan, T. Y., Vanderver, A., Wakeling, E. L., Wassmer, E., Whittaker, E., Lebon, P., Stetson, D. B., Bonthron, D. T. & Crow, Y. J. (2009). 'Mutations involved in Aicardi-Goutieres syndrome implicate SAMHD1 as regulator of the innate immune response', *Nature Genetics,* 41(7), pp. 829-32.

Rice, G. I., Del Toro Duany, Y., Jenkinson, E. M., Forte, G. M., Anderson, B. H., Ariaudo, G., Bader-Meunier, B., Baildam, E. M., Battini, R., Beresford, M. W., Casarano, M., Chouchane, M., Cimaz, R., Collins, A. E., Cordeiro, N. J., Dale, R. C., Davidson, J. E., De Waele, L., Desguerre, I., Faivre, L., Fazzi, E., Isidor, B., Lagae, L., Latchman, A. R., Lebon, P., Li, C., Livingston, J. H., Lourenco, C. M., Mancardi, M. M., Masurel-Paulet, A., McInnes, I. B., Menezes, M. P., Mignot, C., O'Sullivan, J., Orcesi, S., Picco, P. P., Riva, E., Robinson, R. A., Rodriguez, D., Salvatici, E., Scott, C., Szybowska, M., Tolmie, J. L., Vanderver, A., Vanhulle, C., Vieira, J. P., Webb, K., Whitney, R. N., Williams, S. G., Wolfe, L. A., Zuberi, S. M., Hur, S. & Crow, Y. J. (2014). 'Gain-of-function mutations in IFIH1 cause a spectrum of human disease phenotypes associated with upregulated type I interferon signaling', *Nature Genetics,* 46(5), pp. 503-509.

Rice, G. I., Forte, G. M., Szynkiewicz, M., Chase, D. S., Aeby, A., Abdel-Hamid, M. S., Ackroyd, S., Allcock, R., Bailey, K. M., Balottin, U., Barnerias, C., Bernard, G., Bodemer, C., Botella, M. P., Cereda, C., Chandler, K. E., Dabydeen, L., Dale, R. C., De Laet, C., De Goede, C. G., Del Toro, M., Effat, L., Enamorado, N. N., Fazzi, E., Gener, B., Haldre, M., Lin, J. P., Livingston, J. H., Lourenco, C. M., Marques, W., Jr., Oades, P., Peterson, P., Rasmussen, M., Roubertie, A., Schmidt, J. L., Shalev, S. A., Simon, R., Spiegel, R., Swoboda, K. J., Temtamy, S. A., Vassallo, G., Vilain, C. N., Vogt, J., Wermenbol, V., Whitehouse, W. P., Soler, D., Olivieri, I., Orcesi, S., Aglan, M. S., Zaki, M. S., Abdel-Salam, G. M., Vanderver, A., Kisand, K., Rozenberg, F., Lebon, P. & Crow, Y. J. (2013). 'Assessment of interferon-related biomarkers in Aicardi-Goutieres syndrome associated with mutations in TREX1, RNASEH2A, RNASEH2B, RNASEH2C, SAMHD1, and ADAR: a case-control study', *Lancet Neurology,* 12(12), pp. 1159-69.

Rice, G. I., Kasher, P. R., Forte, G. M., Mannion, N. M., Greenwood, S. M., Szynkiewicz, M., Dickerson, J. E., Bhaskar, S. S., Zampini, M., Briggs, T. A., Jenkinson, E. M., Bacino, C. A., Battini, R., Bertini, E., Brogan, P. A., Brueton, L. A., Carpanelli, M., De Laet, C., de Lonlay, P., del Toro, M., Desguerre, I., Fazzi, E., Garcia-Cazorla, A., Heiberg, A., Kawaguchi, M., Kumar, R., Lin, J. P., Lourenco, C. M., Male, A. M., Marques, W., Jr., Mignot, C., Olivieri, I., Orcesi, S., Prabhakar, P., Rasmussen, M., Robinson, R. A., Rozenberg, F., Schmidt, J. L., Steindl, K., Tan, T. Y., van der Merwe, W. G., Vanderver, A., Vassallo, G., Wakeling, E. L.,

Wassmer, E., Whittaker, E., Livingston, J. H., Lebon, P., Suzuki, T., McLaughlin, P. J., Keegan, L. P., O'Connell, M. A., Lovell, S. C. & Crow, Y. J. (2012). 'Mutations in ADAR1 cause Aicardi-Goutieres syndrome associated with a type I interferon signature', *Nature Genetics,* 44(11), pp. 1243-8.

Rice, G. I., Meyzer, C., Bouazza, N., Hully, M., Boddaert, N., Semeraro, M., Zeef, L. A. H., Rozenberg, F., Bondet, V., Duffy, D., Llibre, A., Baek, J., Sambe, M. N., Henry, E., Jolaine, V., Barnerias, C., Barth, M., Belot, A., Cances, C., Debray, F. G., Doummar, D., Fremond, M. L., Kitabayashi, N., Lepelley, A., Levrat, V., Melki, I., Meyer, P., Nougues, M. C., Renaldo, F., Rodero, M. P., Rodriguez, D., Roubertie, A., Seabra, L., Uggenti, C., Abdoul, H., Treluyer, J. M., Desguerre, I., Blanche, S. & Crow, Y. J. (2018). 'Reverse-Transcriptase Inhibitors in the Aicardi-Goutieres Syndrome', *New England Journal of Medicine,* 379(23), pp. 2275-7.

Riess, M., Fuchs, N. V., Idica, A., Hamdorf, M., Flory, E., Pedersen, I. M. & Konig, R. (2017). 'Interferons Induce Expression of SAMHD1 in Monocytes through Down-regulation of miR-181a and miR-30a', *Journal of Biological Chemistry,* 292(1), pp. 264-277.

Robertson, K. A. & Ghazal, P. (2016). 'Interferon Control of the Sterol Metabolic Network: Bidirectional Molecular Circuitry-Mediating Host Protection', *Frontiers in Immunology,* 7, p. 634.

Robertson, K. A., Hsieh, W. Y., Forster, T., Blanc, M., Lu, H., Crick, P. J., Yutuc, E., Watterson, S., Martin, K., Griffiths, S. J., Enright, A. J., Yamamoto, M., Pradeepa, M. M., Lennox, K. A., Behlke, M. A., Talbot, S., Haas, J., Dolken, L., Griffiths, W. J., Wang, Y., Angulo, A. & Ghazal, P. (2016). 'An Interferon Regulated MicroRNA Provides Broad Cell-Intrinsic Antiviral Immunity through Multihit Host-Directed Targeting of the Sterol Pathway', *PLoS Biology,* 14(3), p. e1002364.

Rodel, C. J., Otten, C., Donat, S., Lourenco, M., Fischer, D., Kuropka, B., Paolini, A., Freund, C. & Abdelilah-Seyfried, S. (2019). 'Blood Flow Suppresses Vascular Anomalies in a Zebrafish Model of Cerebral Cavernous Malformations', *Circulation Research,* 125(10), pp. e43-e54.

Rodero, M. P. & Crow, Y. J. (2016). 'Type I interferon-mediated monogenic autoinflammation: The type I interferonopathies, a conceptual overview', *Journal of Experimental Medicine,* 213(12), pp. 2527-2538.

Rodriguez-Acebes, S., de la Cueva, P., Fernandez-Hernando, C., Ferruelo, A. J., Lasuncion, M. A., Rawson, R. B., Martinez-Botas, J. & Gomez-Coronado, D. (2009). 'Desmosterol can replace cholesterol in sustaining cell proliferation and regulating the SREBP pathway in a sterol-Delta24-reductase-deficient cell line', *Biochemical Journal,* 420(2), pp. 305-15.

Rossi, A., Kontarakis, Z., Gerri, C., Nolte, H., Holper, S., Kruger, M. & Stainier, D. Y. (2015). 'Genetic compensation induced by deleterious mutations but not gene knockdowns', *Nature,* 524(7564), pp. 230-3.

Rutherford, H. A., Kasher, P. R. & Hamilton, N. (2020). 'Dirty Fish Versus Squeaky Clean Mice: Dissecting Interspecies Differences Between Animal Models of Interferonopathy', *Frontiers in Immunology,* 11, p. 623650.

Sanchez, G. A. M., Reinhardt, A., Ramsey, S., Wittkowski, H., Hashkes, P. J., Berkun, Y., Schalm, S., Murias, S., Dare, J. A., Brown, D., Stone, D. L., Gao, L., Klausmeier, T., Foell, D., de Jesus, A. A., Chapelle, D. C., Kim, H., Dill, S., Colbert, R. A., Failla, L., Kost, B., O'Brien, M., Reynolds, J. C., Folio, L. R., Calvo, K. R., Paul, S. M., Weir, N., Brofferio, A., Soldatos, A., Biancotto, A., Cowen, E. W., Digiovanna, J. J., Gadina, M., Lipton, A. J., Hadigan, C., Holland, S. M., Fontana, J., Alawad, A. S., Brown, R. J., Rother, K. I., Heller, T., Brooks, K. M., Kumar, P., Brooks, S. R., Waldman, M., Singh, H. K., Nickeleit, V., Silk, M., Prakash, A., Janes, J. M., Ozen, S., Wakim, P. G., Brogan, P. A., Macias, W. L. & Goldbach-Mansky, R. (2018). 'JAK1/2 inhibition with baricitinib in the treatment of autoinflammatory interferonopathies', *Journal of Clinical Investigation,* 128(7), pp. 3041-3052.

Sander, J. D., Cade, L., Khayter, C., Reyon, D., Peterson, R. T., Joung, J. K. & Yeh, J. R. (2011). 'Targeted gene disruption in somatic zebrafish cells using engineered TALENs', *Nature Biotechnology,* 29(8), pp. 697-8.

Santoriello, C. & Zon, L. I. (2012). 'Hooked! Modeling human disease in zebrafish', *Journal of Clinical Investigation,* 122(7), pp. 2337-43.

Sarasin-Filipowicz, M., Wang, X., Yan, M., Duong, F. H., Poli, V., Hilton, D. J., Zhang, D. E. & Heim, M. H. (2009). 'Alpha interferon induces long-lasting refractoriness of JAK-STAT signaling in the mouse liver through induction of USP18/UBP43', *Molecular and Cellular Biology,* 29(17), pp. 4841-51.

Schlunk, F., Fischer, P., Princen, H. M. G., Rex, A., Prinz, V., Foddis, M., Lutjohann, D., Laufs, U. & Endres, M. (2020). 'Effects of Inhibition or Deletion of PCSK9 (Proprotein Convertase Subtilisin/Kexin Type 9) on Intracerebral Hemorrhage Volumes in Mice', *Stroke,* 51(11), pp. e297-e298.

Schmidt, S., Schenkova, K., Adam, T., Erikson, E., Lehmann-Koch, J., Sertel, S., Verhasselt, B., Fackler, O. T., Lasitschka, F. & Keppler, O. T. (2015). 'SAMHD1's protein expression profile in humans', *Journal of Leukocyte Biology,* 98(1), pp. 5-14.

Segal, A. Z., Chiu, R. I., Eggleston-Sexton, P. M., Beiser, A. & Greenberg, S. M. (1999). 'Low cholesterol as a risk factor for primary intracerebral hemorrhage: A case-control study', *Neuroepidemiology,* 18(4), pp. 185-93.

Shalev, H., Kapelushnik, J., Moser, A., Knobler, H. & Tamary, H. (2007). 'Hypocholesterolemia in chronic anemias with increased erythropoietic activity', *American Journal of Hematology,* 82(3), pp. 199-202.

Shewell, L. K., Day, C. J., Jen, F. E., Haselhorst, T., Atack, J. M., Reijneveld, J. F., Everest-Dass, A., James, D. B. A., Boguslawski, K. M., Brouwer, S., Gillen, C. M., Luo, Z., Kobe, B., Nizet, V., von Itzstein, M., Walker, M. J., Paton, A. W., Paton, J. C., Torres, V. J. & Jennings, M. P. (2020). 'All major cholesterol-dependent cytolysins use glycans as cellular receptors', *Sci Adv,* 6(21), p. eaaz4926.

Shinohara, E., Yamashita, S., Kihara, S., Hirano, K., Ishigami, M., Arai, T., Nozaki, S., Kameda-Takemura, K., Kawata, S. & Matsuzawa, Y. (1997). 'Interferon alpha induces disorder of lipid metabolism by lowering postheparin lipases and cholesteryl ester transfer protein activities in patients with chronic hepatitis C', *Hepatology,* 25(6), pp. 1502-6.

Shrivastava-Ranjan, P., Bergeron, E., Chakrabarti, A. K., Albarino, C. G., Flint, M., Nichol, S. T. & Spiropoulou, C. F. (2016). '25-Hydroxycholesterol Inhibition of Lassa Virus Infection through Aberrant GP1 Glycosylation', *mBio,* 7(6).

Sieger, D., Moritz, C., Ziegenhals, T., Prykhozhij, S. & Peri, F. (2012). 'Long-range Ca2+ waves transmit brain-damage signals to microglia', *Developmental Cell,* 22(6), pp. 1138-48.

Simons, K. & Ikonen, E. (2000). 'Cell biology - How cells handle cholesterol', *Science,* 290(5497), pp. 1721-1726.

Singer, E. J., Valdes-Sueiras, M., Commins, D. L., Yong, W. & Carlson, M. (2013). 'HIV stroke risk: evidence and implications', *Therapeutic Advances in Chronic Disease,* 4(2), pp. 61-70.

Sinkevicius, K. W., Morrison, T. R., Kulkarni, P., Caffrey Cagliostro, M. K., Iriah, S., Malmberg, S., Sabrick, J., Honeycutt, J. A., Askew, K. L., Trivedi, M. & Ferris, C. F. (2018). 'RNaseT2 knockout rats exhibit hippocampal neuropathology and deficits in memory', *Disease Models & Mechanisms,* 11(6).

Stainier, D. Y. R., Raz, E., Lawson, N. D., Ekker, S. C., Burdine, R. D., Eisen, J. S., Ingham, P. W., Schulte-Merker, S., Yelon, D., Weinstein, B. M., Mullins, M. C., Wilson, S. W., Ramakrishnan, L., Amacher, S. L., Neuhauss, S. C. F., Meng, A., Mochizuki, N., Panula, P. & Moens, C. B. (2017). 'Guidelines for morpholino use in zebrafish', *PLoS Genetics,* 13(10), p. e1007000.

Stankiewicz, P., Khan, T. N., Szafranski, P., Slattery, L., Streff, H., Vetrini, F., Bernstein, J. A., Brown, C. W., Rosenfeld, J. A., Rednam, S., Scollon, S., Bergstrom, K. L., Parsons, D. W., Plon, S. E.,

Vieira, M. W., Quaio, C., Baratela, W. A. R., Acosta Guio, J. C., Armstrong, R., Mehta, S. G., Rump, P., Pfundt, R., Lewandowski, R., Fernandes, E. M., Shinde, D. N., Tang, S., Hoyer, J., Zweier, C., Reis, A., Bacino, C. A., Xiao, R., Breman, A. M., Smith, J. L., Deciphering Developmental Disorders, S., Katsanis, N., Bostwick, B., Popp, B., Davis, E. E. & Yang, Y. (2017). 'Haploinsufficiency of the Chromatin Remodeler BPTF Causes Syndromic Developmental and Speech Delay, Postnatal Microcephaly, and Dysmorphic Features', *American Journal of Human Genetics,* 101(4), pp. 503-515.

Stetson, D. B., Ko, J. S., Heidmann, T. & Medzhitov, R. (2008). 'Trex1 prevents cell-intrinsic initiation of autoimmunity', *Cell,* 134(4), pp. 587-98.

Sumbria, D., Berber, E., Mathayan, M. & Rouse, B. T. (2020). 'Virus Infections and Host Metabolism-Can We Manage the Interactions?', *Frontiers in Immunology,* 11, p. 594963.

Sun, L., Clarke, R., Bennett, D., Guo, Y., Walters, R. G., Hill, M., Parish, S., Millwood, I. Y., Bian, Z., Chen, Y., Yu, C., Lv, J., Collins, R., Chen, J., Peto, R., Li, L., Chen, Z., China Kadoorie Biobank Collaborative, G., International Steering, C., International Co-ordinating Centre, O., National Co-ordinating Centre, B. & Regional Co-ordinating, C. (2019). 'Causal associations of blood lipids with risk of ischemic stroke and intracerebral hemorrhage in Chinese adults', *Nature Medicine,* 25(4), pp. 569-574.

Tan, J. M. E., van der Stoel, M. M., van den Berg, M., van Loon, N. M., Moeton, M., Scholl, E., van der Wel, N. N., Kovacevic, I., Hordijk, P. L., Loregger, A., Huveneers, S. & Zelcer, N. (2020). 'The MARCH6-SQLE Axis Controls Endothelial Cholesterol Homeostasis and Angiogenic Sprouting', *Cell Reports,* 32(5), p. 107944.

Thiele, H., du Moulin, M., Barczyk, K., George, C., Schwindt, W., Nurnberg, G., Frosch, M., Kurlemann, G., Roth, J., Nurnberg, P. & Rutsch, F. (2010). 'Cerebral arterial stenoses and stroke: novel features of Aicardi-Goutieres syndrome caused by the Arg164X mutation in SAMHD1 are associated with altered cytokine expression', *Human Mutation,* 31(11), pp. E1836-50.

Tirschwell, D. L., Smith, N. L., Heckbert, S. R., Lemaitre, R. N., Longstreth, W. T., Jr. & Psaty, B. M. (2004). 'Association of cholesterol with stroke risk varies in stroke subtypes and patient subgroups', *Neurology,* 63(10), pp. 1868-75.

Tonduti, D., Panteghini, C., Pichiecchio, A., Decio, A., Carecchio, M., Reale, C., Moroni, I., Nardocci, N., Campistol, J., Garcia-Cazorla, A., Perez Duenas, B., Cerebral Calcification International Study, G., Chiapparini, L., Garavaglia, B. & Orcesi, S. (2018). 'Encephalopathies with intracranial calcification in children: clinical and genetic characterization', *Orphanet Journal of Rare Diseases,* 13(1), p. 135.

Tseng, C. H., Muo, C. H., Hsu, C. Y. & Kao, C. H. (2015). 'Increased Risk of Intracerebral Hemorrhage Among Patients With Hepatitis C Virus Infection', *Medicine (Baltimore),* 94(46), p. e2132.

Uggenti, C., Lepelley, A., Depp, M., Badrock, A. P., Rodero, M. P., El-Daher, M. T., Rice, G. I., Dhir, S., Wheeler, A. P., Dhir, A., Albawardi, W., Fremond, M. L., Seabra, L., Doig, J., Blair, N., Martin-Niclos, M. J., Della Mina, E., Rubio-Roldan, A., Garcia-Perez, J. L., Sproul, D., Rehwinkel, J., Hertzog, J., Boland-Auge, A., Olaso, R., Deleuze, J. F., Baruteau, J., Brochard, K., Buckley, J., Cavallera, V., Cereda, C., De Waele, L. M. H., Dobbie, A., Doummar, D., Elmslie, F., Koch-Hogrebe, M., Kumar, R., Lamb, K., Livingston, J. H., Majumdar, A., Lorenco, C. M., Orcesi, S., Peudenier, S., Rostasy, K., Salmon, C. A., Scott, C., Tonduti, D., Touati, G., Valente, M., van der Linden, H., Jr., Van Esch, H., Vermelle, M., Webb, K., Jackson, A. P., Reijns, M. A. M., Gilbert, N. & Crow, Y. J. (2020). 'cGAS-mediated induction of type I interferon due to inborn errors of histone pre-mRNA processing', *Nature Genetics,* 52(12), pp. 1364-1372.

Uggetti, C., La Piana, R., Orcesi, S., Egitto, M. G., Crow, Y. J. & Fazzi, E. (2009). 'Aicardi-Goutieres syndrome: neuroradiologic findings and follow-up', *AJNR: American Journal of Neuroradiology,* 30(10), pp. 1971-6.

Ulrich, F., Ma, L. H., Baker, R. G. & Torres-Vazquez, J. (2011). 'Neurovascular development in the embryonic zebrafish hindbrain', *Developmental Biology,* 357(1), pp. 134-51.

Valappil, A. V., Chaudhary, N. V., Praveenkumar, R., Gopalakrishnan, B. & Girija, A. S. (2012). 'Low cholesterol as a risk factor for primary intracerebral hemorrhage: A case-control study', *Annals of the Indian Academy of Neurology,* 15(1), pp. 19-22.

van Etten, E. S., Kaushik, K., Jolink, W. M. T., Koemans, E. A., Ekker, M. S., Rasing, I., Voigt, S., Schreuder, F., Cannegieter, S. C., Rinkel, G. J. E., Lijfering, W. M., Klijn, C. J. M. & Wermer, M. J. H. (2021). 'Trigger Factors for Spontaneous Intracerebral Hemorrhage: A Case-Crossover Study', *Stroke*, p. STROKEAHA121036233.

Vance, J. E. (2012). 'Dysregulation of cholesterol balance in the brain: contribution to neurodegenerative diseases', *Disease Models & Mechanisms,* 5(6), pp. 746-55.

Vanderver, A., Adang, L., Gavazzi, F., McDonald, K., Helman, G., Frank, D. B., Jaffe, N., Yum, S. W., Collins, A., Keller, S. R., Lebon, P., Meritet, J. F., Rhee, J., Takanohashi, A., Armangue, T., Ulrick, N., Sherbini, O., Koh, J., Peer, K., Besnier, C., Scher, C., Boyle, K., Dubbs, H., Kramer-Golinkoff, J., Pizzino, A., Woidill, S. & Shults, J. (2020). 'Janus Kinase Inhibition in the Aicardi-Goutieres Syndrome', *New England Journal of Medicine,* 383(10), pp. 986-989.

Vandesompele, J., De Preter, K., Pattyn, F., Poppe, B., Van Roy, N., De Paepe, A. & Speleman, F. (2002). 'Accurate normalization of real-time quantitative RT-PCR data by geometric averaging of multiple internal control genes', *Genome Biology,* 3(7), p. RESEARCH0034.

Varatharaj, A., Thomas, N., Ellul, M. A., Davies, N. W. S., Pollak, T. A., Tenorio, E. L., Sultan, M., Easton, A., Breen, G., Zandi, M., Coles, J. P., Manji, H., Al-Shahi Salman, R., Menon, D. K., Nicholson, T. R., Benjamin, L. A., Carson, A., Smith, C., Turner, M. R., Solomon, T., Kneen, R., Pett, S. L., Galea, I., Thomas, R. H., Michael, B. D. & CoroNerve Study, G. (2020). 'Neurological and neuropsychiatric complications of COVID-19 in 153 patients: a UK-wide surveillance study', *Lancet Psychiatry,* 7(10), pp. 875-882.

Virelizier, J. L. & Gresser, I. (1978). 'Role of interferon in the pathogenesis of viral diseases of mice as demonstrated by the use of anti-interferon serum. V. Protective role in mouse hepatitis virus type 3 infection of susceptible and resistant strains of mice', *Journal of Immunology,* 120(5), pp. 1616-9.

Vogt, J., Agrawal, S., Ibrahim, Z., Southwood, T. R., Philip, S., Macpherson, L., Bhole, M. V., Crow, Y. J. & Oley, C. (2013). 'Striking intrafamilial phenotypic variability in Aicardi-Goutieres syndrome associated with the recurrent Asian founder mutation in RNASEH2C', *American Journal of Medical Genetics Part A,* 161A(2), pp. 338-42.

Volpi, S., Picco, P., Caorsi, R., Candotti, F. & Gattorno, M. (2016). 'Type I interferonopathies in pediatric rheumatology', *Pediatric Rheumatology Online Journal,* 14(1), p. 35.

Wang, H., Tang, X., Fan, H., Luo, Y., Song, Y., Xu, Y. & Chen, Y. (2020). 'Potential mechanisms of hemorrhagic stroke in elderly COVID-19 patients', *Aging,* 12(11), pp. 10022-10034.

Wang, Q., Miyakoda, M., Yang, W., Khillan, J., Stachura, D. L., Weiss, M. J. & Nishikura, K. (2004). 'Stress-induced apoptosis associated with null mutation of ADAR1 RNA editing deaminase gene', *Journal of Biological Chemistry,* 279(6), pp. 4952-61.

Wang, S., Li, W., Hui, H., Tiwari, S. K., Zhang, Q., Croker, B. A., Rawlings, S., Smith, D., Carlin, A. F. & Rana, T. M. (2020). 'Cholesterol 25-Hydroxylase inhibits SARS-CoV-2 and other coronaviruses by depleting membrane cholesterol', *EMBO Journal,* 39(21), p. e106057.

Wang, S., Yao, Y., Rao, C., Zheng, G. & Chen, W. (2019). '25-HC decreases the sensitivity of human gastric cancer cells to 5-fluorouracil and promotes cells invasion via the TLR2/NF-kappaB signaling pathway', *International Journal of Oncology,* 54(3), pp. 966-980.

Wang, X., Dong, Y., Qi, X., Huang, C. & Hou, L. (2013). 'Cholesterol levels and risk of hemorrhagic stroke: a systematic review and meta-analysis', *Stroke,* 44(7), pp. 1833-9.

Wang, Y., Pan, L., Moens, C. B. & Appel, B. (2014). 'Notch3 establishes brain vascular integrity by regulating pericyte number', *Development,* 141(2), pp. 307-17.

Wei, Y., Nazari-Jahantigh, M., Chan, L., Zhu, M., Heyll, K., Corbalan-Campos, J., Hartmann, P., Thiemann, A., Weber, C. & Schober, A. (2013). 'The microRNA-342-5p fosters inflammatory macrophage activation through an Akt1- and microRNA-155-dependent pathway during atherosclerosis', *Circulation,* 127(15), pp. 1609-19.

Wen, Y. A., Xiong, X., Zaytseva, Y. Y., Napier, D. L., Vallee, E., Li, A. T., Wang, C., Weiss, H. L., Evers, B. M. & Gao, T. (2018). 'Downregulation of SREBP inhibits tumor growth and initiation by altering cellular metabolism in colon cancer', *Cell Death & Disease,* 9(3), p. 265.

Westerfield, M. (2000). *The zebrafish book. A guide for the laboratory use of zebrafish (Danio rerio)* (4th ed.). Eugene: University of Oregon Press

Widziolek, M., Janik, K., Mojzesz, M., Pooranachandran, N., Adamek, M., Pecio, A., Surachetpong, W., Levraud, J. P., Boudinot, P., Chadzinska, M. & Rakus, K. (2021). 'Type I interferon-dependent response of zebrafish larvae during tilapia lake virus (TiLV) infection', *Developmental & Comparative Immunology,* 116, p. 103936.

Withers, S. E., Parry-Jones, A. R., Allan, S. M. & Kasher, P. R. (2020). 'A Multi-Model Pipeline for Translational Intracerebral Haemorrhage Research', *Translational Stroke Research,* 11(6), pp. 1229-1242.

Wouters, K., Shiri-Sverdlov, R., van Gorp, P. J., van Bilsen, M. & Hofker, M. H. (2005). 'Understanding hyperlipidemia and atherosclerosis: lessons from genetically modified apoe and ldlr mice', *Clinical Chemistry and Laboratory Medicine,* 43(5), pp. 470-9.

Wu, T., Ma, F., Ma, X., Jia, W., Pan, E., Cheng, G., Chen, L. & Sun, C. (2018). 'Regulating Innate and Adaptive Immunity for Controlling SIV Infection by 25-Hydroxycholesterol', *Frontiers in Immunology,* 9, p. 2686.

Xie, Y., Meijer, A. H. & Schaaf, M. J. M. (2020). 'Modeling Inflammation in Zebrafish for the Development of Anti-inflammatory Drugs', *Frontiers in Cell and Developmental Biology,* 8, p. 620984.

Xin, B., Jones, S., Puffenberger, E. G., Hinze, C., Bright, A., Tan, H., Zhou, A., Wu, G., Vargus-Adams, J., Agamanolis, D. & Wang, H. (2011). 'Homozygous mutation in SAMHD1 gene causes cerebral vasculopathy and early onset stroke', *Proceedings of the National Academy of Sciences of the United States of America,* 108(13), pp. 5372-7.

Yamamoto, K., Nogimori, Y., Imamura, H. & Ando, J. (2020). 'Shear stress activates mitochondrial oxidative phosphorylation by reducing plasma membrane cholesterol in vascular endothelial cells', *Proceedings of the National Academy of Sciences of the United States of America,* 117(52), pp. 33660-33667.

Yang, S., Zhan, Y., Zhou, Y., Jiang, Y., Zheng, X., Yu, L., Tong, W., Gao, F., Li, L., Huang, Q., Ma, Z. & Tong, G. (2016). 'Interferon regulatory factor 3 is a key regulation factor for inducing the expression of SAMHD1 in antiviral innate immunity', *Scientific Reports,* 6, p. 29665.

Yang, S. T., Kiessling, V., Simmons, J. A., White, J. M. & Tamm, L. K. (2015). 'HIV gp41-mediated membrane fusion occurs at edges of cholesterol-rich lipid domains', *Nature Chemical Biology,* 11(6), pp. 424-31.

Yao, T., Long, Q., Li, J., Li, G., Ding, Y., Cui, Q. & Liu, Z. (2020). 'Small dense low-density lipoprotein cholesterol is strongly associated with NIHSS score and intracranial arterial calcification in acute ischemic stroke subjects', *Scientific Reports,* 10(1), p. 7645.

York, A. G., Williams, K. J., Argus, J. P., Zhou, Q. D., Brar, G., Vergnes, L., Gray, E. E., Zhen, A., Wu, N. C., Yamada, D. H., Cunningham, C. R., Tarling, E. J., Wilks, M. Q., Casero, D., Gray, D. H., Yu, A. K., Wang, E. S., Brooks, D. G., Sun, R., Kitchen, S. G., Wu, T. T., Reue, K., Stetson, D. B. & Bensinger, S. J. (2015). 'Limiting Cholesterol Biosynthetic Flux Spontaneously Engages Type I IFN Signaling', *Cell,* 163(7), pp. 1716-29.

Yoshimura, A., Naka, T. & Kubo, M. (2007). 'SOCS proteins, cytokine signalling and immune regulation', *Nature Reviews: Immunology,* 7(6), pp. 454-65.

Zang, R., Case, J. B., Yutuc, E., Ma, X., Shen, S., Gomez Castro, M. F., Liu, Z., Zeng, Q., Zhao, H., Son, J., Rothlauf, P. W., Kreutzberger, A. J. B., Hou, G., Zhang, H., Bose, S., Wang, X., Vahey, M.

D., Mani, K., Griffiths, W. J., Kirchhausen, T., Fremont, D. H., Guo, H., Diwan, A., Wang, Y., Diamond, M. S., Whelan, S. P. J. & Ding, S. (2020). 'Cholesterol 25-hydroxylase suppresses SARS-CoV-2 replication by blocking membrane fusion', *Proceedings of the National Academy of Sciences of the United States of America,* 117(50), pp. 32105-32113.

Zhang, X., Bogunovic, D., Payelle-Brogard, B., Francois-Newton, V., Speer, S. D., Yuan, C., Volpi, S., Li, Z., Sanal, O., Mansouri, D., Tezcan, I., Rice, G. I., Chen, C., Mansouri, N., Mahdaviani, S. A., Itan, Y., Boisson, B., Okada, S., Zeng, L., Wang, X., Jiang, H., Liu, W., Han, T., Liu, D., Ma, T., Wang, B., Liu, M., Liu, J. Y., Wang, Q. K., Yalnizoglu, D., Radoshevich, L., Uze, G., Gros, P., Rozenberg, F., Zhang, S. Y., Jouanguy, E., Bustamante, J., Garcia-Sastre, A., Abel, L., Lebon, P., Notarangelo, L. D., Crow, Y. J., Boisson-Dupuis, S., Casanova, J. L. & Pellegrini, S. (2015). 'Human intracellular ISG15 prevents interferon-alpha/beta over-amplification and auto-inflammation', *Nature,* 517(7532), pp. 89-93.

Zhao, J., Chen, J., Li, M., Chen, M. & Sun, C. (2020). 'Multifaceted Functions of CH25H and 25HC to Modulate the Lipid Metabolism, Immune Responses, and Broadly Antiviral Activities', *Viruses,* 12(7), p. 727.

Zhao, K., Du, J., Han, X., Goodier, J. L., Li, P., Zhou, X., Wei, W., Evans, S. L., Li, L., Zhang, W., Cheung, L. E., Wang, G., Kazazian, H. H., Jr. & Yu, X. F. (2013). 'Modulation of LINE-1 and Alu/SVA retrotransposition by Aicardi-Goutieres syndrome-related SAMHD1', *Cell Reports,* 4(6), pp. 1108-15.

Zhou, Q. D., Chi, X., Lee, M. S., Hsieh, W. Y., Mkrtchyan, J. J., Feng, A. C., He, C., York, A. G., Bui, V. L., Kronenberger, E. B., Ferrari, A., Xiao, X., Daly, A. E., Tarling, E. J., Damoiseaux, R., Scumpia, P. O., Smale, S. T., Williams, K. J., Tontonoz, P. & Bensinger, S. J. (2020). 'Interferon-mediated reprogramming of membrane cholesterol to evade bacterial toxins', *Nature Immunology,* 21(7), pp. 746-755.

Zhu, X. Y., Xia, B., Ye, T., Dai, M. Z., Yang, H., Li, C. Q. & Li, P. (2020). 'Ponatinib-induced ischemic stroke in larval zebrafish for drug screening', *European Journal of Pharmacology*, p. 173292.

Appendix 1

Translational stroke research article entitled:

‘A Multi-Model Pipeline for Translational Intracerebral Haemorrhage Research’

This review article discusses the existing pre-clinical models involved in ICH research, ranging from *in vitro* systems, small mammalian models, zebrafish models, larger mammalian models and post-mortem/*ex vivo* studies. We highlight the main advantages and disadvantages associated with each model, and proposed a multi-model pipeline would be of great benefit to the ICH research community. This pipeline should be multidirectional, allowing for both a feedforward and feedback loop to determine the validity of new findings in multiple model systems. Moreover, the use of post-mortem/*ex vivo* tissues have not been widely utilised, and we believe there is a large need for an increase in studies using this precious clinically relevant source of material, which can also help to direct future pre-clinical research, whilst maintaining clinical relevance. Overall, we hypothesise that future collaboration and cross-talk between studies using different ICH models, may facilitate more successful translation in the future, and increases the chances of producing a specific medical treatment for ICH, which is currently lacking, and undoubtedly contributes to the high mortality rates associated with ICH.

Translational Stroke Research (2020) 11:1229–1242
https://doi.org/10.1007/s12975-020-00830-z

REVIEW ARTICLE

A Multi-Model Pipeline for Translational Intracerebral Haemorrhage Research

Sarah E. Withers[1] · Adrian R. Parry-Jones[2,3] · Stuart M. Allan[1] · Paul R. Kasher[1]

Received: 15 May 2020 / Revised: 18 June 2020 / Accepted: 23 June 2020 / Published online: 7 July 2020

Abstract

Apart from acute and chronic blood pressure lowering, we have no specific medications to prevent intracerebral haemorrhage (ICH) or improve outcomes once bleeding has occurred. One reason for this may be related to particular limitations associated with the current pre-clinical models of ICH, leading to a failure to translate into the clinic. It would seem that a breakdown in the 'drug development pipeline' currently exists for translational ICH research which needs to be urgently addressed. Here, we review the most commonly used pre-clinical models of ICH and discuss their advantages and disadvantages in the context of translational studies. We propose that to increase our chances of successfully identifying new therapeutics for ICH, a bi-directional, 2- or 3-pronged approach using more than one model species/system could be useful for confirming key pre-clinical observations. Furthermore, we highlight that post-mortem/ex-vivo ICH patient material is a precious and underused resource which could play an essential role in the verification of experimental results prior to consideration for further clinical investigation. Embracing multidisciplinary collaboration between pre-clinical and clinical ICH research groups will be essential to ensure the success of this type of approach in the future.

Keywords Pre-clinical · Intracerebral haemorrhage · Disease models · Drug discovery

Introduction

Stroke is the second highest cause of death worldwide, surpassed only by ischaemic heart disease [1]. The most devastating sub-type of stroke, intracerebral haemorrhage (ICH), accounts for 10–20% of all strokes in high-income countries, whilst incidences increase in central and East Asia and sub-Saharan Africa [2]. ICH has a mortality rate of 40% at 1-month post-ictus, coupled with a higher loss of disability adjusted life years, exceeding that of ischaemic stroke despite lower prevalence [1, 3]. Knowledge of the molecular pathophysiology surrounding haemorrhagic stroke has vastly increased in recent years, with a plethora of reviews describing the primary and secondary injury phases [4–9]. Key modifiable risk factors for ICH are well recognised, and addressing these can reduce incidence [3, 10–14]. There is still, however, a complete lack of specific treatments available to improve outcomes following ICH, despite many drugs showing efficacy in preclinical models [18]. Therefore, ICH treatment is focussed on quick diagnosis followed by reversal of anticoagulants, blood pressure management and surgery in carefully selected patients as determined by guidelines for the management of spontaneous ICH [15–18]. One reason for the current lack of specific treatments in ICH may be due, in part, to specific limitations associated with the most commonly used existing pre-clinical models of the disease, including constraints related to generating spontaneous brain haemorrhages, difficulties in observing brain pathologies in live animals and sub-optimal experimental study design [19]. It would seem, therefore, that a breakdown in the current 'drug development pipeline' exists for ICH. As such, there is an urgent requirement to rethink our strategies for translational ICH research so that we can investigate new therapeutic avenues for

✉ Paul R. Kasher
paul.kasher@manchester.ac.uk

[1] Division of Neuroscience and Experimental Psychology, School of Biological Sciences, Faculty of Biology, Medicine and Health, Manchester Academic Health Science Centre, The University of Manchester, Oxford Road, Manchester M13 9PT, UK

[2] Division of Cardiovascular Sciences, School of Medical Sciences, Faculty of Biology, Medicine and Health, Manchester Academic Health Science Centre, The University of Manchester, Oxford Road, Manchester M13 9PT, UK

[3] Manchester Centre for Clinical Neurosciences, Salford Royal NHS Foundation Trust, Manchester Academic Health Science Centre, Stott Lane, Salford M6 8HD, UK

future patient treatments, as highlighted in the Haemorrhagic Stroke Academia Industry (HEADS) initiative [20].This review reinforces some of the priorities raised by HEADS, and how these may be implemented within preclinical ICH research, with our main focus highlighting the need for a more efficient, multi-directional pipeline. A more strategic approach to ensure the most appropriate models/systems are selected for each phase of the pre-clinical pipeline (such as studying the occurrence of bleed/risk factors, injury responses or treatments) would be beneficial (Fig. 1). To aid with this decision, the current pre-clinical ICH models will be discussed, including their advantages, disadvantages (see Table 1) and how translational ICH research may be potentially strengthened by adopting multiple models in parallel and embracing multidisciplinary collaboration.

In Vitro Models

In vitro studies dominate the start of the pre-clinical pipeline, where they are commonly used to complement the work from in vivo studies, especially when a pharmacological agent is being tested in rodents. The in vitro work can provide vital information on the mechanism of action, and the effects of the compound on a particular cell type, thus demonstrating the advantages of drug screening in vitro [21–28]. Typically, primary cortical neurons, microglia, astrocyte, mixed glia cultures or endothelial cell cultures are used to emulate the effects of blood on various brain specific cells that are affected following ICH. This can be beneficial for characterising the subsequent response to blood molecules in individual cell types, but less useful for identifying interactions between different brain resident cells. Further advantages of using cell-based systems include the relative ease of genetic manipulation, by using siRNA, gene editing, adenoviruses or plasmid transfections to knock down or over-express various anti- or pro-inflammatory genes or receptors, thus enabling further characterisation of the neuroinflammatory response in a relatively small time period [23, 25–27, 29].

The most conventional approach to producing an in vitro model of ICH is by stimulating the cells with a blood component to mimic the effects of intraparenchymal haemorrhage on brain resident cell types. The serine protease thrombin is activated during coagulation, and has been used to stimulate microglial cultures to determine their response to transforming growth factor β1 (TGF-β1) [30]. Oxyhaemoglobin (oxyHb) and haemoglobin (Hb) have been used to increase understanding of less common cell death mechanisms, such as necroptosis and ferroptosis [23, 24]. Furthermore, whole blood from donor mice has been used with the aid of a porous membrane insert to stimulate primary cortical neurons to allow observation of the full haemotoxic response, specifically erythrocyte lysis and haemoglobin release [31]. However, the most widely used method utilises haemin, the oxidised form of haem, which upon erythrocyte lysis is released from haemoglobin and has been shown to contribute to secondary brain injury following ICH [21, 22, 24–29, 32–34].

One challenge associated with these in vitro models is maintaining relevance to the complexity of the human condition. Following ICH, brain tissue is exposed to approximately 10 mM of haemin, whilst the concentrations used in vitro rarely exceeds 100-μM haemin [29]. Furthermore, individual cell types can exhibit differences in their sensitivity to haemin. This may potentially confound downstream analyses, but could also provide interesting insight into specific functions

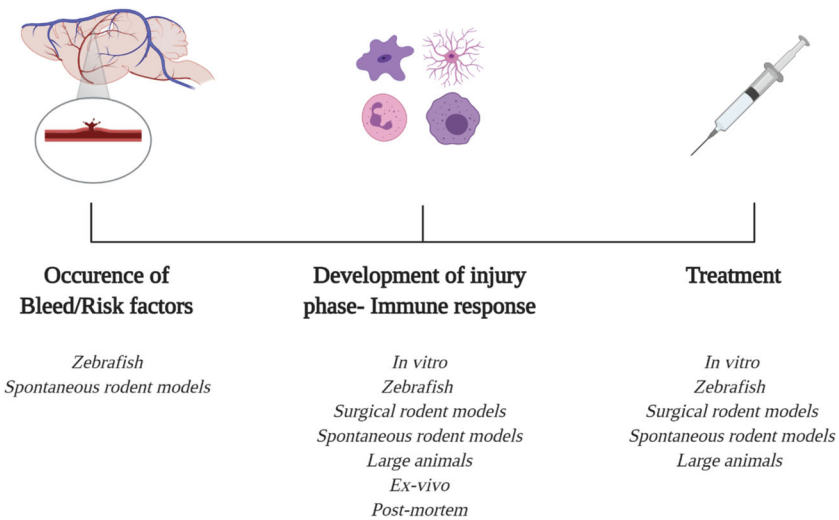

Fig. 1 ICH timeline. This timeline represents the major factors which can be studied in pre-clinical ICH models/systems. Mechanisms that underpin ICH risk can be explored in spontaneous ICH models, such as hypertensive rodents and zebrafish models. Secondary injury progression can be readily observed in all the pre-clinical models, and observations can also be verified in patient tissue such as serum and post-mortem brains. Lastly, potential treatments can be tested across all pre-clinical animal and cell models, where novel candidate therapeutics could be identified through high-throughput screens (e.g. in vitro, zebrafish) and subsequently verified in a mammalian system

Table 1 Comparison between different pre-clinical ICH models

Model	Haematoma expansion	Non-invasive	Spontaneity	Oedema	Intracranial pressure	Mass effect	Live imaging	Aged	High throughput	Drug testing	Behaviour assessment	Cost-effectiveness
Small mammalian												
Autologous blood	+	+	N/A	++	+++	+++	++	++	++	+++	+++	++
Collagenase	+++	+	N/A	++	+++	+++	++	++	++	+++	+++	++
Hypertension	N/D	+++	++++	++	++	++	++	++	++	+++	+++	++
CAA	N/D	++++	++++	++	++	++	++	++++	++	++	+++	+
Col4a1	N/A	++++	++++	++	++	++	++	++	++	++	+++	++
In vitro	N/A	N/A	N/A	N/A	N/A	N/A	++++	N/A	++++	+++	N/A	++++
Zebrafish												
Genetic	++	++++	++++	+	N/A	N/A	++++	+	++++	+++	++	++++
Chemical	++	++	++++	+	N/A	N/A	++++	+	++++	++	++	++++
Large mammalian												
Sheep	+++	+	N/A	++++	++++	++++	++	++	+	++	++	+
Pig	+++	+	N/A	++++	++++	++++	++	++	+	++	++	+

The 12 chosen factors are important when deciding which model, or combination of models can be used, to utilise the advantages of each. Whilst experimentation on sheep and pig can encompass both collagenase and autologous blood, those methods of implementing an ICH follow the same trends as observed in the rodents. *N/D* not determined, *N/A* not applicable

of particular cell types. For example, microglia are less vulnerable to haemin due to their ability to upregulate inducible nitric oxide synthase and haem oxygenase-1 [33]. Goldstein and colleagues hypothesised that in an intact central nervous system (CNS), the toxicity propagated by haemin could be dampened by endogenous antioxidants or other compounds which are not present in these specific cultures, thereby alluding to why such low concentrations of haemin has to be used experimentally [34]. Moreover, only stimulating cells with one blood component do not allow for the full effects of haemotoxicity to be observed, and the time course by which the brain resident cells become affected. Ultimately, simple cell models cannot accurately portray the haematoma expansion or many of the complex mechanisms of primary and secondary injury, hence why they are so often performed alongside in vivo rodent studies.

Small Mammalian Models

The most widely used animals for experimental ICH research are rodents. Although rabbit models also exist, they are predominantly used for subarachnoid haemorrhage research, and as such, will not be discussed here [35–38]. A PubMed assessment of the literature using the search terms 'intracerebral haemorrhage in rats' and 'intracerebral haemorrhage in mice' identified 497 studies published since 2015. These studies could further be divided into two categories: those characterising the pathophysiology of ICH ($n = 303$); and those evaluating candidate therapies ($n = 194$). Despite a large number of the latter reporting beneficial effects, none of the treatments have as yet translated successfully to the clinic. Based on these observations, it would appear therefore that the current translational pipeline is not working. The vast majority of rodent ICH models are non-spontaneous and involve invasive techniques to generate a bleed, through stereotaxic injection of autologous blood or collagenase, and thus do not precisely mimic the human disease, as described below.

Autologous Blood Injection Model

The autologous blood injection model was developed as a controllable and reproducible animal model of ICH, and has undergone many cycles of optimisation since its introduction in 1984. Previously, Ropper et al. had used arterial blood from a donor rat injected into the right caudate nucleus of a recipient rat in order to observe differences in regional blood flow [39]. The use of donor blood quickly became obsolete, leading to the advent of autologous blood taken from the femoral artery before injection into the caudate nucleus [40]. Currently, the most successful model involves a stereotactic injection of autologous blood at two stages into the caudate nucleus. This double injection, first implemented in 1996, was used to allow a small amount of blood to clot, in order to prevent backflow along the needle track, enabling the remaining volume of blood to emulate the haematoma [41]. Following its success in rats, the model has also been implemented for use in mice, where similar effects have been elicited [42–44].

This model is useful at recapitulating a single bleed, which is easily reproducible, and mimics many of the key traits observed in the human condition, such as mass effect, brain oedema, neurological deficits and neuroinflammation [42, 43, 45, 46]. The neuroinflammatory response includes innate immune cell infiltration, activation of brain resident immune cells, oxidative DNA damage and pro-inflammatory cytokine release, all of which have been identified as potential therapeutic targets [43]. However, the autologous blood model lacks the spontaneous nature of haemorrhage, and cannot be used to research haematoma expansion, which is present in 1/3 of patients during the first 24-h post-ictus [7]. Therefore, the primary use of the autologous blood model is to investigate the direct effects of haemotoxicity on the brain.

Collagenase Injection

The collagenase model is the most commonly employed technique for inducing ICH in rodents. This involves the injection of collagenase, a metalloproteinase that degrades interstitial and basement membrane collagen, into the brain via stereotactic injection [47]. Collagenase causes disruption of the basal lamina of the desired cerebral arteries, resulting in blood leaking through the vessels, first achieved in rats by Rosenberg and colleagues in 1990 [47]. Bleeding was observed from 10-min post-injection, with the haematoma volume correlating to the concentration of collagenase used. Various alterations to this model can be made depending on the research question. For example, different brain locations can be injected, although the most commonly used is the right basal ganglia, which reflects the high proportion (35–70%) of patients who develop a 'deep' bleed [48, 49].

As with the autologous blood injection, there are caveats associated with the collagenase model, primarily revolving around the potential neuroinflammatory properties of the enzyme [50, 51]. However, in vitro studies have demonstrated that collagenase alone does not activate microglia, alter prostaglandin E2 production or induce apoptosis [51, 52]. Furthermore, in comparison to the autologous blood model, there is not an increased neuro-immune response attributed to collagenase, as both models display comparable temporal patterns of inflammation [52, 53]. Another disadvantage with the collagenase model is the difficulty in obtaining a relevant sham. Current practice uses a sham model where saline is injected into the brain [54]. However, one could argue that a better sham would be through injection of inactivated collagenase into the brain, thus controlling for potential collagenase-induced inflammation.

Comparative studies between the autologous blood and collagenase model have several key findings. The collagenase injection produces a greater primary injury, most likely attributed to the haematoma expansion which can occur in this model. Interestingly, despite autologous blood generating a more concentrated blood volume and greater initial mass effect, the collagenase model still induces more cell death, oedema and inflammation [45, 55]. There is conflicting literature regarding neurological impairment, which is suggested to be more sustained in the collagenase model, thus rendering it advantageous when observation of long-term deficits of ICH is desirable [45]. Contrastingly, another group saw more long-term motor impairments in the autologous blood model [55]. Ultimately, choice of model depends on the research question being asked. However, the translational relevance of these models has been called into question, thus reiterating the need to develop less invasive and more spontaneous techniques, or coupling these models with other experimental methods in an attempt to more closely recapitulate human ICH [20].

Spontaneous Haemorrhage Models

Although less common, there are rodent models that haemorrhage spontaneously, thus negating the need for surgery, and potentially mimicking the clinical risk factors of ICH more closely. As such, these may be considered as more translationally relevant pre-clinical models, although the location of the bleed and haematoma size cannot be controlled and are often inconsistent between animals, as opposed to the surgically induced ICH models. The main models discussed in this section represent major risk factors for ICH in patients: hypertension, cerebral amyloid angiopathy (CAA) and cerebral small vessel disease (CSVD). The HEADS committee also highlighted the need to develop models of modifiable and non-modifiable risk factors, such as alcoholism and ageing to further understand how ICH can be prevented in these populations, as there are relatively few papers which utilise these risk factors [20, 56–63].

Hypertension

In the 1970s, Okamoto and Aoki generated the spontaneously hypertensive stroke prone (SHRSP) rat model, associated with cerebral lesions that encompassed a wide range of microinfarcts, petechial haemorrhages and larger haemorrhages in locations such as the cerebellum [64, 65]. Furthermore, after the addition of a high salt diet or inhibitor of nitric oxide synthase Nω-nitro-L-arginine methyl ester hydrochloride (L-NAME), the SHRSP rats exhibited larger haemorrhagic events, which were coupled with ischaemia in the L-NAME-treated animals [66, 67]. Ahmad found that after L-NAME treatment, angiotensin receptor antagonist delayed the onset of stroke, thus identifying a potential pathway which may be implemented in hypertension-induced stroke [67].

Following on from the SHRSP rats, Lida and colleagues were the first group to engineer a model of spontaneous ICH in hypertensive mice, where the location of the bleeds identified were similar to those found clinically, such as the brain stem, cerebellum and basal ganglia [65]. Chronic hypertension was achieved by creating a double mutant, overexpressing the human renin and angiotensinogen genes. The mutants were also fed a high salt diet, coupled with L-NAME. A caveat with this study was the survival rates of these mice, which all died within 10 weeks, thereby preventing the ability to observe full recovery following ICH.

The same group then modelled hypertension using a non-transgenic approach by adding L-NAME to the drinking water to induce chronic baseline hypertension, followed by infusion of angiotensin II or norepinephrine to generate an acute hypertensive spike, which was successful at inducing ICH in similar clinical locations to their previous study [65, 68]. This spontaneous model has been valuable in increasing the mechanistic understanding of hypertensive ICH, with particular focus on the role of superoxide and lysyl hydroxylase 3, and how targeting these may act as an intervention to prevent ICH in hypertensive populations [69, 70]. Furthermore, RNAseq analysis from the cerebral vessels of this hypertensive mouse model identified potential key biomarkers for hypertension-induced ICH, including cancer-related pathways, mitochondrion and MHC II proteins, which may help with ICH diagnosis, although these observations need to be confirmed in hypertensive ICH patients [71].

CAA

Rodent models of CAA differ predominantly in the mutated region of the amyloid precursor protein (APP) gene, but they all develop amyloid deposits that bind to the blood vessels and disrupt neurovascular integrity. CAA is a large risk factor for ICH patients above 70 years old; therefore, to mimic the clinical scenario, older animals are utilised in these studies. [14, 20].Winkler et al. were the first group to show that mutations in APP23 mice overexpressing APP_{751} with the Swedish double mutation (K670N/M671L) under the control of a neuron-specific-Thy-1 promoter, exhibited evidence of brain haemorrhage in 27-month old mice [72]. The haemorrhage sites correlated with the CAA vessels, providing rationale for CAA being the driving force behind vessel rupture and bleeds in these transgenic mice. Similarly, a Dutch mutation mouse (E693Q) was generated in the same way, also using APP_{751}. These mice exhibited haemorrhages at 29 months, although the location and frequency of bleeds were not described [73]. Following on from this, a Swedish, Dutch and Iowa (D694N) triple-mutant $A\beta PP_{770}$ mouse was produced, also developing microbleeds [74]. Whilst the frequency of these bleeds was

low, this could be due to the mice being sacrificed at 12 months, and so with a longer life span, it is possible that occurrence of bleeds would have increased. Another study using the Swedish double mutation highlighted the significant increase in the number of microbleeds between 15- and 24-month old mice, further reiterating the need to prolong experimentation when using these models [75].

Some groups have explored the combination of CAA mice and hypertension, which illustrates the importance of investigating multiple risk factors for ICH together, as a patient will often present with a number of comorbidities which can work synergistically to cause a bleed. Over-expression of APP_{695} with the Swedish mutation replicated Alzheimer's pathology, whilst L-NAME treatment and a brief angiotensin II infusion created chronic hypertension. Subsequently, transient acute hypertension was generated by daily doses of angiotensin II. The resulting hypertensive CAA mice had an increased susceptibility to spontaneous ICH at 15 months old [76]. Whilst this is very successful at producing an all-encompassing spontaneous model, major caveats are associated with increased technical demand of generating sufficient hypertension, coupled with the prolonged study time.

Col4a1

Collagen type IV is an integral part of the basement membrane, and is pivotal in providing structural support to tissues. Mutations in the isoform *COL4A1* have been identified in CSVD, haemorrhagic stroke (particularly in younger individuals), familial porencephaly and aneurysm formation of the carotid artery [77]. Newborn mice with mutations in *Col4a1/a2* also exhibit haemorrhage phenotypes. Similarly, older mice experience structural defects in large calibre arteries, as observed in the descending aortae, where focal separation of the endothelium from the media altered the vascular smooth muscle and endothelial cell function. It is hypothesised this may also occur in other large calibre arteries such as the carotid, and may provide rationale for the increased likelihood of ICH in these animals [77]. Another group recreated different *Cola4a1/a2* mutations in mice to understand the genetics and mechanisms that can lead to bleeding, in the hope to improve patient prognosis and treatment for the specific mutations [78]. They also identified several modifiable risk factors which may increase the risk of developing an ICH in this population, such as anticoagulant treatment, acute exercise and vaginal delivery at birth, although these factors would need to be considered on an individual basis, rather than a blanket statement for all *COL4A1* patients [78]. Recently, a *Col4a1* mutant mouse model has been used to mimic deep spontaneous haemorrhages which can occur in patients [79]. A novel segment (transitional segment) was identified between arterioles and capillaries which was hypermuscularised in the mutant mice, thought to play a role in the development of ICH due to subsequent increased intravascular pressure in the upstream feeding arteriole. This study also utilised post-mortem (PM) brain tissue from deep ICH fatalities to corroborate the mouse data. Therefore, this study is a prime example of how using different systems (i.e., mouse models + PM material) can increase confidence in the translational relevance of pre-clinical discoveries.

Despite poor clinical translation in terms of new treatments, the usefulness of both surgical and spontaneous ICH models cannot be disputed, as they have proven vital in studying the multi-faceted effects of ICH within a whole organism. Rodent ICH models have provided the ability to investigate the effects of neurotoxic insults from blood, the infiltrating immune response, neurological deficits and behavioural alterations. However, with the autologous blood and collagenase model, the surgical procedures required to do this are highly invasive and have limitations on how well they truly mimic the clinical scenario. Indeed, the side effects relating to the stress associated with anaesthesia and surgery will undoubtedly confound some aspects of downstream outcome analysis. Moreover, in the past, a disadvantage of rodent models was the presence of the mammalian skull preventing observation of the pathophysiology in real time. However, now various imaging techniques can be implemented such as MRI, PET and laser-speckle. Whilst MRI is commonly used following ICH-induced surgery to view haematoma expansion and/or resolution, and laser speckle to characterise the dynamic changes in blood flow, they are not utilised in identifying bleeds in spontaneous models [55, 80–84]. This is especially apparent in the long-term studies associated with CAA, where the brain is not observed until the animal is 2–3 years old. Prussian blue staining of hemosiderin in the brain is the sole marker used for identifying cerebral bleeds, so the timing of the vessel rupture is largely unknown [72–75]. Furthermore, spontaneous models are rarely used for drug testing, which would be useful to find preventative treatments, or to alleviate symptoms following a bleed, especially as a large proportion of ICH patients suffer from the risk factors modelled in these animals.

Zebrafish Models

Some of the limitations associated with the in vitro and rodent models can be compensated for by the emerging use of zebrafish (*Danio rerio*) models, which can be thought of as an intermediate between in vitro and higher order in vivo systems. Zebrafish possess many benefits as an in vivo model, such as rapid development, transparency of embryos and larvae, non-invasive in vivo imaging and ease of genetic manipulation [85]. Furthermore, as a vertebrate species, the zebrafish genome shares ~ 70% homology with humans thus making them an advantageous system to complement mammalian models [86]. We recognise that zebrafish larvae are

developing animals, and different disease mechanisms may exist in comparison to adult humans. However, we have shown that key characteristics associated with the pathological response to blood in the brain are apparently conserved between young fish and adult humans, suggesting they can be reliably used to model aspects of ICH [87, 88].

In terms of ICH, one of the primary benefits of using zebrafish larvae is that the haemorrhage is produced in a non-invasive manner, thus arguably mimicking the spontaneous nature of human ICH more closely than the surgical rodent models. Several different genetically modified lines exist where haemorrhages are established in this way, whilst chemical induction is another common approach for inducing a brain bleed. There are 2 primary mechanisms by which a bleed can be induced: blood brain barrier (BBB) defects and weakness in the developing blood vessels. With the former, mutations in *notch3*, a regulator in brain pericyte proliferation can result in impaired BBB function and increased frequency of brain haemorrhages [89]. As such, this model may also be useful for studying aspects of CSVD.

Nascent cranial vessel weakness is induced by targeting components important in the stabilisation and development of the cerebrovasculature. βPix is a protein encoded for by the gene *arhgef7b*, thought to play a role in vascular stabilisation. Mutation of βPix results in ICH and hydrocephalus in zebrafish larvae, thus generating the nickname 'bubblehead' for these fish/alleles [90]. Similarly, mutation of the Pak2a protein results in a different, though comparable zebrafish model of ICH, known as the 'redhead' mutant [91]. Defects in primary cilium attached to endothelial cells have been shown to disrupt cerebral-vascular integrity, resulting in ICH in the intraflagellar transport mutant [92].

Aside from genetic alterations to evoke weakness in the neurovasculature, pharmacological agents can be utilised to induce a haemorrhage in zebrafish larvae via water bath incubations and absorption. Statins are most commonly used for this and act by inhibiting the cholesterol biosynthesis rate limiting enzyme 3-hydroxy-3-methylglutaryl-coA reductase (HMGCR). This leads to altered signalling via geranylgeranyl pyrophosphate (GGPP) and reduces activation of Rho GTPases, which act to regulate vascular permeability [93, 94]. Importantly, transient gene knockdown of *hmgcra* using a morpholino (MO) phenocopies, the haemorrhages were observed with statin treatment [94]. Targeting HMGCR not only provides a quick and reliable method of inducing ICH in zebrafish larvae, but may also afford insight into the clinical association between hypocholesterolaemia and increased ICH risk [95–99]. However, statin treatment has been shown to alter myogenesis in developing zebrafish larvae alongside reducing locomotion and heartbeat, which could potentially confound other mechanistic studies which aim to focus solely on the effects of ICH on the larvae [100].

Furthermore, there are rare genetic conditions associated with ICH which cannot be accurately represented in rodents, but can be in zebrafish. An example of this is the rare autosomal recessive interferonopathy: Aicardi-Goutières syndrome subtype 5 (AGS5). Mutations in the viral restriction factor protein SAM and HD domain containing Deoxynucleoside Triphosphate Triphosphohydrolase 1 (SAMHD1) produce an exaggerated type I interferon (IFN) response and cerebrovascular disease in some patients [101–105]. Rodent models of AGS5 exist, but these mice lack any overt physical phenotype [106, 107]. Contrastingly, a MO knockdown of the *samhd1* gene in zebrafish larvae resulted in spontaneous ICH and a significant upregulation of type I IFN [108]. Similar to AGS, another genetic autoimmune disease has been characterised in zebrafish: deficiency of Adenosine Deaminase 2 (ADA2). ADA2 encompasses systemic inflammation and a vascular phenotype arising in childhood, which can result in ischaemic or haemorrhagic cerebral events. A mouse orthologue of the gene encoding ADA2 (*CECR1)* does not exist; however, zebrafish express two paralogues of the *CECR1* gene: *cecr1a* and *cecr1b*. Following MO knockdown of *cecr1b*, these morphants exhibited intracranial bleeding, thus alluding to a role of ADA2 in cranial vessel development or integrity [109].

The use of zebrafish as a disease modelling tool is increasing, and as previously mentioned, they possess several key benefits for studying ICH. However, this is not to suggest that zebrafish should replace any of the well-established models, rather we propose that they should be utilised alongside other in vitro and in vivo studies. For example, using zebrafish for large-scale drug screens, and taking forward the positive hits to interrogate further in mammalian models may increase efficiency of drug development. Furthermore, this approach may also have ethical implications by reducing the numbers of mammals used for primary drug screens. Zebrafish represent a powerful model system for large drug screening studies because of their relatively high-throughput nature, and the high conservation of drug binding sites [110]. There are, however, some caveats associated with zebrafish larval models, such as the lack of skull preventing changes in intracranial pressure and mass effect to be observed following ICH. In addition, as recovery rates are so rapid in zebrafish larvae as demonstrated by Crilly et al., it poses questions on how this may differ to recovery in adult humans. However, understanding these types of processes following ICH during development may provide clues into how we might consider recovering the aged human brain in the future [87].

Larger Mammalian Models

One recurring issue with the animal models described above is their size in comparison to humans, and thus it is difficult to assure accurate translation because of obvious structural differences between rodents, zebrafish and human brains. One

approach to address this is through the use of larger animal species, with brains more comparable to humans, in terms of size, white:grey matter ratios and the presence of gyri. The only 2 species discussed in this section are ovine and swine models; however, this is not to purposefully ignore any additional large mammalian models of ICH. The use of monkeys, canines and cats to study ICH has become largely obsolete, due mainly to ethical considerations [111, 112]. As the main premise of this review is to encourage collaborations between different ICH disciplines, it was thought best to include only those species which are widely used and more broadly accessible.

Boltze and colleagues [113] recently replicated the autologous blood model in adult sheep, observing similar histopathological observations as found in rodent models, such as brain resident cell recruitment and axonal damage. Whilst this preliminary study was used to demonstrate how ovine models can be used as a successful pre-clinical model of ICH, in the future, it is hoped that they will provide additional translational benefits when studying surgical interventions, for example like those performed in the MISTIE and STITCH trials [113–118]. Such candidate intervention techniques are infrequently implemented in other pre-clinical models, and due to the small size of brain and skull, it may be more desirable to perform these types of surgical intervention techniques in an animal model with a larger head [37, 119, 120]. Furthermore, as an aside, this was one of the few pre-clinical ICH studies to include both male and female animals, which as determined by the HEADS initiative needs to be performed more frequently across species, as it is unethical to automatically exclude half of the world's population because female experimental outcomes may differ from males [20]. The other existing pre-clinical studies experimenting on female animals have been used to mainly view hormonal differences between sexes and also how various treatment alters outcome following ICH [82, 121–125].

Swine models of both autologous blood and collagenase injection are implemented for many of the same reasons as ovine models, most notably when characterising the primary injury phase, as comparable haematoma volumes to humans can be produced, making it more beneficial to study mass effect and the mechanism of oedema formation in these larger animals [126–128]. In addition, drug treatments can also be tested in swine models, such as the iron chelator deferoxamine, where it was shown to reduce perihaematomal iron accumulation, neuronal cell death and white matter injury, comparable to its effects in a rat model of ICH [129]. However, the recent i-DEF clinical trial on deferoxamine gave rise to neutral results, thus we should utilise these larger mammalian models to optimise treatment protocols before clinical trials, such as determining the most effective way to administer a drug [130].

Surgical intervention has already been tested in a swine model, whereby following an autologous blood injection, tissue plasminogen activator (tPA) was added to lyse the clot, and the haematoma was aspirated out of the brain, resulting in a significant reduction in oedema [131]. Aside from primary injury, functional changes which occur during ICH can also be measured in the swine model, including alterations within the primary somatic evoked potentials and the resulting cortical spreading depression, which were found to be similar to what was found in a rat model previously [132].

Use of farm animals in ICH research is extremely important to understand the pathophysiology that occurs in a larger brain. However, one limitation of these models in comparison to rodents relates to a relative lack of behavioural assays currently available for measuring neurological outcomes. Furthermore, due to most pre-clinical research being directed towards rodents, it means there is a scarcity of species-specific reagents available for other models, such as sheep, pig and zebrafish, perhaps hindering the ability to look at the secondary injury response as thoroughly as can be observed in mice and rats [128]. The experimentation time is often longer than that of rodent work due to the use of older animals, leading to increased costs, and imaging capabilities are essential. The latter requires infrastructure and resources that few centres currently have.

Post-Mortem/Ex Vivo Studies

Ex vivo studies using PM brain tissue from patients who have died from ICH are surprisingly infrequent, but represent a precious and most clinically relevant source of material. Fortunately, in some instances, what is observed in human samples is comparable to findings in pre-clinical models, as seen in a small proportion of studies [79, 133, 134]. Aside from comparative studies, Wu and colleagues looked at the expression levels of nuclear factor-kappa B (NF-κB), macrophage inflammatory protein-2 (MIP-2) and matrix metalloproteinase-9 (MMP9) using immunohistochemistry. This was successful in enhancing understanding of the time course of brain inflammation following ICH in PM tissues [135]. Furthermore, the robust nature of PM tissue means it can be used for purposes other than just viewing the morphological and cellular characterisation of ICH brains, as demonstrated by a group who performed RNAseq analysis on the frontal and occipital lobes to understand gene expression in hereditary cerebral haemorrhage with amyloidosis-Dutch type (HCHWA-D) [136].

Whilst researching the effect of stroke on the brain is paramount, studies which utilise stroke patient blood can be extremely useful for immune profiling and 'omics-based analyses. This was recently performed by Stamova and colleagues who used RNA from both ischaemic and haemorrhagic stroke patients to reinforce the molecular differences between each condition [137]. Moreover, examining serum from ICH patients has identified the dysregulation of various pro and anti-inflammatory proteins, which have also been confirmed in

rodent ICH models [70, 138, 139]. Additionally, Taylor et al. used ICH patient plasma to determine the role of TGF-β1 following haemorrhage. This ex vivo approach was coupled with both in vitro and in vivo experiments, demonstrating the power of using multiple models/systems, to corroborate discoveries and increase confidence in their validity [30]. Similarly, Lu et al. have recently utilised these three pre-clinical model systems when investigating the effects of the microRNA miR-181c following ICH [140].

There are, however, some problems with PM brain tissue, dependent on factors outside of the researchers' control, such as the availability of particular brain regions, and also the time that the brain is fixed following death [135, 141]. The latter was shown to cause potential exaggeration of glial cell swelling, which is thought to be attributed to the fixation process in devitalised tissue, also seen in delayed fixation in rat brain [141]. Ultimately, the number of studies using PM and ex vivo tissue is minimal. Future work should focus on incorporating these valuable resources into studies, which may become more accessible if cross-discipline collaborations develop, for example, between basic scientists and brain banks.

Conclusion

In this review, we have discussed the multiple models of ICH that exist to inform about a highly disabling condition, currently with no specific medical treatment. To facilitate successful translation in the future, it is clear that there needs to be greater collaboration within the pre-clinical ICH research community to enable cross-talk between studies using different models and by utilising the advantages of each system. The most common multi-model papers exhibit experimentation on rodent and in vitro systems. Moving forward, we suggest a bi-directional 2- or 3-pronged approach for pre-clinical ICH research. For example, using the autologous blood injection rodent model, the thrombin in vitro model, and also incorporating an ex vivo element to the study, as so elegantly illustrated by both Taylor, Lu and colleagues recently [30, 140]. These studies illustrate the power of using multiple systems to investigate a particular question, an approach that will hopefully become more frequently adopted for translational ICH research. Moreover, as one of the key criteria identified by the HEADS committee, we also believe it is essential for pre-clinical findings to be tested and verified in at least two different species (and not both rodents) [20]. By replicating the effect of a drug or compound identified in a smaller animal model in a higher order species such as sheep or pig, it increases the confidence that such a treatment may be efficacious in humans and worthy of consideration for clinical investigation. Furthermore, it is also apparent that the use of brain banks for PM tissue has not been utilised enough for ICH research. Human PM tissue is ideal to validate data obtained from animal models whilst also advancing our understanding of the human pathology and how it may be targeted. Therefore, the use of PM tissue should be implemented when possible, and can work in conjunction with any of the other models (see Fig. 2). Similarly, serum from ICH patients is also understudied, again reinforcing the need for increased cross-talk between pre-clinical scientists and clinicians to obtain this type of material, and to understand key differences which may be observed between comorbid populations which go on to develop an ICH and those that do not. This work would feed into the other pre-clinical work taking place, and can provide validity for the other models, if similar

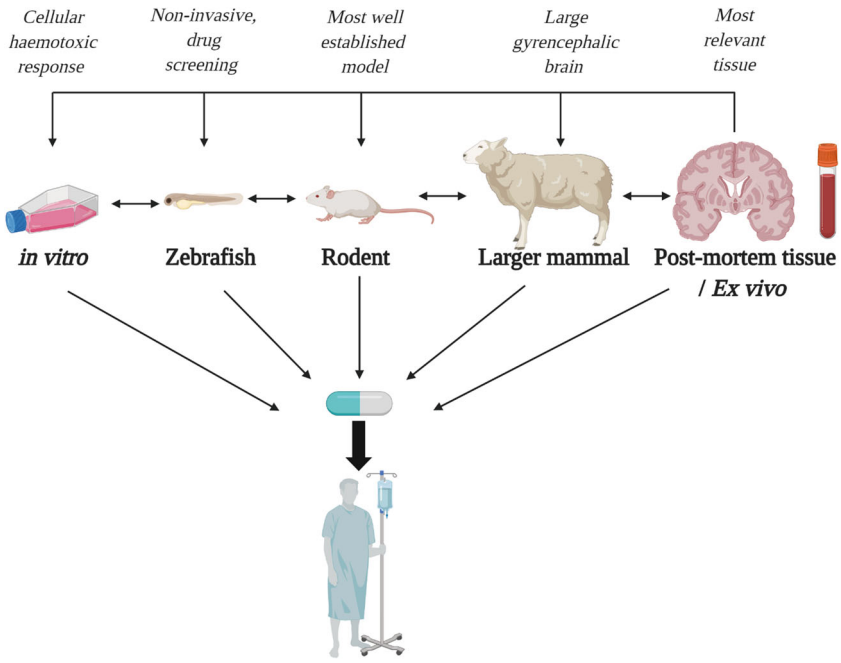

Fig. 2 Multidirectional pipeline of preclinical ICH research. In this pipeline, there is both a feedforward and a feedback loop, to ensure any new findings are valid and observed across multiple models. In addition, the use of post-mortem and ex vivo tissue should feedback into all other pre-clinical models in an attempt to maintain clinical relevance. Fostering multi-discipline collaborations increases the likelihood of creating a drug which will be successful in humans, especially if it is shown to exert positive effects across the pipeline. Maximal advantages are denoted above each model/system

trends are observed. By fostering collaborations with different disciplines, it will strengthen the depth and breadth of ICH research, and will increase the chances of finding new treatment options for ICH patients in the future.

Acknowledgements All authors are thankful to The Natalie Kate Moss Trust for their continued financial support. The figures were created with BioRender.com.

Author Contributions Paul Kasher, Stuart Allan and Adrian Parry-Jones had the idea for the article. Sarah Withers performed the literature search and wrote the first full draft of the review with assistance from Paul Kasher. All authors critically revised the work and produced the final draft.

Funding Information This study was supported by the Medical Research Council Doctoral Training Partnership PhD Programme at the University of Manchester and an English Welsh and Scottish railway (EWS) Exceptional Contribution award to S.E.W; and the Stroke Association for P.R.K. (TSA LECT 2017/02) and A.R.P-J (SA L-RC 19\100,000).

References

1. Collaborators GBDS. Global, regional, and national burden of stroke, 1990-2016: a systematic analysis for the global burden of disease study 2016. Lancet Neurol. 2019;18(5):439–58. https://doi.org/10.1016/S1474-4422(19)30034-1.
2. Krishnamurthi RV, Feigin VL, Forouzanfar MH, Mensah GA, Connor M, Bennett DA, et al. Global and regional burden of first-ever ischaemic and haemorrhagic stroke during 1990-2010: findings from the global burden of disease study 2010. Lancet Glob Health. 2013;1(5):e259–81. https://doi.org/10.1016/S2214-109X(13)70089-5.
3. An SJ, Kim TJ, Yoon BW. Epidemiology, risk factors, and clinical features of Intracerebral hemorrhage: an update. J Stroke. 2017;19(1):3–10. https://doi.org/10.5853/jos.2016.00864.
4. Aronowski J, Zhao X. Molecular pathophysiology of cerebral hemorrhage: secondary brain injury. Stroke. 2011;42(6):1781–6. https://doi.org/10.1161/STROKEAHA.110.596718.
5. Keep RF, Hua Y, Xi G. Intracerebral haemorrhage: mechanisms of injury and therapeutic targets. Lancet Neurol. 2012;11(8):720–31. https://doi.org/10.1016/S1474-4422(12)70104-7.
6. Ziai WC. Hematology and inflammatory signaling of intracerebral hemorrhage. Stroke. 2013;44(6 Suppl 1):S74–8. https://doi.org/10.1161/STROKEAHA.111.000662.
7. Mracsko E, Veltkamp R. Neuroinflammation after intracerebral hemorrhage. Front Cell Neurosci. 2014;8:388. https://doi.org/10.3389/fncel.2014.00388.
8. Shao Z, Tu S, Shao A. Pathophysiological mechanisms and potential therapeutic targets in intracerebral hemorrhage. Front Pharmacol. 2019;10:1079. https://doi.org/10.3389/fphar.2019.01079.
9. Chen S, Yang Q, Chen G, Zhang JH. An update on inflammation in the acute phase of intracerebral hemorrhage. Transl Stroke Res. 2015;6(1):4–8. https://doi.org/10.1007/s12975-014-0384-4.
10. Sturgeon JD, Folsom AR, Longstreth WT Jr, Shahar E, Rosamond WD, Cushman M. Risk factors for intracerebral hemorrhage in a pooled prospective study. Stroke. 2007;38(10):2718–25. https://doi.org/10.1161/STROKEAHA.107.487090.
11. Rost NS, Greenberg SM, Rosand J. The genetic architecture of intracerebral hemorrhage. Stroke. 2008;39(7):2166–73. https://doi.org/10.1161/STROKEAHA.107.501650.
12. Cervera A, Amaro S, Chamorro A. Oral anticoagulant-associated intracerebral hemorrhage. J Neurol. 2012;259(2):212–24. https://doi.org/10.1007/s00415-011-6153-3.
13. O'Donnell MJ, Xavier D, Liu L, Zhang H, Chin SL, Rao-Melacini P, et al. Risk factors for ischaemic and intracerebral haemorrhagic stroke in 22 countries (the INTERSTROKE study): a case-control study. Lancet. 2010;376(9735):112–23. https://doi.org/10.1016/S0140-6736(10)60834-3.
14. Block F, Dafotakis M. Cerebral amyloid angiopathy in stroke medicine. Dtsch Arztebl Int. 2017;114(3):37–42. https://doi.org/10.3238/arztebl.2017.0037.
15. Morotti A, Goldstein JN. Diagnosis and management of acute intracerebral hemorrhage. Emerg Med Clin North Am. 2016;34(4):883–99. https://doi.org/10.1016/j.emc.2016.06.010.
16. Dastur CK, Yu W. Current management of spontaneous intracerebral haemorrhage. Stroke Vasc Neurol. 2017;2(1):21–9. https://doi.org/10.1136/svn-2016-000047.
17. Steiner T, Al-Shahi Salman R, Beer R, Christensen H, Cordonnier C, Csiba L, et al. European stroke organisation (ESO) guidelines for the management of spontaneous intracerebral hemorrhage. Int J Stroke. 2014;9(7):840–55. https://doi.org/10.1111/ijs.12309.
18. Hemphill JC 3rd, Greenberg SM, Anderson CS, Becker K, Bendok BR, Cushman M, et al. Guidelines for the management of spontaneous intracerebral hemorrhage: a guideline for healthcare professionals from the American Heart Association/American Stroke Association. Stroke. 2015;46(7):2032–60. https://doi.org/10.1161/STR.0000000000000069.
19. Frantzias J, Sena ES, Macleod MR, Al-Shahi Salman R. Treatment of intracerebral hemorrhage in animal models: meta-analysis. Ann Neurol. 2011;69(2):389–99. https://doi.org/10.1002/ana.22243.
20. Selim M, Hanley D, Broderick J, Goldstein JN, Gregson BA, Falcione G, et al. Basic and translational research in intracerebral hemorrhage limitations, priorities, and recommendations. Stroke. 2018;49(5):1308–14. https://doi.org/10.1161/Strokeaha.117.019539.
21. Lin S, Yin Q, Zhong Q, Lv FL, Zhou Y, Li JQ, et al. Heme activates TLR4-mediated inflammatory injury via MyD88/TRIF signaling pathway in intracerebral hemorrhage. J Neuroinflammation. 2012;9:46. https://doi.org/10.1186/1742-2094-9-46.
22. Shen X, Ma L, Dong W, Wu Q, Gao Y, Luo C, et al. Autophagy regulates intracerebral hemorrhage induced neural damage via apoptosis and NF-kappaB pathway. Neurochem Int. 2016;96:100–12. https://doi.org/10.1016/j.neuint.2016.03.004.
23. Shen H, Liu C, Zhang D, Yao X, Zhang K, Li H, et al. Role for RIP1 in mediating necroptosis in experimental intracerebral hemorrhage model both in vivo and in vitro. Cell Death Dis. 2017;8(3):e2641. https://doi.org/10.1038/cddis.2017.58.
24. Zille M, Karuppagounder SS, Chen Y, Gough PJ, Bertin J, Finger J, et al. Neuronal death after hemorrhagic stroke in vitro and in vivo shares features of ferroptosis and necroptosis. Stroke.

2017;48(4):1033–43. https://doi.org/10.1161/STROKEAHA.116.015609.

25. Karuppagounder SS, Alin L, Chen Y, Brand D, Bourassa MW, Dietrich K, et al. N-acetylcysteine targets 5 lipoxygenase-derived, toxic lipids and can synergize with prostaglandin E2 to inhibit ferroptosis and improve outcomes following hemorrhagic stroke in mice. Ann Neurol. 2018;84(6):854–72. https://doi.org/10.1002/ana.25356.
26. Luo Q, Li D, Bao B, Wan X, Pan B, Tu J, et al. NEMO-binding domain peptides alleviate perihematomal inflammation injury after experimental intracerebral hemorrhage. Neuroscience. 2019;409:43–57. https://doi.org/10.1016/j.neuroscience.2019.04.041.
27. Hu L, Zhang H, Wang B, Ao Q, Shi J, He Z. MicroRNA-23b alleviates neuroinflammation and brain injury in intracerebral hemorrhage by targeting inositol polyphosphate multikinase. Int Immunopharmacol. 2019;76:105887. https://doi.org/10.1016/j.intimp.2019.105887.
28. Xi ZY, Hu XB, Chen X, Yang Y, Ren J, Wang BF, et al. Protocatechuic acid exerts protective effects via suppression of the P38/JNK- NF-kappa B signalling pathway in an experimental mouse model of intracerebral haemorrhage. Eur J Pharmacol. 2019;854:128–38. https://doi.org/10.1016/j.ejphar.2019.03.008.
29. Sayeed MSB, Alhadidi Q, Shah ZA. Cofilin signaling in hemin-induced microglial activation and inflammation. J Neuroimmunol. 2017;313:46–55. https://doi.org/10.1016/j.jneuroim.2017.10.007.
30. Taylor RA, Chang CF, Goods BA, Hammond MD, Mac Grory B, Ai Y, et al. TGF-beta1 modulates microglial phenotype and promotes recovery after intracerebral hemorrhage. J Clin Invest. 2017;127(1):280–92. https://doi.org/10.1172/JCI88647.
31. Jaremko KM, Chen-Roetling J, Chen L, Regan RF. Accelerated hemolysis and neurotoxicity in neuron-glia-blood clot co-cultures. J Neurochem. 2010;114(4):1063–73. https://doi.org/10.1111/j.1471-4159.2010.06826.x.
32. Mohan S, Glushakov AV, Decurnou A, Narumiya S, Dore S. Contribution of PGE2 EP1 receptor in hemin-induced neurotoxicity. Front Mol Neurosci. 2013;6:31. https://doi.org/10.3389/fnmol.2013.00031.
33. Mohan S, Narumiya S, Dore S. Neuroprotective role of prostaglandin PGE2 EP2 receptor in hemin-mediated toxicity. Neurotoxicology. 2015;46:53–9. https://doi.org/10.1016/j.neuro.2014.10.012.
34. Goldstein L, Teng ZP, Zeserson E, Patel M, Regan RF. Hemin induces an iron-dependent, oxidative injury to human neuron-like cells. J Neurosci Res. 2003;73(1):113–21. https://doi.org/10.1002/jnr.10633.
35. Lyden PD, JacksonFriedman C, LonzoDoktor L. Medical therapy for intracerebral hematoma with the gamma-aminobutyric acid-A agonist muscimol. Stroke. 1997;28(2):387–91. https://doi.org/10.1161/01.Str.28.2.387.
36. Yu Z, Chen LF, Li XF, Zhang DP, Chen YM, Wu WF, et al. A double-injection model of intracerebral hemorrhage in rabbits. J Clin Neurosci. 2009;16(4):545–8. https://doi.org/10.1016/j.jocn.2008.04.026.
37. Wang LK, Wu GF, Sheng F, Wang F, Feng AR. Minimally invasive procedures reduce perihematomal endothelin-1 levels and the permeability of the BBB in a rabbit model of intracerebral hematoma. Neurol Sci. 2013;34(1):41–9. https://doi.org/10.1007/s10072-012-0962-8.
38. Gruter BE, Croci D, Schopf S, Nevzati E, d'Allonzo D, Lattmann J, et al. Systematic review and meta-analysis of methodological quality in in vivo animal studies of subarachnoid hemorrhage. Transl Stroke Res. 2020. https://doi.org/10.1007/s12975-020-00801-4.
39. Ropper AH, Zervas NT. Cerebral blood flow after experimental basal ganglia hemorrhage. Ann Neurol. 1982;11(3):266–71. https://doi.org/10.1002/ana.410110306.
40. Bullock R, Mendelow AD, Teasdale GM, Graham DI. Intracranial haemorrhage induced at arterial pressure in the rat. Part 1: description of technique, ICP changes and neuropathological findings. Neurol Res. 1984;6(4):184–8. https://doi.org/10.1080/01616412.1984.11739687.
41. Deinsberger W, Vogel J, Kuschinsky W, Auer LM, Boker DK. Experimental intracerebral hemorrhage: description of a double injection model in rats. Neurol Res. 1996;18(5):475–7. https://doi.org/10.1080/01616412.1996.11740456.
42. Rynkowski MA, Kim GH, Komotar RJ, Otten ML, Ducruet AF, Zacharia BE, et al. A mouse model of intracerebral hemorrhage using autologous blood infusion. Nat Protoc. 2008;3(1):122–8. https://doi.org/10.1038/nprot.2007.513.
43. Wang J, Fields J, Dore S. The development of an improved preclinical mouse model of intracerebral hemorrhage using double infusion of autologous whole blood. Brain Res. 2008;1222:214–21. https://doi.org/10.1016/j.brainres.2008.05.058.
44. Nakamura T, Xi G, Hua Y, Schallert T, Hoff JT, Keep RF. Intracerebral hemorrhage in mice: model characterization and application for genetically modified mice. J Cereb Blood Flow Metab. 2004;24(5):487–94. https://doi.org/10.1097/00004647-200405000-00002.
45. MacLellan CL, Silasi G, Poon CC, Edmundson CL, Buist R, Peeling J, et al. Intracerebral hemorrhage models in rat: comparing collagenase to blood infusion. J Cereb Blood Flow Metab. 2008;28(3):516–25. https://doi.org/10.1038/sj.jcbfm.9600548.
46. Lei B, Sheng H, Wang H, Lascola CD, Warner DS, Laskowitz DT, et al. Intrastriatal injection of autologous blood or clostridial collagenase as murine models of intracerebral hemorrhage. J Vis Exp. 2014;89. https://doi.org/10.3791/51439.
47. Rosenberg GA, Mun-Bryce S, Wesley M, Kornfeld M. Collagenase-induced intracerebral hemorrhage in rats. Stroke. 1990;21(5):801–7. https://doi.org/10.1161/01.str.21.5.801.
48. Aguilar MI, Brott TG. Update in intracerebral hemorrhage. Neurohospitalist. 2011;1(3):148–59. https://doi.org/10.1177/1941875211409050.
49. Zhu W, Gao Y, Wan J, Lan X, Han X, Zhu S, et al. Changes in motor function, cognition, and emotion-related behavior after right hemispheric intracerebral hemorrhage in various brain regions of mouse. Brain Behav Immun. 2018;69:568–81. https://doi.org/10.1016/j.bbi.2018.02.004.
50. Participants NIW. Priorities for clinical research in intracerebral hemorrhage: report from a National Institute of Neurological Disorders and Stroke workshop. Stroke. 2005;36(3):e23–41. https://doi.org/10.1161/01.STR.0000155685.77775.4c.
51. Wang J. Preclinical and clinical research on inflammation after intracerebral hemorrhage. Prog Neurobiol. 2010;92(4):463–77. https://doi.org/10.1016/j.pneurobio.2010.08.001.
52. Chu K, Jeong SW, Jung KH, Han SY, Lee ST, Kim M, et al. Celecoxib induces functional recovery after intracerebral hemorrhage with reduction of brain edema and perihematomal cell death. J Cerebr Blood F Met. 2004;24(8):926–33. https://doi.org/10.1097/01.Wcb.0000130866.25040.7d.
53. Xue M, Del Bigio MR. Comparison of brain cell death and inflammatory reaction in three models of intracerebral hemorrhage in adult rats. J Stroke Cerebrovasc Dis. 2003;12(3):152–9. https://doi.org/10.1016/S1052-3057(03)00036-3.
54. Zhou Y, Wang Y, Wang J, Anne Stetler R, Yang QW. Inflammation in intracerebral hemorrhage: from mechanisms to clinical translation. Prog Neurobiol. 2014;115:25–44. https://doi.org/10.1016/j.pneurobio.2013.11.003.
55. Barratt HE, Lanman TA, Carmichael ST. Mouse intracerebral hemorrhage models produce different degrees of initial and

delayed damage, axonal sprouting, and recovery. J Cereb Blood Flow Metab. 2014;34(9):1463–71. https://doi.org/10.1038/jcbfm.2014.107.
56. Leclerc JL, Lampert AS, Diller MA, Dore S. PGE2-EP3 signaling exacerbates intracerebral hemorrhage outcomes in 24-mo-old mice. Am J Physiol Heart Circ Physiol. 2016;310(11):H1725–34. https://doi.org/10.1152/ajpheart.00638.2015.
57. Liew HK, Cheng HY, Huang LC, Li KW, Peng HF, Yang HI, et al. Acute alcohol intoxication aggravates brain injury caused by intracerebral hemorrhage in rats. J Stroke Cerebrovasc Dis. 2016;25(1):15–25. https://doi.org/10.1016/j.jstrokecerebrovasdis.2015.08.027.
58. Huang LC, Liew HK, Cheng HY, Kuo JS, Hsu WL, Pang CY. Brain magnetic resonance imaging of intracerebral hemorrhagic rats after alcohol consumption. J Stroke Cerebrovasc Dis. 2018;27(12):3493–502. https://doi.org/10.1016/j.jstrokecerebrovasdis.2018.08.022.
59. Chiu CD, Chiu YP, Lin CL, Ji HR, Shen CC, Lee HT, et al. Acetazolamide alleviates sequelae of hyperglycaemic intracerebral haemorrhage by suppressing astrocytic reactive oxygen species. Free Radic Res. 2018;52(9):1010–9. https://doi.org/10.1080/10715762.2018.1508838.
60. Cao S, Hua Y, Keep RF, Chaudhary N, Xi G. Minocycline effects on intracerebral hemorrhage-induced iron overload in aged rats: brain iron quantification with magnetic resonance imaging. Stroke. 2018;49(4):995–1002. https://doi.org/10.1161/STROKEAHA.117.019860.
61. Leclerc JL, Li C, Jean S, Lampert AS, Amador CL, Diller MA, et al. Temporal and age-dependent effects of haptoglobin deletion on intracerebral hemorrhage-induced brain damage and neurobehavioral outcomes. Exp Neurol. 2019;317:22–33. https://doi.org/10.1016/j.expneurol.2019.01.011.
62. Anqi X, Ruiqi C, Yanming R, Chao Y. Neuroprotective potential of GDF11 in experimental intracerebral hemorrhage in elderly rats. J Clin Neurosci. 2019;63:182–8. https://doi.org/10.1016/j.jocn.2019.02.016.
63. Tao C, Keep RF, Xi G, Hua Y. CD47 blocking antibody accelerates hematoma clearance after intracerebral hemorrhage in aged rats. Transl Stroke Res. 2019;11:541–51. https://doi.org/10.1007/s12975-019-00745-4.
64. Ogata J, Fujishima M, Tamaki K, Nakatomi Y, Ishitsuka T, Omae T. Stroke-prone spontaneously hypertensive rats as an experimental model of malignant hypertension. A pathological study. Virchows Arch A Pathol Anat Histol. 1982;394(3):185–94. https://doi.org/10.1007/BF00430664.
65. Lida S, Baumbach GL, Lavoie JL, Faraci FM, Sigmund CD, Heistad DD. Spontaneous stroke in a genetic model of hypertension in mice. Stroke. 2005;36:1253–8.
66. Smeda JS. Hemorrhagic stroke development in spontaneously hypertensive rats fed a North American, Japanese-style diet. Stroke. 1989;20(9):1212–8. https://doi.org/10.1161/01.str.20.9.1212.
67. Ahmad S. Angiotensin receptor antagonists delay nitric oxide-deficient stroke in stroke-prone rats. Eur J Pharmacol. 1997;333(1):39–45. https://doi.org/10.1016/s0014-2999(97)01089-3.
68. Wakisaka Y, Chu Y, Miller JD, Rosenberg GA, Heistad DD. Spontaneous intracerebral hemorrhage during acute and chronic hypertension in mice. J Cereb Blood Flow Metab. 2010;30(1):56–69. https://doi.org/10.1038/jcbfm.2009.183.
69. Wakisaka Y, Chu Y, Miller JD, Rosenberg GA, Heistad DD. Critical role for copper/zinc-superoxide dismutase in preventing spontaneous intracerebral hemorrhage during acute and chronic hypertension in mice. Stroke. 2010;41(4):790–7. https://doi.org/10.1161/STROKEAHA.109.569616.
70. Li H, Xu H, Wen H, Liu T, Sun Y, Xiao N, et al. Overexpression of LH3 reduces the incidence of hypertensive intracerebral hemorrhage in mice. J Cereb Blood Flow Metab. 2019;39(3):547–61. https://doi.org/10.1177/0271678X18815791.
71. Chen B, Sun H, Zhao Y, Lun P, Feng Y. An 85-gene coexpression module for progression of hypertension-induced spontaneous intracerebral hemorrhage. DNA Cell Biol. 2019;38(5):449–56. https://doi.org/10.1089/dna.2018.4425.
72. Winkler DT, Bondolfi L, Herzig MC, Jann L, Calhoun ME, Wiederhold KH, et al. Spontaneous hemorrhagic stroke in a mouse model of cerebral amyloid angiopathy. J Neurosci. 2001;21(5):1619–27.
73. Herzig MC, Winkler DT, Burgermeister P, Pfeifer M, Kohler E, Schmidt SD, et al. Abeta is targeted to the vasculature in a mouse model of hereditary cerebral hemorrhage with amyloidosis. Nat Neurosci. 2004;7(9):954–60. https://doi.org/10.1038/nn1302.
74. Davis J, Xu F, Deane R, Romanov G, Previti ML, Zeigler K, et al. Early-onset and robust cerebral microvascular accumulation of amyloid beta-protein in transgenic mice expressing low levels of a vasculotropic Dutch/Iowa mutant form of amyloid beta-protein precursor. J Biol Chem. 2004;279(19):20296–306. https://doi.org/10.1074/jbc.M312946200.
75. Fisher M, Vasilevko V, Passos GF, Ventura C, Quiring D, Cribbs DH. Therapeutic modulation of cerebral microhemorrhage in a mouse model of cerebral amyloid angiopathy. Stroke. 2011;42(11):3300–3. https://doi.org/10.1161/STROKEAHA.111.626655.
76. Passos GF, Kilday K, Gillen DL, Cribbs DH, Vasilevko V. Experimental hypertension increases spontaneous intracerebral hemorrhages in a mouse model of cerebral amyloidosis. J Cereb Blood Flow Metab. 2016;36(2):399–404. https://doi.org/10.1177/0271678X15606720.
77. Van Agtmael T, Bailey MA, Schlotzer-Schrehardt U, Craigie E, Jackson IJ, Brownstein DG, et al. Col4a1 mutation in mice causes defects in vascular function and low blood pressure associated with reduced red blood cell volume. Hum Mol Genet. 2010;19(6):1119–28. https://doi.org/10.1093/hmg/ddp584.
78. Jeanne M, Jorgensen J, Gould DB. Molecular and genetic analyses of collagen type IV mutant mouse models of spontaneous intracerebral hemorrhage identify mechanisms for stroke prevention. Circulation. 2015;131(18):1555–U64. https://doi.org/10.1161/Circulationaha.114.013395.
79. Ratelade J, Klug NR, Lombardi D, Angelim M, Dabertrand F, Domenga-Denier V, et al. Reducing hypermuscularization of the transitional segment between arterioles and capillaries protects against spontaneous intracerebral hemorrhage. Circulation. 2020;141:2078–94. https://doi.org/10.1161/CIRCULATIONAHA.119.040963.
80. Knight RA, Han YX, Nagaraja TN, Whitton P, Ding J, Chopp M, et al. Temporal MRI assessment of intracerebral hemorrhage in rats. Stroke. 2008;39(9):2596–602. https://doi.org/10.1161/Strokeaha.107.506683.
81. Matsushita H, Hijioka M, Hisatsune A, Isohama Y, Iwamoto S, Terasawa H, et al. MRI-based analysis of intracerebral hemorrhage in mice reveals relationship between hematoma expansion and the severity of symptoms. PLoS One. 2013;8(7). https://doi.org/10.1371/journal.pone.0067691.
82. Jing C, Bian L, Wang M, Keep RF, Xi G, Hua Y. Enhancement of hematoma clearance with CD47 blocking antibody in experimental intracerebral hemorrhage. Stroke. 2019;50(6):1539–47. https://doi.org/10.1161/STROKEAHA.118.024578.
83. Shi E, Shi K, Qiu S, Sheth KN, Lawton MT, Ducruet AF. Chronic inflammation, cognitive impairment, and distal brain region alteration following intracerebral hemorrhage. FASEB J. 2019;33(8):9616–26. https://doi.org/10.1096/fj.201900257R.
84. Liu C, Xie B, Li M, Yang GY, Tong S. Spatiotemporal changes of cerebral blood flow following hemorrhagic stroke by laser speckle

imaging. Conf Proc IEEE Eng Med Biol Soc. 2011;2011:6150–3. https://doi.org/10.1109/IEMBS.2011.6091519.
85. Lieschke GJ, Currie PD. Animal models of human disease: zebrafish swim into view. Nat Rev Genet. 2007;8(5):353–67. https://doi.org/10.1038/nrg2091.
86. Howe K, Clark MD, Torroja CF, Torrance J, Berthelot C, Muffato M, et al. The zebrafish reference genome sequence and its relationship to the human genome. Nature. 2013;496(7446):498–503. https://doi.org/10.1038/nature12111.
87. Crilly S, Njegic A, Laurie SE, Fotiou E, Hudson G, Barrington J, et al. Using zebrafish larval models to study brain injury, locomotor and neuroinflammatory outcomes following intracerebral haemorrhage. F1000Res. 2018;7:1617. https://doi.org/10.12688/f1000research.16473.2.
88. Crilly S, Njegic A, Parry-Jones AR, Allan SM, Kasher PR. Using zebrafish larvae to study the pathological consequences of hemorrhagic stroke. Jove-J Vis Exp. 2019;(148). https://doi.org/10.3791/59716.
89. Wang Y, Pan L, Moens CB, Appel B. Notch3 establishes brain vascular integrity by regulating pericyte number. Development. 2014;141(2):307–17. https://doi.org/10.1242/dev.096107.
90. Liu J, Fraser SD, Faloon PW, Rollins EL, Vom Berg J, Starovic-Subota O, et al. A betaPix Pak2a signaling pathway regulates cerebral vascular stability in zebrafish. Proc Natl Acad Sci U S A. 2007;104(35):13990–5. https://doi.org/10.1073/pnas.0700825104.
91. Buchner DA, Su F, Yamaoka JS, Kamei M, Shavit JA, Barthel LK, et al. pak2a mutations cause cerebral hemorrhage in redhead zebrafish. Proc Natl Acad Sci U S A. 2007;104(35):13996–4001. https://doi.org/10.1073/pnas.0700947104.
92. Eisa-Beygi S, Benslimane FM, El-Rass S, Prabhudesai S, Abdelrasoul MKA, Simpson PM, et al. Characterization of endothelial cilia distribution during cerebral-vascular development in zebrafish (*Danio rerio*). Arterioscler Thromb Vasc Biol. 2018;38(12):2806–18. https://doi.org/10.1161/ATVBAHA.118.311231.
93. Gjini E, Hekking LH, Kuchler A, Saharinen P, Wienholds E, Post JA, et al. Zebrafish Tie-2 shares a redundant role with Tie-1 in heart development and regulates vessel integrity. Dis Model Mech. 2011;4(1):57–66. https://doi.org/10.1242/dmm.005033.
94. Eisa-Beygi S, Hatch G, Noble S, Ekker M, Moon TW. The 3-hydroxy-3-methylglutaryl-CoA reductase (HMGCR) pathway regulates developmental cerebral-vascular stability via prenylation-dependent signalling pathway. Dev Biol. 2013;373(2):258–66. https://doi.org/10.1016/j.ydbio.2012.11.024.
95. Wang X, Dong Y, Qi X, Huang C, Hou L. Cholesterol levels and risk of hemorrhagic stroke: a systematic review and meta-analysis. Stroke. 2013;44(7):1833–9. https://doi.org/10.1161/STROKEAHA.113.001326.
96. Wieberdink RG, Poels MM, Vernooij MW, Koudstaal PJ, Hofman A, van der Lugt A, et al. Serum lipid levels and the risk of intracerebral hemorrhage: the Rotterdam Study. Arterioscler Thromb Vasc Biol. 2011;31(12):2982–9. https://doi.org/10.1161/ATVBAHA.111.234948.
97. Phuah CL, Raffeld MR, Ayres AM, Viswanathan A, Greenberg SM, Biffi A, et al. Subacute decline in serum lipids precedes the occurrence of primary intracerebral hemorrhage. Neurology. 2016;86(22):2034–41. https://doi.org/10.1212/WNL.0000000000002716.
98. Chang JJ, Katsanos AH, Khorchid Y, Dillard K, Kerro A, Burgess LG, et al. Higher low-density lipoprotein cholesterol levels are associated with decreased mortality in patients with intracerebral hemorrhage. Atherosclerosis. 2018;269:14–20. https://doi.org/10.1016/j.atherosclerosis.2017.12.008.
99. Sun L, Clarke R, Bennett D, Guo Y, Walters RG, Hill M, et al. Causal associations of blood lipids with risk of ischemic stroke and intracerebral hemorrhage in Chinese adults. Nat Med. 2019;25(4):569–74. https://doi.org/10.1038/s41591-019-0366-x.
100. Campos LM, Rios EA, Guapyassu L, Midlej V, Atella GC, Herculano-Houzel S, et al. Alterations in zebrafish development induced by simvastatin: comprehensive morphological and physiological study, focusing on muscle. Exp Biol Med (Maywood). 2016;241(17):1950–60. https://doi.org/10.1177/1535370216659944.
101. Rice GI, Bond J, Asipu A, Brunette RL, Manfield IW, Carr IM, et al. Mutations involved in Aicardi-Goutieres syndrome implicate SAMHD1 as regulator of the innate immune response. Nat Genet. 2009;41(7):829–32. https://doi.org/10.1038/ng.373.
102. Ramesh V, Bernardi B, Stafa A, Garone C, Franzoni E, Abinun M, et al. Intracerebral large artery disease in Aicardi-Goutieres syndrome implicates SAMHD1 in vascular homeostasis. Dev Med Child Neurol. 2010;52(8):725–32. https://doi.org/10.1111/j.1469-8749.2010.03727.x.
103. Thiele H, du Moulin M, Barczyk K, George C, Schwindt W, Nurnberg G, et al. Cerebral arterial stenoses and stroke: novel features of Aicardi-Goutieres syndrome caused by the Arg164X mutation in SAMHD1 are associated with altered cytokine expression. Hum Mutat. 2010;31(11):E1836–50. https://doi.org/10.1002/humu.21357.
104. Xin B, Jones S, Puffenberger EG, Hinze C, Bright A, Tan H, et al. Homozygous mutation in SAMHD1 gene causes cerebral vasculopathy and early onset stroke. Proc Natl Acad Sci U S A. 2011;108(13):5372–7. https://doi.org/10.1073/pnas.1014265108.
105. du Moulin M, Nurnberg P, Crow YJ, Rutsch F. Cerebral vasculopathy is a common feature in Aicardi-Goutieres syndrome associated with SAMHD1 mutations. Proc Natl Acad Sci U S A. 2011;108(26):E232–author reply E3. https://doi.org/10.1073/pnas.1104699108.
106. Behrendt R, Schumann T, Gerbaulet A, Nguyen LA, Schubert N, Alexopoulou D, et al. Mouse SAMHD1 has antiretroviral activity and suppresses a spontaneous cell-intrinsic antiviral response. Cell Rep. 2013;4(4):689–96. https://doi.org/10.1016/j.celrep.2013.07.037.
107. Rehwinkel J, Maelfait J, Bridgeman A, Rigby R, Hayward B, Liberatore RA, et al. SAMHD1-dependent retroviral control and escape in mice. EMBO J. 2013;32(18):2454–62. https://doi.org/10.1038/emboj.2013.163.
108. Kasher PR, Jenkinson EM, Briolat V, Gent D, Morrissey C, Zeef LA, et al. Characterization of samhd1 morphant zebrafish recapitulates features of the human type I interferonopathy Aicardi-Goutieres syndrome. J Immunol. 2015;194(6):2819–25. https://doi.org/10.4049/jimmunol.1403157.
109. Zhou Q, Yang D, Ombrello AK, Zavialov AV, Toro C, Zavialov AV, et al. Early-onset stroke and vasculopathy associated with mutations in ADA2. N Engl J Med. 2014;370(10):911–20. https://doi.org/10.1056/NEJMoa1307361.
110. Walcott BP, Peterson RT. Zebrafish models of cerebrovascular disease. J Cereb Blood Flow Metab. 2014;34(4):571–7. https://doi.org/10.1038/jcbfm.2014.27.
111. Ma Q, Khatibi NH, Chen H, Tang J, Zhang JH. History of preclinical models of intracerebral hemorrhage. Acta Neurochir Suppl. 2011;111:3–8. https://doi.org/10.1007/978-3-7091-0693-8_1.
112. Lin XT, Tang YC, Sun B, Hou ZY, Meng HW, Li ZP, et al. Cerebral glucose metabolism: influence on perihematomal edema formation after intracerebral hemorrhage in cat models. Acta Radiol. 2010;51(5):549–54. https://doi.org/10.3109/02841851003660065.
113. Boltze J, Ferrara F, Hainsworth AH, Bridges LR, Zille M, Lobsien D, et al. Lesional and perilesional tissue characterization by automated

image processing in a novel gyrencephalic animal model of peracute intracerebral hemorrhage. J Cereb Blood Flow Metab. 2019;39(12):2521–35. https://doi.org/10.1177/0271678X18802119.
114. Mendelow AD, Gregson BA, Fernandes HM, Murray GD, Teasdale GM, Hope DT, et al. Early surgery versus initial conservative treatment in patients with spontaneous supratentorial intracerebral haematomas in the International Surgical Trial in Intracerebral Haemorrhage (STICH): a randomised trial. Lancet. 2005;365(9457):387–97. https://doi.org/10.1016/S0140-6736(05)17826-X.
115. Mendelow AD, Gregson BA, Rowan EN, Murray GD, Gholkar A, Mitchell PM, et al. Early surgery versus initial conservative treatment in patients with spontaneous supratentorial lobar intracerebral haematomas (STICH II): a randomised trial. Lancet. 2013;382(9890):397–408. https://doi.org/10.1016/S0140-6736(13)60986-1.
116. Morgan T, Zuccarello M, Narayan R, Keyl P, Lane K, Hanley D. Preliminary findings of the minimally-invasive surgery plus rtPA for intracerebral hemorrhage evacuation (MISTIE) clinical trial. Acta Neurochir Suppl. 2008;105:147–51. https://doi.org/10.1007/978-3-211-09469-3_30.
117. Mould WA, Carhuapoma JR, Muschelli J, Lane K, Morgan TC, McBee NA, et al. Minimally invasive surgery plus recombinant tissue-type plasminogen activator for intracerebral hemorrhage evacuation decreases perihematomal edema. Stroke. 2013;44(3):627–34. https://doi.org/10.1161/STROKEAHA.111.000411.
118. Hanley DF, Thompson RE, Rosenblum M, Yenokyan G, Lane K, McBee N, et al. Efficacy and safety of minimally invasive surgery with thrombolysis in intracerebral haemorrhage evacuation (MISTIE III): a randomised, controlled, open-label, blinded endpoint phase 3 trial. Lancet. 2019;393(10175):1021–32. https://doi.org/10.1016/S0140-6736(19)30195-3.
119. Liu XC, Jing LY, Yang MF, Wang K, Wang Y, Fu XY, et al. Enhanced neuroprotection of minimally invasive surgery joint local cooling lavage against ICH-induced inflammation injury and apoptosis in rats. Cell Mol Neurobiol. 2016;36(5):647–55. https://doi.org/10.1007/s10571-015-0245-z.
120. Pei HT, Jiang T, Liu GF, Li ZX, Luo K, An JJ, et al. The effect of minimally invasive hematoma aspiration on the JNK signal transduction pathway after experimental intracerebral hemorrhage in rats. Int J Mol Sci. 2016;17(5). https://doi.org/10.3390/ijms17050710.
121. Lei B, Wang H, Jeong S, Hsieh JT, Majeed M, Dawson H, et al. Progesterone improves neurobehavioral outcome in models of intracerebral hemorrhage. Neuroendocrinology. 2016;103(6):665–77. https://doi.org/10.1159/000442204.
122. Hsieh JT, Lei B, Sheng H, Venkatraman T, Lascola CD, Warner DS, et al. Sex-specific effects of progesterone on early outcome of intracerebral hemorrhage. Neuroendocrinology. 2016;103(5):518–30. https://doi.org/10.1159/000440883.
123. Xie Q, Xi G, Keep RF, Hua Y. Effects of gender and estrogen receptors on iron-induced brain edema formation. Acta Neurochir Suppl. 2016;121:341–5. https://doi.org/10.1007/978-3-319-18497-5_59.
124. Chen-Roetling J, Kamalapathy P, Cao Y, Song W, Schipper HM, Regan RF. Astrocyte heme oxygenase-1 reduces mortality and improves outcome after collagenase-induced intracerebral hemorrhage. Neurobiol Dis. 2017;102:140–6. https://doi.org/10.1016/j.nbd.2017.03.008.
125. Dai S, Hua Y, Keep RF, Novakovic N, Fei Z, Xi G. Minocycline attenuates brain injury and iron overload after intracerebral hemorrhage in aged female rats. Neurobiol Dis. 2019;126:76–84. https://doi.org/10.1016/j.nbd.2018.06.001.
126. Wagner KR, Xi G, Hua Y, Kleinholz M, de Courten-Myers GM, Myers RE, et al. Lobar intracerebral hemorrhage model in pigs: rapid edema development in perihematomal white matter. Stroke. 1996;27(3):490–7. https://doi.org/10.1161/01.str.27.3.490.
127. Xi G, Wagner KR, Keep RF, Hua Y, de Courten-Myers GM, Broderick JP, et al. Role of blood clot formation on early edema development after experimental intracerebral hemorrhage. Stroke. 1998;29(12):2580–6. https://doi.org/10.1161/01.str.29.12.2580.
128. Wagner KR. Modeling intracerebral hemorrhage: glutamate, nuclear factor-kappa B signaling and cytokines. Stroke. 2007;38(2 Suppl):753–8. https://doi.org/10.1161/01.STR.0000255033.02904.db.
129. Gu Y, Hua Y, Keep RF, Morgenstern LB, Xi G. Deferoxamine reduces intracerebral hematoma-induced iron accumulation and neuronal death in piglets. Stroke. 2009;40(6):2241–3. https://doi.org/10.1161/STROKEAHA.108.539536.
130. Selim M, Foster LD, Moy CS, Xi G, Hill MD, Morgenstern LB, et al. Deferoxamine mesylate in patients with intracerebral haemorrhage (i-DEF): a multicentre, randomised, placebo-controlled, double-blind phase 2 trial. Lancet Neurol. 2019;18(5):428–38. https://doi.org/10.1016/S1474-4422(19)30069-9.
131. Wagner KR, Xi G, Hua Y, Zuccarello M, de Courten-Myers GM, Broderick JP, et al. Ultra-early clot aspiration after lysis with tissue plasminogen activator in a porcine model of intracerebral hemorrhage: edema reduction and blood-brain barrier protection. J Neurosurg. 1999;90(3):491–8. https://doi.org/10.3171/jns.1999.90.3.0491.
132. Mun-Bryce S, Wilkerson AC, Papuashvili N, Okada YC. Recurring episodes of spreading depression are spontaneously elicited by an intracerebral hemorrhage in the swine. Brain Res. 2001;888(2):248–55. https://doi.org/10.1016/s0006-8993(00)03068-7.
133. Shi SX, Li YJ, Shi K, Wood K, Ducruet AF, Liu Q. IL (Interleukin)-15 bridges astrocyte-microglia crosstalk and exacerbates brain injury following intracerebral hemorrhage. Stroke. 2020;51(3):967–74. https://doi.org/10.1161/STROKEAHA.119.028638.
134. Li M, Ren H, Sheth KN, Shi FD, Liu Q. A TSPO ligand attenuates brain injury after intracerebral hemorrhage. FASEB J. 2017;31(8):3278–87. https://doi.org/10.1096/fj.201601377RR.
135. Wu H, Zhang ZY, Hu XL, Zhao RB, Song YJ, Ban XA, et al. Dynamic changes of inflammatory markers in brain after hemorrhagic stroke in humans: a postmortem study. Brain Res. 2010;1342:111–7. https://doi.org/10.1016/j.brainres.2010.04.033.
136. Moursel LG, van Roon-Mom WMC, Kielbasa SM, Mei H, Buermans HPJ, van der Graaf LM, et al. Brain transcriptomic analysis of hereditary cerebral hemorrhage with amyloidosis-Dutch type. Front Aging Neurosci. 2018;10. https://doi.org/10.3389/fnagi.2018.00102.
137. Stamova B, Ander BP, Jickling G, Hamade F, Durocher M, Zhan X, et al. The intracerebral hemorrhage blood transcriptome in humans differs from the ischemic stroke and vascular risk factor control blood transcriptomes. J Cereb Blood Flow Metab. 2019;39(9):1818–35. https://doi.org/10.1177/0271678X18769513.
138. Meng Z, Zhao T, Zhou K, Zhong Q, Wang Y, Xiong X, et al. A20 Ameliorates Intracerebral Hemorrhage-Induced Inflammatory Injury by Regulating TRAF6 Polyubiquitination. J Immunol. 2017;198(2):820–31. https://doi.org/10.4049/jimmunol.1600334.
139. Zhou K, Cui S, Duan W, Zhang J, Huang J, Wang L, et al. Cold-inducible RNA-binding protein contributes to intracerebral hemorrhage-induced brain injury via TLR4 signaling. Brain Behav. 2020:e01618. https://doi.org/10.1002/brb3.1618.
140. Lu X, Zhang HY, He ZY. MicroRNA-181c provides neuroprotection in an intracerebral hemorrhage model. Neural Regen Res. 2020;15(7):1274–82. https://doi.org/10.4103/1673-5374.272612.
141. Del Bigio MR, Deck JH, Davidson GS. Glial swelling with eosinophilia in human post-mortem brains: a change indicative of plasma extravasation. Acta Neuropathol. 2000;100(6):688–94. https://doi.org/10.1007/s004010000236.